THREE-DIMENSIONAL ANALYSIS OF LENTICULAR ORE BODIES USING DISPLACEMENT DISCONTINUITY ELEMENTS

by

Thamer Yacoub

A thesis submitted in conformity with the requirements
for the degree of Doctor of Philosophy
Department of Civil Engineering
University of Toronto

Abstract

Three Dimensional Analysis of Lenticular Orebodies Using Displacement Discontinuity Elements

Doctor of Philosophy, 1999

Thamer Yacoub

Department of Civil Engineering, University of Toronto

The most appropriate numerical techniques for the analysis and design of excavations, pillars and mining sequences in lenticular orebodies is the displacement discontinuity method (DDM). This thesis examines three important facets of the DDM and makes improvements in these areas that affect the efficiency of the method in its application to the crack-type problems, arising in the mining of lenticular or seam deposits.

The introduction of the concept of node sharing between adjacent elements into the DDM, is the first aspect covered in the thesis. The node-sharing formulation of the DDM was made possible after the introduction of a new and unified framework for evaluating the singular boundary integrals that exist in the Green's functions of the displacement discontinuity method. The new integration method is based on the continuation approach.

The formulation of a new displacement discontinuity element – the enhanced displacement discontinuity (EDD) element – was the second major undertaking of the thesis. This new formulation provides information on the in-plane (confinement) stresses in an element, something the conventional DDM does not consider. The EDD element

creates an automated and more flexible way of modelling different degrees of confinement, expected to occur in unmined orebody zones (*i.e.* pillars and abutments). With the inclusion of confinement into the formulation of the enhanced DD element, it can be readily used to analyse yielding pillars, since all components of the stress tensor at a point in a material are explicitly taken into account.

Finally, the thesis looked at the development of a methodology in the EDDM for modelling the post-peak behaviour of pillars. The progressive failure procedure was incorporated into the EDDM to create a program for simulating post-failure pillar response. The progressive failure procedure relies on a simple quasi-elastic constitutive relationship, and uncomplicated failure criteria to model failed pillar material.

Acknowledgements

'Call to me and I will answer you, and will tell you great and hidden things which you have not known.' **(Jeremiah 33:3 RSV)**

At the beginning, I would like to give my everlasting thanks to the one in Whom, I live and move, to my Saviour Jesus Christ. I know that with Him everything is possible. Thank you, Jesus.

I wish to express my thanks to my supervisor, Prof. John H. Curran, for his suggestions and support during the course of this research.

My gratitude also goes to Dr. Reginald E. Hammah for his meticulous work on the editing of the thesis. His assistance and caring were invaluable. I was also fortunate to have met Mr. Vijayakumar Sinnathurai. His strong mathematical background and in-depth knowledge of the methods of integration were of great help.

I am indebted to my parents for their love and encouragement, and sacrifices they have made for the betterment of my life and career. Special thanks go to my father in-law and my mother in-law for providing me with support and encouragement. I also want to thank all the members of my family and my friends, especially Abouna Estephanous, for their continuous prayer and support.

Last, but not the least, I warmly acknowledge and appreciate the encouragement and assistance provided by my wife, Diana, over the years required to complete this work. Her patience and love during these years have been a great source of inspiration to me. Indeed, *a women that fears the LORD, she shall be praised* (Proverb 31:30).

Table of Contents

List of Figures

List of Tables

Contributions of Thesis

The research performed for this thesis has led to the following contributions to the body of engineering knowledge

1. A node-centric formulation to the displacement discontinuity method. The thesis contributed to the node-centric formulation in the following ways:

   i) Established a unified integration methodology for solving singular integrals through the use of boundary functions.

   ii) Derived the required boundary functions for the two- and three-dimensional node-centric displacement discontinuity method.

   iii) Implemented the derived boundary functions in a computer program and tested the performance of the method in the solution of practical problems.

2. An enhanced displacement discontinuity element for the analysis of lenticular orebodies. By extending of the original formulation of the displacement discontinuity method, a new displacement discontinuity element was derived in this thesis. The enhanced formulation introduces an additional displacement discontinuity variation to the traditional DD approach. This new formulation provides information on the confinement stresses in an element in a pillar.

3. The modelling of the post-peak response of pillars using the enhanced displacement discontinuity element. The fact that the enhanced DD element provides the normal, shear and lateral stress in the pillar widens the applicability of the method for the

analysis of yielding pillars. The progressive failure procedure was implemented to show how the EDDM could be used to realistically model the post-peak response in pillars.

Chapter 1

Introduction

1.1 Geomechanical Mine Design and Analysis

The analysis and design of mine structures (shafts, drifts, entries, pillars and other forms of support, etc.) is important for the safe and economic extraction of ore from underground mines, a fact which cannot be overemphasised [1, 2]. The rock mechanics design and analysis of mine structures involves the establishment of parameters such as stope and pillar dimensions, pillar layout, stope mining sequence, pillar extraction sequence and type of rock support [3]. The purpose is to ensure that the local stability of stopes and the general control of rock response in regions close to stope activity are ensured while maintaining the maximum extraction of ore.

The design and analysis of underground structures poses many difficult problems to the rock mechanics expert or rock engineer. For many of these problems, analytical solutions either do not exist, or are extremely difficult to determine. This is often due to factors such as complex problem geometry, non-homogeneous material properties or their combination. More general design tools rely on numerical or empirical techniques [4, 5].

Additional source of considerable difficulty in geomechanical mine design is the uncertainty inherent in data collected on rock strata properties. The properties of geological domains exhibit a very wide range of variability. In certain regions, the properties of rock masses may vary considerably over small volumes, making it very hard to extrapolate or even interpolate rock properties. Aside of the great variability in

properties of rock masses, there is also uncertainty associated with the determination of their properties in localised zones, because the determination of the geomechanical properties of rock samples is not always simple or straightforward. In addition, the behaviour of rock masses differs from that of the small samples tested in lab or field as a result of which the geomechanical properties determined from samples may not be representative of those of the rock mass from which the samples were taken.

The difficulties associated with the uncertainty in the geomechanical properties of rock masses indicate that the design of mining stopes and excavations calls more for a qualitative, rather than purely quantitative, evaluation of the performance of rock in the vicinity of excavations and that in the far-field. The major aim of analyses of this type is therefore to gain physical insight into a problem, and to better understand the influence of the various factors that govern the overall stability of mine structure [6]. Numerical methods are very useful in performing parametric studies under such circumstances. They can be used to evaluate a number of feasible of mining options. These methods are not only appropriate for parametric studies, but can also be used to identify and explore appropriate mine layouts and sequences. The knowledge gained from such analyses can be used to develop detailed ore production schemes.

1.2 Numerical Methods

Numerical methods have undergone major development during the last three decades. Their application in engineering design has seen considerable increase, because of the increasing computing power and falling costs of computers. With numerical

methods, problems that involve complex geometry, non-linear material behaviour, multiple material types, and combinations of these factors, can be solved. Because of their abilities to model a very broad spectrum of engineering problems and handle the modelling difficulties described above, they have made it possible to solve problems that previously could not be attempted with analytical methods.

Based on the form of approximation involved, numerical methods can be classified into two categories: domain methods and boundary methods [7]. In domain methods, boundary conditions are exactly satisfied, while governing differential equations in a material domain are satisfied approximately. On the other hand, boundary methods satisfy governing equations throughout a problem domain, but approximate boundary conditions. The two most popular domain numerical methods are the finite element method (FEM) and the finite difference method (FDM). The boundary element method (BEM) is a boundary method.

Numerical methods do not have the same range of applicability for all classes of problems. Particular numerical methods may be advantageous in some situations and disadvantageous in others. The selection of a numerical technique for a problem depends on the ability of the technique to satisfy the objectives and requirements of the problem. In the following sections, brief descriptions and range of applications for the two most commonly used numerical methods, the FEM and BEM, are provided.

1.2.1 Finite element method (FEM)

As stated earlier, the FEM is the most popular numerical method and is used in a

wide variety of engineering fields. In the method, a material domain or body is divided into elements of various shapes. Each element is connected to others at nodes, which are the corners of elements [8]. Boundary conditions are specified for the problem, and the governing differential equations approximated by developing approximations of the connectivity between elements, and the continuity of displacements and stresses between elements. A system of equations is then assembled for the problem and solved for the unknown nodal stresses and displacements.

The FEM can be used to model mining excavations by replacing the rock continuum around an excavation with a number of individual elements. It can model the enlargement of mining openings or stopes, as well as model the build-up of material (back-fill) in existing stopes. The strength of the FEM in geomechanical mine design lies in its generality and ability to handle problems involving non-homogeneous material domains (different types of material) or geometric non-linearity.

The true boundary conditions on the surfaces of excavations can be easily and correctly represented in the FEM. However, the method cannot explicitly simulate far-field conditions in problems with infinite or semi-infinite domains. To simulate far-field conditions, the FEM requires the definition of an arbitrary outer boundary with boundary conditions that approximate far-field conditions. For cases, in which more than one excavation is to be analysed, the outer boundary has to be located at a considerable distance from the excavations (beyond the zone of influence of the excavations). Errors due to discretization occur throughout a problem domain as a result.

1.2.2 Boundary element methods

Boundary element methods are particularly attractive for solving the class of problems involving large domains and linear material response. It can also be used for non-linear problems [9].

In the BEM, only the boundaries of a problem domain are discretized. This produces a reduction of one in the dimensionality of problems. Unlike the FEM, discretization errors in the BEM occur only on problem boundaries and it correctly models far-field conditions. The BEM uses fundamental solutions that satisfy the governing differential equations of a problem to determine the influence of elements on one another. When the integral equations for all elements are assembled, the resulting system of equations can be solved for unknowns. Once all boundary unknowns have been solved for, field quantities, such as stresses and displacements, at any point in the problem can be obtained [10].

1.3 Requirements of a Mining Stress Analysis Tool

Problems involving analysis of temporary mine excavations such as stopes and drifts, possess characteristics that restrict the choice of numerical methods for their solution. The following are some of the attributes of numerical techniques that are essential and desirable for practical stress analysis in underground mining design:

(i) The numerical method selected for the design of stopes should be capable of efficiently handling the large domains, typically encountered in problems of underground mining [11]. If a method that requires extensive discretization of

domains is used, large numbers of elements and nodes have to be employed to sufficiently represent the problem. This in turn leads to huge systems of equations that demand considerable computational resources and time to solve. In view of the fact that there is a substantial uncertainty associated with mine data, analyses have to be performed several times in order to obtain a proper understanding of the possible consequences of mining activity. Consequently, methods involving extensive discretization are not desirable for such analysis.

(ii) The computational technique used for the analyses of underground mine excavations should be able to accurately model far-field conditions.

(iii) When analysing underground excavations, not all zones require the calculation of very accurate displacements and stresses. For zones that demand high accuracy, finer discretization or meshes have to be used. Away from these areas coarser meshes can be employed to reduce the time required for calculations. This means that numerical methods for such analysis must allow meshes with different sized elements to be used in problems.

(iv) Pillars in underground mine excavations usually have material properties different from that of the host rock. The properties of the pillars are that of the orebody. Therefore, numerical methods for modelling such excavations should have the capability to handle the different material properties.

(v) Pillars are usually subjected to loads, which induce stresses exceeding the elastic limits of the pillar material. Therefore, numerical models for their analysis should be able to capture post-failure material behaviour.

(vi) Mine layouts for flat-lying lenticular orebodies involve parallel-sided openings that are characterised by plan dimensions much greater than opening heights. Stresses around such openings vary greatly over small distances and therefore require either extensive discretization around the openings, or elements that can account for this rapid stress variation.

(vii) For most mining excavations, the assumption of two-dimensional plane strain analysis is violated due to the complex three-dimensional layout of excavations. As a result, three-dimensional analysis has to be performed to determine the states of stress induced in rock material in the vicinity of excavation surfaces (near-field). The difficulties mentioned above, concerning the sizes of equation systems and meshing, are more challenging in three-dimensional numerical analysis than in two-dimensional analysis by an order of magnitude.

1.4 Choice of Numerical Model for the Analysis of Lenticular Orebodies

Although the finite element method is a very powerful and flexible technique, and has been used to analyse a wide range of geomechanics problems, its usefulness for the mining of lenticular orebodies is restricted by many of the above-enumerated practical considerations [11]. Because the FEM requires surface and volume discretization of problem domains, it uses a relatively large number of elements and presents meshing problems, especially in three-dimensional analysis. Even with efficient automated facilities, mesh generation and the checking of meshes for problems involving complex three-dimensional layouts is difficult. Also the FEM does not simulate far-field

conditions accurately unless an extensive region around the excavations is discretized. When the computing resources and time needed to determine solutions of problems is combined with the need for multiple and parametric analyses of the same problem, it becomes evident that the method is not the most suitable for mine stress analysis.

In contrast, the boundary element method requires only the discretization of surfaces, and thus uses much smaller numbers of elements than the FEM. This leads to smaller systems of equations in the BEM, easier mesh generation, faster computing times, and a reduction in the need for significant computing resources. The BEM inherently deals with the infinite and semi-infinite domains of mining problems and matches far-field conditions exactly.

An additional attraction of the BEM is its ability to evaluate stresses and displacements at specific points of interest in a problem domain, without re-meshing or calculating values for the entire domain. For example, if the stresses and displacements along the lengths of extensometers are needed from a model in order to check them with field measurements, those specific values can be readily calculated in the BEM.

1.4.1 Variations of the boundary element method

Generally, for stress analysis, there are two distinct types of boundary element formulations. These are the direct BEM and the indirect BEM. The displacement discontinuity method (DDM), a method commonly used in the analysis of slit-like openings in rock masses, is a type of indirect BEM. Because the DDM is very suitable for the analysis of thin crack-type excavations, the focus of this research, it shall also be described in detail below.

1.4.1.1 The direct boundary element formulation

Direct boundary element methods use fundamental theorems, which relate differential equations over a domain to integrals over the boundaries of the domain, to obtain integral equations. The variables in the direct formulation of the BEM are meaningful physical attributes of a problem, such as tractions and displacements. Solution of the integral equations for the elements into which a boundary is discretized directly yields the desired values of the unknown variables on the boundary.

1.4.1.2 The indirect boundary element formulation

The indirect formulation uses singular solutions, which satisfy the governing differential equations of the problem, with specified unknown densities on the boundaries in a problem. These unknown densities (known as fictitious stresses, for example, in the fictitious stress method) generally have no physical meaning. They can be determined from the boundary integral equations for a set of prescribed boundary conditions. Displacements and stresses on the boundaries, as well as in the domain, can then be obtained indirectly from the fictitious variables.

1.4.1.3 The displacement discontinuity method

For thin slit-like openings or crack-type elements, the boundaries of the two opposing surfaces are very close to each other, thereby practically coinciding. Such conditions create numerical instabilities for both the direct and fictitious stress method. It

follows therefore that special techniques are needed for modelling the mining of seams or lenticular orebodies.

The displacement discontinuity method is ideally suited for solving problems involving crack-type excavations. Although the DDM is technically a type of indirect BEM, the unknown variables in it represent physically meaningful aspects of the problem. The relative movement between the roof and floor of an excavation is treated as a displacement discontinuity. The normal component of the displacement discontinuity vector is called the closure and the transverse components are called the ride components (Fig. 1.1). Since both the top and floor in the mine excavation are included in one element, numerical instability is eliminated. As well, the inclusion of two surfaces in the elements brings about a reduction in the number of elements required for the discretization of problems.

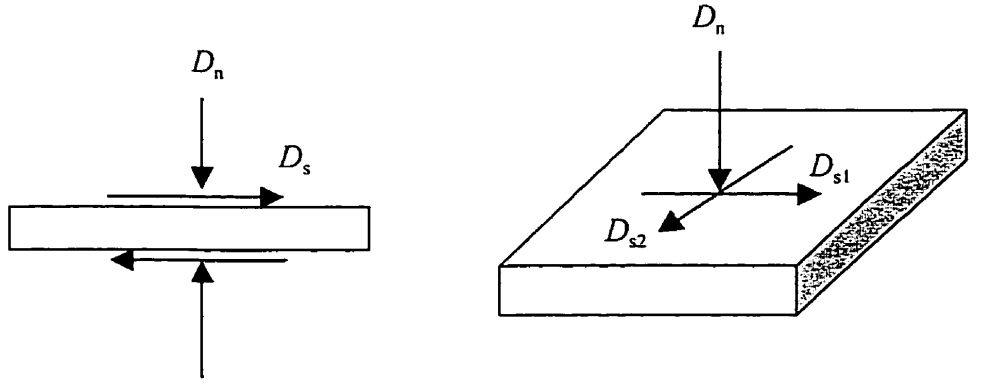

(a) two-dimensional DD element **(b) three-dimensional DD element**

Figure 1.1: Displacement discontinuity components

Although both the direct and indirect boundary element methods can be applied to non-linear and non-homogeneous problems, they are more readily applied to linear homogeneous problems. In order to handle non-homogeneous material, however, the

boundary integral equations have to be augmented by volume integrals, a process that requires internal discretizations of the domain. Such problems are encountered in cases where the strength and deformational properties of an orebody differ from that of the host rock. The presence of volume and surface integrals generates an additional source of difficulty. The displacement discontinuity method, as an exception, is however able to model bimaterial problems very efficiently [12].

1.5 Shortcomings of the Traditional DDM

Several advancements have been made to the original DDM, first proposed by Salamon [13]. These include improvements to the method's accuracy through the formulation of higher-order elements, and enhancements for overcoming difficulties arising in its application to practical problems. Despite all these efforts, the traditional DDM still has some shortcomings. These include the following:

(i) For a constant element in the traditional DDM, unknown parameters are determined at the node of the element, which is located at the element centre. This means that nodes cannot be shared between elements. As a result, the variation of displacements and stresses over adjacent elements is discontinuous [14, 15]. Even when higher-order linear and quadratic DD elements, which increase the number of unknowns for each element, are implemented in the method, the lack of node-sharing means that inter-element continuity cannot be enforced or ensured [16, 17]. Another consequence of the absence of node-sharing in the traditional DDM is that huge influence matrices have to be solved in large-scale mining problems, because

large numbers of nodes are used for problem formulation.

(ii) The conventional DDM provides no information on the in-plane stress in the displacement discontinuity element. As will be seen further on, the in-plane stress is particularly important in the modelling of unmined orebody structures, such as pillars and longwalls, since it induces confinement. To overcome this deficiency, *ad hoc* processes are used to estimate the confining stresses in these zones. One such common procedure is the use of a family of stress-strain curves. The stress-strain curves are assigned to elements based on their location within an unmined structure [18]. This procedure is, however, manual, cumbersome, and requires considerable experience from the analyst in order to assign reasonable curves to elements.

(iii) In practical mining situations, pillars regularly experience some yielding or local failure. It therefore becomes important to model the post-peak performance of orebody material, a problem that involves plastic deformations. Generally, plasticity problems require constitutive models that describe non-linear material behaviour. The traditional DDM cannot use plasticity constitutive models, because it does not provide information on all stress tensor components needed for such analysis. It can, however, be adapted to solve elasto-plastic problems using a method of incremental linear approximations [19] and stress redistribution [20], although the technique still requires cumbersome *ad hoc* means of estimating missing stress tensor components.

1.6 Objective of Research

The primary objective of the research for this thesis was to develop formulations of the displacement discontinuity method for practical mining purposes that would retain the strengths of the method, and surmount its disadvantages. To achieve this goal, the research was divided into three major aspects. Each of these aspects tackled a shortcoming described in the previous section. Attempts were also made to compare results obtained from existing techniques with those from new methods proposed.

The first of the major issues in the DDM considered in this study involved the introduction of node-sharing (node-centric) between DD elements. For node-sharing to work, it was foremost to establish an efficient and accurate method for evaluating integrals of the DDM, especially those associated with singular points in three-dimensional analysis. The problem of ensuring continuous variation of the singularities between elements could then be tackled in order to develop a general framework for the node-sharing procedure.

The absence of confinement effects in elements within unmined regions, it was mentioned earlier, resulted in a major drawback of the traditional DDM. Therefore, the principal focus of the second part of the thesis was on the development of a new DD element that explicitly included confining stress components. This, it was envisaged, would facilitate the use of the DDM for pillar analysis, by overcoming the difficulties of the *ad hoc* approaches.

Finally, the thesis comprehensively looked at the analysis of yielding pillars, and the modelling of post-peak pillar behaviour, using the new formulation of the DDM. The

new DDM is used to simulate the progressive failure of rock.

1.7 Scope and Contents of the Thesis

Apart from this opening chapter, there are five other chapters in the thesis. A general framework for implementing node-sharing in indirect boundary element methods, which imposes continuity of field quantities between the elements, is described in Chapter 2. Difficulties in evaluating the singular integrals of the indirect boundary element formulation are discussed in the chapter, and a method for solving them also provided.

Chapter 3 provides insight into a specific implementation of the node-centric method for the displacement discontinuity method. It also includes examples of the comparison of node-centric results with closed-form solutions.

In Chapter 4, the formulation for a new displacement discontinuity element is presented. The new DD element does away with one of the shortcomings of the conventional DDM. By introducing a lateral discontinuity that considers in-plane (confinement) stresses.

The post-failure behaviour of pillars is discussed in Chapter 5. The analysis of yielding pillars with the simple, yet powerful, progressive failure technique, implemented in the new DDM, is also presented.

A summary of this research, together with its benefits is outlined in Chapter 6. Recommendations for future research and development are in addition discussed.

Four papers, which were written during the work of this thesis and are related to the material in Chapters 2 to 5, are presented in the Appendices.

Chapter 2

Node-Centric Indirect Boundary Element Method

2.1 Elements in the BEM

In the boundary element method, as stated in the previous chapter, only the boundaries of a problem are discretized into elements. The governing differential equations of the problem are satisfied throughout the solution domain by the results obtained from the boundary element method. However, the actual boundary conditions of the problem are only approximated. This gives rise to errors on the boundaries. Consequently, the accuracy of BEM results in regions close to boundaries is dependent on the accuracy of the approximations of the boundary conditions of a problem. It is of vital importance, therefore, to use methods that minimise the errors of boundary approximations.

One way to attain good agreement between the real boundary conditions of a problem and their representation in the BEM is to represent a boundary with a large number of elements. With increasing discretization, the elements used get smaller, as a result of which the expected approximation of the boundary conditions improves. However, this approach demands a lot of computations and therefore requires significant computer resources for most practical problems. A more reasonable approach is to formulate elements that would permit optimal representation of problem boundaries and boundary conditions.

There are two main types of elements that have been formulated for the BEM. These major classes of elements are discontinuous elements and continuous elements.

The nodes of discontinuous elements are located within the interior bounds of elements. They require very simple procedures in determining the element coefficients of the influence matrix. Because the nodes of such elements are in the interior of the elements, matrix contributions from each element reside in their own distinct locations in the influence matrix. In contrast, continuous elements have at least some of their nodes situated at the element ends or corners. The end nodes of continuous elements, therefore, can be shared with adjacent elements [21].

Both discontinuous and continuous elements have advantages and disadvantages in application. Discontinuous elements are widely used in BEMs mainly because of their simplicity in formulation. Because there is no node sharing (adjacent elements do not have common nodes) in their formulation, the computation of the contributions of point sources at nodes is relatively straightforward. However, the lack of node sharing in methods with discontinuous elements means that for the same number of nodes a mesh with discontinuous elements is coarser than a boundary discretization with continuous elements. In addition, there are jumps in values of computed field quantities, such as stress and displacement, at the end nodes. Inter-element continuity between discontinuous elements cannot be attained even with higher order element formulations that use more unknowns.

Typically in the boundary element method, the collection of elements into which a boundary has been discretized is taken to be the approximation of the boundary. The nodes of discontinuous elements are placed at points on an element so that they facilitate convenient integration and interpolation. Since these nodes are chosen to lie in interior nodes of elements, they generally, do not exactly coincide with actual problem

boundaries (Fig. 2.1a). The points at which the boundary conditions are approximated, therefore, do not coincide with points of the boundary.

The node-centric formulation of continuous elements in the BEM allows the nodes of such elements to be chosen such that they lie exactly on a problem boundary (Fig. 2.1b). This feature consequently limits boundary approximations to only the discretization of boundaries into elements, as a result of which boundary approximations no longer include errors due to nodes not being placed on physical problem boundaries. The end nodes of adjacent elements are shared in the node-centric approach. For the same number of nodes as in a problem discretization with discontinuous elements, continuous elements provide a finer mesh, resulting in greater accuracy. At the extreme nodes of continuous elements, there are no jumps in computed values of field quantities such as stresses and displacements. It is expected that a continuous variation of field quantities would more accurately model real behaviour than a discontinuous variation. All this, however, comes at the price of additional mathematical effort in the formulating of the system of equations.

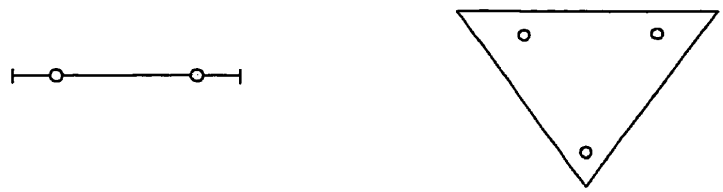

a) Element-centric linear DD element

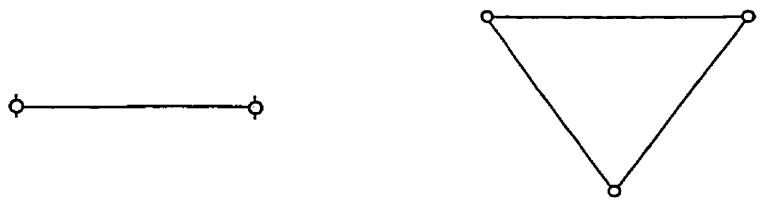

b) Node-centric linear DD element

Figure 2.1: Two and three-dimensional node- and element-centric elements

2.2 Continuous Elements in the Indirect BEM

Continuous elements are used more often than discontinuous elements in the direct BEM, because of the advantages the former offer. The direct BEM requires that implicit integral equations be formulated for a problem. This leads to substantial difficulties in its applications to a number of problems [22], and therefore limits the use of direct methods. The indirect BEM was developed to overcome these difficulties. For a wider variety of problems, it is easier to implement the indirect than the direct BEM.

Despite this advantage of the indirect BEM, researchers have been unable to extensively use the node-centric formulation of elements with the method, owing to some problems with the evaluation of integrals. Integral equations in the node-centric formulation of the direct BEM have lower singularity at the nodes and their integration is therefore not problematic. In the indirect method, however, this is not so. Integral functions are highly singular (hyper-singular) owing to the superposition of fundamental solutions, making them difficult to evaluate. Unlike discontinuous elements, which have all nodes always lying on smooth parts of boundaries, continuous elements, by sharing nodes, require that some functions be integrated at the end nodes of elements. The computation of jump terms at the end nodes of elements in the indirect BEM (nodes that lie on the edges or corners of a boundary) presents significant challenges, due to the meeting of multiple element vertices at such nodes.

2.3 Methods for Integrating Singular Functions

The essence of the boundary element method lies in the transformation of a problem involving a continuum field to an equivalent boundary problem. This

transformation is made possible through the use of fundamental solutions or Green's functions. These functions are generally unbounded at one point, *i.e.* each of the functions has an infinite value at a specific point. Such functions are thus termed as singular functions. The order of singularity can vary from function to function.

The fundamental solutions of the BEM serve as kernels in integrations that provide the transformation from domain problems to boundary problems. To make solutions of the boundary problems feasible and obtainable at reasonable computational cost, boundaries are discretized into elements. The principal idea behind this is that each element can be assigned a prescribed continuous variation of field quantities based on the effects of point loads (values) acting at selected points of the problem domain. The variation of field quantities at elements is chosen so that it approximates the actual variation.

The integrands in boundary element methods are Green's functions multiplied by some weighting functions. The behaviour of these integrands is strongly influenced by the order of singularity of a Green's function, and the position of the singular point. Mathematically, integrals involving the fundamental solutions and Green functions fall into three main classes: non-singular or regular integrals, near-singular integrals, and singular integrals.

Regular or non-singular integrals:

When the distance of a load point (a point at which a load is applied) from an element is far, the integrals are bounded and straightforward to evaluate using any classical numerical quadrature routine or method. Most boundary element integrations

fall in this category. The accuracy of such integrals does not significantly affect results.

Near-singular integrals:

In cases where a load point is close to an element, the value of the integrand over the domain of integration varies rapidly. The values of such integrals can be determined with classical quadrature methods to reasonable degrees of accuracy, only if excessively large numbers of collocation points are used. Accuracy in the evaluation of such integrals has greater influence on results than accuracy for regular integrals.

Singular integrals:

Singular integrals are the most difficult to evaluate, but at the same time the most important to calculate accurately in the BEM. They occur when a load point lies on an element, and represent the influence of elements on themselves (self-influence). Self-influence coefficients form the diagonal terms of coefficient matrices that most strongly affect the overall accuracy of BEM solutions. Classical numerical quadrature methods cannot be applied directly to singular integrals, because of their unbounded nature at singular points. They thus require special treatment [23]. The difference between near-singular and singular integrals is not as sharp as that between near-singular and regular integrals.

The greater degree of singularity of integrals in the DDM, compared to fictitious stress method and direct BEM, has been one of the factors that has constrained the widespread use of continuous elements in the method.

2.4 Techniques for Improving Boundary Approximations in Node-Centric Methods

It was mentioned earlier in the chapter that node-sharing methods reduce the errors of approximation at the boundaries of a problem. However, the boundary approximation errors in the approach can be further reduced through the use of special techniques. These special treatments can be classified into two main categories based on the manner in which errors are minimised. The methods for reducing boundary errors are outlined as follow:

(i) Errors can be minimised by distributing them over elements in an averaged sense. Minimisation of the averaged error can be accomplished through the multiplication of the error function with an interpolation function that approximates boundary conditions, and equating the resulting integral of the product of the two functions to zero. This approach is called the Galerkin technique.

(ii) Values of the error function (the difference between exact boundary values and approximated values) can be forced to be zero at the nodes of elements. This method is called nodal collocation.

2.4.1 The Galerkin Technique

An interpolation function commonly used in the Galerkin technique is the Gaussian quadrature weighting function [24]. An important attribute of the Galerkin method is that it avoids difficulties associated with the evaluation of singular integrals by shifting points of interest from nodal locations to Gaussian quadrature points.

Previous attempts at creating continuous elements in the indirect BEM have used

the Galerkin method to reduce boundary approximation errors. An example of such a work is the application of the Galerkin technique to the displacement discontinuity method by Vandamme and Curran [25]. The number of integrations in the indirect BEM increases by an order of magnitude (*i.e.*, $O(n^2)$) in the Galerkin technique, leading to a rapid growth in the computational effort needed to generate matrices of influence coefficient. For large three-dimensional problems this computational expense gets prohibitive.

2.4.2 Nodal Collocation Method

In the nodal collocation method, boundary integral equations are satisfied at a number of discrete source points on a problem boundary, the nodes of elements. In contrast, the Galerkin technique, described above, satisfies the governing boundary integrals in an integral or weighted residual sense.

The nodal collocation method is attractive because it exactly satisfies boundary integrals at nodal points, and is more economical than the Galerkin method due to fewer number of integrations in the method. Despite its advantages in speed however, there were compelling reasons, in the past, why the nodal collocation method was not applied to the indirect BEM. Primary reasons for using the nodal collocation approach stemmed from the difficulties associated with the evaluation of the hyper-singular integrals of the indirect BEM [26].

Tremendous effort has been devoted in recent years to the development of efficient techniques for the evaluation of singular and near-singular integrals. These techniques employ methods such as analytical integration, modified Gaussian methods,

non-linear transformation of the integration domains, series expansion and row sum methods, to tackle the class of hyper-singular integrals [23]. Although, these methods have been successfully applied to a wide variety of problems, they have their own drawbacks. For example, most of these techniques evaluate singular and non-singular integrals with separate methodologies. In this thesis, an integration technique based on the continuation approach [27-30], originally formulated by Vijayakumar and Cormack [27, 30], that makes it possible to uniformly treat the evaluation of singular and near-singular integrals, was used.

The continuation approach provides an elegant means for treating singular and near-singular integrals. This leads to a unified methodology for evaluating integrals of all kinds. In the continuation approach integration over the domain of the element is converted to integration along the sides (edges) or boundary of the element. Integration along the edges eliminates the need to use a mix of analytical and numerical methods to compute the different types of integrals, thereby providing a uniform way for computing all integrals. Exhaustive details of the continuation approach can be found in the references [27-30], with only an overview of the mathematical derivation of the boundary functions of the method provided further below.

The continuation approach offers robustness, in addition to uniformity in the evaluation of singular and near-singular integrals. Because in the approach, integration is performed along element boundaries, the evaluation of integrands at singular or near-singular points is avoided. Avoidance of the evaluation of integrals at these points is what provides robustness. When a singular point coincides with a node, the values of integration along the element sides that form the node automatically reduce to zero.

Another aspect of the continuation approach is that values of integrals are obtained either as conventional integrals, Cauchy Principal Values or finite-part integrals [31], depending on the type of integrands involved. The computation of integrals is performed more efficiently in the approach, since the number of collocation points required for integration along the boundary of an element is considerably less than the number required if the collocation points were to be selected over the area of the element.

2.5 Adaptive Integration

The new integration formulation described so far simplifies a number of difficulties associated with the evaluation of singular and near-singular integrals. However, numerical difficulties in implementation still arise when a singular point lies in the vicinity of a boundary, because of the steep variation of integrands in the vicinity of singular points. For such a case, closely spaced collocation points are required for the regions of high variation, while sparse collocation points are needed for the rest of the quadrature domain (Fig. 2.2). The traditional approach has been to develop empirical relationships, which roughly indicate the number of uniformly spaced collocation points required for Gaussian quadrature in different parts of an integration domain [26]. Often this number is very large for small sub-regions of extreme variation of an integrand, if the integrand is to be adequately sampled. The empirical approach is very useful, but has the following drawbacks:

(i) Using such a large number of collocation points for a small part of an integration region is grossly inefficient.

(ii) The empirical relationship developed for one type of singularity may be invalid for

another. For example, an empirical relationship that works well for the fictitious stress method may not be applicable to the displacement discontinuity method.

These drawbacks are overcome in this thesis through the use of an adaptive integration scheme that automatically samples different sub-regions of an integration domain with required numbers of collocation points. Quadrature in a region is assumed to be sufficiently accurate, if the computed value of an integral in that region falls within a specified percentage of the sum of the values obtained from the subdivision of the same region into two equal sections. This process of subdivision continues until any subdivided region satisfies the accuracy criterion. The adaptive method therefore ensures that integrals are computed with pre-specified accuracy. Schematically, the subdivision of an integrand (shown in Fig. 2.2a) with collocation points, based on the degree of variation of the integrand in different parts of the domain of quadrature, is illustrated in Fig. 2.2b.

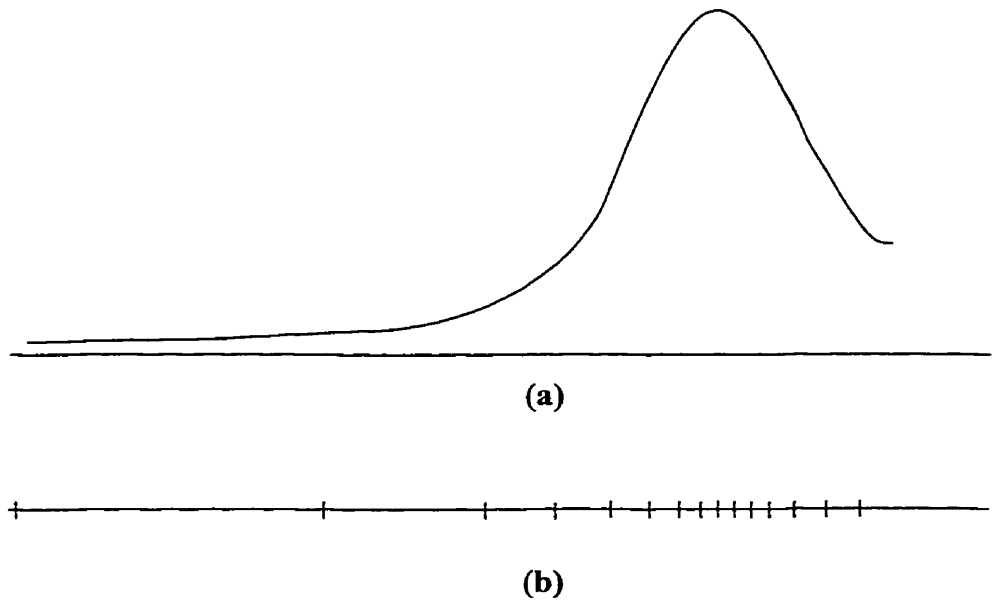

Figure 2.2: Subdivision of side of element

2.6 Mathematical Formulation of Boundary Functions

As stated earlier, the major difficulty associated with the formulation of node-centric elements in the indirect BEM lies in the evaluation of singular integrals. In this section, a brief outline of the mathematical technique, underlying the continuation approach, is discussed. More detailed information on the approach is presented in PAPERS I and II.

Generally, the surface element integrals that appear in BEM formulation are of the form

$$I(q) = \int g(p,q)\, \varphi(p)\, d\Omega\,, \tag{2.1}$$

where Ω is an n-flat finite domain of dimension n, bounded by a piecewise continuous boundary $\partial\Omega$. When n=2, this domain is equivalent to a planar region. g is a Green's function. It is a continuous differentiable function when $p \neq q$, and is infinite when $p = q$. The field point p is a point in the continuum at which field quantities, such as displacements or stresses, due to a source applied at load point q, are calculated. $\varphi(p)$ is an interpolation function. The surface integrals become singular in the limit as the field point p approaches the surface of the integration domain (element).

In the continuation limiting process, the singular integral of eqn. (2.1) is obtained by simply taking the singularity to the surface [27]. An attempt is then made to either integrate the integrand analytically, or to map the integral to one performed on the boundary of the integration domain $\partial\Omega$. When the integral is mapped to the boundary of the integration domain, it is referred to as a continuation integral [27].

We can consider more general forms of integrals arising in the BEM by placing the origin of a local coordinate system at a point $\hat{q} \in \Omega$ (Fig. 2.3). $\hat{q}$, called the proximate singular point (PSP), is the point on the surface of the integration domain closest to the singular point (SP), q. In the local coordinate system, the points p and q can be expressed as $p = (\boldsymbol{X}, \boldsymbol{0})$ and $q = (\boldsymbol{0}, x_{n+1})$, where $\boldsymbol{X}$ is a vector $(x_1, x_2, ..., x_n)$ in the $(n+1)$-dimensional ambient space [28].

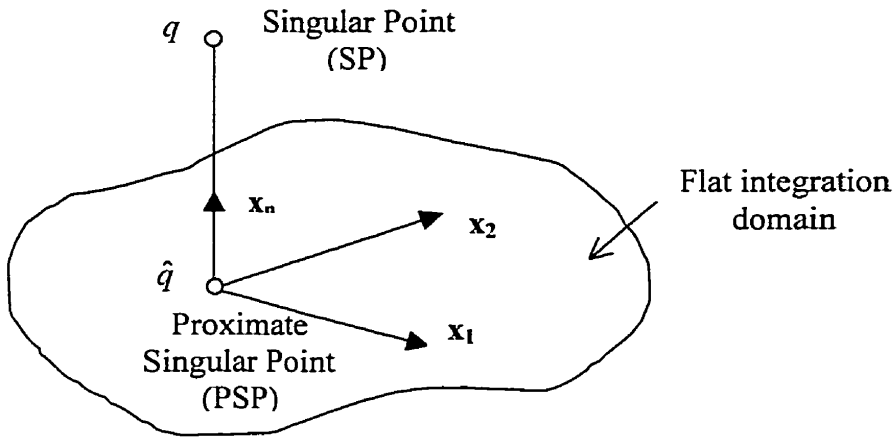

Figure 2.3: Flat integration domain

The integrals encountered in the BEM can be reduced to the following general form

$$I(x_{n+1}) = \int_{\Omega} f_{\beta}(x_1, x_2, ..., x_n, x_{n+1}) d\Omega , \tag{2.2}$$

for any fixed value of x_{n+1}. f_{β} is a homogeneous function of degree β if and only if it satisfies the condition

$$f(\lambda x_1, ..., \lambda x_{n+1}) = \lambda^{\beta} f(x_1, ..., x_{n+1}) , \tag{2.3}$$

where λ is an arbitrary constant, or the Euler's condition

$$\sum x_i \frac{\partial f}{\partial x_i} = \beta f - x_{n+1} \frac{\partial f}{\partial x_{n+1}} \tag{2.4}$$

Although f is homogeneous in the ambient space, it is not homogeneous in the integration domain $x_1,.....,x_{n+1}$. Without loss of generality, it is sufficient to consider the prototypical function f to be of the form

$$f(\boldsymbol{x}, x_{n+1}) = \frac{x_1^{l_1} x_2^{l_2} .....x_n^{l_n} x_{n+1}^{l_{n+1}}}{r^k} \tag{2.5}$$

where the exponents $l_1, l_2 ... l_n, l_{n+1}$, and k are positive integers. The general distance function r is given by the relationship

$$r = (x_1^2 + ... + x_n^2 + x_{n+1}^2)^{\frac{1}{2}} \tag{2.6}$$

When both sides of eqn. (2.4) are integrated on the domain Ω, and Green's theorem is applied to the left-hand side, the continuation formula for $f(\boldsymbol{X}, x_{n+1})$ is obtained in terms of $I(x_{n+1})$ as

$$x_{n+1} \frac{\partial I(x_{n+1})}{\partial x_{n+1}} - \alpha I(x_{n+1}) = -\int f(\boldsymbol{X}, x_{n+1}) \boldsymbol{X} \cdot d\boldsymbol{S}, \tag{2.7}$$

where $d\boldsymbol{S}$ is the directed surface area of the element on the boundary $\partial\Omega$ of the integration domain. α is the degree of singularity, *i.e.* $\alpha = \beta + n$, viz

$$\begin{aligned} \alpha &= l_1 + l_2 + ... + l_{n+1} + d - k \\ &= d - k + \sum_i l_i \end{aligned}$$

where d is the dimension of the integration domain. In two-dimensional Euclidean space, $\boldsymbol{X} \cdot d\boldsymbol{S} = x_1 dx_2 - x_2 dx_1$. Solving equation (2.7) produces the result

$$I(x_{n+1}) = -x_{n+1}^{\alpha} \int_{\eta_o}^{x_{n+1}} \left\{ \frac{1}{\eta^{\alpha+1}} \int_{\partial\Omega} f(\boldsymbol{X},\eta)\boldsymbol{X}\cdot d\boldsymbol{S} \right\} d\eta + \frac{x_{n+1}^{\alpha}}{\eta_o^{\alpha}} I(\eta_o), \tag{2.8}$$

where $I(\eta_o)$ is the initial condition used for integration, corresponding to the initial value of η_o. The value of the integral $I(x_{n+1})$ should be independent of η_o. One way to satisfy this requirement is to choose the initial condition far away from the integration domain. Under such a condition, $\eta_o = \pm\infty$, causing the second term of eqn. (2.8) to vanish for all values of α. $I(x_{n+1})$ can then be computed with regular quadrature. Equation (2.8) can therefore be rearranged to yield

$$I(x_{n+1}) = -x_{n+1}^{\alpha} \int_{\partial\Omega} \left\{ \int_{\eta_0}^{x_{n+1}} \frac{1}{\eta^{\alpha+1}} f(\boldsymbol{X},\eta)\, d\eta \right\} \boldsymbol{X}\cdot d\boldsymbol{S} \tag{2.9}$$

Equation (2.9) suggests the existence of a function F, known as a boundary function, which is represented by the formula

$$F(\boldsymbol{X}, x_{n+1}) = \int \frac{1}{x_{n+1}^{\alpha+1}} f(\boldsymbol{X}, x_{n+1}) dx_{n+1} \tag{2.10}$$

Rosen and Cormack first introduced the boundary function F, in [27], where it was referred to as the *primitive boundary function* (PBF). Note from eqn. (2.10) that the primitive boundary function is independent of the geometry of the integration domain. Using this function, expression (2.2) can be integrated along the boundary as

$$I(x_{n+1}) = x_{n+1}^{\alpha} \int_{\partial\Omega} \{F_{\infty}(\boldsymbol{X}) - F(\boldsymbol{X}, x_{n+1})\} \boldsymbol{X}\cdot d\boldsymbol{S} \tag{2.11}$$

where F_{∞} represents the limit of the primitive boundary function $F(\boldsymbol{X},\eta_o)$ as $\eta_o \to \infty$. For Green's functions that have forms similar to expression (2.5), the function F_{∞} is always bounded and can be obtained analytically.

It is convenient at this stage to introduce an operator $\mathfrak{B}$. When $\mathfrak{B}$ operates on an integrand, it produces the boundary function,

$$\mathfrak{B}(f) = x_3^{\alpha} \int_{x_3}^{\infty} \frac{1}{\eta^{\alpha+1}} f(\boldsymbol{X}, \eta) d\eta . \tag{2.11}$$

Using this operator, the expression (2.2) for evaluating the domain integral becomes

$$I = \int_{\partial\Omega} \mathfrak{B}(f)\, \boldsymbol{X} \cdot d\boldsymbol{S} . \tag{2.12}$$

If $\mathfrak{B}(f)$ is of the form $\mathfrak{B}(f) = \dfrac{f_s(x_1,...,x_n)}{x_{n+1}} + f_R(x_1,...,x_n)$, the first component of the sum represents a divergent part, while the second characterises a regular part. This result demonstrates that the boundary function clearly indicates the degree or nature of divergence of the divergent part.

It has been known in actual physical problems that a property of Green's functions is that the sum of the divergent components of integrals along the boundary of an element equals zero [27]. Because of this phenomenon, the divergent component does not play any role in the solution process for problems of this type, and it is therefore advantageous to retain only the regular part of the integration.

In this thesis, the boundary function approach was developed for node-centric triangular integration domains, for which singular points occupied various positions in relation to flat 2-D triangular element (Fig. 2.4). The conversion of domain integrals to boundary integrals helps satisfy the earlier outlined objectives of developing an efficient integration methodology for the indirect BEM. It provides a unified integration scheme by adopting the same approach for all integrals, regardless of the position of the singular point in relation to the integration domain. The boundary function method is robust

because it is insensitive to the geometry of the integration domain and it is also numerically efficient due to the fact that it reduces the dimension of the quadrature domain by one. By converting integration over a domain to one along a boundary, the number of dimensions is scaled back by one.

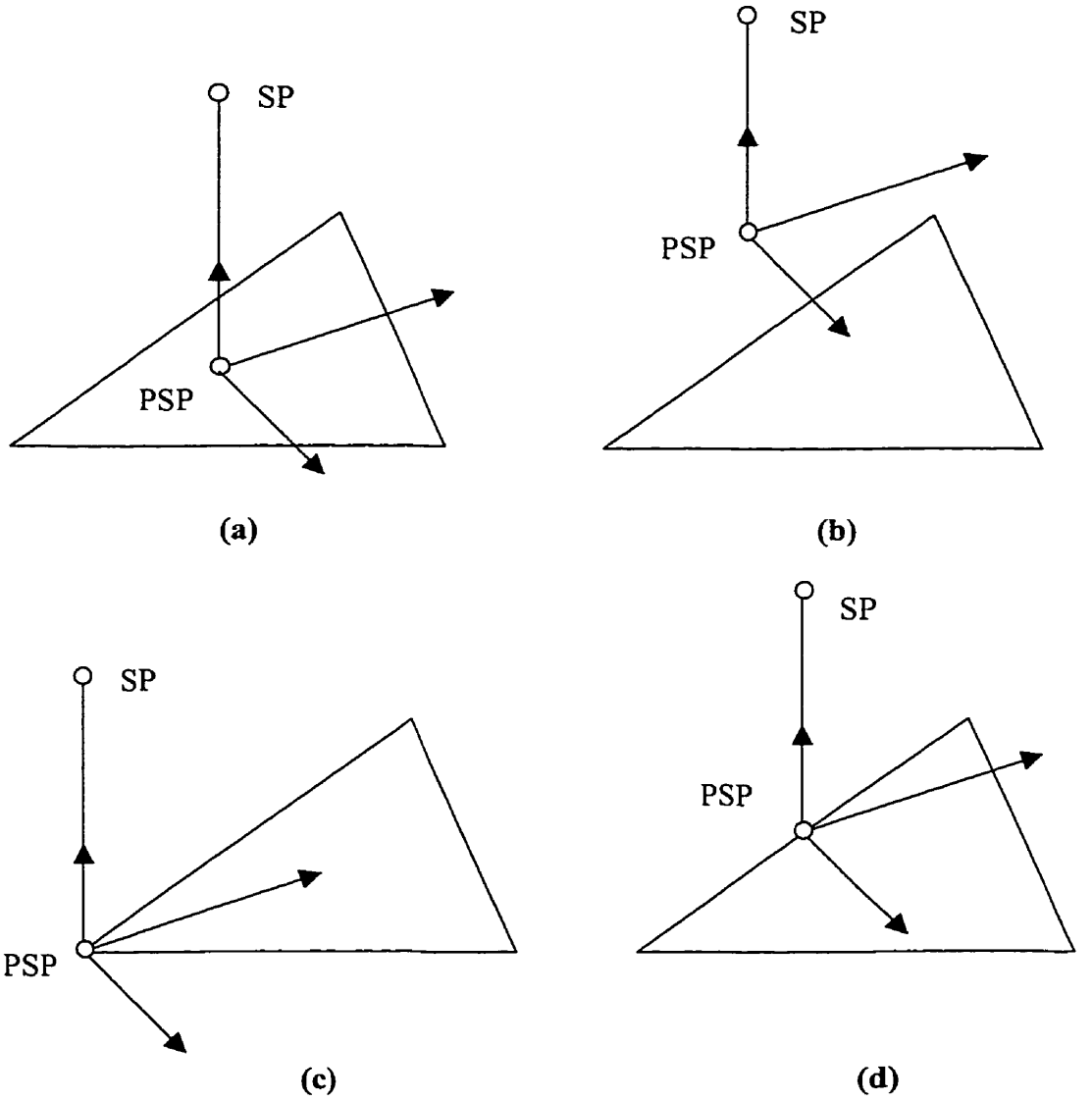

Fig. 2.4 Possible cases of integral domains

A simple example of the conversion of integration from that over a domain to one along a boundary is provided next. Let $g(x_1, x_2, x_3)$ be a Green's function and $\omega(x_1, x_2)$ a

weighting function, both of which are homogeneous in x_1, x_2, x_3. Let it be assumed that the domain Ω lies in the $x_1 - x_2$ plane. Then

$$\int_{\Omega} \omega(x_1, x_2)\, g(x_1, x_2, x_3)\, dV = \int_{\partial\Omega} F(x_1, x_2, x_3)\mathbf{X}.d\mathbf{S} \tag{2.13}$$

The boundary function F for the function ωg is given by the equation

$$F(x_1, x_2, x_3) = x_3^{\alpha} \int_{x_3}^{\infty} \frac{1}{\eta^{\alpha+1}} \omega(x_1, x_2)\, g(x_1, x_2, \eta)\, d\eta \tag{2.14}$$

If the weighting function ω is linear, *i.e.* if the function has the form $\omega(x_1, x_2) = c + ax_1 + bx_2$, it can be separated into two components:

a) $\omega(x_1, x_2) = c$, for which α=-1, and

b) $\omega(x_1, x_2) = ax_1 + bx_2$, for which α=0.

This separation is done, because the degree of homogeneity, α, is different for the constant and linear components. The integration required to produce a boundary function (eqn. (2.14)) can be obtained analytically using standard integrals provided by Dwight [32].

As a concrete example, we shall consider a Green's function that can be expressed as [33]

$$g(x_1, x_2, x_3) = \left[\frac{1}{r^3} + \frac{6x_3^2}{r^5} - \frac{15x_3^2}{r^7} \right]. \tag{2.15}$$

Using the operator $\mathfrak{B}$ on the Green's function, the boundary function can be evaluated as

$$\mathfrak{B}(g(x_1, x_2, x_3)) = \left[\frac{1}{r^3} + \frac{3x_3^2}{r^5} \right]. \tag{2.16}$$

Equation (2.16) represents a conversion to the boundary function using a weighting function of constant variation (the degree of singularity $\alpha = -1$). Similarly, the boundary function using a linear weighting function ($\alpha = 0$) is evaluated to be

$$\mathfrak{B}(g_{333}) = \left[\frac{1}{r^3} + \frac{x_3^2}{r^3\rho^2} + \frac{3x_3^2}{r^5} - \frac{1}{\rho^3}\log\left(\frac{r+\rho}{2H}\right)\right], \tag{2.17}$$

where $\rho = \sqrt{x_1^2 + x_2^2}$ and H is a scale function that is defined as

$$H = \begin{cases} |x_3| & \text{for } x_3 \neq 0 \\ \text{Perpendicular distance from the singular point to the side of the element for } x_3 = 0 \end{cases}.$$

2.7 Summary

The accuracy of BEM results in regions close to boundaries is dependent on the accuracy of the approximations of the boundary conditions of a problem. It is very important therefore to employ techniques that minimise the errors of boundary approximations.

Of the two types of elements available in boundary element methods – discontinuous and continuous elements – continuous elements more accurately model boundary conditions. The node-centric formulation of continuous elements allows the nodes of elements to be chosen such that they exactly coincide with the boundary of a problem. A result of this is that boundary approximations are limited only to the discretization of a boundary into elements. They no longer include errors due to the nodes not being placed on the physical boundary/boundaries of a problem.

For the same number of nodes continuous elements provide a somewhat finer mesh than discontinuous elements. At the extreme nodes of continuous elements, there

are no jumps in computed values of field quantities. It is expected that a continuous variation of field quantities would more accurately model real behaviour than a discontinuous variation.

Despite the relative ease of implementation of the indirect BEM, the node-centric formulation of elements has not found extensive use in the method, owing to the high degree of singularity of the integrals of the indirect BEM at element nodes, making their integration problematic. Also the computation of jump terms at the end nodes of elements in the indirect BEM (nodes that lie on the edges or corners of a boundary) is difficult, due to the meeting of multiple element vertices at such nodes.

Methods for reducing boundary errors at the nodes of elements fall into two main classes- nodal collocation methods and Galerkin techniques. Of the two methods the nodal collocation approach is more attractive, because it exactly satisfies boundary integrals at nodal points, and is due to the lesser number of integrations in the method.

The nodal collocation method also has advantages in speed. However, it was not applied to the indirect BEM in the past, because of the difficulties in evaluating the hyper-singular integrals that occurred at element nodes. In this thesis, an integration technique based on the continuation approach, originally formulated by Vijayakumar and Cormack [25], was used with the nodal collocation method that made it possible to uniformly evaluate all three main types of integrals in the BEM, namely, singular, near-singular and regular integrals.

Because the continuation approach provides an elegant treatment of singular and near-singular integrals, it leads to a unified methodology for evaluating integrals of all kinds. In the continuation approach integrations over the domains of elements are

converted to integrations along the sides (edges) or boundaries of elements. Integration along the edges of elements eliminates the need to use a mix of analytical and numerical methods to compute the different types of integrals thereby providing a uniform way for performing all integrals.

In addition to uniformity, the continuation approach offers robustness and speed. Its computation of integrals is performed efficiently, since the number of collocation points required for integration along the boundary of an integration domain is considerably less than the number required if the collocation points were to be selected over the area of the domain. Although, the continuation approach has existed for a while, until now it had never been applied to the indirect BEM.

Implemented with the continuation approach is an adaptive integration scheme. Adaptive integration overcomes drawbacks of traditional empirical methods for handling the integration of functions that rapidly vary over certain parts of an integration domain and slowly over others. It also makes it possible to evaluate integrals with pre-specified accuracy.

In the next chapter the formulation of node-centric elements for a specific type of indirect boundary element method, the displacement discontinuity method (DDM), is provided.

Chapter 3
Displacement Discontinuity Method (DDM)

3.1 General Scope

For thin slit-like or crack-type openings, such as the excavations commonly encountered in the mining of seams or lenticular orebodies, the distance between opposing surfaces is very small compared to the other dimensions of the openings. As a result the two opposite faces of such excavations practically coincide. The nearness of excavation faces to each other creates serious numerical instabilities for many of the modelling methods available. Such problems can be best solved with a special numerical technique, the displacement discontinuity method (DDM) [34]. The DDM is a boundary element method founded on the analytical solution to the problem of a constant slit-like opening displacement, acting over a line segment of finite size in an infinite elastic domain.

Each surface of an excavation is discretized into elements in a typical BEM. Thus each element lies on only one surface. A single displacement discontinuity element, on the other hand, represents a section of the opposing surfaces of a crack-type opening. Therefore the method is ideal for the analysis of slit-like excavations [35]. This characteristic of the DDM assumes even greater importance in three-dimensional problems. It produces significant economy in the number of elements used for discretizing problem boundaries, which in turn minimizes the effort required of a user during data input.

Technically, the DDM is an indirect BEM. However, unlike other indirect methods, the unknown variables in the DDM represent physically meaningful aspects of a problem. Displacement discontinuities are relative displacements of the opposing surfaces of cracks or slit openings. The displacement discontinuity method has been used to create well-known commercial software packages such as NFOLD [36] and MULSIM [37]. For many years these packages have been widely used for analysis by different institutions and companies in Australia, Canada and the Unites States, because of their practicality for solving mining problems.

Nodes of adjacent elements in the traditional DDM are not shared. As a result of this the number of equations and unknowns for the DDM increases rapidly with increasing number of elements. The situation worsens when higher-order elements are used. Because of this, the commercial packages mentioned above employ only constant DD elements in order to reduce the number of equations, and keep computing times at acceptable levels. Despite the use of constant elements, large numbers of elements are needed for the discretization of regions in which detailed knowledge of stresses (or displacements) is required.

In Chapter 2, it was established that when the end nodes of elements are shared, the number of unknowns in a problem is curtailed, leading to savings in computational time. A general framework for developing such an approach in the indirect BEM was discussed in the same chapter. The current chapter gives an overview of the development a node-centric formulation specifically for the DDM. This new formulation not only preserves the simplicity of the DDM, but also improves the capabilities and efficiency of the DDM in the solution of geomechanics problems. The node-centric formulation of DD

elements ensures inter-element continuity of stresses due to the sharing of nodes, making the new DD element superior to the traditional DD element. Basic examples that outline the capabilities and advantages of the new formulation of the DDM are also presented in the chapter.

3.2 Node-Centric Displacement Discontinuity Element

The three-dimensional displacement discontinuity method is based on the elastic solution for the problem of a displacement discontinuity acting over a finite area in a material domain. For a planar crack with a normal in the x_3 direction (Fig. 3.1), two faces for the crack can be identified - a positive face (or surface) designated as $x_3 = 0^+$, and a negative face $x_3 = 0^-$. When one crosses from one side of the crack to the other, displacements of the faces undergo a jump in value. This jump is known as a displacement discontinuity, D_k, that is mathematically calculated as:

$$D_k = u_k^+ - u_k^-. \tag{3.1}$$

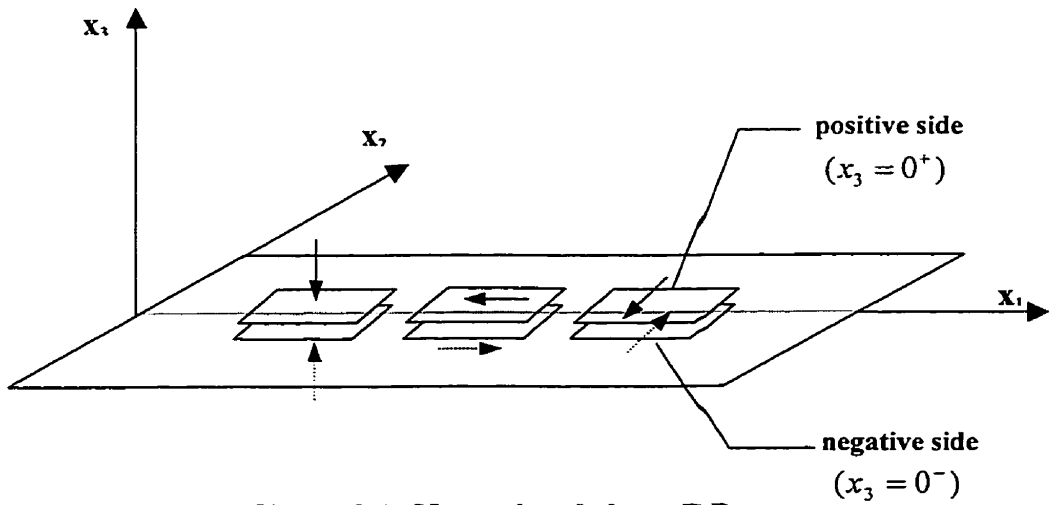

Figure 3.1: Normal and shear DD

The displacement discontinuity of a crack can be resolved into three components along the coordinate axes x_k, k = 1, 2, or 3. These three displacement components are comprised of a normal component (closure) that is perpendicular to the plane of the discontinuity, and two shear components (rides) that lie in the discontinuity plane. They are shown on Fig. 3.1.

We shall let the boundary of a problem be represented with a number of surface patches, s_λ. Three displacement discontinuity density components (one normal density and two shear densities, acting along the directions of local coordinate axes), d_k, can be distributed over the surface patches. Using the principle of superposition, the stresses and displacements at point q in a homogeneous, isotropic, linear elastic material due to the displacement discontinuity densities at point p can be written as

$$\sigma_{ij}(q) = \sum_{\lambda} \int_{s_\lambda} G_{ijk}(p,q) d_k(p) dS(p) \tag{3.2}$$

$$u_i(q) = \sum_{\lambda} \int_{s_\lambda} H_{ik}(p,q) d_k(p) dS(p) \tag{3.3}$$

The Green's functions G_{ijk} and H_{ik} in eqns. (3.2) and (3.3) are defined in PAPER II. The summation is performed over the surface patches, s_λ. If either the stresses σ_{ij}, or displacements u_i, are specified for each s_λ, then eqns. (3.2) and (3.3) can be solved for the unknown DD densities, d_k. In practice, the surface patches s_λ, that form the boundaries, are discretized into planar elements, and a functional form that approximates the variation of d_k over the elements is assumed. For example, in the simplest formulation of the DDM, the density variation over elements is assumed to be constant. As a field point q approaches a point p on the boundary of a problem, eqns. (3.2) and

(3.3) become the standard indirect boundary element equations.

The variation of DD densities over elements can be assumed to be linear in the solution of a problem. This is the basic formulation adopted in this thesis. The nodal values of the displacement discontinuity densities, simply known as displacement discontinuities, of an element are designated as $D_1^{N_j}$, $D_2^{N_j}$ and $D_3^{N_j}$ to denote the two shear, and normal components, respectively. The elements used in discretizing boundaries can have triangular shapes, with nodes placed only at the corners of the elements. In such a case, N_1, N_2 and N_3 represent an element's three nodes. The nodal density values $D_k^{N_j}$ can be defined as the following function of nodal coordinates:

$$D_k^{N_j} = a_0 + a_1 x_1^{N_j} + a_2 x_2^{N_j}, \tag{3.4}$$

where x_1 and x_2 are the coordinates of nodes in the local coordinate system of an element. For a given element, the system of equations for the three components of a nodal DD, supplied by eqn. (3.4), can be rearranged and written in the following matrix form:

$$\begin{bmatrix} a_0 \\ a_1 \\ a_2 \end{bmatrix} = \begin{bmatrix} 1 & x_1^{N_1} & x_2^{N_1} \\ 1 & x_1^{N_2} & x_2^{N_2} \\ 1 & x_1^{N_3} & x_2^{N_3} \end{bmatrix}^{-1} \begin{bmatrix} D_k^{N_1} \\ D_k^{N_2} \\ D_k^{N_3} \end{bmatrix}. \tag{3.5}$$

For three-dimensional problems, generally, if a boundary is represented with p triangular surface elements, the components of stress and displacement induced at a node m, due to the distribution of normal and shear displacement discontinuities D_k at a node n, can be written as:

$$\sigma_{ij}^m = A_{ijk}^{mn} D_k^n \quad , \quad \text{and} \tag{3.6}$$

$$u_i^m = B_{ik}^{mn} D_k^n \quad , \tag{3.7}$$

where the influence coefficient matrices A_{ijk} and B_{ik} are given by

$$A_{ijk}^{mn} = \sum_{e} t_{il} \left(\sum_{side} \alpha_{lpk}^{mn}(e) \right) t_{pj} \tag{3.8}$$

and

$$B_{ik}^{mn} = \sum_{e} t_{il} \left(\sum_{side} \beta_{lk}^{mn}(e) \right) . \tag{3.9}$$

The t_{ij},'s are the coefficients of the direction cosine matrix. Each coefficient, t_{ij}, is defined as the dot product, $X_i \cdot Y_j$, of the two unit vectors X_i and Y_j, of the axes of the local coordinate systems at the field point and load point, respectively. α_{ijk}^{mn} is evaluated as

$$\begin{bmatrix} \alpha_{ijk}^{mN_k}(e) \\ \alpha_{ijk}^{mN_{k+1}}(e) \end{bmatrix} = \frac{1}{x_p^{N_{k+1}} - x_p^{N_k}} \begin{bmatrix} x_p^{N_{k+1}} & -1 \\ -x_p^{N_k} & 1 \end{bmatrix} \begin{bmatrix} \bar{I}_{ijk}^{0}(e) \\ \bar{I}_{ijk}^{1}(e) \end{bmatrix} , \tag{3.10}$$

where $x_p^{N_k}$ and $x_p^{N_{k+1}}$ are the local coordinates of the two nodes of each side of the element (Fig. 3.2).

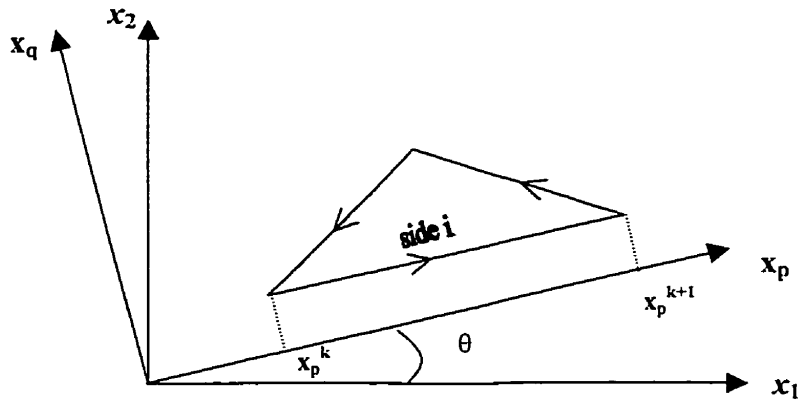

Figure 3.2: Coordinate system used to compute line integrals

$\bar{I}_{ijk}^{0}$ and $\bar{I}_{ijk}^{1}$ are calculated from the formulae:

$$\bar{I}^{0}_{ijk} = \int_{side} \Phi^{0}_{ijk}.(x_p \cos\theta - x_q \sin\theta)dx_p, \text{ and} \tag{3.11}$$

$$\bar{I}^{1}_{ijk} = \int_{side} \Phi^{1}_{ijk}.(x_p \cos\theta - x_q \sin\theta)dx_p, \tag{3.12}$$

through the use of the boundary functions Φ^{0}_{ijk} and Φ^{1}_{ijk} of the continuation approach. These boundary functions can be obtained analytically, as discussed in Chapter 2, and they are presented in Paper II. The integrals of eqns. (3.11) and (3.12) are evaluated with the adaptive integration scheme. θ is the angle measured between the x_1-axis of the element local coordinate system and the side of the element along which integration is performed. β^{mn}_{ik} is evaluated likewise using eqns. (3.11) and (3.12), and replacing the boundary functions Φ's with Γ's.

Eqns. (3.8) and (3.9) represent a system of linear algebraic equations, which after the substitution of appropriate boundary conditions, can be solved for the unknown values of nodal displacement discontinuities D^{n}_{k}. After calculating the displacement discontinuities, stress, as well as displacement, components at any interior points of the domain of a problem can then be computed by substituting values of D^{n}_{k} into eqns (3.6) and (3.7).

3.3 Numerical Implementation

3.3.1 Penny-shaped crack

A standard problem for testing the validity of the results of the three-dimensional DDM is the penny-shaped planar crack [38]. In this thesis, a penny-shaped crack was discretized into 108 elements with 61 nodes. A uniform internal unit pressure was applied

in the crack (Fig. 3.3). The boundary conditions at the nodes on the rim of the crack demanded that DD values be zero at those nodes. This stipulation, together with node-sharing, reduces the number of unknowns in the problem from 3x108 for the conventional constant DDM, to 3x49 for the node-centric formulation.

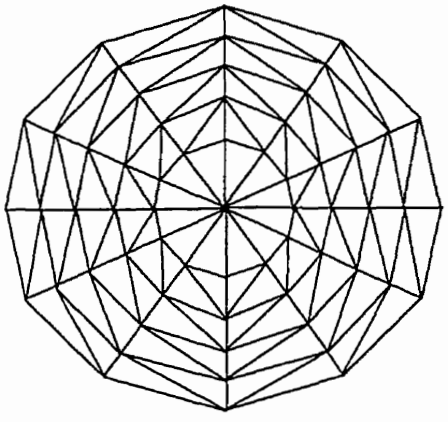

Figure 3.3: Mesh used for the penny-shaped crack problem

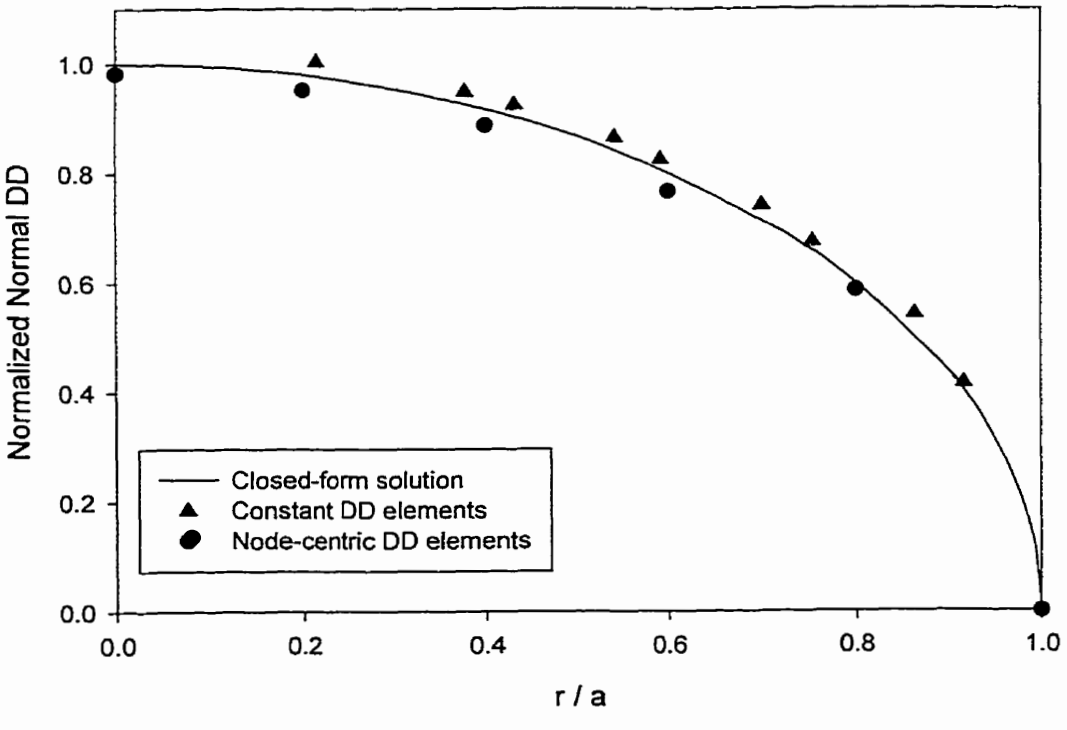

Figure 3.4: Normal displacement variation over the crack boundary

Values of the normal DD components, computed with node-centric elements, were compared with results obtained from the constant DDM and the closed-form solution in Fig. 3.4. The comparison showed that the node-centric method, although using a significantly smaller number of unknowns, produced results comparable to that of the conventional DDM, and that were close to the analytical solution.

3.3.2 Long cylindrical tunnel

Stresses and displacements around a long cylindrical tunnel under far-field in-situ stresses, computed from a numerical technique such as the DDM, can be assessed for accuracy by comparing them with those obtained from the closed-form solution. Stresses and displacements at the central cross-section of the tunnel must be close to the results of Kirsch's analytical solution to the two-dimensional problem of a circular hole subjected to biaxial loading in an infinite elastic medium [3]. A three-dimensional form of this problem can be formulated if the length of the tunnel is chosen to be large in relation to its diameter so that the assumption of plane strain conditions becomes valid.

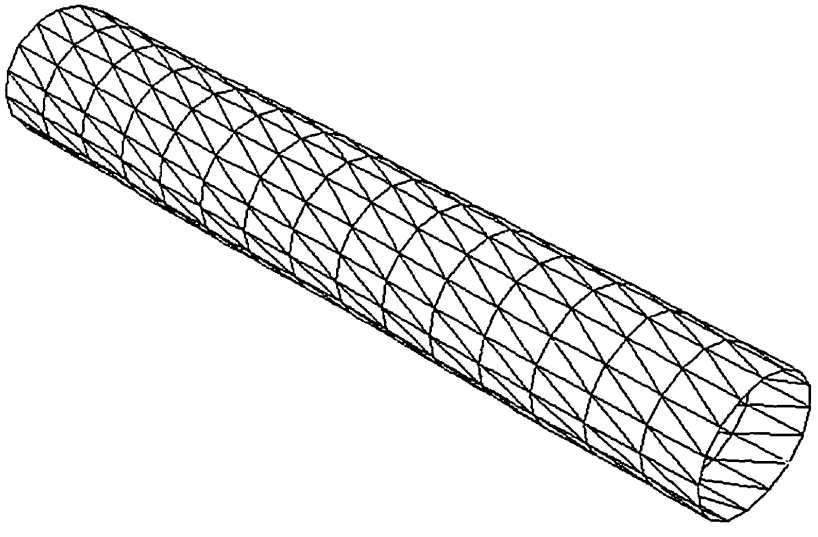

Figure 3.5: Tunnel discretization

Figure 3.5 shows the mesh of node-centric DD elements used for analysing a three-dimensional cylindrical tunnel. The dimensions of the tunnel and the properties of the rock used for the analysis are provided in Table 3.1.

Table 3.1: Details of tunnel model

Dimension	Radius (a) = 0.5 m Length (L) = 8m
Material properties	Young's modulus (E) = 2.5 MPa Poisson's ration (ν) = 0.25
Far-field stress	Vertical in-situ stress (p) = 1.0 MPa horizontal in-situ stress (kp) = 1.0 MPa

The Kirsch solution for radial, tangential and shear stresses around a circular excavation with radius a, subjected to biaxial loading in an infinite elastic medium (Fig. 3.6), is

$$\sigma_{rr} = \frac{P}{2}\left\{(1+k)(1-\beta^2) + (1-k)(1-4\beta^2+3\beta^4)\cos 2\theta\right\}$$

$$\sigma_{\theta\theta} = \frac{P}{2}\left\{(1+k)(1+\beta^2) + (1-k)(1+3\beta^4)\cos 2\theta\right\} \qquad (3.13)$$

$$\sigma_{r\theta} = \frac{P}{2}\left\{(1-k)(1+2\beta^2-3\beta^4)\sin 2\theta\right\},$$

where σ_{rr}, $\sigma_{\theta\theta}$ and $\sigma_{r\theta}$ are the total radial, tangential and shear stresses at the point in the rock mass with polar coordinates (r, θ), and $\beta = \frac{a}{r}$.

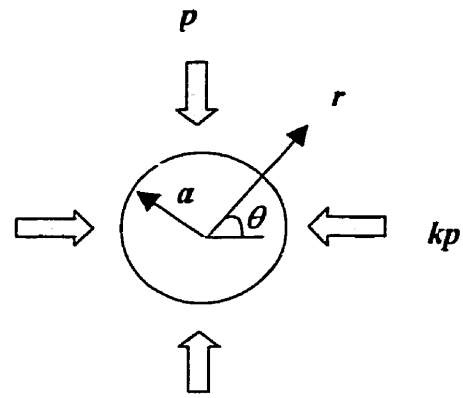

Figure 3.6: Circular excavation

Plots of the variation of radial and tangential stresses with distance, obtained analytically from equations (3.13) and numerically from the node-centric DDM, are shown in Fig. 3.7. It is seen from the plots that the stresses predicted by the node-centric DDM are in very close agreement with those obtained from the Kirsch solution.

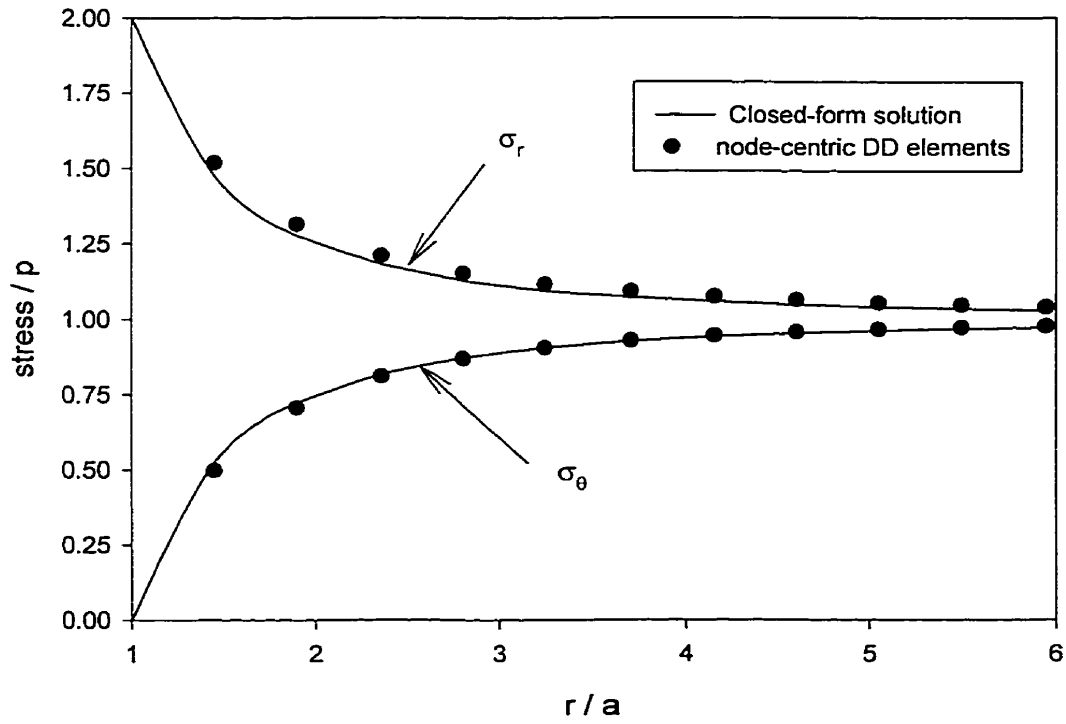

Figure 3.7: Tangential and radial stresses along horizontal line at the central cross-section of cylindrical tunnel

3.3.3 Spherical Excavation

On figure 3.8 is shown a spherical excavation in an infinite elastic medium. The dimensions of this excavation, and the strength and deformational properties of the surrounding rock mass, are summarized in Table 3.2.

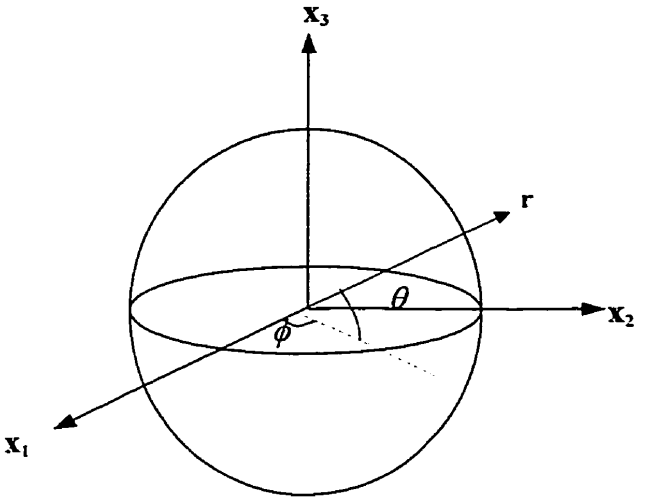

Figure 3.8: Spherical excavation

Table 3.2: Details of spherical cavity model

Dimension	Radius (a) = 1m
Material properties	Young's modulus (E) = 2.5 MPa Poisson's ration (ν) = 0.25
Far-field stress	In-situ field stress (P) = 1.0 MPa

This spherical cavity was subjected to two different loading conditions – a hydrostatic state of stress and a uniaxial stress field. The spherical excavation problem was then solved with the node-centric DD elements.

1. Hydrostatic stress field

This was an excellent test case since the problem has a well-known closed-from solution [39]. The external radial and tangential stresses along the direction of $\theta = 0^\circ$ and $\phi = 90^\circ$ can be determined from the following equations:

$$\sigma_{rr} = P\left[1 - \beta^3\right]$$
$$\sigma_{\theta\theta} = \sigma_{\phi\phi} = P\left[1 + \tfrac{1}{2}\beta^3\right] \tag{3.14}$$

Plots, shown in Fig. 3.9, of these stresses computed with the node-centric DDM and the equations in (3.14) reveal that the results of the numerical method closely match the analytical solution at every point along the direction of radius of the sphere.

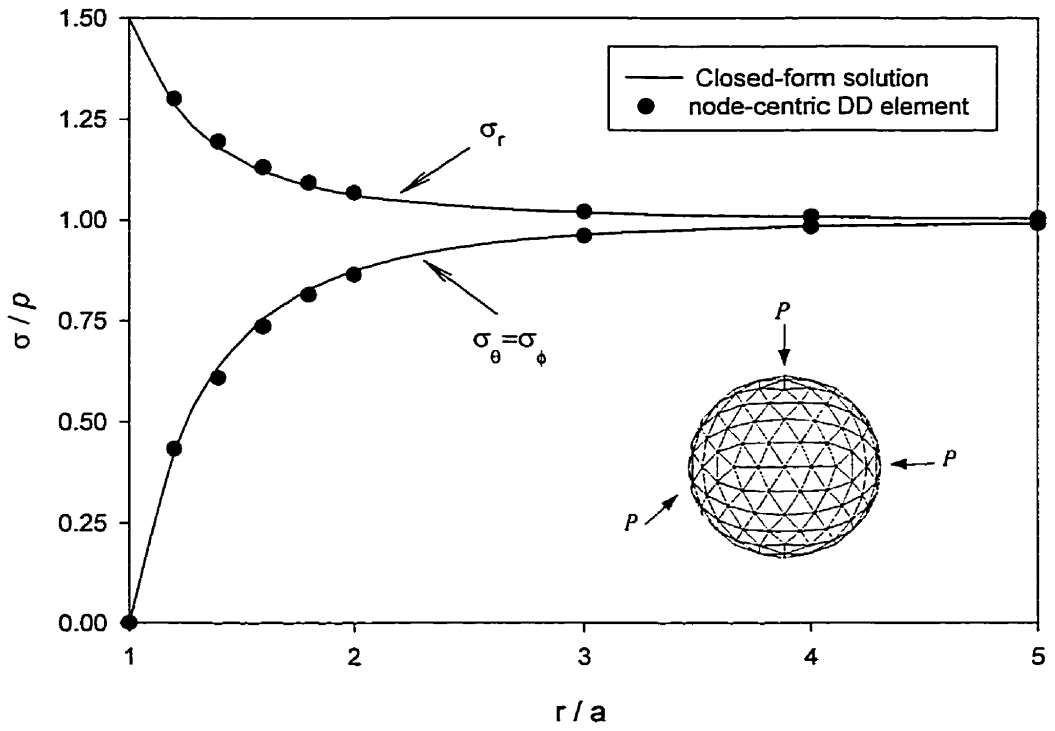

Figure 3.9: The distribution of stresses outside spherical cavity subjected to a hydrostatic pressure at infinity

2. *Uniaxial stress field*

The case of the spherical excavation, subjected to a uniaxial *in-situ* field stress, was considered in order to verify the validity of the node-centric formulation, when used in solving problems in which different normal and shear loads are applied to element nodes. The total stresses (radial and tangential) at any point (r, θ, ϕ) in the elastic medium can be computed from the equations

$$\sigma_{rr} = P\left[\frac{6\beta^3(1-\beta^2)(3\cos^2\theta-2)}{(7-5\nu)} + (1-\beta^3)\sin^2\theta\right]$$

$$\sigma_{\theta\theta} = P\left[\frac{3\beta^3\left[(3+7\beta^2)\cos^2\theta-4(1+\beta^2)\right]}{2(7-5\nu)} + (1-\beta^3)\cos^2\theta + \frac{3\beta^3}{2}\right] \qquad (3.15)$$

$$\sigma_{\phi\phi} = P\left[\frac{3\beta^3\left[(9+5\beta^2)\cos^2\theta-4(1+\beta^2)\right]}{2(7-5\nu)} + \frac{3\beta^3}{2}\cos^2\theta\right]$$

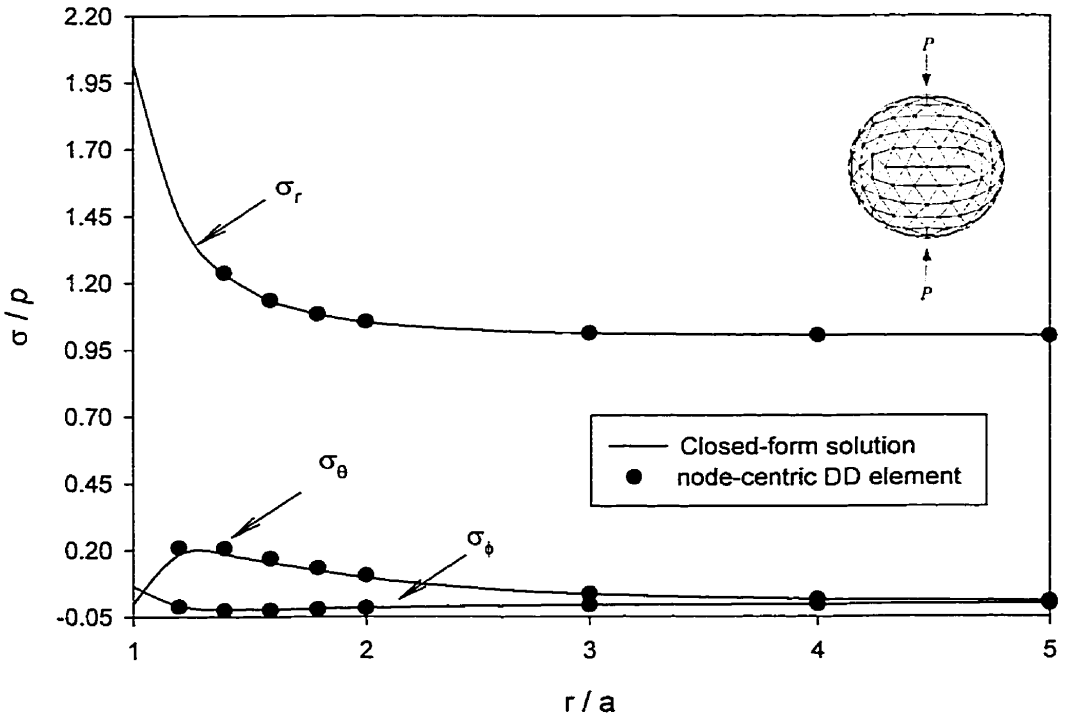

Figure 3.10: The distribution of stresses outside a spherical cavity subjected to a uniaxial stress at infinity

Stresses computed for this problem, using the new DDM, were compared with those from the analytical solution. Plots of the variation of the different stresses with increasing distance from the excavation are shown in Fig. 3.10. Observation of the plots shows that for all stresses the results of the node-centric DDM were in good agreement with the analytical solution.

3.4 Concluding Remarks

In the node-centric framework for three-dimensional problems, the number of nodes used in discretizing boundaries is generally much less than the number of elements (Table 4.3). To obtain the same degree of accuracy of analysis with constant DD elements, the node-centric DDM requires a much smaller number of degrees of freedom. This results in computational efficiency, attested to by the results in Table 4.4. For example, when boundary of the penny-shaped crack described above is discretized with 108 constant DD elements, 324 unknowns result. When 108 node-centric DD elements are used, the number of unknowns drops to only 147. Also, the node-centric approach allows the boundary condition of zero displacement on crack perimeters to be satisfied exactly. The solution of the penny-shaped crack problem exemplifies this attribute of the node-centric formulation.

Because the new formulation assumes a continuous variation of DD values, no anomalous changes of stresses occur in neighborhoods where elements are connected to each other. This facilitates the use of node-centric approach in practical geomechanics problems, where great attention must be paid to regions in which two excavations

intersect (*e.g.* where a tabular orebody intersects another orebody, or a joint intersects with an excavation).

Table 3.3: Comparison of number of nodes for constant, linear and quadratic DDM to node-centric DDM for closed boundary and crack type problems

	Constant	Linear	Quadratic	Node-centric
Closed boundary problem	N_e	$3N_e$	$6N_e$	$\frac{N_e}{2}+2$
Spherical cavity	320	960	1920	162
Crack type problem	N_e	$3N_e$	$6N_e$	$\frac{N_e-N_b}{2}+1$
Penny-shaped crack	108	324	648	49

Where N_e is the number of elements and N_b is the number of nodes on the edge of crack.

Table 3.4: Percentage error for normal DD for penny-shaped crack and spherical cavity problems

		Number of D.O.F	%Error
Pressurized penny-shaped crack	**Constant DD [14]**	3x108	3.278
	Node-centric DD	3x97	0.698
Spherical cavity under hydrostatic pressure	**Constant DD [14]**	3x120	14.32
	Node-centric DD	3x62	14.44

Chapter 4

Analysis of Pillars Using Enhanced Displacement Discontinuity Method

4.1 General Scope

Room and pillar and longwall mining techniques are regularly employed during the mining of flat-lying lenticular orebodies. Pillars, which are ore remnants left standing between the resulting excavations of the aforementioned mining methods, control both the local performance of immediate rock roof and the global response of the host rock medium. Pillars provide local rock support for individual excavations, and control the extents of deformation of rock material in the zone of mining activity. The degree to which the local and near-field stability of mining stopes are maintained to a considerable extent depends on the dimensions of the pillars providing support, their layout, and the strength and deformational properties of both the ore and host rock material.

A comprehensive understanding of the behaviour of pillars, and the ability to predict this behaviour are very important for the economic and safe mining of ore. From the economic point of view, it is desirable that the least possible amount of ore be committed to support. On the other hand, the commitment of greater amounts of ore to support is preferable from the perspective of safety. For an effective solution between the competing factors to be reached, some failure of peripheral pillar material in practical mining is permitted [1].

Stress states in pillars, and consequently pillar behaviour, are complicated. For example, in the case of the simplest loading of a pillar, when it is compressed uniaxially,

the stress state in the pillar is triaxial. The stress state cannot only be triaxial, but it can also be non-homogeneous. This is due to the interaction between the ends of the pillar and the surrounding host rock mass. The geometry of orebodies and other factors often combine to produce irregular mine layouts that cannot be accurately analysed with simple or analytical methods. Numerical modelling techniques are best suited for solving problems of such degrees of complexity. The computational tool most appropriate for the analysis of the slit-type excavations encountered in the mining of lenticular orebodies is the displacement discontinuity method (DDM) [40], described in the previous chapter.

4.1.1 The traditional DDM for stress mine analysis

During mining activity in a stope, stresses are redistributed around the excavation and in the pillars supporting the excavation. When the stresses in the pillars are less than the strength of the orebody material, the pillars behave elastically. One of the principal aims of such an analysis is to determine the load-bearing capacities of pillars. For analysis of pillars in this category, elastic analysis such as that offered by the traditional DDM is adequate. The formulation of displacement discontinuity elements for pillars (unmined zones of orebodies) differs from that for elements in mined regions. To model the behaviour of material in pillars, springs that respond to the normal and shear stresses are included in the formulation of DD elements used in representing pillar supports. By formulating DDs for different orebody zones it has been possible to solve a number of practical mining problems.

Useful as the conventional DD formulation for unmined regions is, however, it has a major shortcoming. For orebodies that extend over large areas or that have low in

situ strength, pillars necessarily have to be designed to undergo plastic deformations, unless exceedingly large amounts of ore are to be used to provide support. The traditional DDM for unmined material, however, cannot appropriately model plastic or yielding pillar behaviour without considerable changes being made to its formulation, or implementation.

An important component for modelling plastic material behaviour in pillars, lateral confinement, is absent from the formulation of the conventional DD element for unmined material. Plastic material behaviour involves post-peak material behaviour. The determination of peak loads, post failure strength and the plastic behaviour of material all require knowledge of the complete stress tensor at a point in the material. This includes the lateral confining stresses omitted from the conventional DDM.

The degree of confinement in a pillar influences its strength. Irrespective of the shape of a pillar, it typically has a confined core [41, 42] and the bearing capacity of the pillar increases with increasing radius of this confined core. The higher the confining stresses in the pillar are, the higher are both the peak and residual strengths of its core. Because of this phenomenon, any mathematical formulation for solving pillar problems that neglects confinement in the analysis, is expected to introduce significant error in the calculated values of displacements and stresses in pillars.

4.1.2 Conventional methods for improving DDM for the design of yielding pillars

In recognition of the inadequacies of the conventional DDM, in its practical application to mining problems *ad hoc* approaches are used to account for confinement. One such procedure acknowledges the presence of confinement in unmined zones

through the use of a family of stress strain curves. After discretization of pillars, elements are assigned stress-strain curves based on their locations in pillars. Those close to pillar centres or cores are assigned the highest strength curves, while the ones adjacent to pillar surfaces have the lowest curves. Intermediate elements are assigned intermediate curves. This was the approach implemented in the commercial software package, MULSIM [18].

The *ad hoc* approaches, however, have some disadvantages. The procedure described above, for example, is tedious and requires considerable experience in order to determine the appropriate stress-strain curves to assign to elements in a pillar, making the technique quite subjective. The approach used in MULSIM can be used for pillar geometries of varying complexity. However, even slight complications of pillar geometries, make the technique difficult to use.

4.2 The Enhanced Displacement Discontinuity Method (EDDM)

In this thesis an enhanced displacement discontinuity method (EDDM) that explicitly and objectively accounts for the effects of confinement is proposed. This enhancement is achieved through the addition of a displacement discontinuity singularity perpendicular to the normal DD, to the original formulation of DDs. With the addition of this new DD, all stresses - normal, shear and confining stresses - are now accounted for in the modelling of unmined material. The newly created DD elements can accommodate general constitutive relationships, ranging from elastic models to general plasticity formulations, in the representation of pillar material behaviour, because of the inclusion of confining stress.

An additional advantage of the EDDM is that it accounts for confinement in a manner more general than those advocated by *ad hoc* approaches such as the technique used in MULSIM. Instead of using a discrete set of strength curves to model the effects of confinement, the EDDM allows strengths at different locations in a material to be calculated as functions of the stress states at the locations. It therefore offers more than the mere automation of the procedure advocated in MULSIM (automation of the process translates into considerable timesaving for geomechanical mine design) by also modelling confinement more realistically. A discussion of the advantages of the EDDM and its full development is provided in Paper III. However the essentials of the approach are discussed next.

4.2.1 Fundamentals of the EDDM

The original formulation of the displacement discontinuity method (DDM) combined the idea of modelling cracks as distributions of dislocations with the method of integral equations [43, 44]. It assumed a constant distribution of dislocations in modelling crack problems.

Confinement can be incorporated into the DDM by deriving DDs starting from the basic definition of discontinuities as singularities created by strain nuclei, which are volumetric strain densities in three-dimensional problems, and surface strain densities for two-dimensional problems. There are two fundamental types of nuclei of strain, d^* - shear and normal strain nuclei. These strain nuclei can be distributed such that the necessary boundary conditions in crack problems are satisfied [43].

4.2.2 Conceptual framework

A displacement discontinuity, as originally defined, is the relative movement between the two surfaces of a crack [40]. This definition of a displacement discontinuity can be generalized to cover the relative movement between two points on a crack. Because the relative movement of opposing points on the surfaces of a crack is uniform along the length of the crack, it becomes possible to define the displacement discontinuity as the relative movement between surfaces. For the traditional displacement discontinuity element (Fig. 4.1a), the shear DD is calculated as $D_1 = u_1^+ - u_1^-$, while the DD in the normal direction is defined as $D_2 = u_2^+ - u_2^-$.

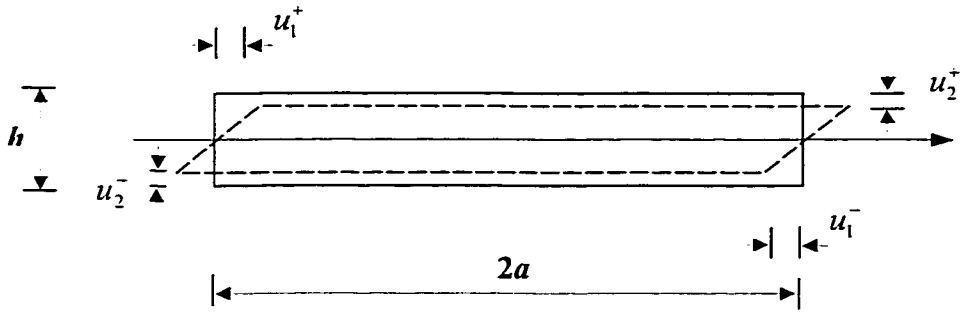

(a) Traditional DD element

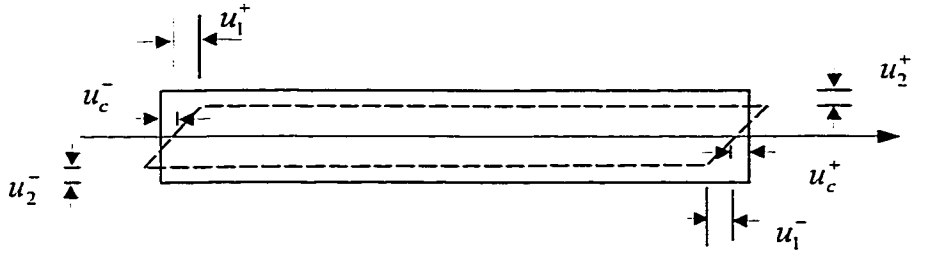

(b) New DD element

Figure 4.1: Definition of displacement discontinuity

By examining the generalised definition of a DD, a third DD, which shall be named the lateral or confinement DD, D_c, can be defined for an element. It is the relative

movement between the ends of a DD element as shown on Fig. 4.1b, and is defined by the relationship $D_c = u_c^+ - u_c^-$.

A strain nucleus d^* is the displacement discontinuity per unit volume in a continuum [45]. The cumulative or total displacement discontinuity, Ω, in a unit volume can be kept constant while the height of the volume is collapsed to zero. This can be written mathematically as $\Omega = \int d^* dV = \int d\, dA$, where d is a new quantity, which shall be termed the displacement discontinuity per unit area, or surface displacement discontinuity density.

When a two-dimensional element of height h and length $2a$ in a homogeneous, linear elastic material is subjected to normal strain nuclei d_2^*, distributed throughout the element, stresses are induced in the medium. The stresses induced at a point q, sufficiently far from the element, by the distribution of strain nuclei can be (closely) replicated by replacing the element with a displacement discontinuity density, d, acting along the centreline of the element. (It is only when q is sufficiently far from the element that the stresses induced by strain nuclei distributed throughout the element will be well approximated by those induced by a displacement discontinuity density acting at the centreline of the element.)

Stresses induced by the strain nuclei distribution d_2^* can be determined using the following integral equation:

$$\sigma(q) = \int_{-h/2}^{+h/2} g(p,q) \cdot d^*(p)\, dx_2, \tag{4.1}$$

where g is a Green's function, and p is a point in the domain of the distribution of strain nuclei. Since the Green's function is continuous in the domain of integration

$(-h/2, h/2)$, we can use the mean-value theorem to evaluate equation (4.1) as

$$\sigma(q) = g(p_o, q) \cdot d_2^*(p_o) h, \tag{4.2}$$

where p_o is the point between $-h/2$ and $h/2$ at which the integrand takes on its average value. p_o can be approximated to be located at the mid-height (centreline) of the element in order to simplify computations. From this point forth, p_o shall be simply referred to as p.

Equivalent stresses at q can be induced by a displacement discontinuity density d placed along the centre line of the element. These stresses can be evaluated from the formula:

$$\sigma(q) = g(p, q) \cdot d_2(p). \tag{4.3}$$

Equating (4.2) to (4.3), the strain nucleus distribution can be expressed in terms of the displacement discontinuity density as:

$$d_2^*(p) = d_2(p)/h \tag{4.4}$$

When the displacement discontinuity density d has a constant variation in the x_1-direction, it becomes equal to a displacement discontinuity D acting at the centre of the element (see further explanation in the next section).

Similar to the above development of the normal DD, a shear displacement discontinuity, D_1, can be formulated by replacing the normal strain nuclei with nuclei that produce shear displacements in the element.

We shall now consider another distribution of strain nuclei d_c^* that act on the element. We shall label these nuclei as confinement strain nuclei. This new distribution takes care of the effect of confinement in the element and produces lateral strain within

the element. Analogous to the case of normal strain nuclei d_2^*, a lateral (or confinement) displacement discontinuity density d_c can be obtained from the confinement strain nuclei d_c^*. They are related through the equation

$$d_c^*(p) = d_c(p)/h \tag{4.5}$$

Assuming a constant distribution of lateral displacement discontinuity density in the x_1-direction, the total lateral displacement discontinuity in the element can be evaluated as

$$D_c(p) = \int_{-a}^{+a} d_c^*(p)\,dx_1 = d_c(p)\frac{2a}{h}. \tag{4.6}$$

Expression (4.6) defines the lateral (confinement) displacement discontinuity. This new DD will be employed in the development of the enhanced DD element, which will be presented in the next section.

4.2.3 Mathematical formulation

As mentioned earlier, distributions of shear and normal strain nuclei throughout an element of height h and length $2a$ located at a point p in a homogenous, linear elastic material, induce stresses in the continuum. The components of the stress tensor, σ_{ij}, and the displacements, u_i, that arise at a point q in the continuum due to the strain nuclei can be determined from the following equations:

$$\sigma_{ij}(q) = \int_{-a}^{+a}\int_{-h/2}^{+h/2} g_{ijk}^*(p,q)d_k^*(p)\varphi_m(x_2)\,dx_2dx_1\,, \tag{4.7}$$

$$u_i(q) = \int_{-a}^{+a}\int_{-h/2}^{+h/2} h_{ik}^*(p,q)d_k^*(p)\varphi_m(x_2)\,dx_2dx_1\,, \tag{4.8}$$

where the repeated indices represent the usual summation convention. For two-dimensional problems $i, j, k = 1, 2$. g^*_{ijk} and h^*_{ik} are normal and shear influence functions for stresses and displacements, respectively, due to the strain density at p. φ_m is an interpolation function. It can range from the simple square function, φ_0, to the Dirac delta function, φ_n (or δ) (Fig. 4.2).

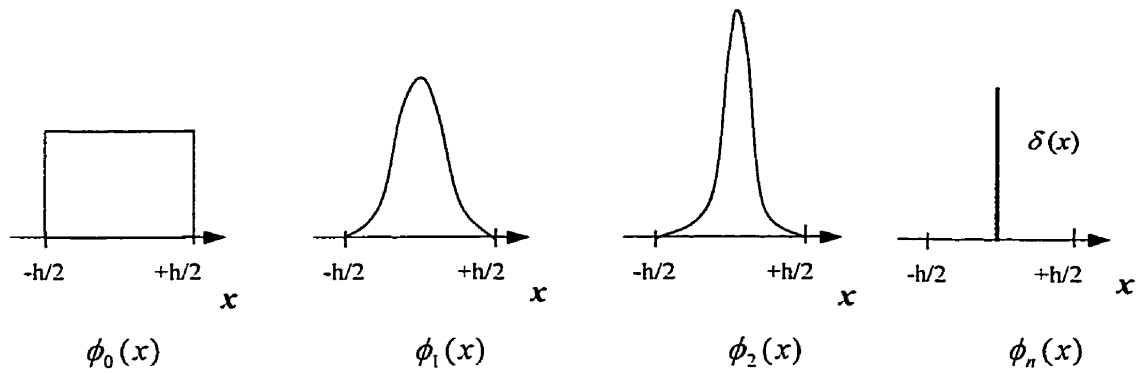

Figure 4.2: Interpolation functions

We shall select the Dirac delta function for the problem at hand, *i.e.* $\varphi_m = \delta$, and shall also look to simplify the resulting expression $\int_{-h/2}^{+h/2} g^*_{ijk}(p,q) d^*_k(p)\, \delta(x_2)\, dx_2$ in equation (4.7). The Dirac delta function has an important property that for two functions $f(t)$ and $\varphi(t)$, both continuous at the origin, the following relationship holds [19]

$$\int_{-\infty}^{+\infty} [f(t)\, \varphi(t)]\, \delta(t)\, dt = f(0)\varphi(0) \tag{4.9}$$

Using the well-known property of the Dirac function: $\int_{-\infty}^{+\infty} f(t)\, \delta(t)\, dt = f(0)$, equation (4.9) can be written as:

$$\int_{-\infty}^{+\infty}[f(t)\ \varphi(t)]\ \delta(t)\ dt = \int_{-\infty}^{\infty} f(t)\ \delta(t)\ dt\ \int_{-\infty}^{\infty}\varphi(t)\ \delta(t)\ dt\,. \qquad (4.10)$$

The above property, applied to the expression we are trying to simplify, leads to the following result:

$$\int_{-h/2}^{+h/2} g_{ijk}^{\bullet}(p,q)d_k^{\bullet}(p)\,\delta(x_2)\,dx_2 = \int_{-h/2}^{+h/2} g_{ijk}^{\bullet}(p,q)\,\delta(x_2)\,dx_2 \int_{-h/2}^{+h/2} d_k^{\bullet}(p)\,\delta(x_2)\,dx_2\,. \qquad (4.11)$$

By letting

$$\int_{-h/2}^{+h/2} d_k^{\bullet}(p)\,\delta(x_2)\,dx_2 = d_k(p)\ \text{, and}\quad \int_{-h/2}^{+h/2} g_{ijk}^{\bullet}\ (p,q)\delta(x_2)\,dx_2 = g_{ijk}(p,q)\,, \qquad (4.12)$$

equation (4.11) can be reduced to the form:

$$\int_{-h/2}^{+h/2} g_{ijk}^{\bullet}(p,q)d_k^{\bullet}(p)\,\delta(x_2)\,dx_2 = g_{ijk}(p,q)\,d_k(p)\,. \qquad (4.13)$$

d_k is the displacement discontinuity density (where d_1 is the ride or shear DD density, and d_2 is the closure or normal DD density). Similar operations can be performed to simplify the corresponding expression in the equation for computing displacements.

These mathematical operations lead to the important result that for two-dimensional problems, the stresses and displacements in equations (4.7) and (4.8) can be calculated as:

$$\sigma_{ij}(q) = \int_{-a}^{+a} g_{ijk}(p,q)d_k(p)\,dx_1 \qquad (4.14)$$

$$u_i(q) = \int_{-a}^{+a} h_{ik}(p,q)d_k(p)dx_1\,. \qquad (4.15)$$

g_{ijk} and h_{ik} are the normal and shear influence functions for stresses and displacements, respectively, due to the displacement discontinuity density d_k at the point p. These

influence functions are given in [33]. The equations (4.14) and (4.15) constitute the formulation of the classical displacement discontinuity method.

We shall now consider the case of a crack divided into N discrete line segments or elements. Acting over each of these elements is a DD density. Each element is defined by nodes at which displacement discontinuities (DDs) can be evaluated. By multiplying values of the nodal DDs with coefficients of an interpolation function, the DD density variation over the length of the crack can be approximated [7]. The approximation of the DD density at a point p along the crack, coincident with the nodes of the elements, is represented by the expression:

$$d_k(p) = \sum_e \Phi_e(p)\, D_k^e, \quad k = 1, 2. \tag{4.16}$$

Φ is an interpolation function identical to the shape functions of elements [7], which is evaluated at the nodes e. Substituting eqn. (4.16) into eqns. (4.14) and (4.15) we obtain the following equations:

$$\sigma_{ij}(q) = \sum_e \int_a g_{ijk}(p,q)\Phi_e(p)D_k^e\, dx_1 \tag{4.14}$$

$$u_i(q) = \sum_e \int_a h_{ik}(p,q)\Phi_e(p)D_k^e\, dx_1 \tag{4.15}$$

If we assume a constant variation of the displacement discontinuity over each element, $\Phi_e(p)$ at node p is equal to unity and zero everywhere else, and eqns. (4.17) and (4.18) become:

$$\sigma_{ij}(q) = \sum_e D_k^e \int_a g_{ijk}(p,q)\, dx_1 \tag{4.16}$$

$$u_i(q) = \sum_e D_k^e \int_a h_{ik}(p,q)\, dx_1\,, \tag{4.17}$$

In this case the total number of nodes is equal to the number of elements N. Equations (4.16) and (4.17) form the classical formulation of the constant DDM.

The formulation of the enhanced displacement discontinuity (EDD) element shall begin with strain densities. Revisiting the problem of shear and normal strain nuclei acting at a point in a material, let an additional nucleus, d_c^*, orthogonal to the normal strain nucleus be included in the problem. Other than direction, this new strain nucleus behaves similarly to the normal strain density. The solution of the new problem differs from the original only by the addition of an extra term to each of the equations (4.9) and (4.10), that accounts for the influence of the newly introduced strain density.

A new displacement discontinuity, D_c, which is perpendicular to the normal DD, can be formed from the new strain nucleus. Relying on the same approach used in the formulation of the classical DDM, the density d_c of this new lateral or confinement displacement discontinuity can be determined from the additional strain nucleus d_c^* using the relationship

$$d_c(p) = \int_{-h/2}^{+h/2} d_c^*(p)\,\delta(x_2)\,dx_2 . \tag{4.18}$$

For discretized problems, the DD density at a point p along a crack can be approximated by nodal DD values through interpolation functions and the equation:

$$d_c(p) = \sum_e \Phi_e(p)\, D_c^e, . \tag{4.19}$$

The stresses and displacements induced at an arbitrary point q in an infinite, homogeneous, linear elastic domain with the application of a shear, normal, and lateral constant DD can be written as:

$$\sigma_{ij}(q) = \sum_e D_k^e \int_a g_{ijk}(p,q)\, dx_1 + \sum_e D_c^e \int_a v_{ij}(p,q)\, dx_1 \qquad (4.20)$$

$$u_i(q) = \sum_e D_k^e \int_a h_{ik}(p,q)\, dx_1 + \sum_e D_c^e \int_a w_i(p,q)\, dx_1 \,. \qquad (4.21)$$

v_{ij} and w_i are the confinement displacement discontinuity influence functions for stresses and displacements, respectively. The definitions of the influence functions are presented in Paper III. Equation (4.20) and (4.21) represent the enhanced DD element.

4.2.4 System of equations for EDDM

The enhanced DD element can be applied to the problem of determining the total stresses and mining-induced displacements in the room-and-pillar or longwall mining of lenticular orebodies. As stated earlier, such mining involves slit-type excavations. It is necessary to identify the appropriate boundary conditions specific for problems of the type described above.

As a first step in solving the problem of mining lenticular orebodies employing room-and-pillar or longwall techniques, discrete EDD elements are placed along the centre lines of the excavations, pillars and panels. The next step is to determine values of normal, shear and confinement DDs that produce total stress and displacement components consistent with the boundary conditions of the problem. In general, if the problem involves boundaries that are represented by N elements, M of which are unmined ($M<N$), induced stresses σ_{ij}^p and displacements u_i^p at element p due to the distribution of normal, shear and confinement DDs at element q can be computed as

$$\sigma_{ij}^p = A_{ijk}^{pq} D_k^q + \delta_{ik} K_{jk}^{pq} D_c^q \qquad (4.22)$$

$$u_i^p = B_{ik}^{pq} D_k^q + L_i^{pq} D_c^q \ , \tag{4.23}$$

where $i, j, k = 1, 2$ and δ_{ij} is Kronecker's delta. The influence coefficients A_{ijk}^{pq} are obtained from the expression

$$A_{ijk}^{pq} = t_{il} G_{lmk}^{pq} t_{mj} \ , \tag{4.24}$$

where G_{lmk}^{pq} is the integral in the element local coordinate system of $g_{lmk}(p,q)$ in equation (4.19), and t_{il} is the rotation matrix. The other coefficients K_{jk}^{pq}, B_{ik}^{pq} and L_i^{pq} of equations (4.21) and (4.22) are determined in similar fashion through the integration and transformation of $v_{ij}(p,q)$, $h_{ik}(p,q)$, and $w_i(p,q)$ in equations (4.20) and (4.21), respectively. The system of linear algebraic equations given by equations (4.22) and (4.23) can be solved for the unknown displacement discontinuities D_k^p and D_c^p, after substitution into the equations of the appropriate boundary conditions.

In underground excavation problems, it is convenient to separate total stresses σ_{ij} into two stress components - initial stresses $(\sigma_{ij})_o$ and induced stresses due to excavation (or simply induced stresses) $(\sigma_{ij})'$. The separation can be expressed mathematically as:

$$\sigma_{ij} = (\sigma_{ij})_o + (\sigma_{ij})' . \tag{4.25}$$

Crouch and Starfield [40] introduced mining-specific boundary conditions and material relationships that accounted for the differences in the boundary conditions of mined and unmined orebody zones into the DDM. These boundary conditions can be used in the solution of problems with the EDDM. There is however one principal difference. Because of the presence of a third DD, the confinement DD (D_c) in the EDDM, an additional equation and condition are needed to make the system of equations

assembled for the EDDM fully determinate. This extra equation is supplied by the constitutive relationship for seam material in unmined zones.

Boundary conditions and system of equations for elements in mined zones

In the mined portions of a seam or orebody, if there is no contact between the roof and the floor of excavations. Crouch and Starfield defined the boundary conditions[1] for the roof and floor to be:

$$\sigma_{22} = -(\sigma_{22})_o \tag{4.26}$$

$$\sigma_{12} = -(\sigma_{12})_o, \tag{4.27}$$

where $(\sigma_{22})_o$ and $(\sigma_{12})_o$ are the initial normal stress and shear stress, respectively. These same boundary conditions are applied to EDD elements in mined zones. It is important to mention here that the lateral confinement of EDD elements in these zones is zero, since those elements have no material. When these boundary conditions are inserted into equations (4.20), the resulting system of equation is:

$$-(\sigma_{22}^p)_o = A_{222}^{pq} D_2^q + A_{221}^{pq} D_1^q \tag{4.28}$$

$$-(\sigma_{12}^p)_o = A_{122}^{pq} D_2^q + A_{121}^{pq} D_1^q . \tag{4.29}$$

$$D_c^p = 0 \tag{4.30}$$

Boundary conditions and system of equations for elements in unmined zones

For elements in unmined zones, the EDDM accounts for the effect of confinement with the introduction of the confinement displacement discontinuity, D_c (Fig. 4.3).

---

[1] σ_{12} and σ_{22} in equations (4.26) and (4.27) are equivalent to the stresses denoted in [40] as σ_s and σ_n.

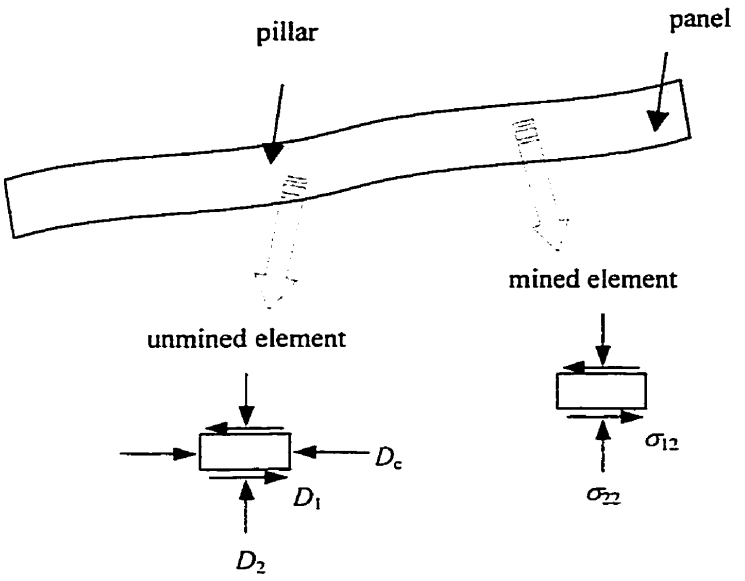

Figure 4.3: Boundary conditions for mined and unmined elements in a seam

If it is assumed that the seam material is homogeneous, isotropic, and linearly elastic, its constitutive relationship connecting stresses, σ_{ij}, and strains, ε_{ij}, can be written as:

$$\sigma_{ij} = \lambda_s \, \delta_{ij} \, \varepsilon_{kk} + 2G_s \, \varepsilon_{ij} \ , \tag{4.31}$$

where λ is Lame's constant defined by the relationship:

$$\lambda_s = \frac{2\nu}{(1-2\nu)} G_s \ . \tag{4.32}$$

Let strain nuclei acting on thin strips of material with height equal to element height h_s, be distributed along the length of a crack [43]. The strain nuclei, d_c^*, d_1^* and d_2^*, discussed earlier in the development of the EDD element (see section 4.2.2), can be defined as

$$d_c^* = \varepsilon_{11} = \frac{\partial u_1}{\partial x_1} \tag{4.33}$$

$$d_2^* = \varepsilon_{22} = \frac{\partial u_2}{\partial x_2} \tag{4.34}$$

$$d_1^* = \varepsilon_{12} = \frac{1}{2}\left(\frac{\partial u_1}{\partial x_2} + \frac{\partial u_2}{\partial x_1}\right) \tag{4.35}$$

where ε_{11}, ε_{22}, and ε_{12} are the lateral, normal and shear strain, respectively. The strain nuclei distributions ε_{12} and ε_{22} corresponding to the displacement discontinuity densities d_1 and d_2 for an element of finite height h_s, as shown previously in eqns. (4.2) and (4.4), can be expressed as

$$\varepsilon_{12} = d_1^* = d_1 / h_s \tag{4.36}$$

$$\varepsilon_{22} = d_2^* = d_2 / h_s \tag{4.37}$$

The lateral strain in the element, ε_{11}, due to the lateral displacement discontinuity density can be defined as the total lateral deformation D_c over the length of the element $2a$ and thus can be represented as

$$\varepsilon_{11} = \frac{D_c}{2a} = \frac{1}{2a}\left(d_c \frac{2a}{h_s}\right) = \frac{d_c}{h_s}. \tag{4.38}$$

Subsequently, the following relationship holds true for ε_{11}:

$$\varepsilon_{11} = d_c^* = d_c / h_s. \tag{4.39}$$

When the variation of the displacement discontinuity density over the length of an element is considered to be constant, the values of d_k and d_c at a node equal D_k and D_c, respectively. Therefore, by replacing the strains in the constitutive relationship (4.31) with the quantities $\frac{D_k}{h_s}$ and $\frac{D_c}{h_s}$, the normal, lateral and shear stresses induced on an element in an unmined zone through the application of DDs are determined to be:

$$(\sigma_{22})^{\cdot} = \frac{(\lambda_s + 2G_s)}{h_s} D_2 + \frac{2G_s}{h_s} D_c \tag{4.40}$$

$$(\sigma_{11})^{\cdot} = \frac{(\lambda_s + 2G_s)}{h_s} D_c + \frac{2G_s}{h_s} D_2 \tag{4.41}$$

$$(\sigma_{12})^{\cdot} = \frac{G_s}{h_s} D_1 \tag{4.42}$$

The use of the constitutive relationship for the seam material has provided the additional equation needed to make the system of assembled equations fully determinate. Observation of equations (4.40) and (4.42) shows that only the confinement and the normal discontinuities are coupled. This is consistent with the expected behaviour of pillars under axial loads.

If it is assumed that elements in unmined zones initially have zero displacement, and that they deform only in response to induced stresses [40], the following system of equations can be assembled for this type of element:

$$0 = \frac{(\lambda_s + 2G_s)}{h_s} D_2^p + \frac{2G_s}{h_s} D_c^p + A_{222}^{pq} D_2^q + A_{221}^{pq} D_1^q + K_{22}^{pq} D_c^q \tag{4.43}$$

$$0 = \frac{(\lambda_s + 2G_s)}{h_s} D_c^p + \frac{2G_s}{h_s} D_2^p + A_{112}^{pq} D_2^q + K_{11}^{pq} D_c^q \tag{4.44}$$

$$0 = \frac{G_s}{h_s} D_1^p + A_{122}^{pq} D_2^q + A_{121}^{pq} D_1^q \tag{4.45}$$

This system of equations, together with the system of equations (4.28) - (4.30), forms the basis of the EDDM, and can be solved for the values of the unknowns DDs.

The EDDM algorithm for three-dimensional is developed through straightforward extension of the two-dimensional model. A detailed account of its formulation is presented in Paper III.

4.3 Sample Applications

In this section, two examples (one two-dimensional and the other a three-dimensional case) that demonstrate the functionality and advantages of the enhanced displacement discontinuity method (EDDM) are described. More examples of problems solved with the new method are given in Paper III.

4.3.1 Example 1: Analysis of a pillar between two stopes

The model of a pillar between two stopes presented by Brady and Wassyng [46] is analysed with the EDDM. The geometry of the problem is shown in Fig. 4.4. The pillar and stopes were each modelled with 12 discrete EDD elements. Since there are no analytical solutions for this problem, stresses computed in the pillar and around the stopes by the EDDM were verified through comparison with those generated from the coupled FEM/BEM developed by Brady and Wassyng [46]. (The Brady and Wassyng solution was used in checking stresses in the pillar only.) They were also compared to stresses calculated from *Phase*^{2}, a FE software program developed in the Rock Engineering Group of the University of Toronto [47]. In the finite element-boundary element coupling technique presented by Brady and Wassyng [46], the boundaries of the stopes (excavations) were modelled with boundary elements while a finite element mesh was used for the pillar. *Phase*^{2} solely employs the finite element method.

Figure 4.5 contains plots of the major and minor stresses in the pillar computed by the three methods. From the results, it can be seen that all three methods give similar solutions to the problem. (The stress values at the ends of the pillar are different for the coupled FEM/BEM technique because a finer mesh is needed in that region for the

technique.) These comparisons demonstrate that the EDDM, as well as its additional capability of including confining effects (which are very important when pillar yielding is modelled), can provide accurate results when used for elastic analysis.

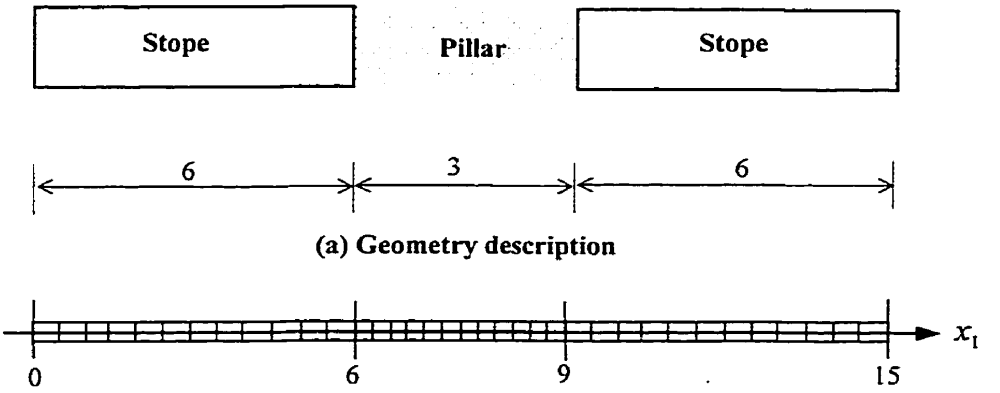

(a) Geometry description

(b) Discretized configuration

Figure 4.4: Pillar and stope geometry description

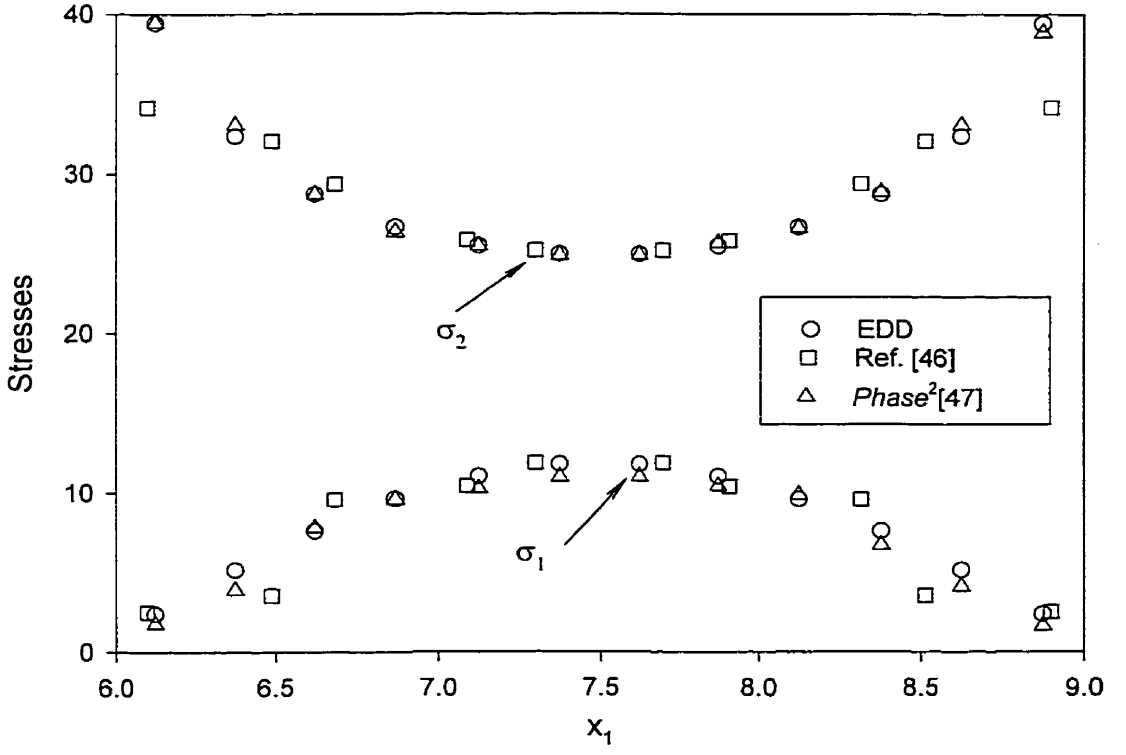

Figure 4.5: Stress distribution for the pillar

4.3.2 Example 2: Three-dimensional analysis of a pillar in a room

Confinement controls the overall behaviour of pillars. A detailed study of the failure process in pillars [48, 49], showed that failure commenced on pillar boundaries and migrated towards the centres of the pillar, where the cores had not reached their full load-bearing capacities. The observed increase in the strength of material from pillar boundaries towards the core is attributable to the effects of confinement.

Previous approaches for handling lateral confinement in DD methods relied on manual techniques to account for the influence of confinement. Figure 4.6 shows a typical scheme in MULSIM for assigning stress-strain curves to the elements of a square pillar in a room-and-pillar mining scheme [50]. Elements used in discretizing the square pillar are designated with letters from A to D in Fig. 4.6. These elements are assigned strength curves (shown on the stress-strain diagram) according to the degree of confinement they experience. The element at the core of the pillar, being in the most confined region, is assigned the highest strength curve (curve A).

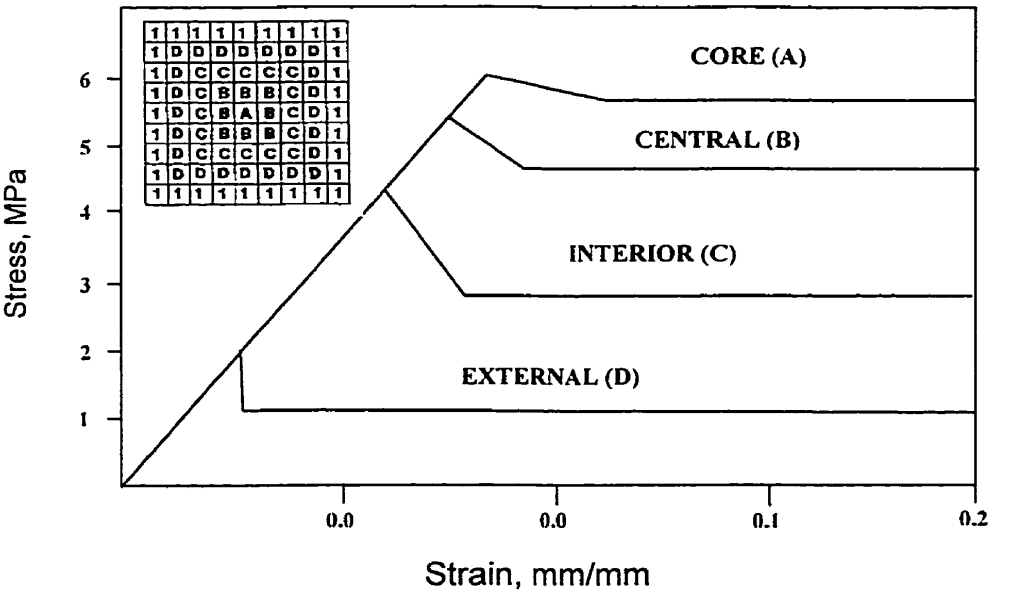

Figure 4.6: Assignment of material properties to different elements [50]

For the three-dimensional EDDM to be considered successful it must correctly capture the variation of the degree of confinement in pillars. The normalised confinement DD adequately captures the degree of confinement in a pillar. An example of a single pillar in a room similar to the pillar of Fig. 4.6 is depicted in Fig. 4.7. Figure 4.8 shows the contours of equal normalised confinement DDs calculated for the square pillar. Due to the inclusion of the lateral singularity in the EDDM, it has been able to effectively model confinement in the square pillar.

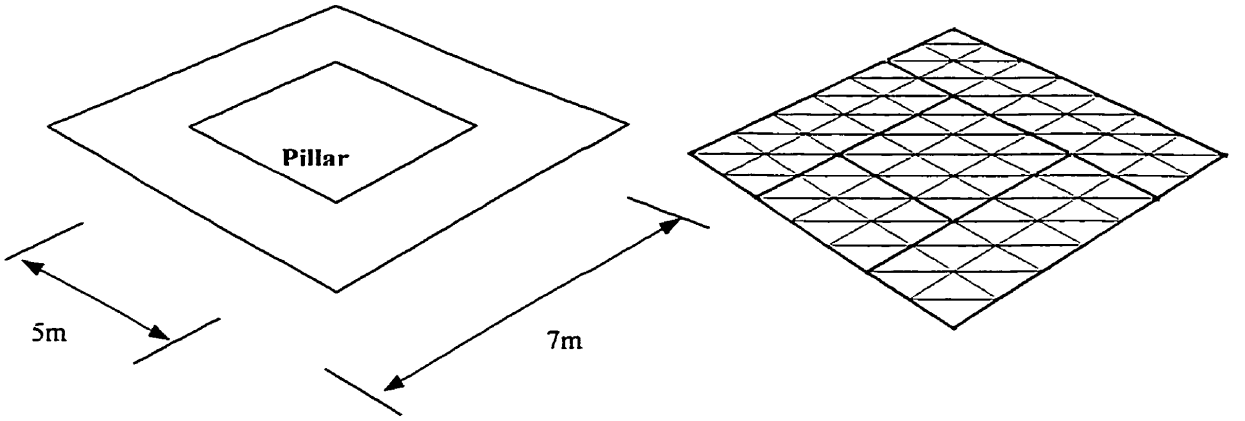

Figure 4.7: Geometry and discretization of problem involving a square pillar in a room

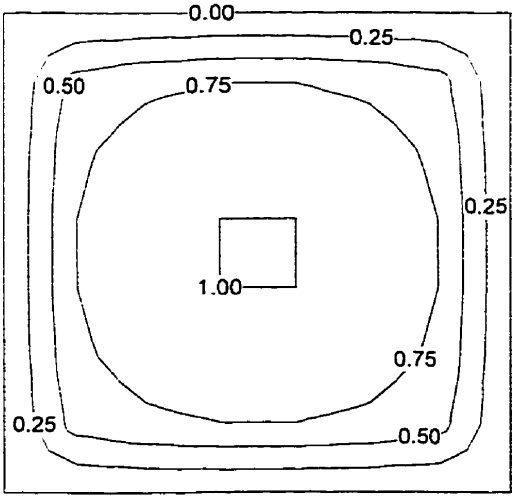

Figure 4.8: Contours of normalised confinement DD for the pillar

4.4 Summary

The EDDM makes use of all the components of the stress tensor and assumes a homogeneous stress distribution along the height of pillars or panels. It has a principal advantage over the classical DDM because of its ability to model material behaviour effects which depend on confining stresses. Whereas the DDM is limited in its application, the EDDM can accommodate general material constitutive equations including plasticity and damage models. By explicitly accounting for confinement in its formulation, the new procedure generalizes and automates the process of assigning strength curves to elements. As a result, it simplifies data preparation by eliminating the need for any artificial means for accounting for the effects of confining stresses.

Sample problems involving boundaries and pillars of simple geometry were solved (mainly described in Paper III) to validate the performance of the EDDM. The results obtained from the EDDM compared well with analytical solutions for problems for which they were available, and showed good agreement with the results of other numerical techniques that have been established to perform well. Although the examples used in validating the new formulation involved simple shapes, the procedure is by no means limited to such cases.

The EDDM in this chapter was formulated using constant elements. However, higher-order elements can be implemented, requiring only a few and relatively simple modifications. This ability of the EDDM to accommodate a variety of constitutive models, combined with its ability to account for confinement, makes it even more attractive and important in the analysis of failing or yielding pillars.

Chapter 5

Stability Analysis of Pillars Using Enhanced Displacement Discontinuity Method

5.1 General Scope

During the simple uniaxial compression of mine pillars, frictional forces perpendicular to the direction of compression arise in the pillars, because of the effects of clamping at the ends of the pillars. Because these horizontal frictional forces resist the bulging effects of uniaxial compression on pillars, the stresses they generate in pillar material are termed confining stresses.

Due to the effects of confinement, pillars do not experience failure uniformly across their cross-sections. Close to pillar surfaces, the degree of confinement is lesser than for points further away from exposed faces. Under such triaxial stress conditions, the strength of pillar material increases from the boundaries towards the core. It can therefore be said that pillar material strength increases with increasing confinement [51, 52]. Confinement is more pronounced in the cores of short squat pillars, and reduces with increasing pillar slenderness.

The presence of confining effects, which render pillar strength non-uniform across pillar cross-sections, means that the practical design and analysis of pillars yielding without the inclusion of confining stresses is inaccurate. Yielding of pillars or plastic pillar response, as stated in Chapter 4, occurs in mining operations in which ore is recovered from pillars and pillars, are allowed to collapse in a controlled fashion [52].

In some contemporary design methods, parameters and relationships used for computing pillar sizes are obtained through the back analysis of failed and stable pillars. The application of these techniques is however limited in range, because they can be used to analyse and design only pillars with the same properties and operating under the same conditions as those from which the equations and parameters were obtained. More general approaches can be devised through theoretical considerations of the behaviour of rock material in pillars.

The yielding behaviour of pillars can be modelled with constitutive relationships such as elasto-plastic models. These constitutive models can be used with various numerical techniques including the FEM and EDDM. The practical application of elaborate models is, however, restricted due to the number of material parameters involved, and the difficulties associated with the determination of their appropriate values. A simpler approach involves the use of elasticity constitutive relationships, together with failure criteria such as the Mohr-Coulomb criterion or Hoek-Brown criterion, to model yielding in pillars. These simple approaches perform analysis through iterative procedures. One such technique is the progressive failure method developed for the FEM [53-56].

Although quite simple in its formulation, the progressive failure method adequately captures the essence of the yield behaviour of materials. The parameters needed for the failure criterion incorporated in the method are easy to determine, and therefore make the practical application of this method very attractive. Although the progressive failure procedure has been successfully implemented with the FEM to analyse individual pillars, the large number of elements required to adequately model

large-scale mine problems, and the uncertainty in mine input data do not justify the approach for practical geomechanical mine design. A progressive failure approach, implemented in the EDDM, will be introduced in this chapter. This new method offers all the advantages of the speed of the BEM, and produces results of enough detail to facilitate accurate engineering decision-making on mine pillar design.

5.2 Stress-Strain Behaviour of Rock

After rock is fractured it has reduced resistance to loads. This in turn leads to increased deformation under loads, because of the increased external energy supplied to the rock. These observations were confirmed by experimental data obtained by Bieniawski [51]. His results showed that the post-peak response of intact rock samples was characterised by a progressive decrease in both load-bearing capacity and elastic stiffness.

The stress-strain behaviour of rock material, however, depends to a great extent on the confining stresses acting on the material. At higher confining stresses, both the failure loads and residual strength for rock samples increase in triaxial tests. At low levels of confinement, the post-peak strength of rock is reduced to very small fractions of the load-bearing capacities of samples, whereas the post-peak loss of strength is not so pronounced at high confining stresses.

5.3 Progressive Failure Procedure

In the rock mass surrounding excavations, and for rock material in pillars, extensive redistribution of stresses occurs due to post-peak deformations. When local

failure of material occurs at points in rock where stresses have exceeded strength, the loss of load-bearing capacity has to be sustained by surrounding material. Stresses are therefore redistributed, with regions in the immediate vicinity of failed material acquiring increased stresses. Stress redistribution continues (progresses) until a stable state is attained in which no new local failures of material occur.

Progressive failure of rock material was first included in analysis by Kidybinski and Babcock [57], when they represented failed rock zones around longwall faces with material of reduced elastic moduli. Kripakov [53] developed a more sophisticated approach to simulating progressive failure. This approach, implemented in the FEM, more realistically modelled the process of progressive failure. The progressive failure approach of Kripakov uses an iterative pseudo-elastic method of analysis to simulate the progressive yield zone in pillar material. In the method, it is assumed that local failure of an element representing a section of a material occurred, when the stress on the element exceeded the calculated strength of the material at that point. This strength is calculated using a failure criterion such as Mohr-Coulomb.

If after the computation of element stresses any elements have failed, a new iteration is begun in which stresses were recalculated, with the difference between the calculated stress of a failed element and its admissible residual stress being distributed to surrounding elements. Redistribution of stresses is achieved through the modification of the element material stiffnesses. Every time the failure stress of an element is exceeded, its elastic modulus is reduced by the ratio of the failure stress predicted by a failure criterion to the stress computed at the element.

Since failure criteria generally do not provide any information on the post-failure

behaviour of material, the procedure developed by Kripakov models post-peak material constitutive behaviour by reducing the stiffness and strength of material as iterations progressed. The amounts of reductions after failure are determined by an empirical local material factor of safety, F_S. This index is not a global safety factor that indicates the danger of collapse of excavations or mine pillars, but rather one that measures how close material at a point is to failure. The local factor of safety is computed from the formula:

$$F_S = \frac{maximum\ material\ strength}{applied\ stress} = \frac{\sigma_F}{\sigma_1}, \tag{5.1}$$

where σ_1 is the maximum principal stress calculated at a point in the material. The maximum material strength, σ_F, is calculated from a failure criterion. A factor of safety greater than 1.0 implies that no failure has occurred, while factors of safety less than 1.0 indicate failure.

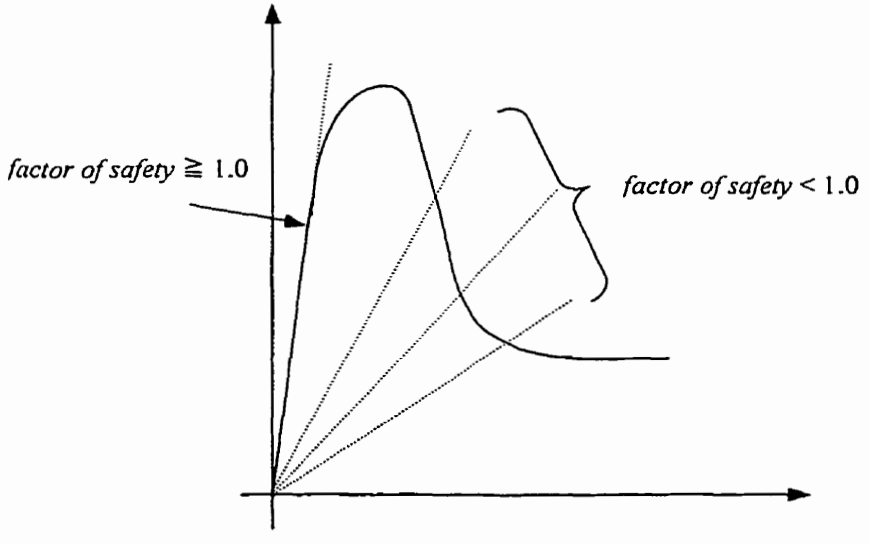

Figure 5.1: Reduced post-peak elastic moduli of material

The reduced modulus of elasticity and uniaxial strength (Fig. 5.1) of failed material are calculated from the equations:

$$E_{(\text{modified})} = F_S \cdot E_{(\text{original})} \tag{5.2}$$

$$\sigma_{c(\text{modified})} = F_S \cdot \sigma_{c(\text{original})}, \tag{5.3}$$

respectively. If an element fails in tension, that element is assumed to have yielded completely and therefore does not retain any residual strength.

After the first iteration of the progressive failure algorithm, the degrees of failure (factors of safety) of the elements of a discretized structure or domain are assessed for values less than 1.0 (indications of failed elements). If all elements have factors of safety greater than 1.0, the analysis is terminated. For elements that have factors of safety less than 1.0, reductions are applied to their stiffness and strength and the analysis repeated. At the end of each iteration a termination condition, which compares element factors of safety from the previous iteration to that of the current, is checked. If the differences between previous and current values of the factors of safety for elements are smaller than a set tolerance, i.e. when the factors of safety practically stop changing, the algorithm is adjudged to have converged. Results of studies by Kripakov and others [53, 56] show that the criterion produces stable results that are not affected by the accuracy of the convergence ratio.

5.4 Failure criteria

Failure at points of a material occurs when the stresses at these points, or in elements used in modelling the material, exceed the material's strength limit. Strength limits are determined or predicted from failure criteria [58]. For isotropic material, a failure criterion is an invariant function of the state of stress, and is commonly represented with principal stresses as:

$$f(\sigma_1, \sigma_2, \sigma_3) = 0, \tag{5.4}$$

where $\sigma_1, \sigma_2, \sigma_3$ are, respectively, the major, intermediate and minor principal stress components.

Failure criteria for uniaxial stress conditions cannot be used in progressive failure, because the stress-strain behaviour of rock material depends on the magnitude of confining stresses. Therefore failure criteria that take into consideration other principal stresses are required. The material parameters needed in failure criteria for rock masses are critical to the design of underground excavations, but can be at times difficult to estimate. As a result, it is desirable that failure criteria chosen for practical analysis include only parameters that can be evaluated realistically and reliably [59]. Two such criteria, which are very widely used for predicting failure loads of rock under triaxial stress states, and that satisfy these conditions, are the Mohr-Coulomb and the Generalised Hoek-Brown criteria.

The Mohr-Coulomb and Generalised Hoek-Brown failure models [60] have great appeal when applied to practical problems involving progressive failure of rock material, because of their relative simplicity. Although it is possible that more complicated models may be able to predict failure stresses more accurately than these two criteria, the ease of the determination of the values of their parameters, and the simplicity of their forms, renders them very effective for routine use.

5.5 Progressive Failure Simulation Using EDDM

For progressive failure to be implemented in the EDDM, the stress tensor for each unmined element is calculated and rotated to obtain principal stresses. The strength of

each element is calculated using either the Mohr-Coulomb or Hoek-Brown failure criteria. If the stress computed for an element exceeds the element material strength, then the factor of safety for that element is modified in the next run of the algorithm. The strength and deformational properties of that element are reduced, thereby simulating progressive partial failure of the element. As failed and softened elements will not support as much load as before, extra stresses are transferred to other more competent elements. This procedure continues until all elements reach an equilibrium state in which the computed stresses for all elements do not exceed failure stresses.

5.6 Sample Applications

Two examples of the application of progressive failure with the EDDM are provided in this chapter. These examples help demonstrate the applicability of the proposed method to mine pillar analysis. The examples presented in this chapter were selected such that the results obtained from analysing them with progressive failure in the EDDM could be readily verified. In all the examples it is assumed that the host rock is much stronger than the seam or orebody. Under such conditions, the host rock behaves in a linear elastic manner. Only material in the seam undergoes yielding.

5.6.1 Two-dimensional analysis of a pillar (Example 1)

The application of progressive failure with the EDDM to the two-dimensional analysis of a pillar is demonstrated in this example. Figs. 5.2a and 5.2b provide a description of the problem and the discrete representation of the stopes and pillar with EDD elements. The elastic properties for both the host rock and orebody in the problem,

and material parameters for determining failure stresses are given in Table 5.1 [51]. This problem was solved with progressive failure in the FEM [51]. It is assumed in the problem that only vertical stresses due to the weight of rock overburden are applied to the excavations. The underground excavations shown in Fig. 5.2a are at a depth of 457m.

Table 5.1: Rock properties for Example 1

Rock type	*E (MPa)*	*ν*	*ϕ (degree)*	*C (MPa)*	*m*
Host	11324	0.3	40	4	9
Orebody	3248	0.3	30	2	7

In the analysis, stresses in the pillars were calculated using the EDDM. The ratios of the normal stresses to the vertical stress, p, (normalised normal stresses) at various points across the width of the pillar are plotted in Fig. 5.3. From the plots it is evident that the results of the approach advocated in this paper compare very well with those obtained from the FEM with progressive failure modelling.

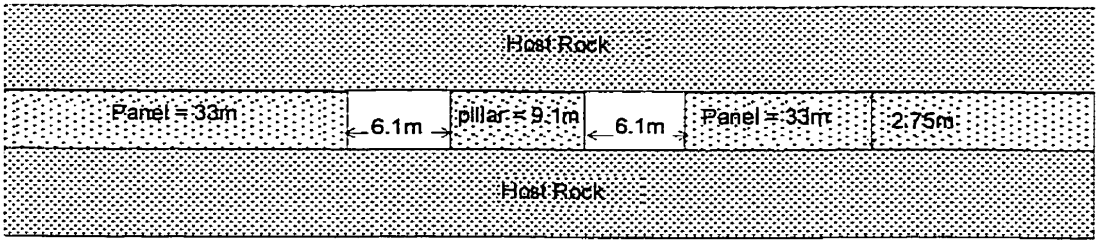

(a) Geometrical description

(b) Discretized mesh

Figure 5.2: Two-dimensional model for mining problem

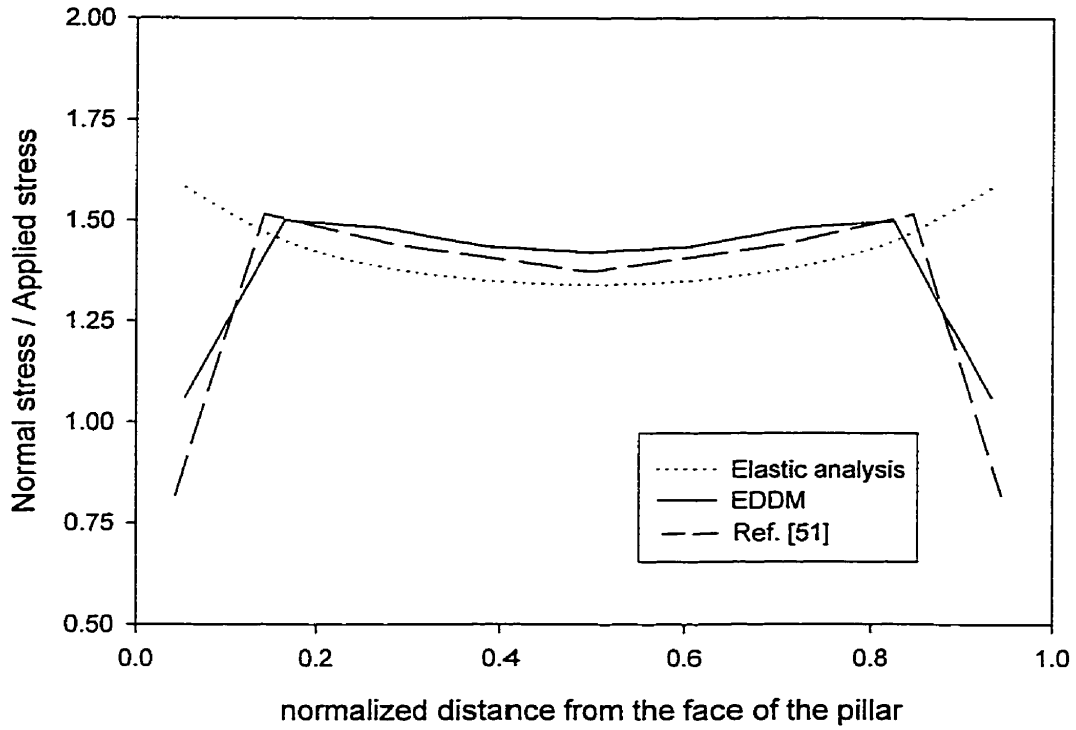

Figure 5.3: Normal stress variation across the pillar

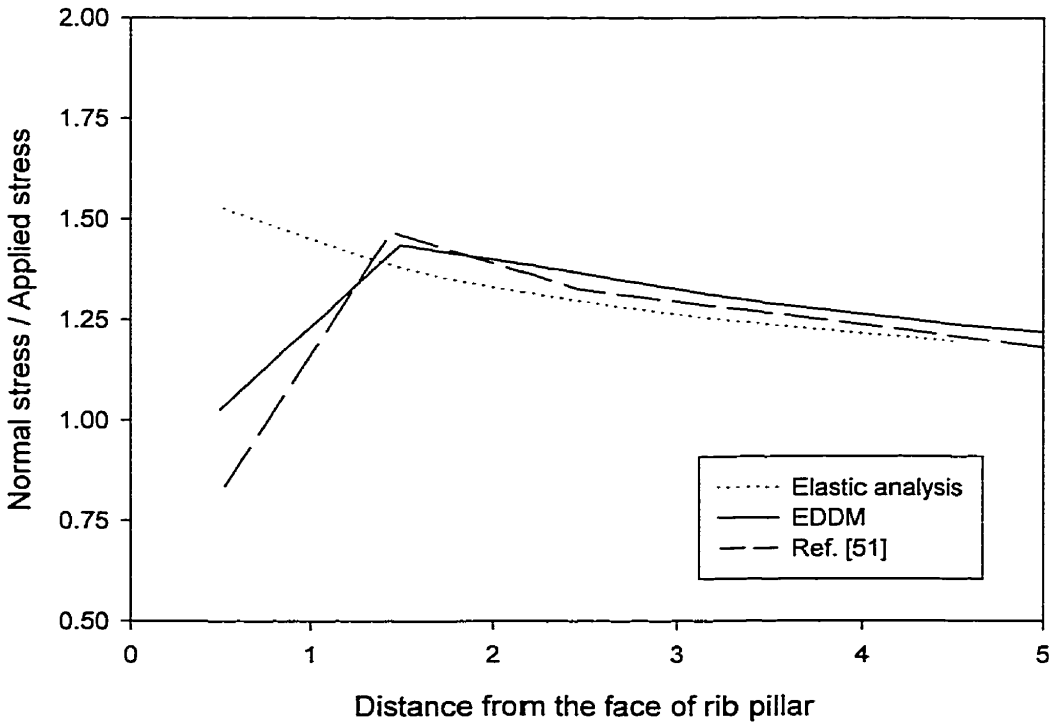

Figure 5.4: Normal stress variation along the panel

In addition to verifying the stresses in the pillar, the stresses computed for the panels were also checked. Normalised normal stresses for the panels are plotted in Fig. 5.4. Again, there is good agreement between the results of the EDDM with progressive failure, and those computed from progressive failure in the FEM. Plots of the normalised normal stresses in the pillar and panels produced by an elastic analysis are provided in Figs. 5.3 and 5.4, respectively, for comparison with stresses obtained from the yield models.

5.5.2 Three-dimensional analysis of a pillar (Example 2)

Example 2 examined the analysis of a pillar in a longwall mining scheme, in which ore from a panel was removed in two stages. The material properties of the host rock and orebody analysed in the example are provided in Table 5.2. The mining depth was again assumed to be at 457m, with the primitive stress field assumed to be uniform and equal to overburden pressure [61].

Table 5.2: Rock properties for Example 2

Rock type	E *(MPa)*	ν	ϕ *(degree)*	C *(MPa)*	m
Host	17241	0.3	30	4	9
Orebody	1724	0.3	30	2	7

Fig. 5.5a shows the geometry and dimensions of the excavations, panels and pillar at each of the mining stages. If the length of the panels, orebody, and pillar were to be infinitely long, this three-dimensional problem would be equivalent to a two-dimensional analysis of the central cross-section of the problem. For practical purposes, however, an

infinite length is not possible and therefore a length to width ratio of 4:1 was selected for the problem.

The mesh used in discretizing the problem domain is shown in Fig. 5.5b. This mesh remained unchanged for both stages of the problem. Boundary conditions, however, were chosen to correctly represent the physical conditions prevailing at the different stages.

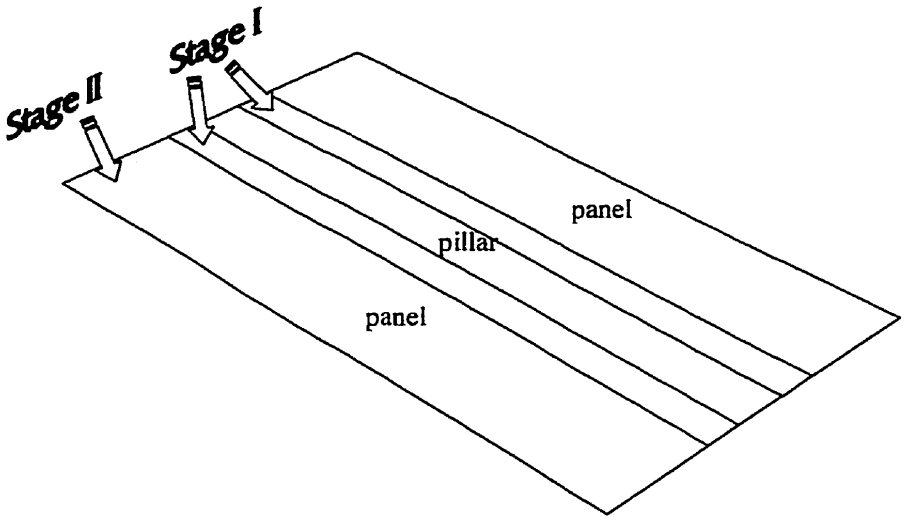

(a) Geometry description

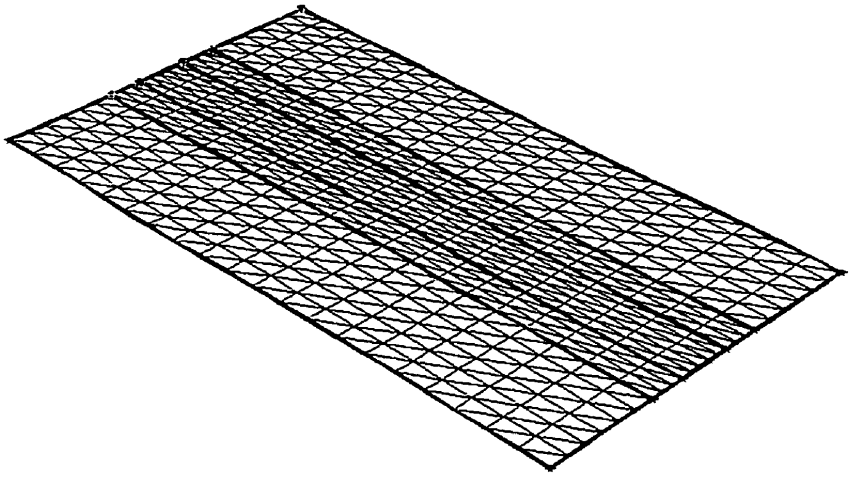

(b) Used mesh

Figure 5.5: Geometry and discretization of the orebody

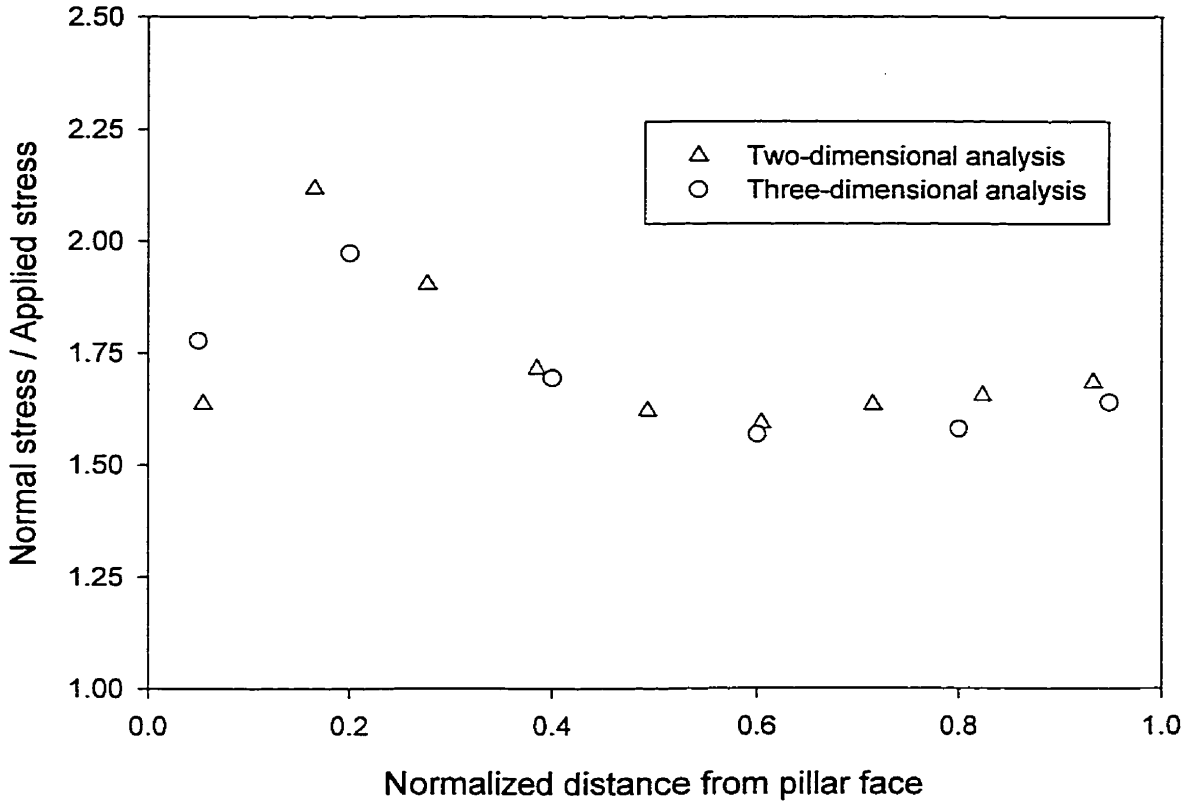

Figure 5.6: Variation of normal stress across the pillar for stage II

Stresses around the excavations and in panels and pillars were computed for the different stages of the analysis. During stage I, no failure occurred in either pillar or panel material. Progressive failure of rock occurred only during stage II of mining. The normalised normal stresses computed in the plane of the central cross-section of the pillar are plotted in Fig. 5.6. These results are compared with the results of a two-dimensional analysis of the central cross-section of the problem. There is good agreement between the results of the three-dimensional and two-dimensional analyses, even though the mesh used for the latter was much finer.

5.7 Summary and Conclusions

The yield behaviour of rock pillars and the analysis of yielding pillars are generally very difficult to model numerically, because of the non-linearity of the yielding process. The prediction however of pillar behaviour is of great importance to the design of room-and-pillar mining schemes. Due to difficulties in estimating the *in-situ* strength properties of pillar material and the complexities of pillar loading conditions, any tool for the practical analysis of yielding pillars must be simple and yet capable of producing acceptable results. The progressive failure technique, implemented in the EDDM, was initiated in an effort to develop a quick and efficient numerical technique for pillar post-failure analysis in the mining of lenticular orebodies.

Although very simple in formulation, the progressive failure technique overcomes many of the numerical programming difficulties associated with the simulation of strain-softening behaviour. It also provides efficient ways of generating results that conform with the pillar rapture mode which involve spalling from the pillar surfaces. The results of the analysis of sample problems in both two and three dimensions with the progressive failure procedure in the EDDM proposed in this thesis, compared very favourably with those obtained from other methods.

Although only the progressive failure method was used with the EDDM, additional models for analysing pillar yielding in the EDDM could be readily developed. For example, more complex plasticity constitutive models can be used in place of the pseudo-elastic model in the EDDM.

Chapter 6
Summary and Future Development

6.1 General Summary

The design and analysis of mining excavations has great significance for the profitable and safe mining of mineral resources. It involves the geomechanical analysis of mine structures, and requires the use of numerical techniques that are more powerful and flexible than analytical methods. One of the difficulties of mine analysis is that it involves large-scale problems, due to the sizes of orebodies and influence zones of mining activity. The geometry of orebodies, excavations and mine support structures pose additional challenges in practical mining situations, because of their irregular shapes and layouts. For example, mine excavation analysis for the extraction of ore from deposits such as seams or lenticular orebodies, is difficult, because of the unique property of these excavations that their boundaries consists of two parts in very close proximity to each other. These factors combine to impose a number of restrictions on the numerical method that can be for practical stress mine analysis. The mining of orebodies with shapes as those just mentioned above is of particular interest in this thesis.

Another major problem in geomechanical mine analysis and design is the uncertainty in data collected on rock properties. Uncertainty makes it uneconomical to perform elaborate design, especially at preliminary stages of mining. It often brings about changes in analysis and design, because new data collected on rock properties from a

location as mining progresses show that input parameters are not what they were initially estimated to be.

Of the numerical methods available for engineering design, the displacement discontinuity method (DDM) is most suitable for solving mine design and analysis problems of lenticular orebodies. Its advantages stem from the use of a boundary element method in which the two surfaces of thin slit-like excavations are treated as one entity, and the relative displacements between these surfaces are handled as unknown physical parameters.

The research conducted in this thesis was aimed at resolving a broad spectrum of issues related to the practical application of the DDM to stress analysis problems of mining excavations. The new formulations for the DDM derived in this thesis were verified by implementing them in a C/C++ program code and comparing its results with those of available software programs. Although results produced by the new code were very good, it is important to outline some of the simplifying assumptions used in its formulation that lead to limitations in its application. These limitations are related to the DDM itself, and can be outlined as follows:

The method assumes

1. homogeneous, isotropic, linear elastic behaviour for domain (host rock) material,
2. average stress components in pillars that are distributed along the centreline of DD elements,
3. only rupture modes that involve spalling from pillar surfaces.

Also, although different plasticity models can be used with the method, they were not actually implemented.

6.2 Contributions

This thesis has made key contributions to research on the theoretical development of the DDM and on the practical application of the method to mining stress-analysis problems. These contributions are outlined in the sections below.

6.2.1 Node-centric framework

In the first part of this work, a node-centric formulation, applicable to indirect boundary element methods, was developed. This had not been done previously, because of difficulties associated with the evaluation of the highly singular integrals of the indirect method, despite the proven advantages of node sharing in the BEM. The node-centric indirect BEM was made possible only after the creation of a new and unified framework for evaluating hyper-singular boundary integrals in the thesis. Original boundary functions, based on an assumption of linear variation of unknowns in the indirect BEM, were derived in the thesis. They were used in the new approach for evaluating singular integrals. The technique of boundary functions significantly reduces complications in the integration of singular functions, and also uniformly treats singular, near-singular and regular integrals. It has additional advantages of being robust and fast, and used adaptive integration to make it possible to evaluate integrals with predetermined accuracy.

The practical implementation of the node-centric method for indirect BEMs was demonstrated on the displacement discontinuity method (DDM). PAPER I, in the appendix to this thesis, discusses the application of the method to two-dimensional

analysis with the DDM, while in PAPER II, a three-dimensional DDM implementation of the node-centric is provided.

The node-centric formulation together with the unified integration scheme produced more accurate results than the conventional DDM, and demonstrated greater robustness in comparison to other DD formulations. The node-centric DD formulation extends the range of application of the DDM to non-standard problems such as those involving the intersection of excavations by faults. Without a node-centric formulation, the application of the DDM to such geomechanics problems is quite cumbersome. Usually, to overcome the physically impossible large stresses that are calculated in-between elements in the conventional DDM for problems of this kind, careful and fine discretization had to be used. The node-centric formulation obviates this problem by imposing stress continuity.

6.1.2 Analysis of pillars using EDDM

The second part of the thesis described the derivation of a new DD element - the enhanced displacement discontinuity method (EDDM). Elements of this new displacement discontinuity approach were formulated by adding a centre of dilation singularity to the formulation of the conventional DD element. The dilation singularity is coupled with the normal singularity through the use of a constitutive relationship. This new formulation provides information about the in-plane (confinement) stress in an element, something the conventional DD does not include. These developments are discussed in Paper III, a summary of which is provided in Chapter 4.

The EDDM allows the process of assigning degrees of confinement, expected to occur in pillar and abutment elements under a given set of mining conditions, to be automated. A primary advantage of this feature is that it provides a means to simplify data preparation, because it eliminates the need for *ad hoc* means for accounting for the effects of lateral stresses.

With the inclusion of confinement into the formulation of the enhanced DD element, it can be readily used for the analysis of yielding pillar, since all components of the stress tensor at a point in a material are explicitly accounted for in elements. The new element displays greater flexibility and power in handling two- as well as three-dimensional mining problems.

6.1.3 Pillar yielding

The final focus of the thesis research was on the implementation of the EDDM for modelling the behaviour of yielding pillars. The technique selected was the progressive failure method, previously used with only the FEM. Its application to the BEM, and specifically to the EDDM, is new. The implementation of the progressive failure procedure in the EDDM was undertaken in an effort to develop a quick and efficient numerical tool for pillar post-failure analysis in the mining of lenticular orebodies. PAPER III, summarized in Chapter 5, contains the full formulation of the progressive failure method applied in the EDDM. The progressive failure procedure is a simple and yet very efficient way of simulating real rock behaviour. It uses a quasi-elastic approach,

accompanied by iterative modifications to element material deformation and strength properties.

The motivation behind the proposed numerical procedure for modelling yielding pillars was quite straightforward. Often, not enough is known about rock properties to justify a complete elastic-plastic analysis, especially since elastic-plastic analyses require considerable computational resources, effort and time. The input data for the progressive failure procedure, outlined in the thesis, include well-understood parameters, easily obtained from laboratory tests on rock samples.

6.3 Future Development

Further developments to the methods described in this thesis can be directed in two principal directions: improvements to modeling techniques and the resolution of practical application issues. Some of the aspects that need to be investigated in these two areas are discussed below:

1. The node-centric formulation of the DDM implemented in this work assumed a linear variation of unknowns, which is the lowest order of interpolation functions that could be used for node sharing. Higher order of elements can be developed for special design or analysis cases, where results of higher accuracy are desired.
2. The node-centric framework developed in this research can be applied to other indirect boundary element methods such as the fictitious stress method. This could facilitate the coupling of fictitious stress methods with the displacement discontinuity method, because of node sharing.

3. The node-centric displacement discontinuity method developed here can be extended to multiple material problems.
4. Extensive studies oriented at comparing practical mine data with the numerical results obtained from the new DD model can be carried out. In these studies, the performance of both elastic analysis and progressive failure analysis of pillars can be evaluated.
5. More complicated models can be developed for the behaviour of unmined material, close to excavation boundaries, by incorporating non-linear material constitutive relationships into the progressive failure method.
6. The EDDM developed in the thesis can be used for modelling mining sequences. It can thus be used to study history dependent phenomena such as those arising from mining activities in the vicinity of faults. The ability to model mining sequences is also necessary when considering the non-linear behaviour of the seam material.
7. A study directed at the effects of back-filling mined zones can be conducted using the progressive failure method and the EDDM. Adding a routine that changes the properties of unmined elements during every mining stage can help accomplish this objective.

References

1. Jeremic, M.L. (1987) *Ground mechanics in hard rock mining,* A.A. Balkema, Netherlands.
2. Franklin, J. A. and Dusseault, M. B. (1989) *Rock Engineering*, McGraw-Hill, New York.
3. Brady, B.H.G. and Brown, E.T. (1985) *Rock Mechanics for Underground Mining,*, Chapman & Hall, London.
4. Wardle, L.J. (1993) The use of numerical modeling for underground coal mine design, *Comprehensive Rock Engineering* (Eds. J.A. Hudson, E.T. Brown, C. Fairhurst and E. Hoek), Chp. 28, Vol.2, 733-748.
5. Coates, D. F. (1975) *Rock Mechanics Principles*, Ottawa Mines Branch Dept of Mines and Technical Surveys, Canada
6. Eberhardt E., Stead D., Reeves M.J. and Connors C. (1997) Design of tabular excavations in foliated rock: and integrated numerical modelling approach, *Geotechnical and Geolegical Engineering*, **15**, 47-85.
7. Beer, G. and Watson, J.O. (1992) *Introduction to Finite Element and Boundary Element Methods for Engineers*, John Wiley & Sons Inc., England.
8. Zienkiewicz, O.C. (1986) *The Finite Element Method,* Tata McGraw-Hill, New Delhi.
9. Banerjee, P.K. (1994) *Boundary Element Methods in Engineering* McGraw-Hill, London.
10. Brebbia, C.A. and Dominguez, J. (1989) *Boundary Elements: An Introductory Course,* Computational Mechanics Publications, Southampton.
11. Meek, J.L. (1993) Stress analysis in mine design, *Comprehensive Rock Engineering* (Eds. J.A. Hudson, E.T. Brown, C. Fairhurst and E. Hoek), Chp. 21, Vol.2, 529-546.
12. Starfield, A.M. and Crouch, S.L. (1973) Elastic analysis of single seam extraction, *In New Horizons in Rock Mechanics* (Ed. H.R. Hardy Jr., R. Stefanko), Proceedings 14th. U.S. Rock Mechanics Symposium, 421-439.

13. Salamon, M.D.G. (1963) Elastic analysis of displacements and stresses induced by the mining of seam or reef deposits, Part I, *J. S. Afr. Inst. Min. Metall.*, **64**, 128-149.

14. Kuriyama, K. and Mizuta, Y. (1993) Three-dimensional elastic analysis by the displacement discontinuity method with boundary division into triangular leaf elements. *Int. J. Rock Mech. Min. Sci.*, **30(2)**, 111-123.

15. Cayol, V. and Cornet, F.H. (1997) 3D mixed boundary elements for elastostatic deformation field analysis. *Int. J. Rock Mech. Min. Sci.*, **34(2)**, 275-287.

16. Shou, K. J. and Crouch, S.L. (1995) A higher order displacement discontinuity method for analysis of crack problems, *Int. J. Rock Mech. Min. Sci. & Geomech. Abst.*, **32**, 49-55.

17. Shou, K. J., Siebrits, E. and Crouch, S. L. (1997) A higher order displacement discontinuity method for three-dimensional elastostatic problems. *Int. J. Rock Mech. Min. Sci,* **34(2)**, 317-322.

18. Zipf, R.K. (1992) *MULSIM/NL Theoretical and Programmer's Manual* BuMines IC 9322.

19. Fotoohi, K. and Mitri, H.S. (1996) Non-linear fault behaviour near underground excavations - A boundary element approach, *Int. J. Numer.Anal. Meth. Engngi,* **20**, 173-190.

20. Duncan Fama, M.E. (1993) Numerical modeling of yield zones in weak rock, *Comprehensive Rock Engineering* (Eds. J.A. Hudson, E.T. Brown, C. Fairhurst and E. Hoek), Chp. 3, Vol.2, 49-75.

21. Kane, J.H. (1994) *Boundary Element Analysis in Engineering Continuum Mechanics*, Prentice-Hall Inc.

22. Medina, D.E. and Liggett, J.A. (1988) Three-dimensional boundary-element computation of potential flow in fractured rock, *Int J. Numer Methods Eng.*, **26**, 2319-2330.

23. Hall, W.S. (1988) Integration methods for singular boundary element integrands, In *New Developments in Boundary Elements X*, Vol.1 (ed. Brebbia C. A.), Computational Mechanics Publications, Southampton, 219-236.

24. Vijayakumar, S. and D.E. Cormack, Canonical representation of influence functions in elastic media, *Mechanics Research Communications*, **14(3)**, 159-164 (1987).de

Paula, F.A. and Telles, J.C.F. (1989) A comparison between point collocation and Galerkin for stiffness matrices obtained by boundary elements. *Engineering Analysis with Boundary Elements,* **6(3)**, 123-126.

25. Vandamme, L. and Curran, J.H. (1989) A three-dimensional hydraulic fracturing simulator. *Int. J. Numer. Meth. Engng.*, **28**, 909-927.
26. Shah, S. (1993) *Practical Implementation of the Direct Boundary Element Method for Three-Dimensional Stress Analysis of Underground Excavations*, Ph.D. Thesis, University of Toronto.
27. Vijayakumar, S. and Cormack, D.E. (1988) An invariant imbedding method for singular integral evaluation on finite domains. *SIAM J. App. Math.*, **48**, 1335-1349.
28. Rosen, D. and Cormack, D.E. (1994) The continuation approach for singular and near-singular integration. *Engineering Analysis with Boundary Elements,* **13**, 99-113.
29. Rosen, D. (1993) *A Unified Interpretation for Singular and Near Singular Integrals in the Boundary Element Method*, Ph.D. Thesis, University of Toronto.
30. Vijayakumar, S. and Cormack, D.E. (1989) A new concept in near-singular integral evaluation: The continuation approach, *SIAM J. App. Math.*, **49**, 1285-1295.
31. Hadamard J. *Lectures on Cauchy's Problem in Linear Partial Differential Equations*, Yale University Press, New Haven, CT (1923).
32. Dwight, H.B. (1961) *Tables of Integrals and other Mathematical Data,* 4th Ed., Macmillan.
33. Wiles, T.D. and Curran, J.H. (1982) General 3-D displacement discontinuity method, *Proceedings of the 4th Int. Conf. on Numerical Methods in Geomechanics*, (Z. Eisenstein, Ed.) Edmonton, Canada .
34. Mack, M.G. (1993) The displacement discontinuity method, *in Boundary Element Techniques in Geomechanics,* (Eds. G.D. Manolis and T.G. Davis) Computational Mechanics Publications, Elsevier Applied Science.
35. Sinha, K.P. (1979) *Displacement Discontinuity Technique for Analyzing Stresses and Displacements Due to Mining in Seam Deposits,* Ph.D. Thesis, University of Minnesota.
36. *NFOLD* (1989) *Program user manual*, Golder Associates

37. Donato, D. (1992) *MULSIM/PC A Personal Computer Based Structural Analysis Program for Mine Design in Deep Tabular Deposits,* BuMines IC 9325.

38. Sneddon, I.N. and Lowengrub, M. (1969) *Crack Problems in the Classical Theory of Elasticity*, John Wiley & Sons, Inc.

39. Timoshenko, S.P. and Goodier, J.N. (1970) *Theory of Elasticity*, McGraw Hill, New York.

40. Crouch, S. L. and Starfield, A. M. (1983) *Boundary Element Methods in Solid Mechanics*, George Allen & Unwin, London.

41. Wagner, H. (1974) Determination of the complete load-deformation characteristics of coal pillars, *3rd. Int. Congress on Rock Mechanics*, 1076-1081.

42. Bieniawski, Z.T. (1972) Propagation of brittle fracture in rock, *Proceedings 10th Symposium on Rock Mechanics (AIME)*, 409-427.

43. Hills, D.A., Kelly, P.A., Dai, D.N. and Korsunsky, A.M. (1994) *Solution of Crack Problems The Distributed Dislocation Technique,* Kluwer Academic Publishers, Netherlands.

44. Brady, B.H.G. and Bray, J.W. (1978) The boundary element method for elastic analysis of tabular orebody extraction, assuming complete plane strain, *Int. J. Rock Mech. Min. Sci. Geomech. Abstr.*, **15**, 29-37.

45. Westergaard, H. M. (1964) *Theory of Elasticity and Plasticity*, Dover Publications.

46. Brady, B.H.G. and Wassyng, A. (1981) A coupled finite element-boundary element method of stress analysis, *Int. J. Rock Mech. Min. Sci. Geomech. Abstr.*, **18**, 475-485.

47. *Phase*^{2}, (1996) *Implicit-Explicit Finite Element*, Rock Engineering Group, University of Toronto, Canada.

48. Bieniawski, Z.T. (1969) Deformational behavior of fractured rock under multiaxial compression. *Proc. Int. Conf. Structures Solid Mech. Engng Materials,* Southampton, England, Paper 50, 589-598.

49. Grobbelaar, C. (1970) *A Theory for the Strength of Pillars*, Johannesburg Voortrekkerpers; distributed by Pillarco.

50. Campoli, A. A. (1994) Boundary element method applied to coal mine bump control, *Computer Methods and Advances in Geomechanics*, (Siriwardane & Zaman, Eds.), 1817-1822.

51. Bieniawski, Z.T. (1984) *Rock mechanics design in mining and tunneling,* A.A. Balkema, Netherlands.

52. Duncan Fama, M.E. and Wardle, L.J. (1987) Numerical analysis of coal mine chain pillar stability, *Int. Congress on Rock Mechanics* (Eds. G. Herget and S. Vongpaisal), Vol. 2, 859-863.

53. Kripakov N.P. (1981) Finite element analysis of yielded-pillar stability, *Comp. & Struct.*, **13**, 575-593.

54. Kripakov, N.P. and Melvin, M.T. (1983) A computer procedure to simulate progressive rock failure around coal mine entries. *Proceedings of the 1st conference on the use of computers in the coal industry,* (Eds. Y. J. Wang, R.L. Sanford), Chp. 56, 487-502 .

55. Ash, N.A. and Park, D. (1987) 3-D finite element modeling of longwall mining using progressive failure concept. *Proc. 28th US Symp. Rock Mech.,* (Eds. I.W. Farmer, J.J. K. Daemen, C.S. Desai, C.E. Glass, S.P. Neuman), Tucson, 725-734.

56. Park, D. and Gall, V. (1989) Supercomputer assisted three-dimensional finite element analysis of a longwall panel. *Proc. 30th US Symp. Rock Mech.,* (Ed. A. Wahab Khair), 133-140.

57. Kidybinski, A. and Babcock, C.O. (1973) Stress distribution and rock fracture zones in the roof of longwall face in a coal mine. *Rock Mech. J.* **5(1)**.

58. Chen, W.F. (1982) *Plasticity in reinforced concrete*, McGraw-Hill, New York.

59. Andreev, G.E. (1995) *Brittle Failure of Rock Materials, Test Results and Constitutive Models,* A. A. Balkema, Netherlands.

60. Hoek, E., Kaiser, P.K. and Bawden, W.F. (1995) *Support of underground excavations in hard rock*, A. A. Balkema, Netherlands.

61. Kipakov, N.P., Sun, M.C. and Donato, D.A. (1995) ADINA applied toward simulation of progressive failure in underground mine structures, *Comp. & Struct.*, **56**, 329-344.

Appendix A

Paper I - "Node-Centric Displacement Discontinuity Method for Plane Elasticity Problems"

To appear in the International Journal for Numerical and Analytical Methods in Geomechanics

Node-Centric Displacement Discontinuity Method for Plane Elasticity Problems

S. Vijayakumar, J. H. Curran[§] and T. E. Yacoub

Rock Engineering Group, Dept. of Civil Engineering,
University of Toronto
Toronto, Ontario, Canada, M5S 1A4

Abstract

A new two-dimensional displacement discontinuity formulation, which preserves inter-element continuity of tractions and displacements at nodes, is introduced. The continuous displacement discontinuity variation between elements is achieved by treating inter-element nodes as the points of specification of unknown displacement discontinuity values. Thus, the most important source of error in the displacement discontinuity method implementation is eliminated. This, in turn, widens the applicability of the displacement discontinuity method. The trade off is that certain conceptual and computational difficulties with respect to element integrations arise. By employing the ideas of invariant imbedding and continuation of singular and near-singular integrals, a suitable integration ansatz is developed. The efficacy of the method is shown using several examples which are designed to explore its potency as a general purpose method for solving large scale field problems.

(No. of Figures: 15 No. of tables: 0 No. of Refs: 17)

Keywords: Indirect Boundary Element Method, Displacement Discontinuity Method, Singular integrals, collocation, Node-centric

---

§ Author to whom correspondence should be addressed

1. INTRODUCTION

Rock mechanics and mining engineering problems are distinguished form other engineering problems in the sense that they are often very large in scale with infinite, inhomogeneous and discontinuous material domains. The boundary element method (BEM) is suitable for the mining problems since in this method only the boundary of the problem requires discretization. The displacement discontinuity method (DDM) is a boundary element method for solving problems in solid mechanics with fractures. Although it can be used for conventional problems involving underground excavations, such as holes in infinite media, it is most appropriate for problems involving faults or joints, mining in tabular orebodies [1, 2].

The first reference to the application of DDM to mining engineering was in Salamon [3]. His work was followed by Starfield and Crouch [4] who generalized it and used to solve various types of problems related to geomechanics.

Displacement discontinuities possess a higher-order mathematical singularity than the well-known direct boundary element method or fictitious stress method. This higher-order singularity has been found to be a hindrance towards widespread applicability of the method. The higher-order singularity has a direct bearing on the singular behavior of the element integration. The difficulty in integration is largely due to limitations of the traditional integration schemes that have been applied to the singular integrals.

In this paper, a new and powerful displacement discontinuity element formulation for plane linear elastic problems is introduced. In this new formulation, the nodes, and not the elements, play the central role. We shall illustrate through several examples that this node-centric DD method proves to be more efficient and robust than the traditional element-centric

formulation. With the traditional constant DD technique, the two unknown parameters (normal and shear displacement discontinuities) are represented at the node located at the centre of the element. This leaves the displacements and stresses between the elements discontinuous. Even higher-order linear and quadratic DD elements, while increasing the number of unknown parameters to 4 and 6, respectively, for each element, fail to provide inter-element continuity (Fig. 1a). On the other hand, node-centric elements provide inter-element continuity of stresses and displacements (Fig. 1b). We shall provide several examples which traditionally have been considered intractable by the conventional boundary element formulations.

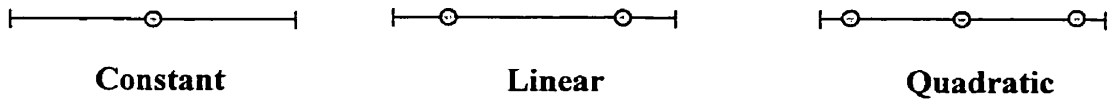

Constant **Linear** **Quadratic**

a) Element-centric elements

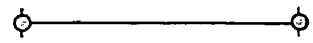

b) Node-centric element

Figure 1. Node- and element-centric elements

The node-centric formulation is a general purpose boundary element methodology that we have developed for the numerical solution of large-scale field problems. Traditionally, the boundary element method is formulated by first discretizing the boundary into elements. Subsequently, the ensemble of all elements is considered to be the boundary and the nodes are placed at suitable points on the elements in order to perform integration and

interpolation. Thus, the nodes as well as the elements do not necessarily coincide with the actual boundary. On the other hand, in the node-centric method all nodes are chosen to lie precisely on the actual boundary. The boundary approximation results only from the discretization of the boundary into elements. Furthermore, the geometry of the elements is needed only for the element integrations and occasional interpolation of field quantities.

2. Node-Centric Displacement Discontinuity Method

In this section we present the two-dimensional formulation of the node-centric DD method. For an excellent overview of the DD method the reader is referred to the book by Crouch and Starfield [5].

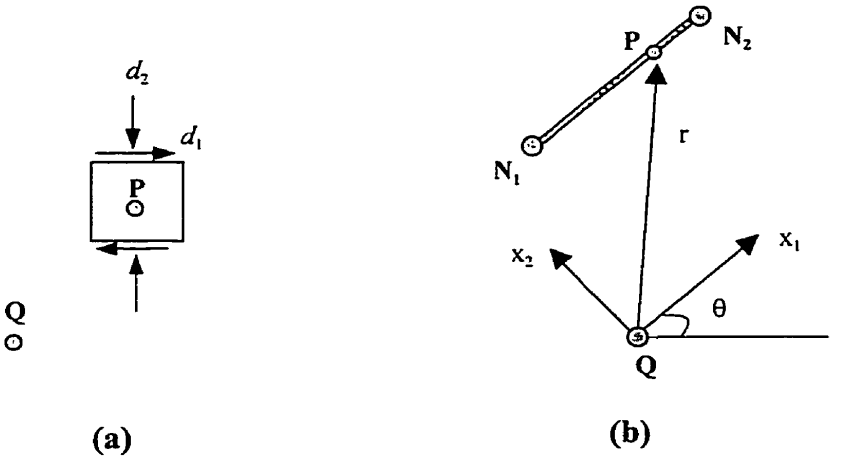

Figure 2. Notation

Consider a homogenous, isotropic, linear elastic material subjected to a displacement discontinuity with density, d_k, at a point P (Fig. 2a). The stresses, σ_{ij}, and the displacements, u_i, at any point Q, in the domain can be represented as

$$\sigma_{ij}(Q) = G_{ijk}(P,Q)\, d_k(P) \tag{1}$$

$$u_i(Q) = H_{ik}(P,Q)\, d_k(P) \tag{2}$$

Throughout this paper repeated indices indicate the usual summation convention and $i, j, k = 1, 2$. The Green's functions, G_{ijk} and H_{ik} in eqns. (1) and (2) for a shear DD density, d_1, are given by

$$G_{111} = \frac{G}{\pi(\kappa+1)}\frac{1}{r^6}\left[12x_1^3x_2 - 4x_2^3x_1\right] \tag{3}$$

$$G_{221} = \frac{G}{\pi(\kappa+1)}\frac{1}{r^6}\left[12x_2^3x_1 - 4x_1^3x_2\right] \tag{4}$$

$$G_{121} = G_{211} = \frac{-G}{\pi(\kappa+1)}\frac{1}{r^6}\left[2x_1^4 + 2x_2^4 - 12x_1^2x_2^2\right] \tag{5}$$

$$H_{11} = \frac{-G}{2\pi(\kappa+1)}\frac{1}{r^2}\left[(\kappa-1)x_2 + 4\frac{x_1^2x_2}{r^2}\right] \tag{6}$$

$$H_{21} = \frac{-G}{2\pi(\kappa+1)}\frac{1}{r^2}\left[(\kappa-1)x_1 + 4\frac{x_2^2x_1}{r^2}\right] \tag{7}$$

where

$$\kappa = \begin{cases} 3-4\nu & \text{for plane strain} \\ \dfrac{3-\nu}{1+\nu} & \text{for plane stress} \end{cases}$$

G and ν are the shear modulus and Poisson's ratio, respectively and $r = \sqrt{x_1^2 + x_2^2}$. For a normal DD density, d_2, the Green's functions are

$$G_{112} = \frac{-G}{\pi(\kappa+1)}\frac{1}{r^6}\left[2x_1^4 + 2x_2^4 - 12x_1^2x_2^2\right] \tag{8}$$

$$G_{222} = \frac{-G}{\pi(\kappa+1)}\frac{1}{r^6}\left[2x_1^4 - 6x_2^4 + 12x_1^2x_2^2\right] \tag{9}$$

$$G_{122} = G_{212} = \frac{G}{\pi(\kappa+1)}\frac{1}{r^6}\left[12x_1x_2^3 - 4x_1^3x_2\right] \tag{10}$$

$$H_{12} = \frac{G}{2\pi(\kappa+1)}\frac{1}{r^2}\left[(\kappa-1)x_1 - 4\frac{x_2^2x_1}{r^2}\right] \tag{11}$$

$$H_{22} = \frac{-G}{2\pi(\kappa+1)} \frac{1}{r^2}\left[(\kappa-1)x_2 + 4\frac{x_2^3}{r^2}\right] \tag{12}$$

If we distribute displacement discontinuities of densities, d_k, over a number of curves, c_λ, then by superposition, the stresses and displacements at point Q become

$$\sigma_{ij}(Q) = \sum_{\lambda} \int_{c_\lambda} G_{ijk}(P,Q) d_k(P) dS(P) \tag{13}$$

$$u_i(Q) = \sum_{\lambda} \int_{c_\lambda} H_{ik}(P,Q) d_k(P) dS(P) \tag{14}$$

where the summation is performed over each of the curves, c_λ. If σ_{ij} or u_i are specified along c_λ, then eqns. (13) and (14) can be solved for the unknown DD densities, d_k. In practice it is necessary to discretize the curves, c_λ (*i.e.*, boundaries) into elements and assign a simple approximate functionality for d_k. For the case when Q approaches P, eqns. (13) and (14) become the standard indirect boundary element equations.

The main difference between the constant element and the node-centric formulation lies in the functionality of the DD distribution (Fig. 3). In the node-centric method, we assume a linear variation for the displacement discontinuity density, d_k, *i.e.*,

$$d_k(e) = D_k^{N_1} + \frac{x_1}{L}(D_k^{N_1} + D_k^{N_2}) \tag{15}$$

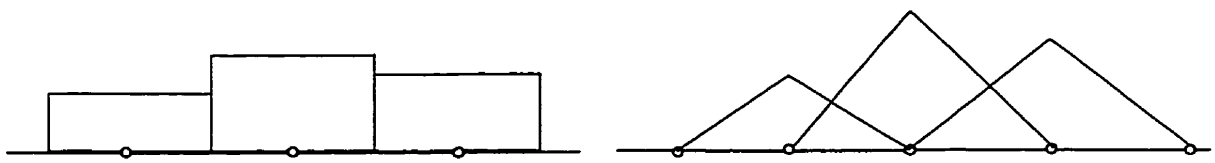

(a)
Block function
for a constant element

(b)
Hat function
for a node-centric element

Figure 3. Functionality of the distribution

where e denotes an element with length L, and N_1 and N_2 are the nodes located at the element ends. The integrals that need to be evaluated in eqns. (13) and (14) have the form

$$I^0_{ijk}(e) = \int G_{ijk}(x_1, x_2)\, dx_1 \tag{16}$$

$$I^1_{ijk}(e) = \int x_1 G_{ijk}(x_1, x_2)\, dx_1 \tag{17}$$

$$J^0_{ik}(e) = \int H_{ik}(x_1, x_2)\, dx_1 \tag{18}$$

$$J^1_{ik}(e) = \int x_1 H_{ik}(x_1, x_2)\, dx_1 \tag{19}$$

The integrations in eqns. (16)-(19) are done analytically and are tabulated in the appendix. Suppose the boundary of the problem to be considered is divided into P elements. It is necessary to find the values of the displacement discontinuities (normal and shear) which give the total stress and displacement components consistent with the boundary conditions. In general, if the boundary is represented by P elements, induced stresses and displacements at node m due to distributions of normal and shear displacement discontinuities (D_k) at node n can be written as

$$\sigma^m_{ij} = A^{mn}_{ijk} D^n_k \tag{20}$$

$$u^m_i = B^{mn}_{ik} D^n_k \tag{21}$$

where A_{ijk} and B_{ik} are the coefficient matrices. The influence coefficients for each node in the element are evaluated as

$$A^{mn}_{ijk} = \sum_e \alpha^{mn}_{ijk}(e) \tag{22}$$

with

$$\begin{bmatrix} \alpha^{mN_1}_{ijk}(e) \\ \alpha^{mN_2}_{ijk}(e) \end{bmatrix} = \frac{1}{x_1^{N_2} - x_1^{N_1}} \begin{bmatrix} x_1^{N_2} & -1 \\ -x_1^{N_1} & 1 \end{bmatrix} \begin{bmatrix} \bar{I}^0_{ijk}(e) \\ \bar{I}^1_{ijk}(e) \end{bmatrix}$$

where $x_1^{N_1}$ and $x_1^{N_2}$ are the local coordinates of the two nodes of the element (Fig. 2) and $\bar{I}_{ijk}$ and $\bar{J}_{ik}$ are defined as

$$\bar{I}^0_{ijk}(e) = t_{il}(e) I^0_{mlk}(e)\, t_{mj}(e)$$

$$\bar{I}^1_{ijk}(e) = t_{il}(e) I^1_{mlk}(e)\, t_{mj}(e) \tag{23}$$

$$\bar{J}^0_{ik}(e) = t_{il}(e) J^0_{lk}(e)$$

$$\bar{J}^1_{ik}(e) = t_{il}(e) J^1_{lk}(e) \tag{24}$$

and t_{ij} is the rotation matrix for the element, *i.e.*

$$t_{ij}(e) = \begin{bmatrix} \cos\theta_e & -\sin\theta_e \\ \sin\theta_e & \cos\theta_e \end{bmatrix} \tag{25}$$

where θ_e is the angle between the local x_1 and global x axis.

The displacement coefficient matrix, B_{ik}, is evaluated in the same manner of eqn. (22) by replacing I's by J's. The summation in eqn. (22) is performed over all the elements e which contain the node n, where n is either N_1 or N_2 of the element, based on the global node numbering system.

Eqns. (20) and (21) represent a set of linear algebraic equations which, after substitution of the appropriate boundary conditions, can be solved for the unknown displacement discontinuities D_k^n for each node.

2.1 Integration Ansatz

A mathematically rigorous handling of singular integrals involves smooth weighting functions, *i.e.*, C^n functions on smooth boundaries and C^m on boundaries at infinity. The values of m and n depend on the order of the singularity [*10*]. In the case of the DD method, the value of n and m should be at least 1. However when we use flat elements in discretizing the boundary, smooth boundaries cannot be maintained. Furthermore, even with a smooth boundary we have to deal with finite domains where the point of singularity is coincident with one of the end points.

Since we are using flat elements, the integrals are regular when the field point does not lie in the domain of the integration. The integrals can thus be obtained using standard integration. The integrations in eqns. (16)-(19) are done analytically and are tabulated in the appendix.

The procedure for dealing with the non-integrable singularity lying within the domain of integration is based on Hadamard's idea of the finite part integral. Accordingly, the integration is performed formally and evaluated by ignoring the infinite terms. Further justification for using the finite part integral is given in [*9*] using the continuation approach.

Hence, the formal integrals given in the appendix can be used with proper interpretation and modification. When the field point lies on one of the nodes, there will be two neighboring elements which exhibit singular behaviour. Following Hadamard's procedure, the integrals for the two elements are evaluated separately in the finite part sense. Thus when the element contains a singular point, we need to evaluate the integrals given in the appendix only at the non-singular end of the element.

In summary, we use the following integration ansatz:

1. If the singularity is at one of the end points, the integration is performed formally and evaluated at the opposite end, *i.e.* 'the non-singular end' of the domain (Fig. 4a).
2. When the domain is non-smooth, the normal direction at the node is assumed to be the mean of the normal directions of the elements which form the node (Fig. 4b).

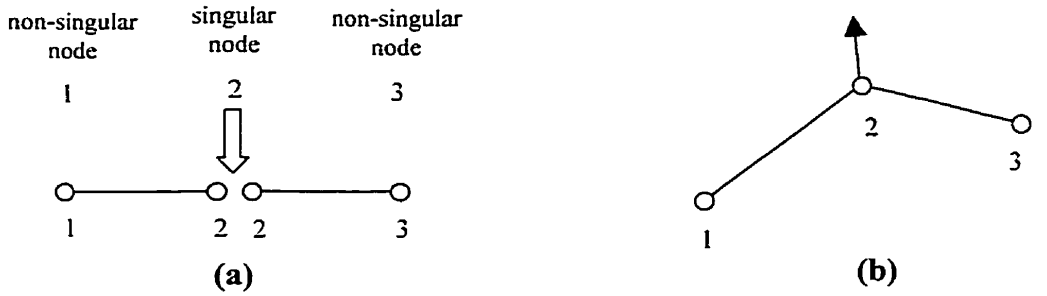

Figure 4. Integration procedure

In carrying out these integrations we note the special way the variation of the functions is constructed. Since this functionality (*i.e.*, the hat function) is dependent on the scale of the element, the integral should also possess the same scale dependency (or the scale invariance, so to speak). This means that when the element length is scaled by a factor λ, the value of the integral should scale by a factor λ^{α} where α is the order of the singularity [*10*]. This imposes the condition that the log r term in the integration appears with proper scaling of the element length H (Fig. 5) as the term $\log(r/H)$. For the limiting case $r \rightarrow 0$, the evaluation of the integrals is done in Hadamard's finite part sense [7].

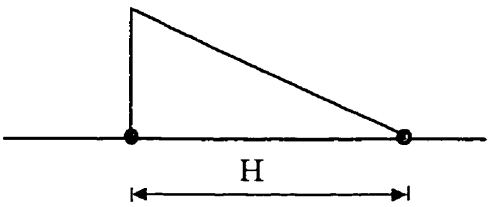

Figure 5. Element scaling factor H

3. Applications

In this section, two categories of applications using displacement discontinuities are presented. The first category, which we will refer to as Category A, deals only with crack problems which are inherently singular. The second Category B, involves problems with both cracks and holes. The crack problems are the traditional mainstay of the DD method while the hole or finite domain problems have been solved using either the direct boundary element method or the indirect fictitious stress technique.

In order to illustrate the versatility and robustness of the new node-centric DD method, we are presenting two groups of problems to test the validity of this method for both types of problems mentioned above, *i.e.*, applications with cracks and those involving both cracks and holes. The first group consists of test problems which have closed-form solutions and can also be analyzed with the classical boundary element method. These problems are used to evaluate the node-centric method for accuracy and efficiency. The second group of test problems is selected to show the versatility of the node-centric method. These more difficult problems have hitherto been considered intractable by the classical boundary element method.

3.1 Crack Problems – Category A

3.1.1 Single line crack in an infinite medium – Test problem (first group)

The single line crack problem typifies the early application of the DD method. It is an excellent test case because the closed-form solution is available [8, 9]. Consider a line crack discretized into 10 elements. Applying zero displacement discontinuity conditions at the ends of the crack, there remain 9 nodes where 18 unknown DD (normal and shear) values need to be calculated. For comparison, we use the same disretization with constant displacement discontinuities which requires that 20 unknowns be determined.

The analytical solution for the normal DD, D_2, for a single crack with constant internal pressure p is given in [9] as,

$$D_2 = \frac{(\kappa+1)p}{2G}\sqrt{b^2 - x_1^2} \tag{26}$$

where b is half the width of the crack. The cleavage stress distribution from the tip of the crack is given by

$$p\left\{\frac{|x_1|}{\sqrt{b^2 - x_1^2}} - 1\right\} \tag{27}$$

Fig. 6 compares the 9 values of the normal DD computed by the linear node-centric method with the 10 values computed by the constant element method and the analytical solution given by eqn. (26). A comparison of the cleavage stress distribution along the crack tip is provided in Fig. 7.

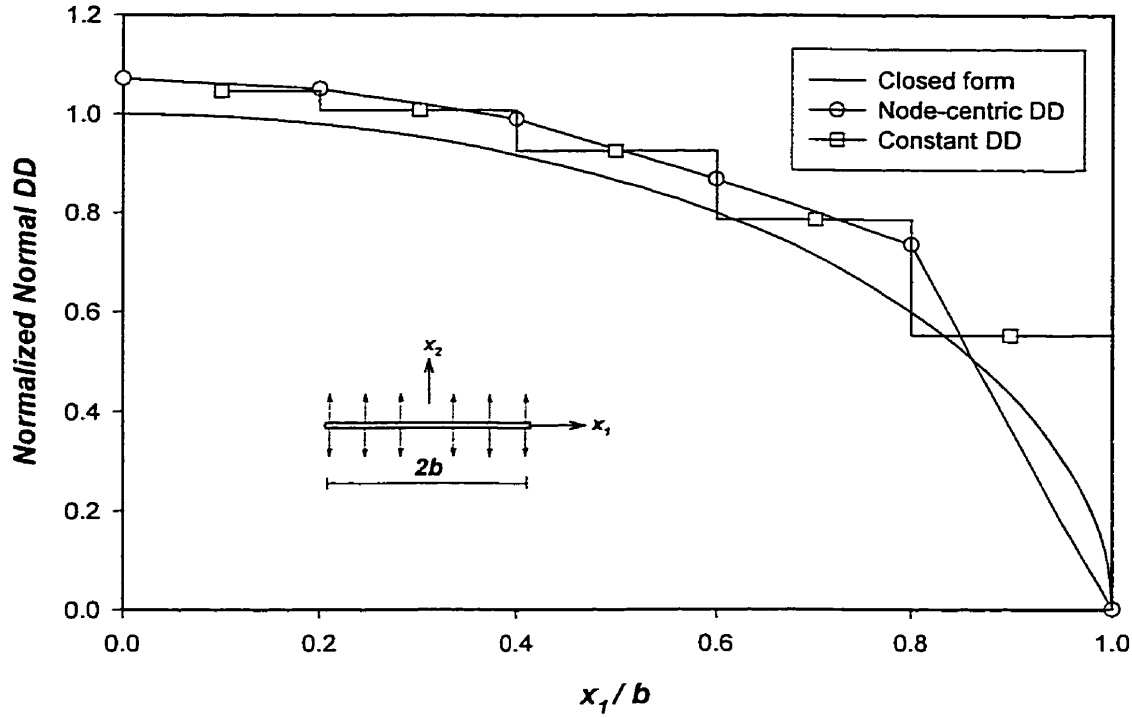

Figure 6. Normal displacement discontinuity solution for single crack

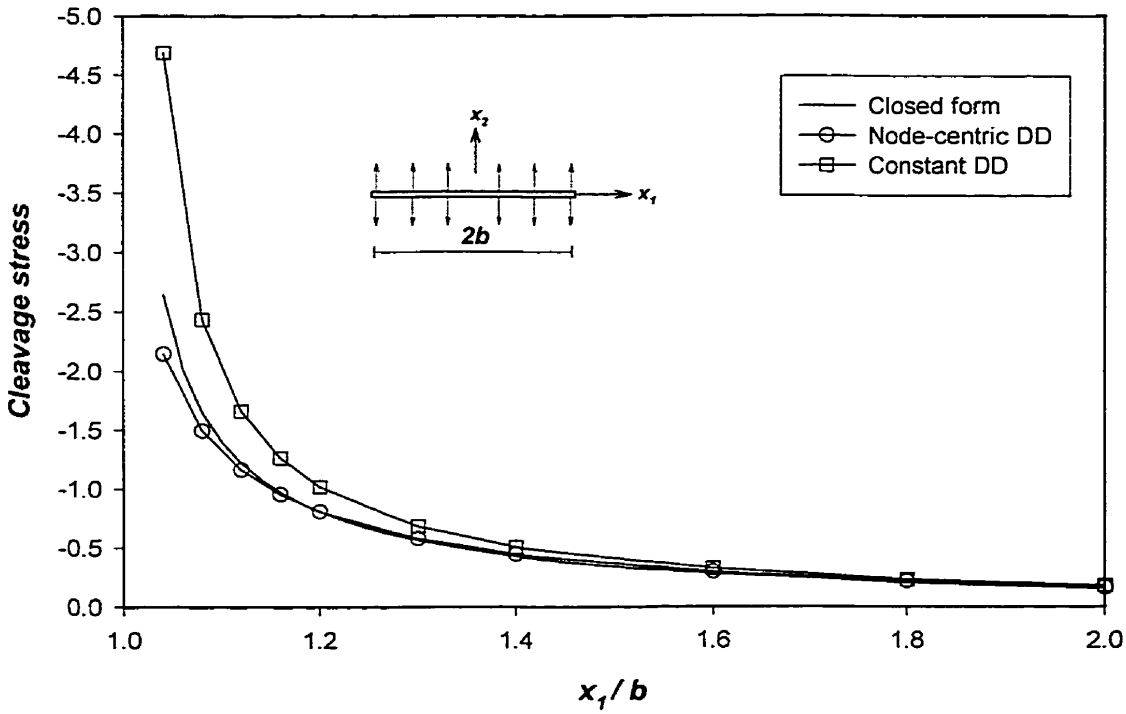

Figure 7. Cleavage stress variation along the crack tip

From Fig. 6 and Fig. 7, one can see that while the DD values computed by the new formulation and the conventional method are comparable, the clevage stress variation exhibits a remarkable improvement.

In order to test the robustness of the node-centric method with regard to relative element size, we subdivided the last element into two elements with a 10:1 ratio of the original length. The aim here is to show that such a subdivision, however small, always tends to improve the result. As shown in Fig. 8 the value of the normal DD is improved at every node.

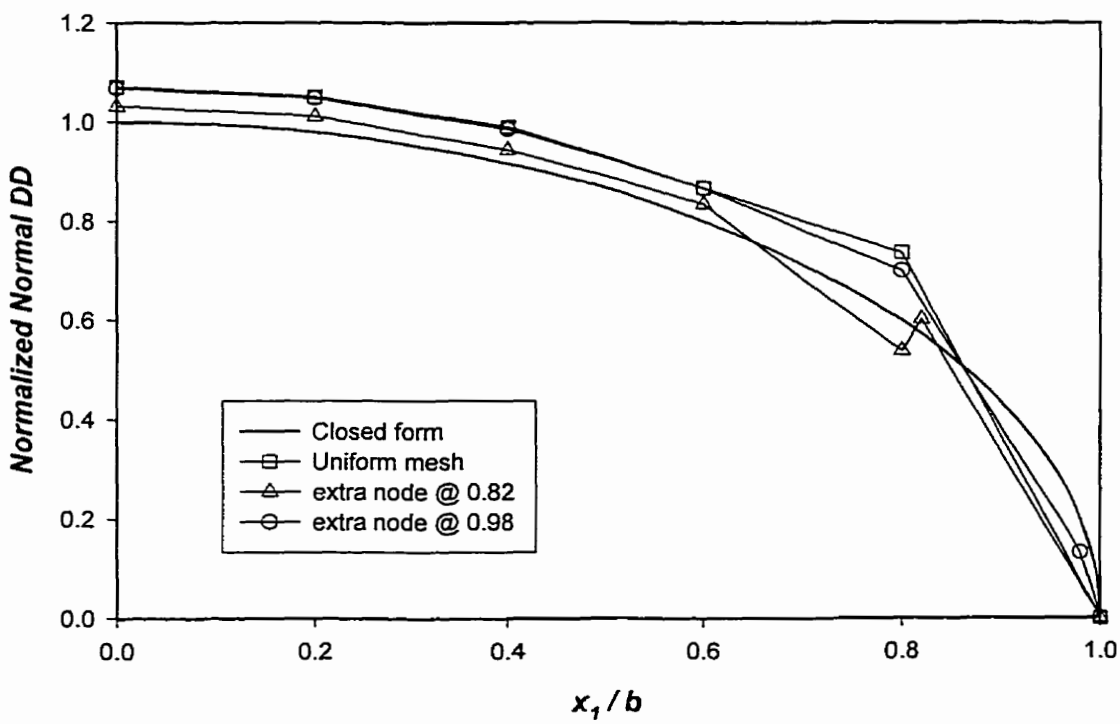

Figure 8. Influence of element size for the single crack problem

3.1.2 Intersecting Cracks – Test problems (second group)

Here, we consider two intersecting pressurized cracks in the form of a cross. This is an example of the class of physico-geometric situations which using the traditional DD method would need much finer discretization in the vicinity of the intersection because of the lack of inter-element continuity of the displacement discontinuities. Similar to the single crack problem, we discretize each crack into 10 elements. Since both cracks are subdivided uniformly, the centre node of one crack coincides with that of the other crack. We assign the unknown displacement discontinuities to each of the coinciding nodes independently. This is possible since in the DD method the cracks are modeled as a superposition of forces, instead of two separate boundaries. However, the stress state at the intersection point, which needs to be taken into consideration for the traction collocation of the external pressure, provides only one condition for the two intersecting nodes. As a consequence, we are left with only one pair of independent collocation equations at the intersecting nodes. This results in an under-determined system of equations. However, one can easily furnish an additional pair of equations by collocating tractions at any non-nodal boundary point such as the mid-point of an element at the nodes of coincidence. The conventional wisdom is that the best performance is obtained by collocating at the points at which the unknown parameters are assigned. By collocating at a point other than a node, we are not straying away from this convention since all the nodal positions have already been taken care of. In order to test the robustness of the method, we carried out three sets of numerical experiments:

1. The two cracks share nodes at the intersection (Fig. 9a),

2. the centre node of the horizontal crack is moved along the vertical crack a distance of 20% of the element length (Fig. 9b),
3. both centre nodes are moved by 20% of the element length along their respective cracks from the original positions (Fig. 9c).

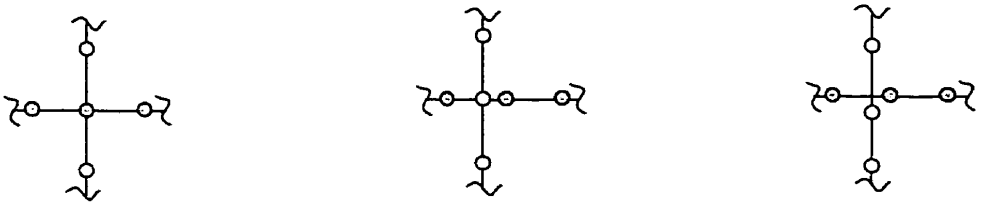

a - Node sharing **b - Node lies on one of the elements** **c - No node sharing**

Figure 9. Different node configurations for the intersection of two cracks

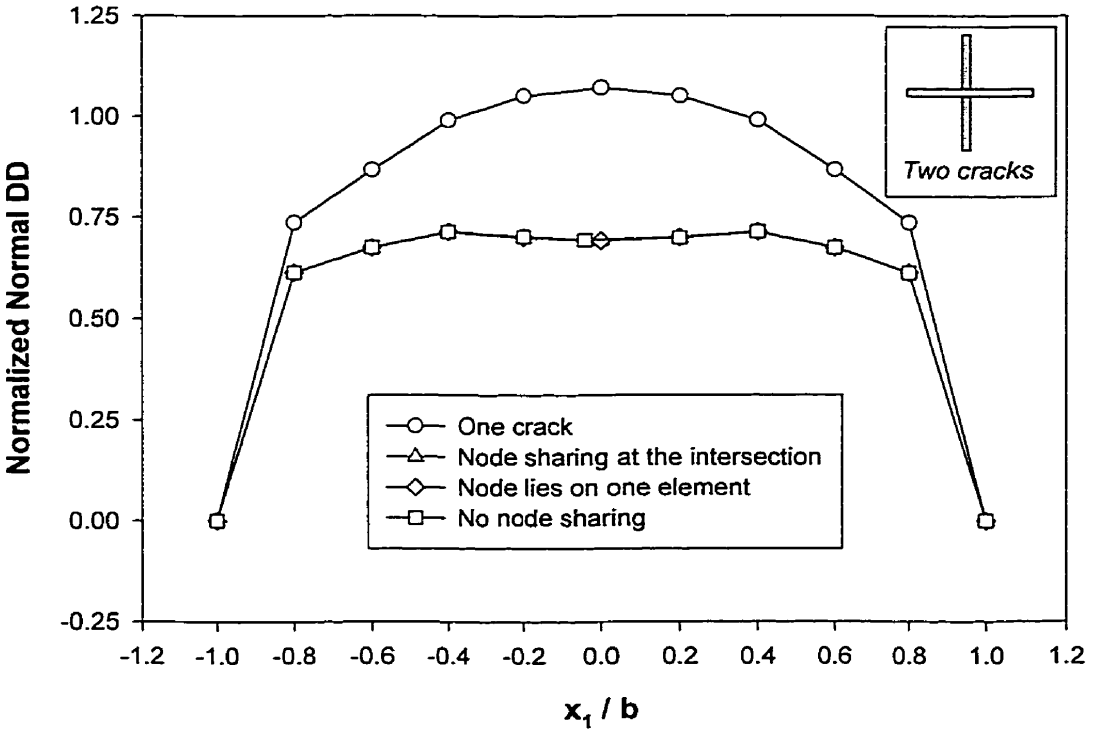

Figure 10. Normal DD variation along horizontal crack for different "centre" node positions

Fig. 10 depicts the DD values for the horizontal crack for several positions of the "centre" node. The solution for a single crack is also provided as a convenient magnitude comparison. It is difficult to get an explicit analytical expression as the DD distribution of the cruciform crack in order to evaluate the accuracy of the node-centric method. However, from [10] we can obtain the strain energy, W, of the system as

$$W = 1.4914\pi\frac{(\kappa+1)}{8G} \tag{28}$$

for a curciform crack of unit half length subjected to uniform unit pressure. From our DD calculations using 10 elements, we get a value of $1.55\pi\frac{(\kappa+1)}{8G}$ for the strain energy which is within 4.1% of the exact answer while the constant DD method gives $1.64\pi\frac{(\kappa+1)}{8G}$ which is about 9.8% of the exact answer.

It should be emphasized here that the 9.8% accuracy for the constant DD is achieved only by careful discretization so that the collocation points lie farthest to the inter-element discontinuity. Otherwise the accuracy will be much worse. This problem does not arise in the node-centric approach.

As shown in Fig. 10, the results are very insensitive to the node configuration of the intersecting cracks. In a second set of experiments, we considered the non-symmetric intersection of the two cracks (Fig. 11). The results for different positions of the intersection point are given in Fig. 12.

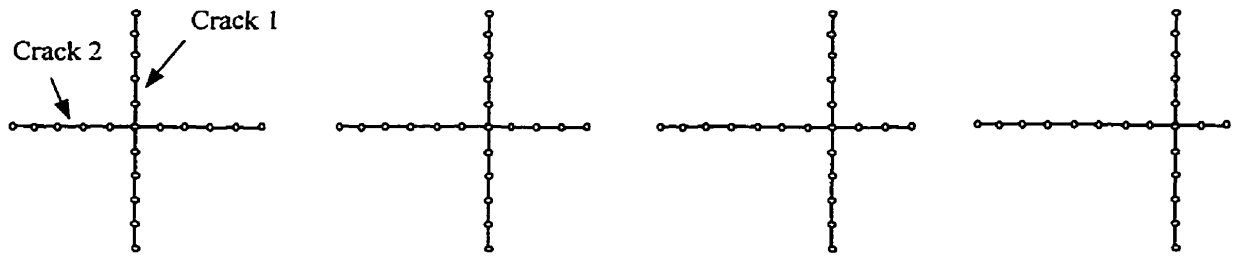

At the centre | **At 1 element from the centre** | **At 2 elements from the centre** | **At 3 elements from the centre**

Figure 11. Different locations of crack 1 relative to the centre of crack 2

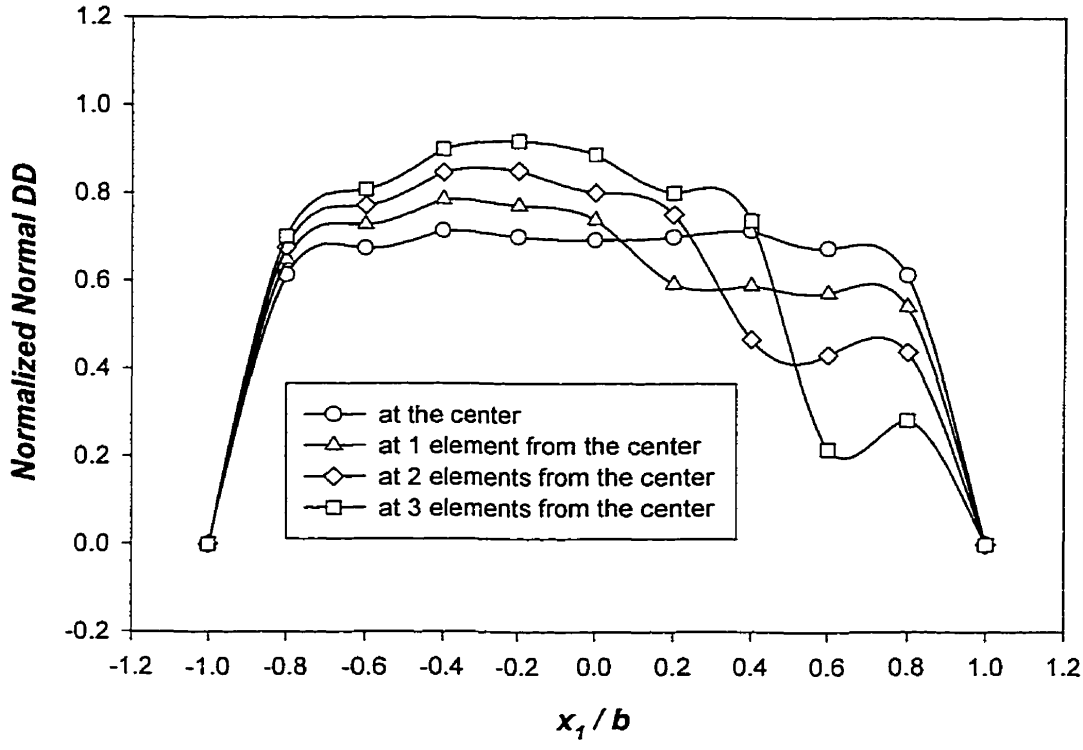

Figure 12. Normal DD variation along the horizontal crack for two cracks intersecting at different locations

In the third set of numerical experiments, we considered the symmetric intersection of three cracks. As in the previous cases, each crack is subdivided into equal length elements. For this problem there are three nodes which share the same physical location. Each node can again be assigned independent unknown discontinuities which leaves us with a deficiency of four equations after the boundary conditions are specified at the nodes. So, similar to the two crack case, the collocation is done at two non-nodal points along the other two cracks. Fig. 13 shows the displacement discontinuity profile along one of the three cracks. The displacement discontinuity profiles along the other two cracks are undistinguishable from the horizontal one.

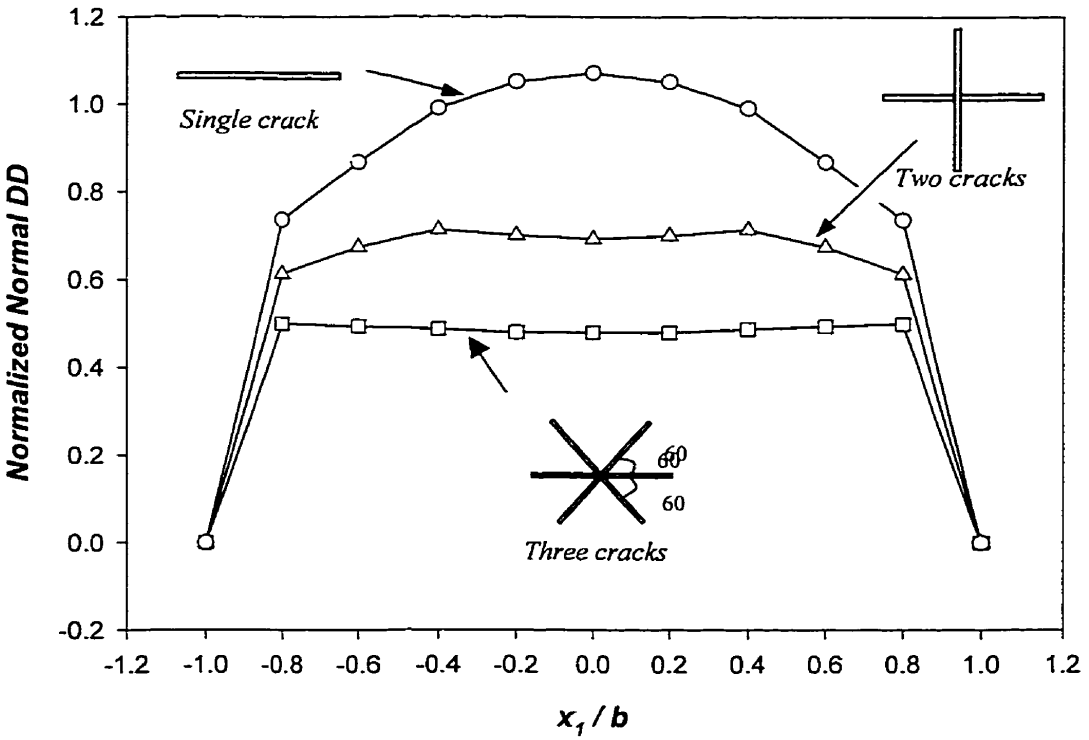

Figure 13. Displacement discontinuity variation along the horizontal crack

3.2 Excavation Type Problems with and without Intersecting Cracks – Category B

3.2.1 Uniformly pressurized circular hole – Test problem (first group)

This problem is analysed using 36 nodes uniformly placed along the boundary of a circle of radius, a. The tractions at the nodes are based on the tangent plane of the circular hole.

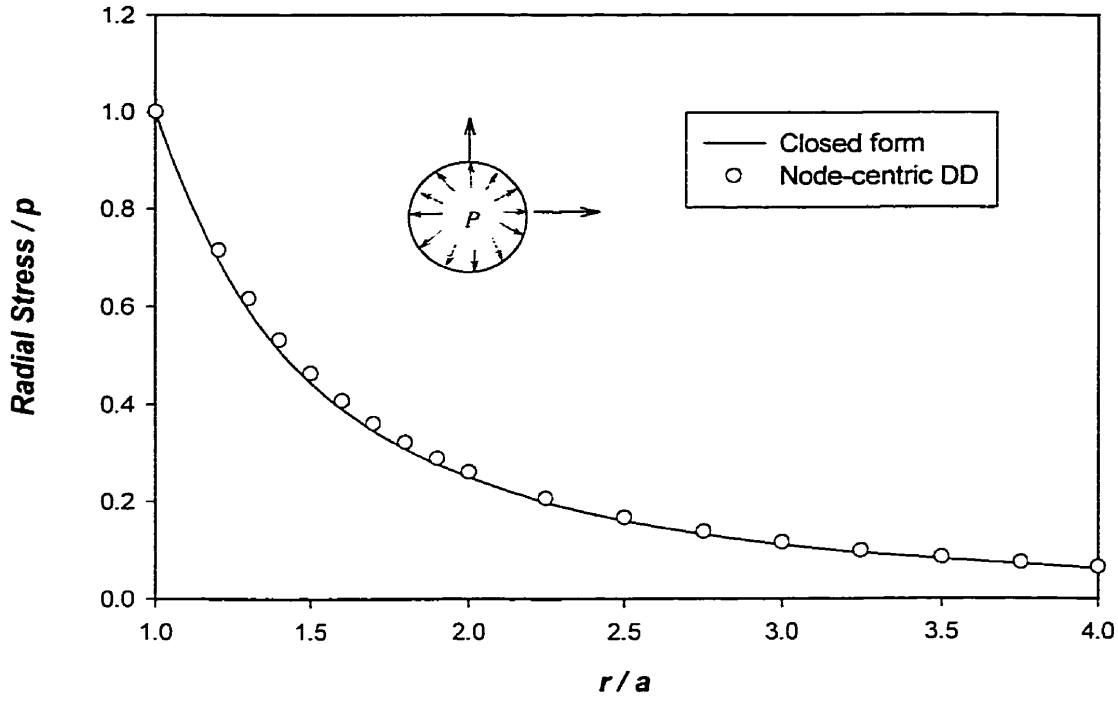

Figure 14. Radial stress variation for a circular hole

Fig. 14 compares the radial stress distribution outside the hole obtained from the node-centric DD method with the analytical solution [8]

$$\sigma_{rr} = p\frac{a^2}{r^2}. \tag{29}$$

3.2.2 Circular hole with intersecting crack – Test problem (second group)

Having established the applicability of the node-centric DD method to external problems, we consider the more difficult problem of the intersection of a joint or fault with the boundary of an excavation. Again we need to deal with the issue of stress collocation when nodes coincide (node sharing) as discussed in section 3.1.

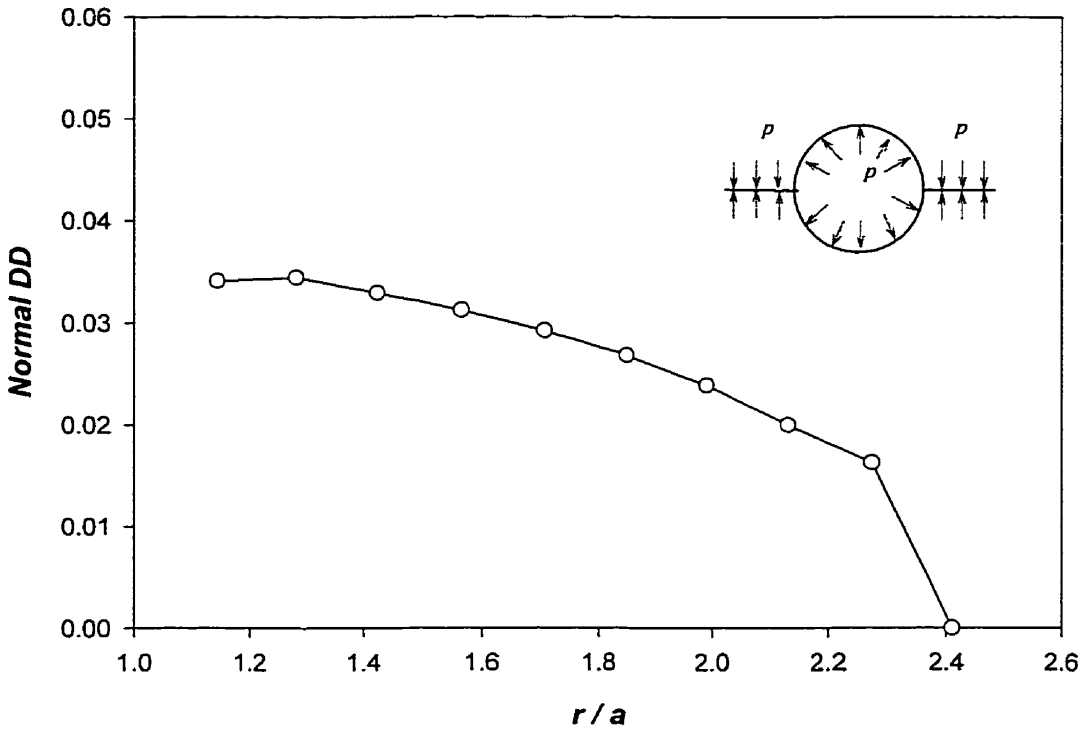

Figure 15. Displacement discontinuity solution along the crack

Fig. 15 illustrates the normal DD variation along the crack when the same uniform pressure is applied in the hole as well as in the crack. The variations of the shear and normal displacement discontinuities along the periphery of the circle are depicted in Fig. 16. We

emphasize here that with the node-centric DD method, the crack and the hole are discretized independently. It has common practice with the constant DD elements to discretize them in conjunction so that the effects of the infinite stresses at the element ends are minimized.

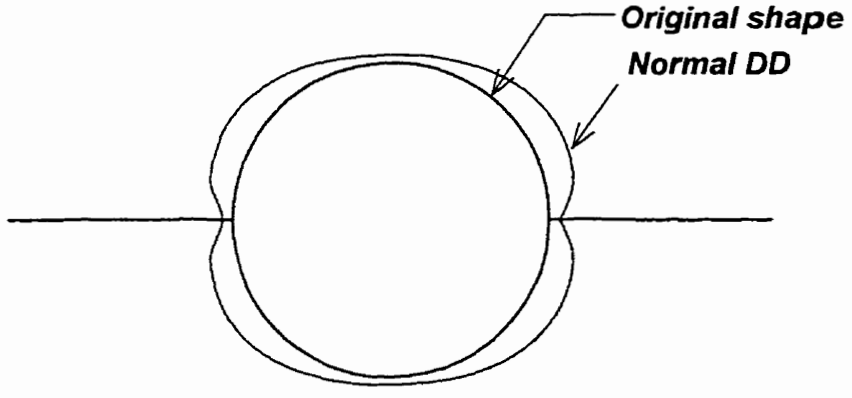

(a) Normal displacement discontinuity variation on the surface of the hole

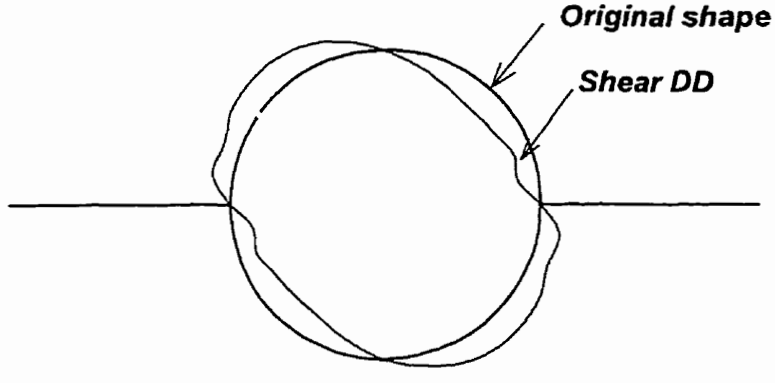

(b) Shear displacement discontinuity variation on the surface of the hole

Figure 16. Variation of normal and shear displacement discontinuities on the surface of the hole

4. Discussions

Through several examples, we sought to test the viability of the node-centric DD method as a general purpose numerical technique for plane linear elastic stress analysis.

4.1 Flexibility of indirect formulation

We have shown that the indirect formulation is highly adaptable for a variety of physico-geometric problems. Traditionally, the direct boundary element method has been considered too inflexible to be considered as a general purpose method since it implicitly requires construction of an integral equation. However its other incarnation, the indirect boundary element formulation, eliminates this requirement. In the indirect method, distributions of various forms of multiple forces (single force, doublet etc.) can be used to solve a wide range of physico-geometric problems. The DD method in which distributions consist of double forces appears to be the most flexible of all. Of course one must deal with the pathological nature of the singularities. In the light of the integration ansatz presented in this paper, this difficulty has been overcome.

4.2 Inter-element continuity and node-sharing

A significant breakthrough of the node-centric formulation is the handling of node-sharing and coincidence of nodes (node-sharing of higher types) in a systematic way (see examples in 3.1.2). The issue of node sharing has been one of the stumbling blocks of the DD method. In the present context, it was the inability to formulate the DD method in a node-centric manner. In the node-centric formulation, assignment of quantities at the nodes ensures inter-element continuity of these quantities in a natural way. As shown in references [5] and [12], lack of inter-element continuity can introduce such large errors in the stress calculations as to render them useless for highly interacting elements. In contrast, the node-centric formulation is particularly attractive in this respect.

4.3 Higher-order displacement discontinuity method

A superficial perusal of the present work may mislead the reader into thinking that this is an attempt to use a higher-order DD variation than the constant DD element originally presented by Crouch [11]. This was the case with the early work by Crawford and Curran [12] and by Shou and Crouch [13]. But all of the previous works did not, to quote Shou and Crouch, 'make the tractions and displacements continuous at the nodes between elements'. This is precisely the aim of the node-centric method. Regarding the order of the displacement discontinuity, we should emphasize here that, a linear variation along the element is the lowest order one can use.

4.4 New integration scheme

The salient features of the node-centric DD formulation are the C^0 inter-element continuity of the displacement discontinuities and the need for a suitable integration scheme that takes into account the linear piece-wise functionality of the loading. In a general three-dimensional problem, this would require a new integration methodology (see [6], [14] and [15] for a background to the new integration methodology). One could use the same approach for the two-dimensional node-centric method. But as we have shown in this paper, it is possible to develop closed-form integrations which results in less bookkeeping effort. A suitable integration ansatz was developed using closed-form solutions available from integral tables [16].

4.5 Influence of element size and its impact on general purpose large scale field problems

In general purpose large scale applications, very complex physico-geometric situations can arise. Certainly for many practical problems discretizing the boundary into uniformly sized elements is not possible. The unbounded stresses due to a discontinuous DD at the node adversely affect the stress calculations in the surrounding elements. One may encounter complex situations arising from intersection of simpler geometric elements such as the intersection of cracks or cracks emanating from holes or passing through them. In such geometric situations, it is virtually impossible to avoid the unbounded stress regions in the calculations. In the case of intersecting cracks, for example, unless careful re-discretization is done, unbounded stresses along one crack would adversely affect the stress calculations along the other crack. The present node-centric DD formulation intrinsically avoids having unbounded stresses unless otherwise warranted by the geometry of the problem, e.g., a corner. There would not be any need for a re-discretization. Hence the method should be robust for general purpose large scale applications.

4.6 Special case of a general framework

As alluded to earlier, this two-dimensional DD method is part of a much wider framework of a node-centric boundary element method for two-dimensional and three-dimensional problems. Here, the nodes play the central role and the elements take up the supporting role of acting as support for integration and interpolation. The C^0 continuity should be viewed as a special case of general C^N continuity in which case the node can be thought of possessing continuity of differentials up to order N. As mentioned earlier, the element shape function

plays its part mainly during the integration stage. Although this element shape function can be defined independently, in order to maintain conformity between adjacent elements, one needs to adhere to the same set of differentials for each element surrounding the node. In the present work, we have formally defined the tractions to possess C^1 continuity at the nodes. However, for the element discretization and integration, we assumed only a C^0 continuity.

Conclusion

We have shown the efficacy of node-centric formulation through several examples presented in this paper. Even though node sharing has been implemented in both the direct boundary method and fictitious stress technique, node sharing using the DD method has not been possible until because of its higher-order singularity.

Through a proper integration ansatz, we have overcome the associated difficulties by imposing a continuous variation of the displacement discontinuities. Without a node-centric formulation, the ability of the DD method to solve practical geomechanics problems such as joints intersecting excavations is limited. In such problems, a more careful and finer discretization is usually required to overcome the infinite stresses generated at the element end. The node-centric formulation obviates this problem by imposing stress continuity.

The extension of the methodology presented in this paper to three-dimensional problems has been completed by the authors and has been accepted for publication [17].

Acknowledgment

The financial support provided by NSERC through an operating grant (J.H. Curran) and postgraduate scholarship (T.E. Yacoub), CANMET through the Canada/Ontario Mineral Development Agreement (Contract # 23440-4-1310/01-SQ) and *Rocscience* Inc. are gratefully acknowledged.

References

1. Brady B. H. G. and J. W. Bray, 'The boundary element method for elastic analysis of tabular orebody extraction, assuming complete plane strain', *Int. J. Rock Mech. Min. Sci. & Geomech. Abstr.* **15**, 29-37 (1978).
2. Wiles T. D. and J. H. Curran 'A general 3-D displacement discontinuity method', *Proc. 3rd Int. Conf. Num. Meth. Geomech.*, 103-111 (1982).
3. Salamon M.D.G., 'Elastic analysis of displacements and stresses induced by the mining of seam or reef deposits - part I', *J. South African Inst. Mining Metallurgy*, **64**, 129-149 (1963).
4. Starfield, A.M. and S.L. Crouch, 'Elastic analysis of single seam extraction', Rock Mechanics (H.R. Hardy Jr. and R. Stefhanko (eds.), ASCE, New York, 421-439, 1972
5. Crouch S. L. and A. M. Starfield, *Boundary Element Methods in Solid Mechanics*, George Allen & Unwin, London, 1983.
6. Vijayakumar S. and D. E. Cormack, 'An invariant imbedding method for singular integral evaluation on finite domains', *SIAM J. App. Math.*, **48**, 1335-1349 (1988).
7. Hadamard, J., *Lectures on Cauchy's Problem in Linear partial Differential Equations*, Yale University Press, New Haven, CT, 1923.

8. England A. H., *Complex Variable Methods in Elasticity*, Wiley-Interscience, 1971.

9. Sneddon I. N. and M. Lowengrub, *Crack Problems in the Classical Theory of Elasticity*, John Wiley & Sons, Inc., 1969.

10. Stallybrass M. P., 'A Pressurized crack in the form of a cross', *Quart. Journ. Mech. and Applied Math.*, **23**, Part I (1970).

11. Crouch S. L. 'Solution of plane elasticity problems by the displacement discontinuity method', *Int. J. Num. Meth. Engng.* 10, 301-343 (1976).

12. Crawford A. M. and J. H. Curran, 'Higher order functional variation displacement discontinuity elements', *Int. J. Rock Mech. Min. Sci. & Geomech. Abst.*, **19**, 143-148 (1982).

13. Shou K. J. and S. L. Crouch, 'A higher order displacement discontinuity method for analysis of crack problems', *Int. J. Rock Mech. Min. Sci. & Geomech. Abst.*, **32**, 49-55 (1995).

14. Vijayakumar S. and D. E. Cormack, 'A new concept in near-singular integral evaluation: The continuations approach', *SIAM J. App. Math.*, **49**, 1285-1295 (1989).

15. Rosen D. and D. E. Cormack, 'The continuation approach: A general framework for the analysis and evaluation of singular and near-singular integrals', *SIAM J. App. Math.*, **55**, 723-762 (1995).

16. Toma J. J., *Engineering Mathematics Handbook*, Third Edition, McGraw-Hill, New York, 1987.

17. Vijayakumar S., Yacoub T.E. and Curran J.H. A node-centric indirect boundary element method: Three-dimensional displacement discontinuities, *accepted for publication in Comput. and Structures.*

Appendix

2-D Green's function integrals for constant and linear variation of shear and normal displacement discontinuities

	Constant	Linear
Shear DD	$I^0_{111} = \frac{G}{\pi(\kappa+1)}\left[\frac{3x_2}{r^2} - \frac{2x_2^3}{r^4}\right]$	$I^1_{111} = \frac{G}{\pi(\kappa+1)}\left[\frac{4x_1x_2}{r^2} - \frac{2x_1x_2^3}{r^4} - 2\tan^{-1}\left(\frac{x}{z}\right)\right]$
	$I^0_{221} = \frac{G}{\pi(\kappa+1)}\left[-\frac{x_2}{r^2} + \frac{2x_2^3}{r^4}\right]$	$I^1_{221} = \frac{G}{\pi(\kappa+1)}\left[-\frac{2x_1x_2}{r^2} + \frac{2x_1x_2^3}{r^4}\right]$
	$I^0_{121} = \frac{G}{\pi(\kappa+1)}\left[-\frac{x_1}{r^2} + \frac{2x_2^2x_1}{r^4}\right]$	$I^1_{121} = \frac{G}{\pi(\kappa+1)}\left[\frac{4x_2^2}{r^2} - \frac{2x_2^4}{r^4} + \ln\left(\frac{r}{H}\right)\right]$
	$J^0_{11} = \frac{1}{2\pi(\kappa+1)}\left[\frac{x_1x_2}{r^2} - \frac{(\kappa+1)}{2}\tan^{-1}\left(\frac{x_1}{x_2}\right)\right]$	$J^1_{11} = \frac{1}{2\pi(\kappa+1)}\left[-\frac{x_2^3}{r^2} - \frac{(\kappa+3)}{2}x_2\ln\left(\frac{r}{H}\right)\right]$
	$J^0_{21} = \frac{1}{2\pi(\kappa+1)}\left[\frac{x_2^2}{r^2} - \frac{(\kappa-1)}{2}\ln\left(\frac{r}{H}\right)\right]$	$J^1_{21} = \frac{1}{2\pi(\kappa+1)}\left[-\frac{(\kappa-1)}{2}x + \frac{x_1x_2^2}{r^2} + \frac{(\kappa-3)}{2}\tan\left(\frac{x_1}{x_2}\right)\right]$
Normal DD	$I^0_{112} = \frac{G}{\pi(\kappa+1)}\left[-\frac{x_1}{r^2} + \frac{2x_2^2x_1}{r^4}\right]$	$I^1_{112} = \frac{G}{\pi(\kappa+1)}\left[\frac{4x_2^2}{r^2} - \frac{2x_2^4}{r^4} + \ln\left(\frac{r}{H}\right)\right]$
	$I^0_{222} = \frac{G}{\pi(\kappa+1)}\left[-\frac{x_1}{r^2} - \frac{2x_2^2x_1}{r^4}\right]$	$I^1_{222} = \frac{G}{\pi(\kappa+1)}\left[-\frac{2x_2^2}{r^2} + \frac{2x_2^4}{r^4} + \ln\left(\frac{r}{H}\right)\right]$
	$I^0_{122} = \frac{G}{\pi(\kappa+1)}\left[-\frac{x_2}{r^2} + \frac{2x_2^3}{r^4}\right]$	$I^1_{122} = \frac{G}{\pi(\kappa+1)}\left[-\frac{2x_1x_2}{r^2} + \frac{2x_1x_2^3}{r^4}\right]$
	$J^0_{12} = \frac{1}{2\pi(\kappa+1)}\left[\frac{x_2^2}{r^2} + \frac{(\kappa-1)}{2}\ln\left(\frac{r}{H}\right)\right]$	$J^1_{12} = \frac{1}{2\pi(\kappa+1)}\left[\frac{(\kappa-1)}{2}x_1 + \frac{x_1x_2^2}{r^2} - \frac{(\kappa+1)}{2}x_2\tan^{-1}\left(\frac{x_1}{x_2}\right)\right]$
	$J^0_{22} = \frac{1}{2\pi(\kappa+1)}\left[\frac{x_1x_2}{r^2} + \frac{(\kappa+1)}{2}\tan^{-1}\left(\frac{x_1}{x_2}\right)\right]$	$J^1_{22} = \frac{1}{2\pi(\kappa+1)}\left[-\frac{x_2^3}{r^2} + \frac{(\kappa-1)}{2}x_2\ln\left(\frac{r}{H}\right)\right]$

Appendix B

Paper II - "A Node-Centric Indirect Boundary Element Method: Three-Dimensional Displacement Discontinuities"

To appear in the Computers and Structures

A Node-Centric Indirect Boundary Element Method: Three-Dimensional Displacement Discontinuities

S. Vijayakumar, T. E. Yacoub and J. H. Curran[§]

Rock Engineering Group, Dept. of Civil Engineering, University of Toronto
Toronto, Ontario, Canada, M5S 1A4

Abstract

An indirect boundary element formulation based on unknown physical values being defined only at the nodes (vertices) of a boundary discretization of a linear elastic continuum is introduced. As an adaptation of this general framework, a linear displacement discontinuity density distribution using a flat triangular boundary discretization is considered. A unified element integration methodology based on the continuation principle is introduced to handle regular as well as near-singular and singular integrals. The boundary functions that form the basis of the integration methodology are derived and tabulated in the appendix for linear displacement discontinuity densities.

The integration of the boundary functions is performed numerically using an adaptive algorithm which ensures a specified numerical accuracy. The applications include verification examples which have closed-form analytical solutions as well as practical problems arising in rock engineering. The node-centric displacement discontinuity method is shown to be numerically efficient and robust for such problems.

(No. of Figures: 14 No. of Tables: 1 No. of Refs: 21)

Keywords: Displacement Discontinuity Method, Node-centric, Adaptive integration, Singular integrals, collocation, continuation

---

§ Author to whom correspondence should be addressed

1. Introduction

The displacement discontinuity method (DDM), which is an offshoot of the classical boundary element method (BEM), has been successfully applied to geomechanics and fracture mechanics problems [1, 2, 3] which, using traditional numerical techniques were considered to be intractable due to differing geometric scales. In fracture mechanics, one deals with cracks of lengths several orders of magnitude greater than the surface separation. Similarly, in geomechanics, one considers faults and joints which have very large aspect ratios. In essence, DDM is ideally suited to such problems.

For the first generation of DDM applications, a constant element formulation was sufficient to obtain reasonably accurate numerical results. When higher accuracy is required or more intricate geometries are involved, the general tendency has been merely to increase the number of sub-divisions of the boundary while keeping the same functionality. This is akin to the *h*-version approach in finite element method. This approach is taken due to conceptual difficulties arising from the mathematics related to the principal value [4] and finite part integrals [5].

In subsequent developments, researchers have taken several directions in improving DDM. These improvements have focused on specific aspects of the method. However these improvements have either been inadequate or have created new difficulties. Notable among them are the following:

(i) Increasing the order of the weighting (or interpolation) function in order to obtain higher accuracy. For instance, recently Shou *et. al.* [6] introduced a higher-order (bi-quadratic) DD formulation in which nine collocation points are spread over a nine element patch, centered at the source element. This method, however, does not

ensure continuity between elements.

(ii) Developing new integration methods to improve efficiency and robustness. Kuriyama and Mizuta [7] performed closed-form integrations for 3D triangular elements. An important shortcoming of their derivation is that the integrations become unbounded when the center of gravity of an element lies on the prolongation of the side of another element.

(iii) Introducing hybrid methods to widen the scope of applicability. For example, Cayol and Cornet [8] coupled direct linear boundary elements with constant DD elements. The extension of their method to higher order DD elements requires internal nodes. The lack of node sharing between elements greatly increases the overall number of nodes in comparison with the node-centric approach (Fig. 1).

(iv) Using the Galerkin technique to overcome the difficulty involved in the evaluation of the singular integrals [9]. However, the required number of integrations increases exponentially (*i.e.*, $O(n^2)$) in the Galerkin formulation which considerably increases the computational effort in generating the matrix of influence coefficients [10].

The node-centric method being proposed in this paper examines the DDM in a more general way and thus solves several of the aforementioned problems.

One of the major obstacles to the development of a continuous DD formulation has been the absence of a suitable integration methodology for singular and near-singular integrals. Notwithstanding the problems associated with the element integration, there is a natural way to formulate DDM that avoids these difficulties. This is achieved by considering nodes as the primary geometric entity along with the normal vectors to the surface, and other geometric primitives such as curvatures at the nodes. The shape of an

element should play a subordinate role as support for interpolation and integration. This is the underlying philosophy of the node-centric formulation. In the node-centric context, the element shape can be thought of as an artifact rather than as an intrinsic parameter of the problem. The unknown values of the DD distribution are, in conformation to the philosophy of node-centricity, defined at the nodes only. An important advantage of defining DD values at the nodes rather than at some convenient collocation points inside the element is that the nodes lie on the actual boundary. All the boundary conditions are specified only at these nodes, thus maintaining fidelity to the physical problem.

In this paper, we start with a general outline of the node-centric displacement discontinuity method. We then specialize the node-centric method to a linear boundary discretization (*i.e.* flat elements). Since unknown values are defined at the nodes, the minimum functionality of the DD density variation is linear. The unified boundary element integration approach developed by Vijayakumar, Yacoub and Curran [11] is used to derive boundary functions for the displacement discontinuity Green's functions with constant and linear distributions. These boundary functions can then be integrated numerically along the edges of the elements.

Several numerical examples are presented in this paper. The examples are divided into two categories. The first category deals with problems that have closed-form solutions which can be used to test the accuracy and robustness of the method. The second category deals with geomechanics applications that require a more robust DD formulation than provided by the constant DDM.

2. Node-centric formulation

Consider a homogenous, isotropic, linear elastic material subjected to a displacement discontinuity density, d_k, at a point P (Fig. 2). The stresses, σ_{ij}, and the displacements, u_j, at any point Q, in the domain can be represented by

$$\sigma_{ij}(Q) = G_{ijk}(P,Q)\, d_k(P) \tag{1}$$

$$u_i(Q) = H_{ik}(P,Q)\, d_k(P) \tag{2}$$

Throughout this paper repeated indices indicate the usual summation convention where i, j, k = 1, 2, 3. The Green's functions G_{ijk} and H_{ik} in eqns. (1) and (2) are given in Appendix 1.

If we distribute displacement discontinuities of densities, d_k, over surface patches s_λ, using the superposition principle, the stresses and displacements at point Q can be written as

$$\sigma_{ij}(Q) = \sum_{\lambda} \int_{s_\lambda} G_{ijk}(P,Q) d_k(P) dS(P) \tag{3}$$

$$u_i(Q) = \sum_{\lambda} \int_{s_\lambda} H_{ik}(P,Q) d_k(P) dS(P) \tag{4}$$

where the summation is performed over the number of the surface patches, λ. If σ_{ij} or u_i are specified over s_λ then eqns. (3) and (4) can be solved for the unknown DD densities, d_k. In practice it is necessary to discretize the surface patches, s_λ (*i.e.*, boundaries) into elements and assign an approximate functionality for d_k. For the case where Q approaches P on the boundary, eqns. (3) and (4) become the standard indirect boundary element equations.

In this paper, the DD densities, d_k are assumed to have a linear functionality.

Thus, the nodal values $D_k^{N_j}$ (Fig. 3) are given by

$$D_k^{N_j} = a_0 + a_1 x_1^{N_j} + a_2 x_2^{N_j} \tag{5}$$

where N_j are the nodes of the element k, and x_1 and x_2 are local coordinate axes in the plane of the element. For any element, k, the solution of eqn. (5) can be written as

$$\begin{bmatrix} a_0 \\ a_1 \\ a_2 \end{bmatrix} = \begin{bmatrix} 1 & x_1^{N_1} & x_2^{N_1} \\ 1 & x_1^{N_2} & x_2^{N_2} \\ 1 & x_1^{N_3} & x_2^{N_3} \end{bmatrix}^{-1} \begin{bmatrix} D_k^{N_1} \\ D_k^{N_2} \\ D_k^{N_3} \end{bmatrix} \tag{6}$$

For a given problem, the boundary is discretized into a number of surface elements (in our case triangles). The solution is given by the nodal displacement discontinuities (normal and two components of shear) which give total stress and displacement components consistent with the given boundary conditions.

In general, if the boundary is represented by p surface elements, components of induced stress and displacement at node m due to the distribution of normal and shear displacement discontinuities, D_k, at node n can be written as

$$\sigma_{ij}^m = A_{ijk}^{mn} D_k^n \tag{7}$$

$$u_i^m = B_{ik}^{mn} D_k^n \tag{8}$$

where the influence coefficient matrices A_{ijk} and B_{ik} are given by

$$A_{ijk}^{mn} = \sum_e t_{il} \left(\sum_{side} \alpha_{lpk}^{mn}(e) \right) t_{pj} \tag{9}$$

and

$$B_{ik}^{mn} = \sum_e t_{il} \left(\sum_{side} \beta_{lk}^{mn}(e) \right) \quad . \tag{10}$$

The index e indicates the element. The t_{ij}'s are the terms of the direction cosine matrix. Each term, t_{ij}, is defined as the dot product $l_i \cdot m_j$ of the two unit vectors l_i and m_j. The

l_i's and the m_j's represent the axes of the coordinate systems at the field point and the load point, respectively. α_{ijk}^{mn} can be evaluated as

$$\begin{bmatrix} \alpha_{ijk}^{mN_k}(e) \\ \alpha_{ijk}^{mN_{k+1}}(e) \end{bmatrix} = \frac{1}{x_p^{N_{k+1}} - x_p^{N_k}} \begin{bmatrix} x_p^{N_{k+1}} & -1 \\ -x_p^{N_k} & 1 \end{bmatrix} \begin{bmatrix} \bar{I}_{ijk}^{0}(e) \\ \bar{I}_{ijk}^{1}(e) \end{bmatrix} \tag{11}$$

where $x_p^{N_k}$ and $x_p^{N_{k+1}}$ are the local coordinates of the two nodes of each side of the element (Fig. 4). $\bar{I}_{ijk}^{0}$ and $\bar{I}_{ijk}^{1}$ are given by

$$\left.\begin{aligned} \bar{I}_{ijk}^{0} &= \int_{side} \Phi_{ijk}^{0}.(x_p \cos\theta - x_q \sin\theta)dx_p \\ \bar{I}_{ijk}^{1} &= \int_{side} \Phi_{ijk}^{1}.(x_p \cos\theta - x_q \sin\theta)dx_p \end{aligned}\right\} \tag{12}$$

The boundary functions Φ_{ijk}^{0} and Φ_{ijk}^{1}, which will be explained in section 3, are presented in Appendix 2. The angle θ is measured from x_1-axis of the element local coordinate system to the side on which the integration is performed.

In the same manner, β_{ik}^{mn} is evaluated using eqn. (12) by replacing the Φ's by Γ's (definitions of which are given in Appendix 2). Eqns. (7) and (8) represent a system of linear algebraic equations. After substitution of the appropriate boundary conditions, it can be solved for the unknown displacement discontinuities D_k^n at each node. The stress components as well as the displacement components at any interior points can then be calculated by substituting for D_k^n in eqns (7) and (8).

3. Integration methodology

The most intuitive notion of multi-dimensional integration is the summation of an area

measure multiplied by a function. This is the underlying principle in all numerical quadrature schemes. However, the element integration in the boundary element method involves the Green's function which is unbounded at one point. The Green's function at this singular point generally has an infinite value of varying order. The integrand is the Green's function multiplied by a weighting function. The position of the singular point and the order of singularity affect the behavior of the integrand dramatically.

Table 1: Various situations of singular, near-singular and non-singular integrals

	CASE 1	*CASE 2*	*CASE 3*	*CASE 4*
Singular	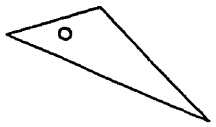	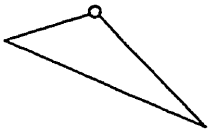	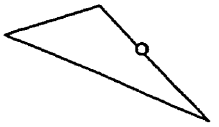	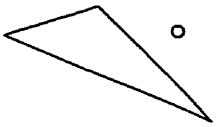
Near Singular	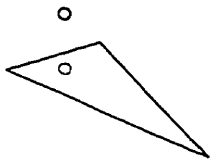	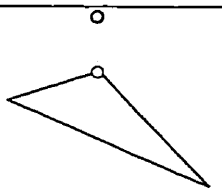	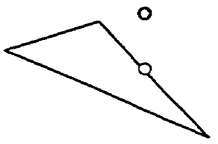	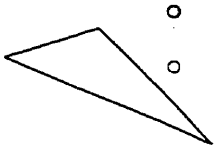
Non Singular				

o singular point o proximate singular

The boundary element integrals can be classified into three main groups: Non-singular (regular) integrals, near-singular integrals and singular integrals. The difference between the near-singular integrals and the regular integrals is not as sharp as the difference between the singular integrals and the near-singular integrals. Table 1 illustrates various situations that can arise during the integration of an arbitrary triangular

flat (linear) domain and a field point. In table 1, the singular point is the field point where the Green's function becomes unbounded and the proximate singular point is located at the base of the perpendicular to the element from the singular point.

As we move through the table from non-singular integral to singular integral, the level of difficulty of numerical quadrature by classical methods ranges from straightforward to outright impossible.

In addition to the above classification, there is an additional factor that contributes to the difficulty of the integral *i.e.*, type of the Green's function. The displacement discontinuity density possesses a higher order of singularity than either the direct BEM or indirect fictitious stress method.

In order to develop a unified method of integration for non-singular, near-singular and singular integrals of varying order of singularity, the continuation approach is used [12, 13, 14]. The basis of the continuation approach is that the value of the integral must vary smoothly as we continuously move from the non-singular integral to singular integral. Based on the continuation approach, a simplified form, called the *boundary function,* is derived. A systematic analysis of the *boundary function* for the Green's functions of continuum mechanics is presented in [11]. Here we briefly outline the approach.

The element integration is based on the observation that the Green's functions for homogeneous problems are functionally homogeneous, *i.e.*, they satisfy the condition that for an arbitrary real number λ

$$f(\lambda x_1, ..., \lambda x_n) = \lambda^{\alpha} f(x_1, ..., x_n) \tag{13}$$

where α is the degree of homogeneity [12].

In three dimensions, for an integration carried out over the $x_1 - x_2$ plane, the equation for the boundary function becomes

$$\int_{\Omega} f(x_1, x_2, x_3)\, dV = \int_{\partial\Omega} F(x_1, x_2, x_3) \boldsymbol{X} \cdot d\boldsymbol{S} \tag{14}$$

where $F = x_3^{\alpha} \int_{x_3}^{\infty} \frac{1}{\xi^{\alpha+1}} f(x_1, x_2, \xi)\, d\xi$, $\boldsymbol{X} = x_1 \boldsymbol{i} + x_2 \boldsymbol{j}$, $d\boldsymbol{S} = \hat{\boldsymbol{n}}\, ds$ and $\hat{\boldsymbol{n}}$ is the unit normal vector to the $x_1 - x_2$ plane. The function $F(x_1, x_2, x_3)$ is called the boundary function of the function $f(x_1, x_2, x_3)$ [11, 13]. Here Ω is considered to be a non-pathological (regular) domain. However the function $f(x_1, ..., x_n)$ may include certain pathological points as in the case of Green's functions [9]. The interpretation of these integrals varies according to the nature of the singularity.

In general, the results of [14] can be automatically carried to the special cases. An important point is that a scaling parameter H is required wherever a logarithm term occurs. For example, a term such as $\log \phi(x_1, x_2, x_3)$ becomes $\log \frac{\phi(x_1, x_2, x_3)}{H}$ where H is the scale parameter (see Appendix 2 for the definition of H).

Let $G(x_1, x_2, x_3)$ be a Green's function and $\omega(x_1, x_2)$ a weighting function, which are homogeneous in x_1, x_2, x_3 and take the domain Ω to lie in the $x_1 - x_2$ plane. Then

$$\int_{\Omega} \omega(x_1, x_2)\, G(x_1, x_2, x_3)\, dV = \int_{\partial\Omega} \Phi(x_1, x_2, x_3) \boldsymbol{X}.d\boldsymbol{S} \tag{15}$$

The *boundary function* Φ for the composed function ωG is given by

$$\Phi(x_1, x_2, x_3) = x_3^{\alpha} \int_{x_3}^{\infty} \frac{1}{\xi^{\alpha+1}} \omega(x_1, x_2)\, G(x_1, x_2, \xi)\, d\xi \tag{16}$$

For the linear weighting function, ω of the form, $\omega(x_1, x_2) = c + a x_1 + b x_2$, we need to

decompose ω into two components, $\omega(x_1,x_2)=c$ for (α=-1) and $\omega(x_1,x_2)=ax_1+bx_2$ for (α=0) since the degree of homogeneity α is different for the constant and linear components. The integrations required to obtain the boundary functions are evaluated analytically using standard integrals given in Dwight [15]. The complete displacement discontinuity boundary functions are given in Appendix 2.

The expression (16) is derived for the domain as indicated in Fig. 6a. The application of the integral formula is required for a typical domain as shown in Fig. 6b. The following definitions will simplify further discussion.

Angle of deficit: The difference of 2π radians and the solid angle subtended at a vertex. Note that the solid angle at a vertex approaches 2π if the vertex is flattened out.

Asymptotically planar: A surface discretization is asymptotically planar at a vertex if gradual refinement of the discretization produces an angle of deficit at that vertex that asymptotically approaches zero.

In this paper, we shall deal only with asymptotically planar discretizations at all vertices. It should be emphasized that a proper discretization of a section of a surface without corners will yield an asymptotically planar discretization (Fig. 6b).

Since the integration formula is valid for a planar integration domain, the natural idealization of the domain is as shown in Fig. 6c. The different orientation of each segment, although asymptotically small, can be assigned during the integration process. This is done by transforming from the local coordinate system of each node to the local coordinate system of the element.

3.1 Adaptive integration scheme

Even though, the boundary function integration method dramatically simplifies the difficult near-singular integral evaluation by converting the integration from the domain to integration along the boundary of each element, numerical difficulties can still arise when the singular point lies in the vicinity of the boundary.

Numerical quadrature, in these situations, requires closer collocation points when the gradient of the integrand is high while the rest of the quadrature domain requires only sparsely placed collocation points. The challenge is how to identify the region of rapid variation [16].

We have developed an adaptive scheme which subdivides the integration domain as required. For example, quadrature in a region is assumed to be sufficiently accurate if the computed value of that region falls within a specified percentage of the summation of the values obtained from the two equal subdivisions of the same region. We can use a simple quadrature for each subdivision such as the two point Gaussian scheme. This process of subdivision continues until any subdivided region satisfies the accuracy criterion.

4. Applications

In this section, two categories of applications using the new node-centric formulation are presented. The first category, verification examples, was chosen to demonstrate the accuracy and robustness of the method. The method has been verified through several examples that have closed-form solutions. These examples include the pressurized penny-shaped crack, a spherical cavity under an external hydrostatic pressure, and a

spherical cavity subjected to a uniaxial stress field at infinity. A second category, which involves practical examples, shows the versatility of the three-dimensional node-centric method for solving challenging geomechanics problems.

4.1 Verification examples

4.1.1 Penny-shaped crack

A standard test problem for DDM is the penny-shaped planar crack [17]. The crack is discretized into 108 elements with 61 nodes and a uniform internal unit pressure is applied. The boundary conditions at the outermost nodes require that the DD values be set to zero. Thus the number of unknowns for the problem is reduced from 3x108 unknowns for the constant DD to 3x49 unknowns for the node-centric. The normal DD for the node-centric DDM, the constant DDM and the closed-form solution are plotted in Fig. 7. Despite the reduction in the number of unknowns for the node-centric method, its percentage error (0.698%) is much smaller than the error (3.278%) for the constant DD method.

4.1.2 Randomly discretized penny-shaped crack

In order to demonstrate the robustness of the node-centric formulation, four different meshes for the penny-shaped crack have been tested (Fig. 8). The first three meshes were created using a random number generator in the radial direction. The fourth mesh is based on uniform spacing.

The results, which are presented in Fig. 9, show that even with elements having very large aspect ratios such as in mesh #1, the node-centric DD values are in a good

agreement with the closed-form solution.

4.1.3 Circular fracture embedded in an elastic half-space

This example considers a pressurized circular horizontal fracture with 235 elements and a ground surface with two mesh discretizations. The first mesh for the ground surface has 800 elements and the second has 1800 elements. Young's modulus and Poisson's ratio are taken as 50,000 MPa and 0.21, respectively. Fig. 10 compares the variation of both displacement components for the ground surface obtained from the node-centric method with the analytical solution [18]. The percentage error decreased from 6.5% for the mesh of 800 elements to 2.7% when 1800 elements were used.

4.1.4 Spherical cavity under an external hydrostatic pressure

A sphere of unit radius subjected to an external hydrostatic pressure, P, was modeled using 320 elements with 162 nodes. The value of the normal DD predicted by the node-centric method is

$$0.812\frac{(1-\nu)P}{(1+\nu)G}$$

whereas the closed-form solution [19] gives the value of

$$0.75\frac{(1-\nu)P}{(1+\nu)G}$$

where G and ν are the shear modulus and Poisson's ratio, respectively. This represents an error of 8.26%. The induced stress components in the r-direction are very close to the analytical solution (Fig. 11). Although the number of degrees of freedom for the node-centric method (3x62) is only about half that of the constant DDM (3x120), its

percentage error (14.44%) is approximately equal to the percentage error (14.32%) of the constant DDM.

4.1.5 Spherical cavity under uniaxial loading condition

In the previous example, both components of the shear DD are zero. In order to test the influence of the shear DD on the accuracy of the method, a uniaxial loading condition is applied to the spherical cavity of unit radius using the same discretization as in example 4.1.4. The error in the numerical value of the calculated normal DD at the top of the sphere as compared to the closed-form [19] is 17%. The percentage error in the uniaxial case is about double that of the case of hydrostatic pressure. This is due to the large variation of shear displacement discontinuity along the longitudes while the uniaxial stress is applied vertically.

As shown in Fig. 12, the variation of the induced stress components in the *r*-direction closely follow the analytical solution.

4.2 Practical examples

In this category of examples, we shall consider the class of physico-geometric problems which are modeled by intersecting boundaries. The lack of inter-element continuity in the constant DDM yields unbounded stresses around the edges of the elements. As a result, in the case of intersecting boundaries which have been independently discretized, it is inevitable that one encounters unbounded stresses. Hence, considerable care is required in generating the boundary mesh in the vicinity of intersections using the constant DDM. The node-centric approach obviates this problem by ensuring inter-element continuity.

4.2.1 Intersection of two penny-shaped cracks

In this example, we consider the intersection of two perpendicular pressurized penny-shaped cracks. The unknown displacement discontinuities are assigned to each of the coinciding nodes independently. This is possible because in DDM, the cracks are modeled as a superposition of forces, instead of two separate boundaries. However, the stress state at the intersection point, which needs to be taken into consideration for the traction collocation of the external pressure, provides only one set of conditions for the two intersecting nodes. As a consequence, we are left with only one pair of independent collocation equations at the intersecting node. This results in an under-determined system of equations. But one can easily furnish an additional pair of equations by collocating tractions at any non-nodal boundary point, e.g., the center-point of the elements that have the connecting node.

Similar to the single penny-shaped crack example, each crack is discretized using 108 elements and 61 nodes. Two sets of meshes have been used. The first set provides node sharing along the line of intersection while for the second set node sharing occurs only at the node at the centre. As shown in Fig. 13, the variation of the normal DD for both sets is insensitive to the node configuration along the line of the intersection.

4.2.2 Crack intersecting a spherical cavity

In this application, a crack passing through the centre of a spherical cavity is analyzed. We emphasize that with the node-centric DD, because the DD variation is continuous between elements, the cavity and the crack can be independently discretized. With the

conventional DD, the lack of continuity can introduce such large errors in the stress calculations as to render the results unreliable for highly interacting elements [6, 8].

Two discretizations for the same geometry have been analyzed. Similar to the previous application, with the first mesh (test #1), node sharing occurs along the intersection while with the second mesh (test #2), there is no node sharing. The variation of the stress components for points along line b-b for the two meshes is given in Fig. 14. This graph shows that results are similar for the two meshes.

5. Comparative Evaluation

An important contribution of the present work is the development of the complete set of the boundary functions for the linear node-centric DD. These boundary functions reduce the computing effort required for the element integrations considerably. There have been several works which address the issue of element integration. Notably, Vandamme and Curran [9] and Kuriyama and Mizuta [7] provided closed-form integrations for triangular elements. A serious restriction in Kuriyama and Mizuta's work is that the centre of gravity of any element must not lie on any prolongation of the side of another element. Since the possibility of this restriction being violated is high for many practical problems, the robustness of their approach is questionable. The boundary function method that is presented in this paper provides a unified method to evaluate singular, near-singular and regular integrals without imposing any restrictions.

Cayol and Cornet [8] use a mixed BEM (DD and direct method) to solve the problem of a pressurized horizontal fracture embedded in an elastic half-space. They model the fracture using constant DD elements and use direct boundary elements for the

ground surface. According to Cayol and Cornet, the direct method is more exact than the DD method when dealing with real topographies. Since the direct method requires closed boundary surfaces, they use a modified row-sum technique using a virtual closed surface to augment the free surface. We have modeled the same problem using node-centric DD's for both the fracture and the free surface (example 4.1.3). It is important to note that the numerical accuracy of the mixed method deteriorated with a finer mesh whereas the accuracy improved for the node-centric DD. The percentage error increased for the mixed method increased from 3.5% to 4.9% when the number of elements was increased from 800 to 1800 elements.

Shou *et. al.* [6] developed a higher-order DDM which provides a quasi continuity between the boundary elements. The main disadvantage of their method is that it requires a uniform rectangular mesh be used which is impractical for many practical problems. However, the node-centric method presented in this paper can accomodate any boundary shapes. Furthermore the node-centric method has the ability to precisely satisfy the zero displacement boundary condition at the crack tip, i.e., there is no need to introduce a special crack tip elements.

6. Discussion

6.1 The node-centric framework enables one to clearly identify the geometrical factors which remain invariant from the original physical problem through various approximations made in obtaining a numerical solution. Among these invariants are the normal vector and curvature (for higher-order formulations) in addition to the coordinates of the nodes where the unknown physical parameters are sought. The

linear variation used in this paper is also the lowest order of interpolation function that is applicable. The node-centricity is a general framework. The direct linear BEM is usually implemented in this manner. The apparent reason for choosing the unknown values at the nodes, rather than at points inside the element, is that the number of degrees of freedom is kept to a minimum. There is also a deeper reason which is more significant for numerical stability. In the parlance of the emerging field of wavelets [20], this is referred to as 'choosing a short compact support'. The enhanced numerical stability is due to the self-similarity of the interpolation function.

6.2 Since the main role of the element is to act as support for integration, we can choose any approximation which facilitates integration as long as the geometric measure of the ensemble of elements asymptotically matches that of the actual boundary. This naturally obviates any use of overlapping elements. The flat element subdivision of the boundary is the lowest-order geometrical representation which allows inter-element continuity.

6.3 The node-centricity provides a mathematical machinery for clearly separating the actual parameters from their approximations. Since the nodes precisely lie on the boundary and the geometric shape of the element Ω and the interpolation function f are approximations, we can consider the combined entity

$$\langle f, \Omega \rangle \equiv \int_{\Omega} f \, dV$$

as the quantity that quantifies the error. This mathematical entity is called *'current'* following deRham [20] in his work on differential geometry. We can think of the above expression as an approximation to the actual current

$$\langle f^{\bullet}, \Omega^{\bullet} \rangle \equiv \int_{\Omega^{\bullet}} f^{\bullet} \, dV$$

The error, *Err*, is denoted by

$$Err = \langle f, \Omega \rangle - \langle f^*, \Omega^* \rangle$$

The symmetrical relationship between space and function embedded in the concept of current unifies function and space. This is a first step towards a unified error analysis.

6.4 The number of vertices for a discretization is generally much less than the number of elements. Hence compared to the constant DD element for the same accuracy the node-centric DDM requires a much smaller number of degrees of freedom, resulting in enhanced computational efficiency. An additional efficiency results from the way the zero boundary conditions are exactly satisfied. This is clearly evident from the penny-shaped crack examples where, for a discretization of 108 elements, there are 324 unknowns for the constant DD approach while there are only 147 in the node-centric formulation.

6.5 The efficient solution of problems involving the intersection of geometric entities, such as when a fault intersects an excavation, is greatly facilitated if the fault and excavation can be independently discretized. The continuous DD variation ensures that no anomalous changes of stresses occur in the inter-element neighborhood. As we have shown by examples 4.2.1 and 4.2.2, the numerical solutions remain essentially the same regardless of which of the two meshes was used.

6.6 We emphasize that without the streamlined integration method afforded by the continuation approach, the node-centric displacement discontinuity method would not be feasible. Through the use of the boundary function we are able to

(i) provide a unified integration routine regardless of the integrals, whether they are regular, near-singular, or singular.

(ii) obtain the values of the integrals as conventional integrals, as Cauchy Principal value integrals and as finite-part integrals according to the type of the integrands.

(iii) compute the integration efficiently since the number of collocation points required along the boundary is considerably less than the number required if the collocation points are selected over the element area.

6.7 The method of adaptive quadrature used for the integration along the boundary of the elements ensures that a pre-determined accuracy is always attained. The adaptive method of quadrature automatically provides a finer subdivision in the region where rapid variation of the integrand occurs while keeping the number of collocation points low where the integrand varies very little.

7. Conclusion

In this paper, we have shown the efficacy of node-centric indirect BEM through a DD formulation based on flat triangular discretrization. The main strengths of the present approach are:

1. Node sharing which preserves inter-element continuity.
2. Unified integration methodology.
3. Robustness of the method with respect to variable element sizes.
4. Precise matching of the boundary conditions especially for crack problems.

As the verification examples show, the node-centric formulation together with the unified element integration scheme outperforms other DD formulations in accuracy and robustness. In addition, we have also shown how the node-centric DD method widens the scope of applicability through some non-standard applications such as the intersection of

a cavity and a crack. Comparison of the present method with some recently published work has been made.

Acknowledgment

The financial support provided by NSERC through an operating grant (J.H. Curran) and postgraduate scholarship (T.E. Yacoub), CANMET through the Canada/Ontario Mineral Development Agreement (Contract # 23440-4-1310/01-SQ) and *Rocscience* Inc. are gratefully acknowledged.

References

1. Salamon, M. D. G., Elastic analysis of displacements and stresses induced by the mining of seam or reef deposits, Part I, *J. S. Afr. Inst. Min. Metall.*, 1963, **64**, 128-149.
2. Crouch, S. L. and Starfield A. M., *Boundary Element Methods in Solid Mechanics*, George Allen & Unwin, London, 1983.
3. Wiles, T. D. and Curran, J. H., A general 3-D displacement discontinuity method. *Proc. 3rd Int. Conf. Num. Meth. Geomech.*, 1982, 103-111.
4. Beer, G. and Watson, J. O., *Introduction to Finite Element and Boundary Element Methods for Engineers*, John Wiley & Sons Inc., England, 1992.
5. Hadamard, J., *Lectures on Cauchy's Problem in Linear Partial Differential Equations*, Yale University Press, New Haven, CT, 1923.
6. Shou, K. J., Siebrits, E. and Crouch, S. L., A higher order displacement discontinuity method for three-dimensional elastostatic problems. *Int. J. Rock Mech. Min. Sci,* 1997 **34(2)**, 317-322.
7. Kuriyama, K. and Mizuta, Y., Three-dimensional elastic analysis by the displacement discontinuity method with boundary division into triangular leaf elements. *Int. J. Rock Mech. Min. Sci.*, 1993 **30(2)**, 111-123.

8. Cayol, V. and Cornet, F.H., 3D mixed boundary elements for elastostatic deformation field analysis. *Int. J. Rock Mech. Min. Sci.,* 1997, **34(2)**, 275-287.
9. Vandamme, L. and Curran, J. H., A three-dimensional hydraulic fracturing simulator. *Int. J. Numer. Meth. Engng.,* 1989, **28**, 909-927.
10. de Paula, F. A. and Telles, J. C. F., A comparison between point collocation and Galerkin for stiffness matrices obtained by boundary elements. *Engineering Analysis with Boundary Elements,* 1989, **6(3)**, 123-126.
11. Vijayakumar, S., Yacoub, T. E. and Curran, J. H., Unified boundary element integration using boundary functions (in preparation).
12. Vijayakumar, S. and Cormack, D. E., An invariant imbedding method for singular integral evaluation on finite domains. *SIAM J. App. Math.*, 1988, **48**, 1335-1349.
13. Vijayakumar, S. and Cormack, D. E., A new concept in near-singular integral evaluation: The continuation approach, *SIAM J. App. Math.*, 1989, **49**, 1285-1295.
14. Rosen, D. and Cormack, D. E., The continuation approach for singular and near-singular integration. *Engineering Analysis with Boundary Elements,* 1994, **13**, 99-113.
15. Dwight, H. B., *Tables of Integrals and other Mathematical Data,* 4th Ed., Macmillan, 1961.
16. Kane, J. H., *Boundary Element Analysis in Engineering Continuum Mechanics*, Prentice-Hall Inc. 1994.
17. Sneddon, I. N. and Lowengrub, M., *Crack Problems in the Classical Theory of Elasticity*, John Wiley & Sons, Inc., 1969.
18. Sun, J. R., Theoretical size of hydraulically induced horizontal fracture and corresponding surface uplift in an idealized medium. *J. Geophys. Res.*, 1969, **74**, 5995-6011.
19. Timoshenko, S. P. and Goodier, J. N., *Theory of Elasticity*, McGraw Hill, New York, 1970.
20. Erlebacher, G., Hussaini, M. Y. and Jameson, L. M., *Wavelets Theory and Applications*, Oxford University Press, 1996.
21. Vijayakumar, S. and Cormack, D. E., Differential geometric foundation of the boundary element method, *Mech. Res. Comm.,* 1987, **14**(2), 73-80.

Appendix 1

Green's Functions for Three-dimensional Displacement Discontinuities

	Green's functions in x_1-direction	Green's functions in x_2-direction	Green's functions in x_3-direction
σ_{11}	$-\frac{G}{4\pi(1-\nu)}\left[\frac{3x_1x_3}{r^5}-\frac{15x_1^3x_3}{r^7}\right]$	$-\frac{G}{4\pi(1-\nu)}\left[(1-2\nu)\frac{3x_2x_3}{r^5}-\frac{15x_2x_1^3x_3}{r^7}\right]$	$-\frac{G}{4\pi(1-\nu)}\left[2(1-\nu)\frac{1}{r^3}-3(1-2\nu)\frac{x_2^2}{r^5}-\frac{15x_1^2x_3^2}{r^7}\right]$
σ_{22}	$-\frac{G}{4\pi(1-\nu)}\left[(1-2\nu)\frac{3x_1x_3}{r^5}-\frac{15x_1x_2^3x_3}{r^7}\right]$	$-\frac{G}{4\pi(1-\nu)}\left[\frac{3x_2x_3}{r^5}-\frac{15x_2^3x_3}{r^7}\right]$	$-\frac{G}{4\pi(1-\nu)}\left[2(1-\nu)\frac{1}{r^3}-3(1-2\nu)\frac{x_1^2}{r^5}-\frac{15x_2^2x_3^2}{r^7}\right]$
σ_{33}	$-\frac{G}{4\pi(1-\nu)}\left[\frac{3x_1x_3}{r^5}-\frac{15x_1x_3^3}{r^7}\right]$	$-\frac{G}{4\pi(1-\nu)}\left[\frac{3x_2x_3}{r^5}-\frac{15x_2x_3^3}{r^7}\right]$	$-\frac{G}{4\pi(1-\nu)}\left[\frac{1}{r^3}+\frac{6x_3^2}{r^5}-\frac{15x_3^4}{r^7}\right]$
σ_{12}	$-\frac{G}{4\pi(1-\nu)}\left[3\nu\frac{x_2x_3}{r^5}-\frac{15x_1^2x_2x_3}{r^7}\right]$	$-\frac{G}{4\pi(1-\nu)}\left[3\nu\frac{x_1x_3}{r^5}-\frac{15x_2^2x_1x_3}{r^7}\right]$	$-\frac{G}{4\pi(1-\nu)}\left[3(1-2\nu)\frac{x_1x_2}{r^5}-\frac{15x_1x_2x_3^2}{r^7}\right]$
σ_{23}	$-\frac{G}{4\pi(1-\nu)}\left[3\nu\frac{x_1x_2}{r^5}-\frac{15x_1x_2x_3^2}{r^7}\right]$	$-\frac{G}{4\pi(1-\nu)}\left[(1+\nu)\frac{1}{r^3}-3\nu\frac{x_1^2}{r^5}-\frac{15x_2^2x_3^2}{r^7}\right]$	$-\frac{G}{4\pi(1-\nu)}\left[\frac{3x_2x_3}{r^5}-\frac{15x_2x_3^3}{r^7}\right]$
σ_{13}	$-\frac{G}{4\pi(1-\nu)}\left[(1+\nu)\frac{1}{r^3}-3\nu\frac{x_2^2}{r^5}-\frac{15x_1^2x_3^2}{r^7}\right]$	$-\frac{G}{4\pi(1-\nu)}\left[3\nu\frac{x_1x_2}{r^5}-\frac{15x_1x_2x_3^2}{r^7}\right]$	$-\frac{G}{4\pi(1-\nu)}\left[\frac{3x_1x_3}{r^5}-\frac{15x_1x_3^3}{r^7}\right]$
u_1	$\frac{-1}{8\pi(1-\nu)}\left[(1-2\nu)\frac{x_3}{r^3}+\frac{3x_1^2x_3}{r^5}\right]$	$\frac{-1}{8\pi(1-\nu)}\left[\frac{3x_1x_2x_3}{r^5}\right]$	$\frac{-1}{8\pi(1-\nu)}\left[-(1-2\nu)\frac{x_1}{r^3}+\frac{3x_1x_3^2}{r^5}\right]$
u_2	$\frac{-1}{8\pi(1-\nu)}\left[\frac{3x_1x_2x_3}{r^5}\right]$	$\frac{-1}{8\pi(1-\nu)}\left[(1-2\nu)\frac{x_3}{r^3}+\frac{3x_2^2x_3}{r^5}\right]$	$\frac{-1}{8\pi(1-\nu)}\left[-(1-2\nu)\frac{x_2}{r^3}+\frac{3x_2x_3^2}{r^5}\right]$
u_3	$\frac{-1}{8\pi(1-\nu)}\left[(1-2\nu)\frac{x_1}{r^3}+\frac{3x_1x_3^2}{r^5}\right]$	$\frac{-1}{8\pi(1-\nu)}\left[(1-2\nu)\frac{x_1}{r^3}+\frac{3x_2x_3^2}{r^5}\right]$	$\frac{-1}{8\pi(1-\nu)}\left[(1-2\nu)\frac{x_3}{r^3}+\frac{3x_3^3}{r^5}\right]$

Note: G, ν are the elastic shear modulus and Poisson's ratio, respectively, and $r^2 = x_1^2 + x_2^2 + x_3^2$.

Appendix 2

Boundary Functions (BF) for Three-dimensional Node-centric Displacement Discontinuities

i. Stress constant boundary functions

	BF in x_1-direction	**BF in x_3-direction**
σ_{11}	$\frac{G}{4\pi(1-\nu)}\frac{1}{x_3}\left[-\frac{x_1}{r^3}+\frac{3x_1^3}{r^5}\right]$	$\frac{G}{4\pi(1-\nu)}\left[\left(2(1-\nu)\frac{1}{\rho^2 r}-3(1-2\nu)\frac{x_2^2}{\rho^4 r}\right)+\left((1-2\nu)\frac{x_2^2}{\rho^4 r^3}-\frac{5x_1^2}{\rho^4 r^3}\right)x_3^2+\frac{3x_1^2}{\rho^4 r^5}x_3^4\right]$ $\pm\frac{G}{4\pi(1-\nu)}\frac{1}{x_3}\left[-2\nu\frac{1}{\rho^2}+4\nu\frac{x_2^2}{\rho^4}\right]$
σ_{22}	$\frac{G}{4\pi(1-\nu)}\frac{1}{x_3}\left[-(1-2\nu)\frac{x_1}{r^3}+\frac{3x_1x_2^2}{r^5}\right]$	$\frac{G}{4\pi(1-\nu)}\left[\left(2(1-\nu)\frac{1}{\rho^2 r}-3(1-2\nu)\frac{x_1^2}{\rho^4 r}\right)+\left((1-2\nu)\frac{x_1^2}{\rho^4 r^3}-\frac{5x_2^2}{\rho^4 r^3}\right)x_3^2+\frac{3x_2^2}{\rho^4 r^5}x_3^4\right]$ $\pm\frac{G}{4\pi(1-\nu)}\frac{1}{x_3}\left[-2\nu\frac{1}{\rho^2}+4\nu\frac{x_1^2}{\rho^4}\right]$
σ_{33}	$\frac{G}{4\pi(1-\nu)}\frac{1}{x_3}\left[\frac{4x_1}{r^3}-\frac{3\rho^2 x_1}{r^5}\right]$	$\frac{G}{4\pi(1-\nu)}\left[\frac{1}{r^3}+\frac{3x_3^2}{r^5}\right]$
σ_{12}	$\frac{G}{4\pi(1-\nu)}\frac{1}{x_3}\left[-\nu\frac{x_2}{r^3}+\frac{3x_1^2x_2}{r^5}\right]$	$\frac{G}{4\pi(1-\nu)}\left[\left(3(1-2\nu)\frac{x_1x_2}{\rho^4 r}\right)-\left(2(3-\nu)\frac{x_1x_2}{\rho^4 r^3}\right)x_3^2+\left(\frac{3x_1x_2}{\rho^4 r^5}\right)x_3^4\right]$ $\pm\frac{G}{4\pi(1-\nu)}\frac{1}{x_3}\left[4\nu\frac{x_1x_2}{\rho^4}\right]$
σ_{23}	$\frac{G}{4\pi(1-\nu)}\left[\left(3\nu\frac{x_1x_2}{\rho^4 r}\right)-\left((5+\nu)\frac{x_1x_2}{\rho^4 r^3}\right)x_3^2+\left(\frac{3x_1x_2}{\rho^4 r^5}\right)x_3^4\right]$ $\pm\frac{G}{4\pi(1-\nu)}\left[2(\nu-1)\frac{x_1x_2}{\rho^4 x_3}\right]$	$\frac{G}{4\pi(1-\nu)}\frac{1}{x_3}\left[\frac{4x_2}{r^3}-\frac{3\rho^2 x_2}{r^5}\right]$
σ_{13}	$\frac{G}{4\pi(1-\nu)}\left[\left((1+\nu)\frac{1}{\rho^2 r}-3\nu\frac{x_2^2}{\rho^4 r}\right)+\left(\nu\frac{x_2^2}{\rho^4 r^3}-\frac{5x_1^2}{\rho^4 r^3}\right)x_3^2+\left(\frac{3x_1^2}{\rho^4 r^5}\right)x_2^4\right]$ $\pm\frac{G}{4\pi(1-\nu)}\frac{1}{x_3}\left[(1+\nu)\frac{1}{\rho^2}-2(\nu x_2^2+x_1^2)\frac{1}{\rho^4}\right]$	$\frac{G}{4\pi(1-\nu)}\frac{1}{x_3}\left[\frac{4x_1}{r^3}-\frac{3\rho^2 x_1}{r^5}\right]$

ii. ***Stress linear boundary functions***

	BF in x_1-direction	**BF in x_3-direction**
σ_{11}	$\frac{G}{4\pi(1-\nu)}\left[\left(\frac{3x_1}{\rho^4 r}-\frac{15x_1^3}{\rho^6 r}\right)x_3-\left(\frac{x_1}{\rho^4 r^3}-\frac{10x_1^3}{\rho^6 r^3}\right)x_3^3-\frac{3x_1^3}{\rho^6 r^5}x_3^5\right]\pm\frac{G}{4\pi(1-\nu)}\left[\frac{2x_1}{\rho^4}-\frac{8x_1^3}{\rho^6}\right]$	$\frac{G}{4\pi(1-\nu)}\left[\left\{2(1-\nu)\frac{1}{\rho^2 r}-(1-2\nu)\left(\frac{x_2^2}{\rho^2 r^3}+\frac{3x_2^2}{\rho^4 r}\right)+\frac{3x_1^2}{r^5}\right\}\right]+\frac{G}{4\pi(1-\nu)}\left[\left(-2(1-\nu)\frac{1}{\rho^3}+3(1-2\nu)\frac{x_2^2}{\rho^5}\right)\log\left(\frac{r+\rho}{2H}\right)\right]$
σ_{22}	$\frac{G}{4\pi(1-\nu)}\left[\left(3(1-2\nu)\frac{x_1}{\rho^4 r}-\frac{15x_1x_2^2}{\rho^6 r}\right)x_3-\left((1-2\nu)\frac{x_1}{\rho^4 r^3}-\frac{10x_1x_2^2}{\rho^6 r^3}\right)x_3^3-\left(\frac{3x_1x_2^2}{\rho^6 r^5}\right)x_3^5\right]\pm\frac{G}{4\pi(1-\nu)}\left[2(1-2\nu)\frac{x_1}{\rho^4}-\frac{8x_1x_2^2}{\rho^6}\right]$	$\frac{G}{4\pi(1-\nu)}\left[\left\{2(1-\nu)\frac{1}{\rho^2 r}-(1-2\nu)\left(\frac{x_1^2}{\rho^2 r^3}+\frac{3x_1^2}{\rho^4 r}\right)+\frac{3x_2^2}{r^5}\right\}\right]+\frac{G}{4\pi(1-\nu)}\left[\left(-2(1-\nu)\frac{1}{\rho^3}+3(1-2\nu)\frac{x_1^2}{\rho^5}\right)\log\left(\frac{r+\rho}{2H}\right)\right]$
σ_{33}	$\frac{G}{4\pi(1-\nu)}\left[\left(\frac{3x_1}{\rho^4 r}\right)x_3-\left(\frac{6x_1}{\rho^4 r^3}\right)x_3^3+\left(\frac{3x_1}{\rho^4 r^5}\right)x_3^5\right]$	$\frac{G}{4\pi(1-\nu)}\left[\frac{1}{r^3}+\frac{x_3^2}{r^3\rho^2}+\frac{3x_3^2}{r^5}-\frac{1}{\rho^3}\log\left(\frac{r+\rho}{2H}\right)\right]$
σ_{12}	$\frac{G}{4\pi(1-\nu)}\left[\left(3\nu\frac{x_2}{\rho^4 r}-\frac{15x_1^2x_2}{\rho^6 r}\right)x_3-\left(\nu\frac{x_2}{\rho^4 r^3}-\frac{10x_1^2x_2}{\rho^6 r^3}\right)x_3^3-\left(\frac{3x_1^2x_2}{\rho^6 r^5}\right)x_3^5\right]\pm\frac{G}{4\pi(1-\nu)}\left[2\nu\frac{x_2}{\rho^4}-\frac{8x_1^2x_2}{\rho^6}\right]$	$\frac{G}{4\pi(1-\nu)}\left[3(1-2\nu)\frac{x_1x_2}{\rho^4 r}+(1-2\nu)\frac{x_1x_2}{\rho^2 r^3}+\frac{3x_1x_2}{r^5}-3(1-2\nu)\frac{x_1x_2}{\rho^5}\log\left(\frac{r+\rho}{2H}\right)\right]$
σ_{23}	$\frac{G}{4\pi(1-\nu)}\left[3\nu\frac{x_1x_2}{\rho^4 r}+\nu\frac{x_1x_2}{\rho^2 r^3}+\frac{3x_1x_2}{r^5}-3\nu\frac{x_1x_2}{\rho^5}\log\left(\frac{r+\rho}{2H}\right)\right]$	$\frac{G}{4\pi(1-\nu)}\left[\frac{3x_2x_3}{r^5}\right]$
σ_{13}	$-\frac{G}{4\pi(1-\nu)}\left[(1+\nu)\frac{1}{\rho^2 r}-\nu\frac{x_2^2}{\rho^2 r^3}-3\nu\frac{x_2^2}{\rho^4 r}+\frac{3x_1^2}{r^5}+\left(3\nu\frac{x_2^2}{\rho^5}-(1+\nu)\frac{1}{\rho^3}\right)\log\left(\frac{r+\rho}{2H}\right)\right]$	$-\frac{G}{4\pi(1-\nu)}\left[\frac{3x_1x_3}{r^5}\right]$

iii. ***Displacement constant boundary functions***

	BF in x_1-direction	**BF in x_3-direction**
u_1	$\frac{1}{8\pi(1-\nu)}\left[\left((1-2\nu)\frac{1}{\rho^2 r}+\frac{3x_1^2}{\rho^4 r}\right)x_3-\left(\frac{x_1^2}{\rho^4 r^3}\right)x_3^3\right]\pm\frac{1}{8\pi(1-\nu)}\left[(1-2\nu)\frac{1}{\rho^2}+\frac{2x_1^2}{\rho^4}\right]$	$\frac{1}{8\pi(1-\nu)}\left[\left(-(1-2\nu)\frac{x_1}{\rho^2 r}-\frac{x_1}{r^3}\right)+(1-2\nu)\frac{x_1}{\rho^3}\log\left(\frac{\rho+r}{2H}\right)\right]$
u_2	$\frac{1}{8\pi(1-\nu)}\left[\frac{3x_1x_2}{\rho^4 r}x_3-\frac{x_1x_2}{\rho^4 r^3}x_3^3\right]\pm\frac{1}{8\pi(1-\nu)}\left[\frac{2x_1x_2}{\rho^4}\right]$	$\frac{-1}{8\pi(1-\nu)}\left[\left(-(1-2\nu)\frac{x_2}{\rho^2 r}-\frac{x_2}{r^3}\right)+(1-2\nu)\frac{x_2}{\rho^3}\log\left(\frac{\rho+r}{2H}\right)\right]$
u_3	$\frac{-1}{8\pi(1-\nu)}\left[\left((1-2\nu)\frac{x_1}{\rho^2 r}-\frac{x_1}{r^3}\right)-(1-2\nu)\frac{x_1}{\rho^3}\log\left(\frac{\rho+r}{2H}\right)\right]$	$\frac{1}{8\pi(1-\nu)}\left[(1-2\nu)\frac{1}{\rho^2 r}x_3+\frac{1}{\rho^2 r^3}x_3^3\right]\pm\frac{1}{8\pi(1-\nu)}\left[2(1-\nu)\frac{1}{\rho^2}\right]$

iv. ***Displacement linear boundary functions***

	BF in x_1-direction	**BF in x_3-direction**
u_1	$\frac{1}{8\pi(1-\nu)}x_3\left[(1-2\nu)\frac{1}{\rho^2 r}+\frac{x_1^2}{\rho^2 r^3}+\frac{3x_1^2}{\rho^4 r}-\left((1-2\nu)\frac{1}{\rho^3}+\frac{3x_1^2}{\rho^5}\right)\log\left(\frac{\rho+r}{2H}\right)\right]$	$\frac{1}{8\pi(1-\nu)}\left[(1-2\nu)\frac{rx_1}{\rho^4}+2(2-\nu)\frac{x_1}{\rho^4 r}x_3^2-\frac{x_1}{\rho^4 r^3}x_3^4\right]\pm\frac{1}{8\pi(1-\nu)}\left[4(1-\nu)\frac{x_1x_3}{\rho^4}\right]$
u_2	$\frac{1}{8\pi(1-\nu)}x_3\left[\frac{x_1x_2}{\rho^2 r^3}+\frac{3x_1x_2}{\rho^4 r}-\left(\frac{3x_1x_2}{\rho^5}\right)\log\left(\frac{\rho+r}{2H}\right)\right]$	$\frac{1}{8\pi(1-\nu)}\left[(1-2\nu)\frac{rx_2}{\rho^4}+2(2-\nu)\frac{x_2}{\rho^4 r}x_3^2-\frac{x_2}{\rho^4 r^3}x_3^4\right]\pm\frac{1}{8\pi(1-\nu)}\left[4(1-\nu)\frac{x_2x_3}{\rho^4}\right]$
u_3	$\frac{1}{8\pi(1-\nu)}\left[-(1-2\nu)\frac{rx_1}{\rho^4}+2(1+\nu)\frac{x_1}{\rho^4 r}x_3^2-\frac{x_1}{\rho^4 r^3}x_3^4\right]\pm\frac{1}{8\pi(1-\nu)}x_3\left[4\nu\frac{x_1}{\rho^4}\right]$	$\frac{1}{8\pi(1-\nu)}x_3\left[(1-2\nu)\frac{1}{\rho^2 r}-\frac{1}{r^3}-(1-2\nu)\frac{1}{\rho^3}\log\left(\frac{\rho+r}{2H}\right)\right]$

Notes: In the above expressions the + and - signs are used for $x_3 > 0$ and $x_3 < 0$, respectively and $\rho^2 = x_1^2 + x_2^2$.

H is scale function, which is defined:

$$H = \begin{cases} |x_3| & \text{for } x_3 \neq 0 \\ \text{Perpendicular distance from the singular point to the side of the element for } x_3 = 0 \end{cases}$$

The respective expressions due to shear DD in the x_2-direction can be obtained by interchanging the indices 1 and 2.

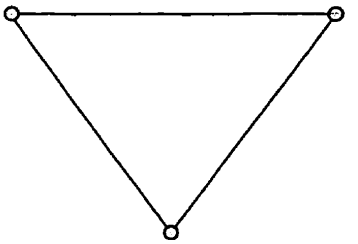

Node-centric linear DD element

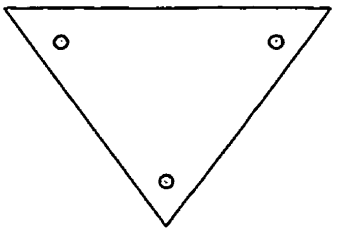

Element-centric linear DD element

Figure 1: Three-dimensional node- and element-centric elements

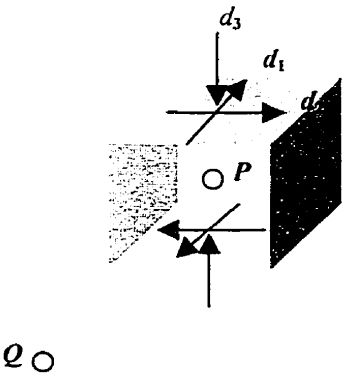

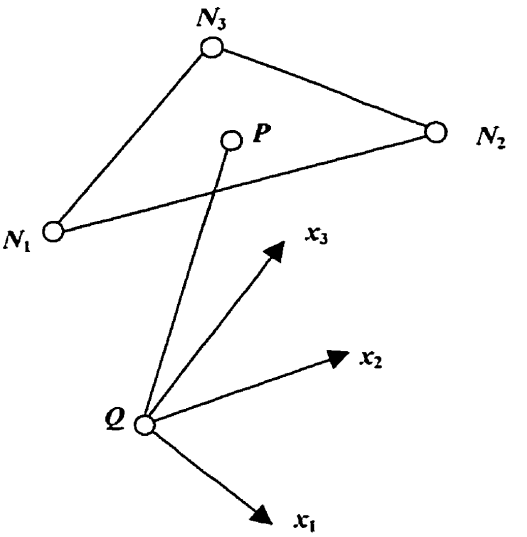

Figure 2: Notations

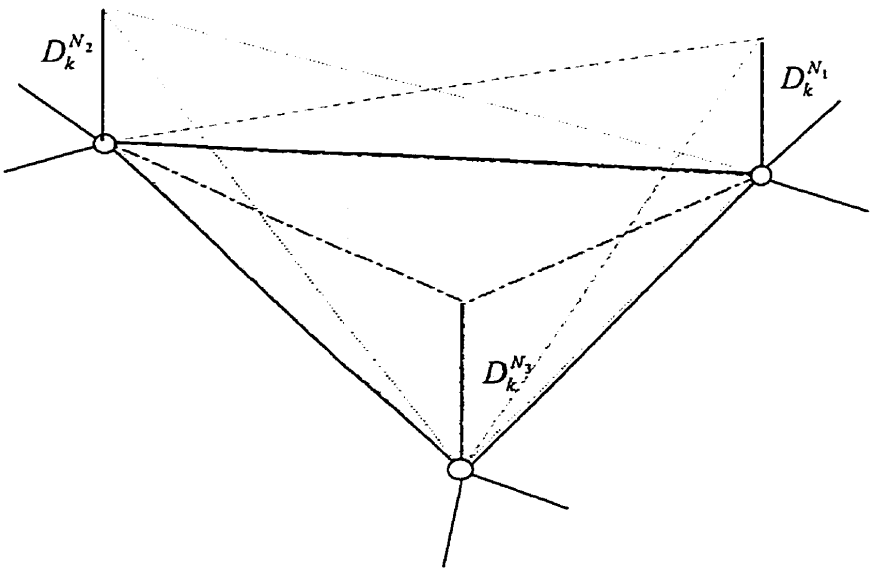

Figure 3: Node-centric pyramid function

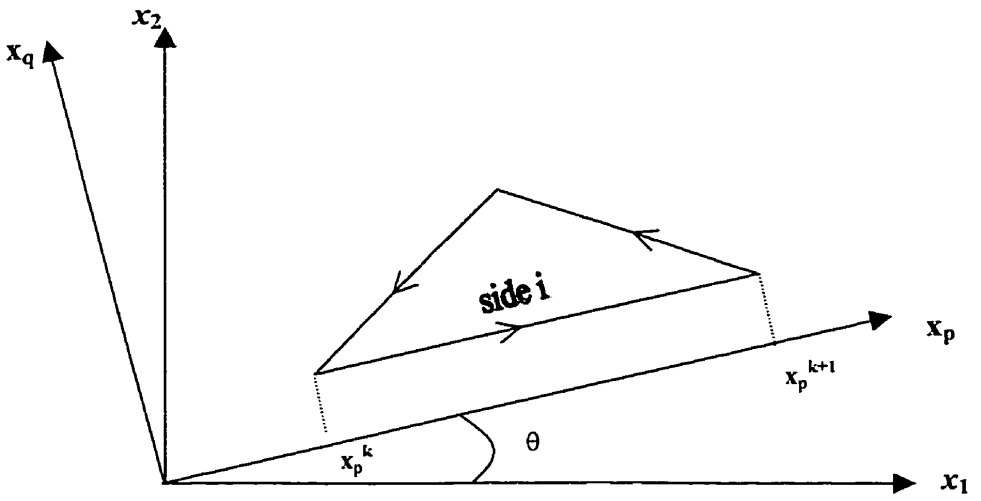

Figure 4: Coordinate system used to compute line integrals

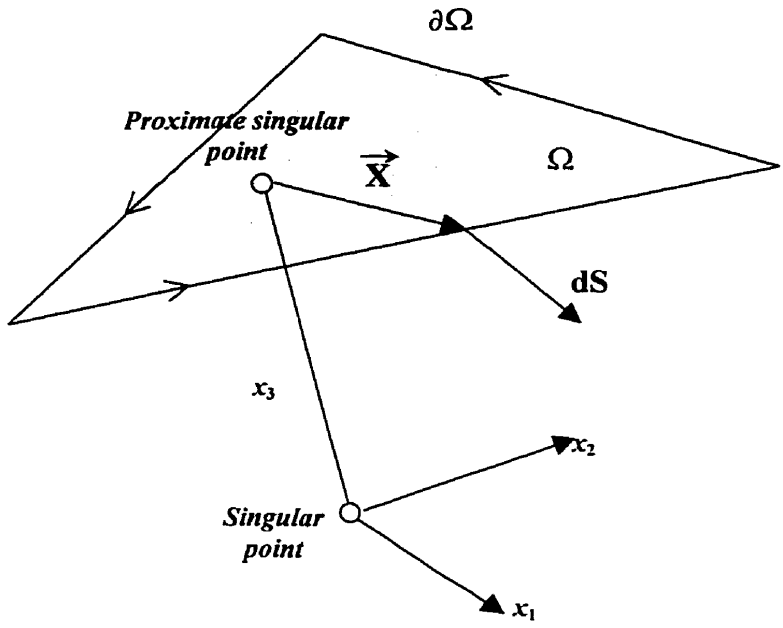

Figure 5: Schematic diagram

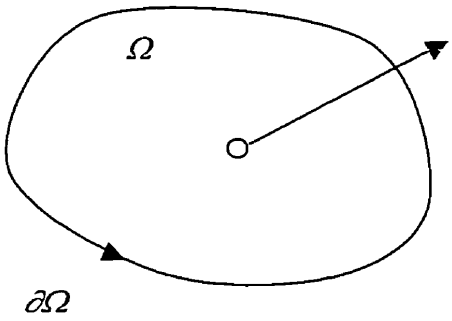

(a) Smooth integration domain

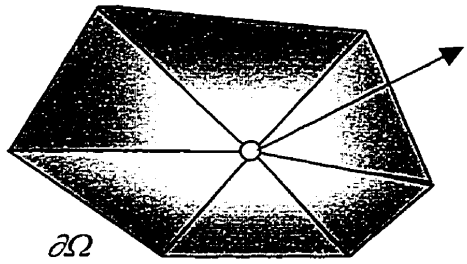

(b) Actual 3D discretization

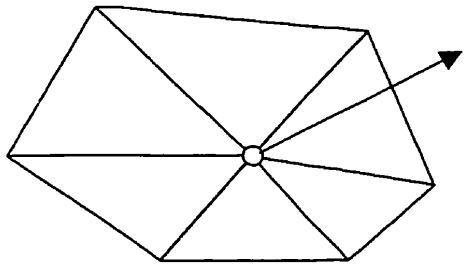

(c) Flattened version of the discretization

Figure 6: Integration domain

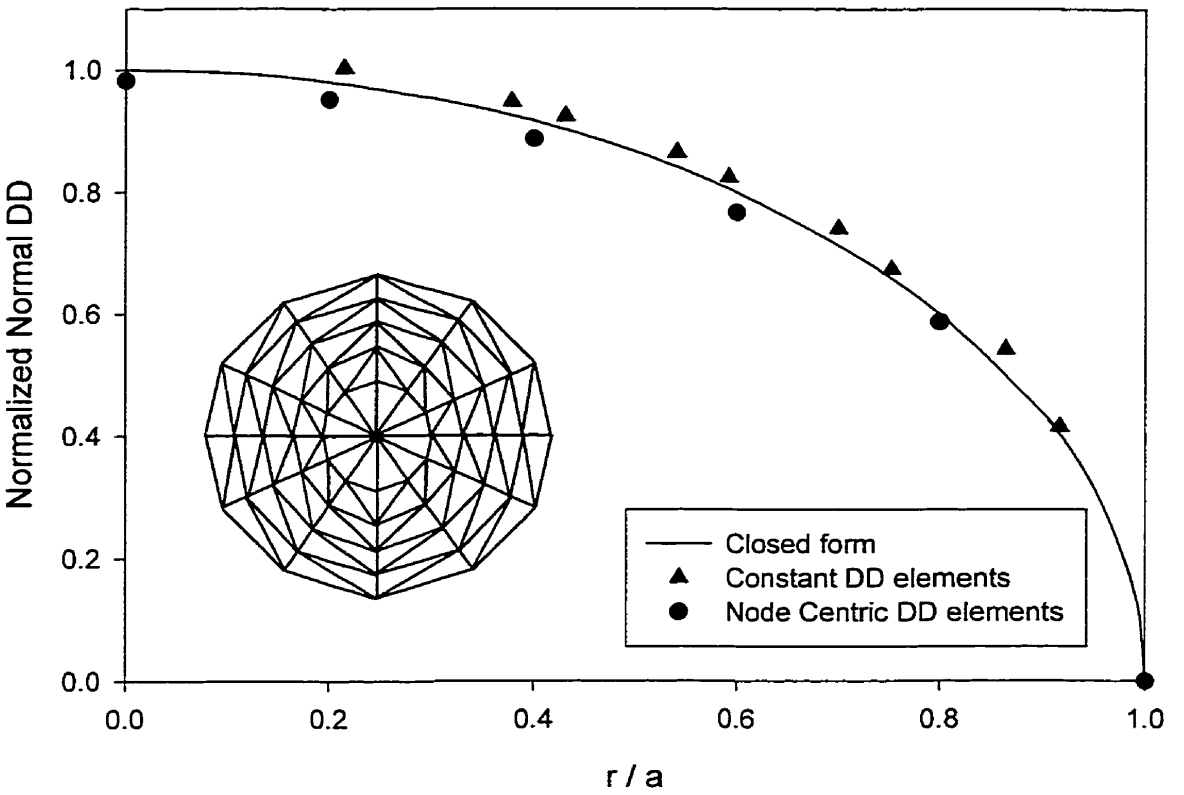

Figure 7: Normal displacement variation over the crack boundary

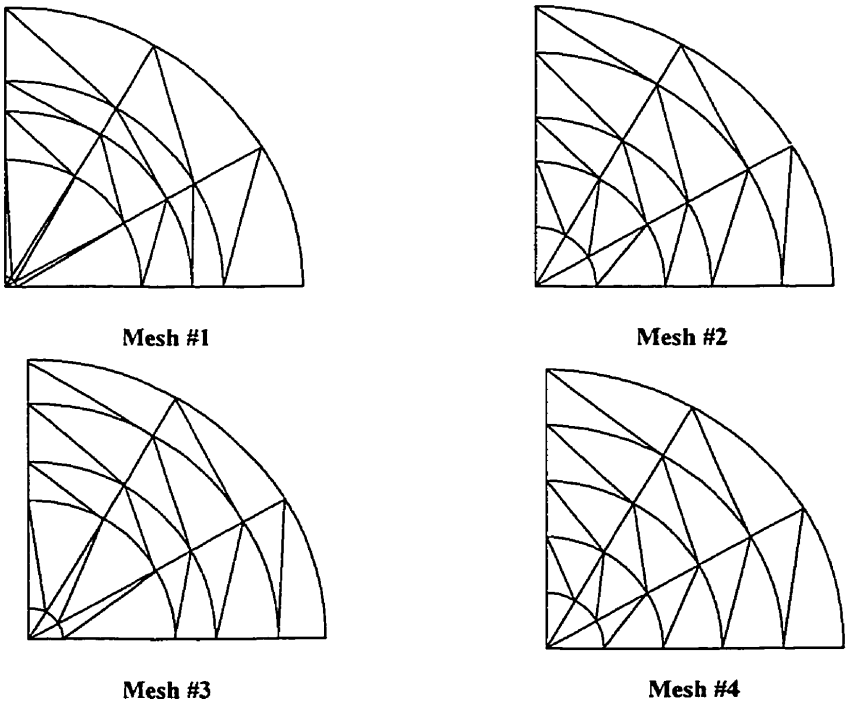

Figure 8: Meshes randomly discretized in radial direction

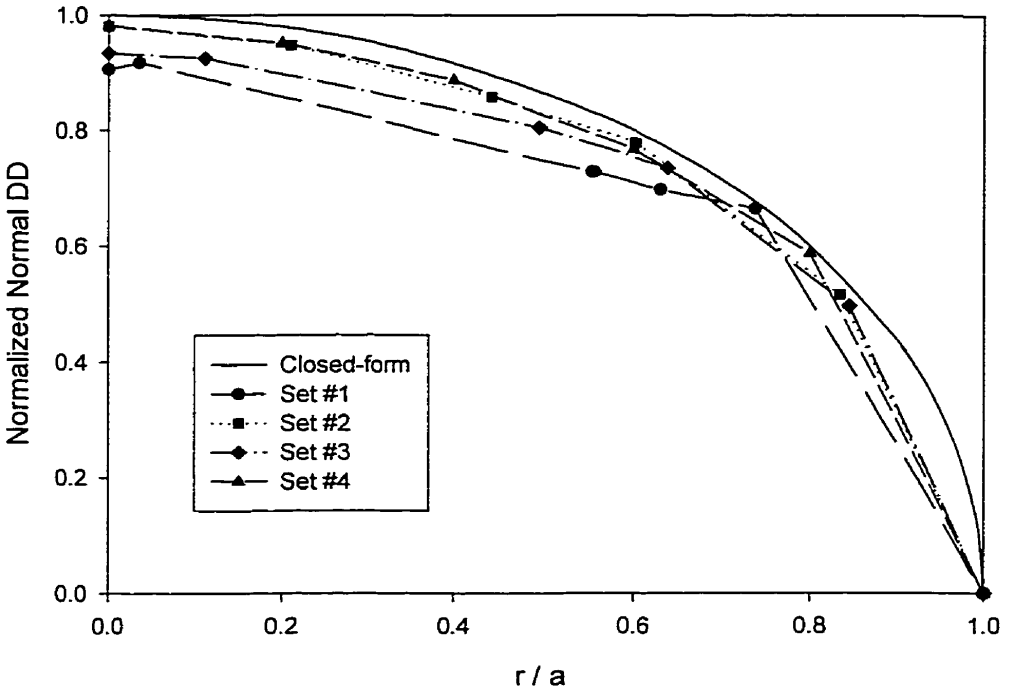

Figure 9: The distribution of normal DD for randomly sized meshes

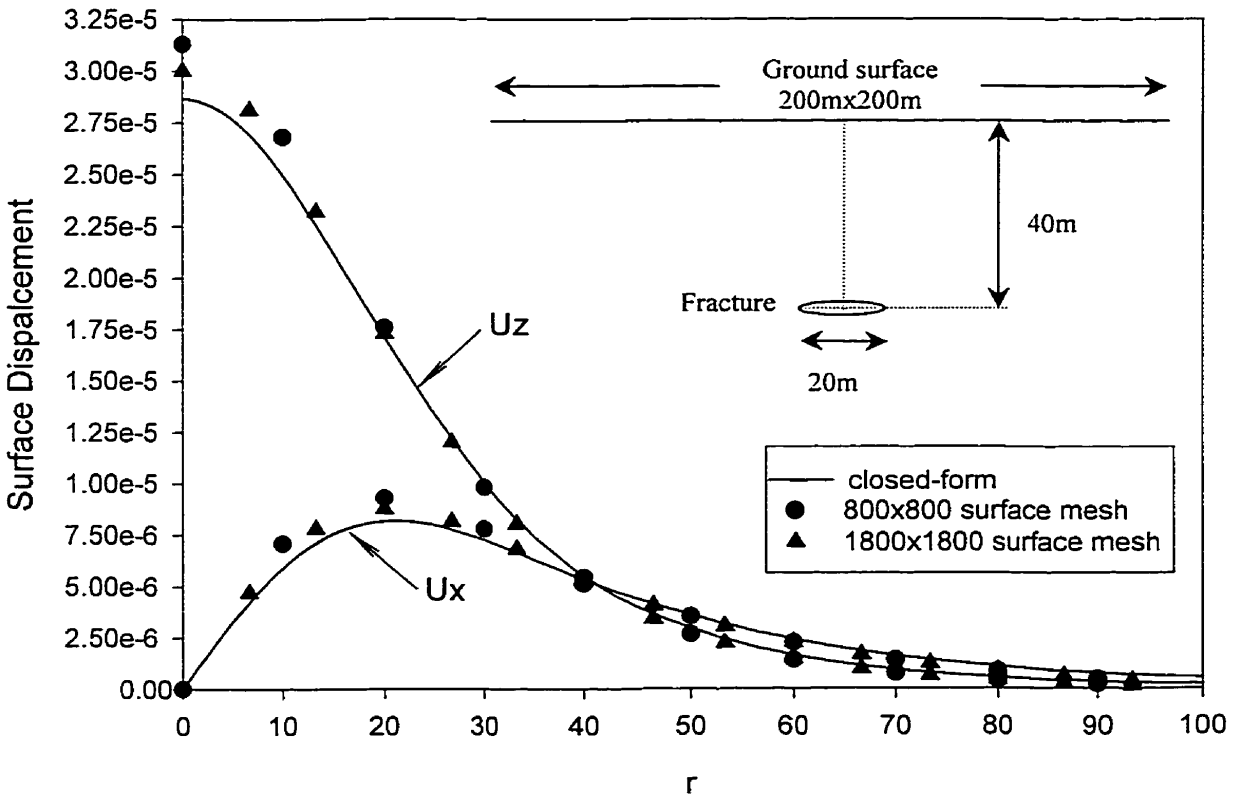

Figure 10: The distribution of displacements along the ground surface

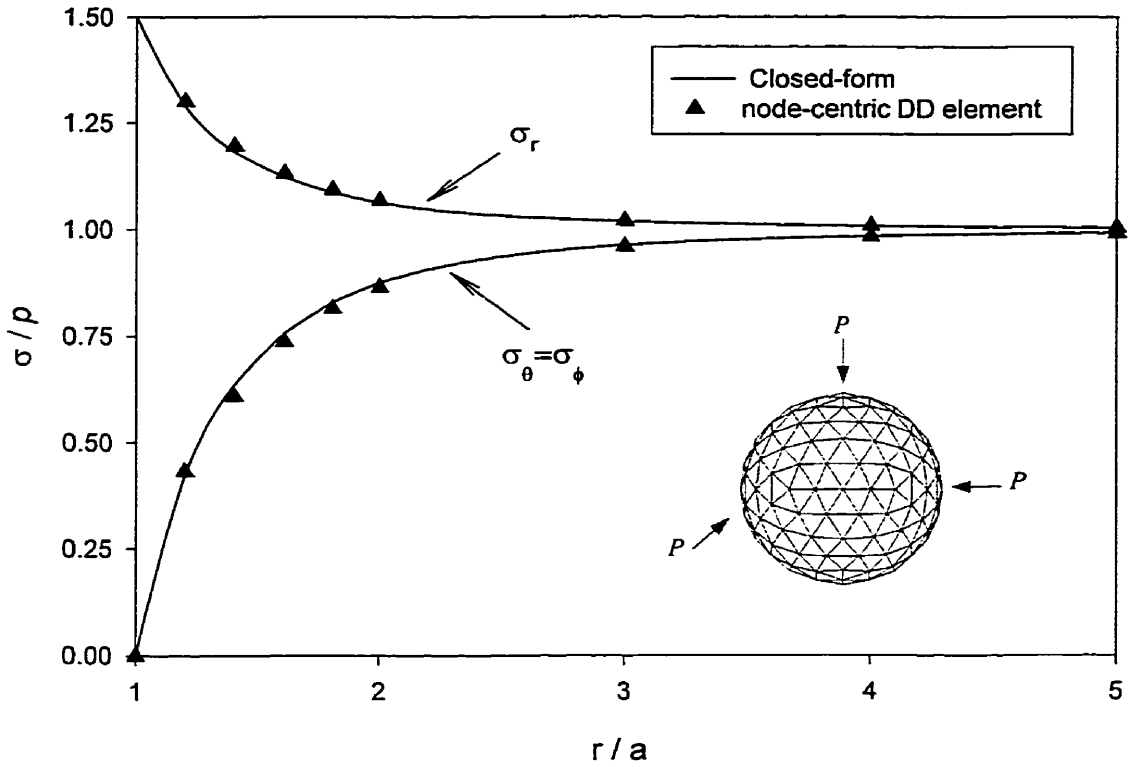

Figure 11: The distribution of stresses outside spherical cavity subjected to a hydrostatic pressure at infinity

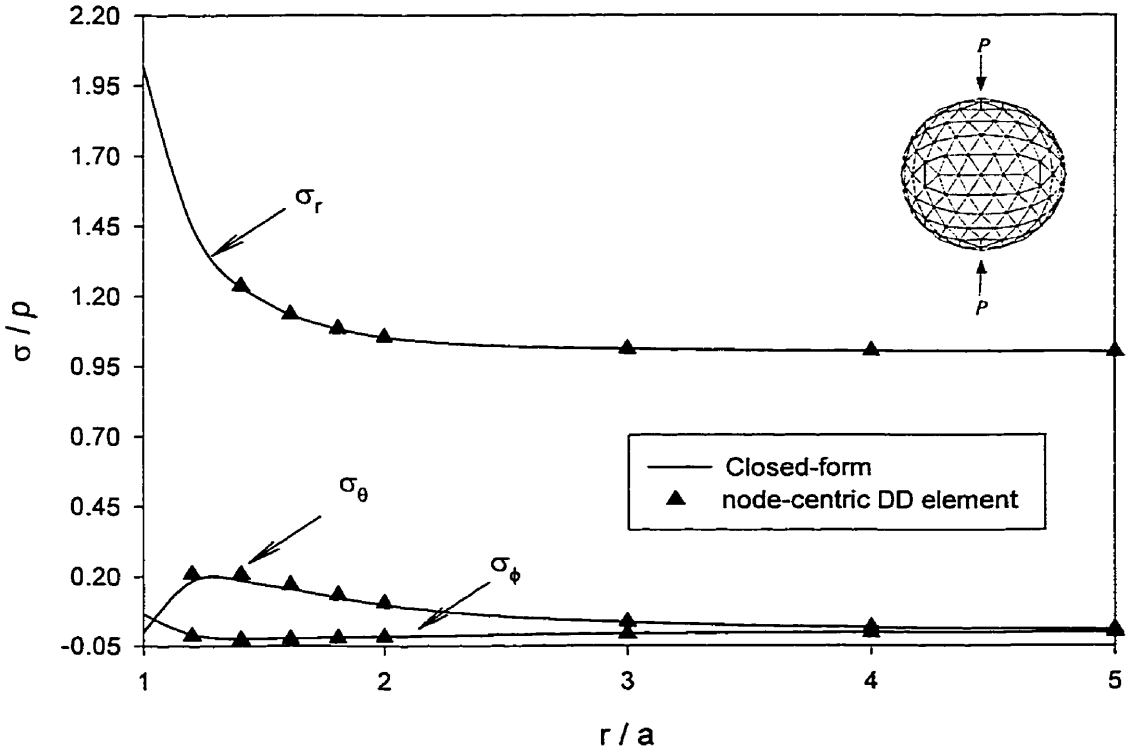

Figure 12: The distribution of stresses outside a spherical cavity subjected to a uniaxial stress at infinity

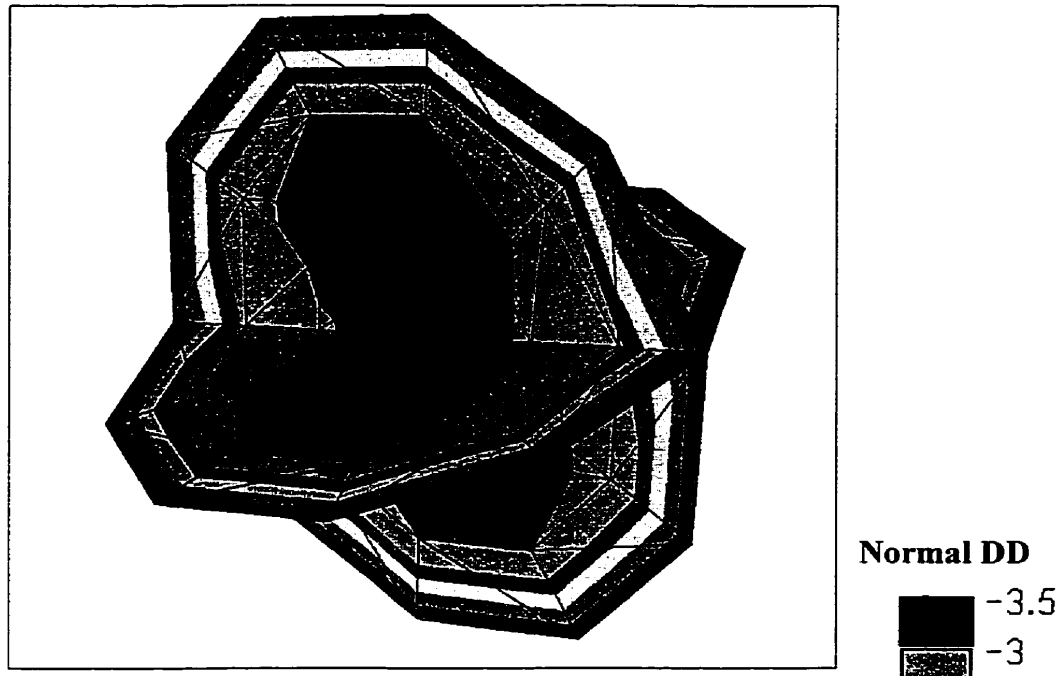

(a) node sharing along line of the intersection (set #1)

(b) no node sharing (set #2)

Figure 13: The variation of normal DD for two intersecting penny-shaped cracks

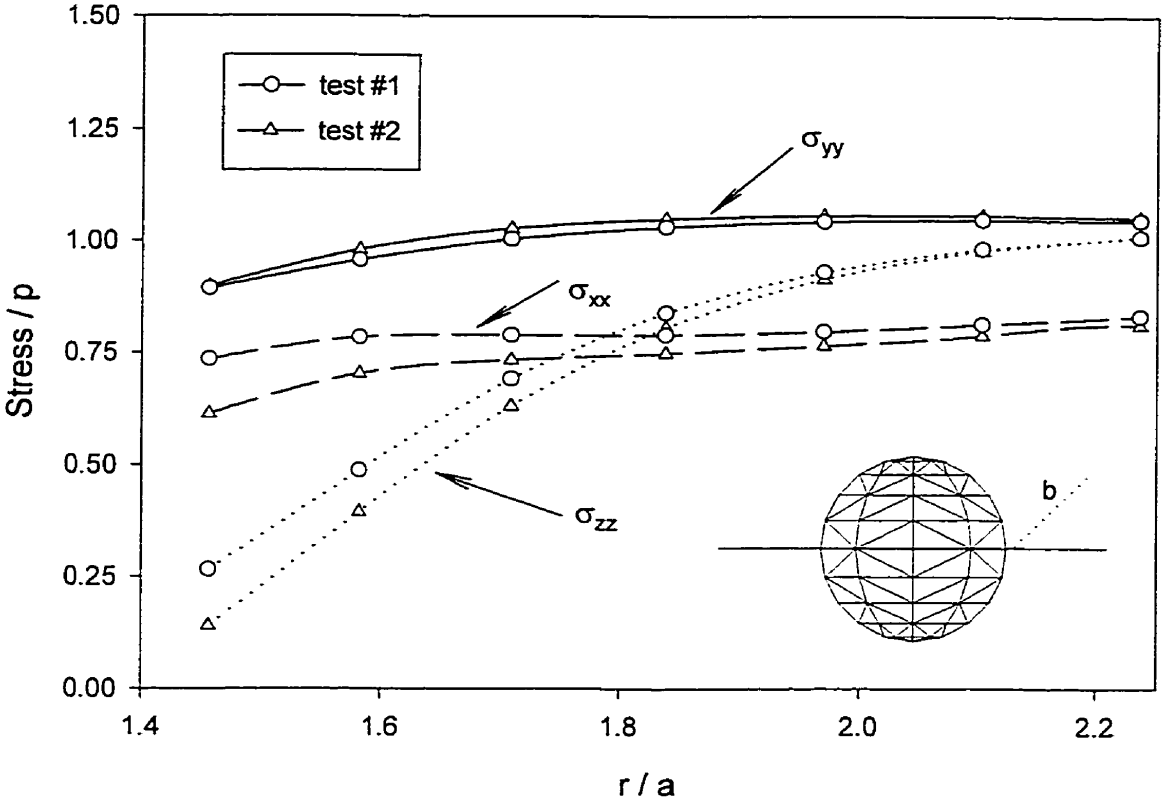

Figure 14: The variation of stress components

Appendix C

Paper III - "An Enhanced Displacement Discontinuity Method for the Analysis of Lenticular Orebodies"

To be submitted to the International Journal of Rock Mechanics and Mining Sciences

An Enhanced Displacement Discontinuity Method for the Analysis of Lenticular Orebodies

T. E. Yacoub[1] and J. H. Curran[2]
Rock Engineering Group, Dept. of Civil Engineering,
University of Toronto
Toronto, Ontario, Canada, M5S 1A4

Abstract

The displacement discontinuity method (DDM) - an indirect BEM - is very suitable for calculating stresses and displacements associated with the mining of lenticular orebodies (orebodies that are at most only a few meters in one direction and tens of meters in the other two). The original formulation of the DDM, however, omits the effects of confining stresses, which are important to pillar strength.

In this paper, a new DD method, the enhanced displacement discontinuity method (EDDM), which explicitly models confining stresses in pillars in the formulation of DD elements, is presented. The new DD element is derived through the inclusion of an additional singularity that accounts for confining stresses to the formulation of the conventional DD. The inclusion of the confinement DD enables the EDDM to accommodate all components of the stress tensor, and requires a new equation to make the resulting system of equations fully determinate. This equation is obtained via the material constitutive relationship. The use of the full stress tensor grants the EDDM the capability to employ general material constitutive relationships for the modelling of different types of material behaviour. It is developed for both two- and three-dimensional problems. Sample applications of the new method to pillar problems are provided in the paper. These examples illustrate the viability of the EDDM.

Keywords: Displacement Discontinuity, DD, enhanced displacement discontinuity, EDD, strain nucleus or nuclei, pillar confinement effect.

---

[1] Ph. D. Candidate and [2]Professor

1. INTRODUCTION

During the (room-and-pillar or longwall) mining of lenticular orebodies, sections of the orebody are left intact for the purposes of providing support for excavated rooms. These unexcavated orebody portions are known as pillars. The analysis of stresses and displacements around the resulting excavations and in the pillars often requires the use of numerical techniques, because closed-form solutions exist only for a very small set of problems.

There are two competing demands that control pillar sizes in the design of pillars. Mining economics demands that as much ore as possible be recovered from mining operations implying that pillars must have minimal sizes. Safety demands however require that pillars be designed such that they have adequate load carrying capacity to prevent catastrophic collapse of excavations. For an optimal solution between the competing factors to be reached, some failure of peripheral pillar material in practical mining is permitted.

Numerical Modelling Techniques

Today there are a variety of numerical techniques available for performing stress analysis and design of rock engineering structures. These techniques include the finite element method (FEM), finite difference method (FDM) and the boundary element method (BEM). In principle, all of these methods can be used for the detailed modelling of features such as stopes and pillars that result from mining excavation works [1].

The finite element method is a very powerful and versatile numerical modelling technique that can be used to solve a very broad range of engineering problems. Overall it enjoys greater popularity in engineering applications than other numerical methods. In finite element modelling, the material region of interest is divided (discretised) into a network of elements. The solution to the problem of finding displacements and stresses induced by applied stress states is determined at the nodes of the elements. The FEM can be used to obtain detailed information on the distribution of stresses and strains that other methods are either incapable of producing, or can produce but with significantly more effort. It can also readily model non-linear material behaviour and non-homogeneous material domains.

As the name suggests, the boundary element method (BEM) involves the representation of only excavation boundaries with elements. Analytical solutions obtained for problems entailing the application of singular loads in generally homogeneous domains supply the basis for the BEM to satisfy the problem boundary conditions at the nodes of its elements. Based on the integral formulations involved, BEMs can be separated into two main classes - direct methods and indirect methods. In direct boundary element methods, stresses and displacements are calculated directly from the system of equations that is assembled for a problem. The indirect approach involves the initial computation of fictitious quantities. Stresses and displacements are thereafter calculated from these fictitious quantities. Unlike the FEM, however, the BEM does not accommodate heterogeneous material domains or non-linear material behaviour very readily.

Selection of Numerical Methods for Mining Applications

The success of these numerical techniques, when applied to mine design, depends on the level of effort needed to define or formulate problems in the techniques, their ability to produce solutions fairly rapidly, and the flexibility they offer in analysing alternate mine layouts reasonably quickly. The application of methods that demand tedious and subjective input such as the manual assignment of strength parameters to elements is limited by these constraints. A distinctive characteristic of the modelling of mining excavations is that problems involve large domains. As a result, when the FEM is applied to mining problems, relatively large regions around excavations have to be divided into elements. This approach necessarily leads to large numbers of nodes and elements, which in turn translate into considerable computational times for each mining layout or sequence examined. For three-dimensional problems, meshing becomes a significant issue in the FEM. It is not easily performed and subsequently hampers its use in the examination of alternate mining schemes. In the BEM, on the other hand, because only problem boundaries are discretized into elements, the amount of time needed to generate and check meshes is much reduced, especially for three-dimensional problems [1]. The smaller numbers of elements in the BEM result in much smaller systems of equations than are found in equivalent FEM representations of problems. These attributes of the BEM grant it significant advantages in computational speed and flexibility over the FEM in solving the large domain problems of mining.

A most important issue in the choice between the FEM and BEM for mine modelling centres on the justification for selecting one or the other method for design. Characteristically in mining, data on stress states and other input design parameters are

not recorded with great precision. A reasonably high degree of uncertainty therefore surrounds input parameters for the design of mining stopes and pillars. Also, in typical mine operations stopes need to be supported or kept standing only for a few weeks before either being backfilled, or being allowed to collapse. For the design of mine pillars therefore, the main purpose of stress analysis is to provide insight into the overall physical behaviour of mine pillars, rather than into the specifics of the behaviour of individual pillars. The desire of designers in such cases is to only obtain results that sufficiently capture the essential character of the problem. Due to these factors (the relatively high uncertainty in input data, moderate levels of required stress detail, and the short lengths of time over which excavations are required to stand or be supported), the use of the FEM is not always recommended for problems of analysing stopes and pillars. BEMs, on the other hand, meet the above criteria for mine design by requiring less effort in formulating problems and supplying the required amounts of information and insight, necessary for design. Despite their difficulties in handling heterogeneous materials, they are often more fitting for mine analysis and design because detailed knowledge on the material properties needed for the modelling of such material domains is not well established in many mining cases.

The Displacement Discontinuity Method (DDM). Advantages and Disadvantages

The displacement discontinuity method (DDM) is a type of indirect boundary element technique. It is well suited for modelling a particular class of mining problems, namely those involving thin, slit-like openings, and discontinuities such as faults or joints [2, 3]. Thin, slit-like openings are commonly encountered in the mining of lenticular ore

bodies (seam-type deposits) - orebodies that have relatively small thickness compared to their other two dimensions. In the analysis of such features, both excavated and unexcavated regions can be represented as crack-type elements.

Since the original papers on the DDM were published, advancements of the method have followed two principal directions [2]. In the first direction, researchers have sought for improvements to the accuracy of the method by formulating higher-order DD elements [4, 5]. The second direction has mainly pursued enhancements in the practical application of the DDM. These efforts have led to the development of several well-known commercial software packages [6, 7].

Displacement discontinuities can represent relative displacements of crack surfaces under the influence of imposed stresses. Because rock discontinuities and the features formed during the mining of lenticular orebodies have proportions similar to cracks, when compared to problem domains, they can be readily analysed with DDs. Although, generally, the initial unknown quantities computed in indirect methods are of a fictitious nature, the unknown variables in the DDM represent physical features in the modelling of mining excavations in lenticular orebodies, and rock discontinuities. For the mined sections of a lenticular orebody, the rides (the relative movements of the roof and floor of excavations parallel to each other) and closure (the relative displacement of the roof and floor perpendicular to their surfaces) can be treated as the unknown parameters in the DDM [2].

The formulation of DDs for pillars (unmined zones) differs from that of elements in mined regions of an orebody. To model the behaviour of material in pillars, springs that respond to the normal and shear stresses are included in the formulation of DD

elements for unmined orebody regions. The formulation of DDs for the different zones (*i.e.* mined or unmined) has allowed a number of practical mining problems to be solved.

Useful as the conventional DD formulation for unmined regions is, it has a major shortcoming. It is a well-established fact in rock mechanics that confining stresses significantly influence the strength of pillars. Because pillar cores, for example, experience much higher confining stresses than pillar regions abutting pillar surfaces, cores have much greater bearing capacities. The hourglass shape of failed pillars provides evidence of the phenomenon of confinement in rock material. This important effect of lateral confinement is omitted from the formulation of the conventional DD element for unmined material. The modelling of confinement in the pillar material is especially important when yielding or post-peak response of pillars is being analysed.

Yielding or failure of pillars cannot properly be analysed if confinement in pillars is ignored. In recognition of this problem, *ad hoc* approaches are used to account for confinement in the practical application of the DDM to mining problems. One such procedure recognises confinement in unmined zones through the use of a family of stress-strain curves. In this method, each pillar is discretised into several elements. Elements are then assigned stress-strain curves based on their locations in pillars. Those close to pillar centres or cores are assigned the highest strength curves, while the ones adjacent to pillar surfaces have the lowest curves. Intermediate elements are assigned intermediate curves. This approach has been implemented in the commercial software package MULSIM [7].

The *ad hoc* approaches, however, have some principal deficiencies. The procedure described above, for example, is tedious and requires considerable experience in order to determine the appropriate stress-strain curves to assign to elements in a pillar. This makes

the technique subjective in nature. In principle, the approach used in MULSIM/NL can be used for pillar geometries of varying complexity. However, even slight complications of pillar geometries, make the technique difficult to use.

Proposed Enhancement to the DDM

This paper proposes an enhanced displacement discontinuity method (EDDM) that explicitly accounts for the effect of confinement in an objective manner. This enhancement is achieved through the addition of a displacement discontinuity singularity that is perpendicular to the normal DD present in the original formulation of DDs. With the addition of this new DD, three stress types, instead of two, are now accounted for in the modelling of unmined material. The three stress types accounted for now are normal, shear and confining stresses. By including confining stress in its formulation, the newly created DD elements can accommodate general constitutive relationships, ranging from elastic models to general plasticity formulations, to represent pillar material behaviour. An additional advantage of the EDDM is that it accounts for confinement in a manner more general than those advocated by *ad hoc* approaches such as the technique used in MULSIM. Instead of using a discrete set of strength curves to model the effects of confinement, the EDDM allows strengths at different locations in a material to be calculated as functions of the stress states at the locations. It therefore offers more than the mere automation of the procedure advocated in MULSIM (automation of the process translates into considerable timesaving for mine design) by also modelling confinement more realistically.

2. PILLAR BEHAVIOR

In room-and-pillar and longwall mining, pillars are generated as ore remnants between excavations, to control both the local performance of roof rock and the global response of the host rock medium. These pillars have the capability to transmit axial and shear loads [8].

The degree of confinement implicitly influences pillar strength. Fig. 1 shows the stress-strain behaviour of rock cores under confining stresses. The higher the confining stress, the higher are both the peak and residual strengths of rock cores. Irrespective of the shape of a pillar, it typically has a confined core. Under normal overburden pressure, horizontal in-situ stresses are generated in pillar cores due to the effect of Poisson's ratio [9, 10]. The bearing capacity, thus, of a pillar increases with increasing radius of its confined core. Pillar deformability is inversely proportional to the area of confined cores [11, 12].

From the above discussion on the effects of confinement, it is reasonable to expect that in any mathematical formulation of problems involving pillars, significant error is introduced in the calculated values of displacements and stresses, if confinement is neglected in the analysis. As earlier mentioned, one of the disadvantages of the classical DDM for analysis involving pillars is that the formulation involves only two types of singularities that account for normal and shear stresses [13]. A lateral discontinuity that can model the effects of confinement is not considered. It is to overcome this disadvantage that in the current work the effect of confinement is explicitly included in the formulation of elements for the EDDM. The incorporation of the missing lateral

component leads to the generalisation of *ad hoc* techniques (that compensate for this missing component) used in the practical implementation of the DDM to mining problems. In modelling pillars and unmined panels with the assumption that the average stress state (*i.e.* stress averaged over the height of a pillar) is representative of pillar response, the new method supplies all components of the stress tensor. As a result of these particular attributes of the EDDM, it can use any constitutive relationships to model the behaviour of the orebody material.

3. FORMULATION OF THE EHANCED DISPLACEMENT DISCONTINUITY METHOD

The original formulation of the displacement discontinuity method (DDM) combined the idea of modelling cracks as distributions of dislocations with the method of integral equations [14, 15]. The original DD formulation assumed a constant distribution of dislocations in modelling crack problems. This formulation was refined by Crawford and Curran [4], and later on by Vandamme and Curran [16], using higher-order dislocation distributions. These higher-order DD elements required that nodes be located in the interior of elements due to mathematical difficulties with integral equations. Despite an increase in accuracy with the use of higher-order elements, this approach could not eliminate inaccuracies in the modelling of lenticular orebody mining, because of the neglect of confining effects in pillars.

Confinement can be incorporated into the DDM by deriving DDs starting from the basic definition of discontinuities as singularities created by strain nuclei, which are volumetric strain densities in three-dimensional problems, and surface strain densities for

two-dimensional problems. There are two fundamental types of nuclei of strain, d^* - shear and normal strain nuclei. These strain nuclei can be distributed such that the necessary boundary conditions in crack problems are satisfied [17].

3.1 Conceptual framework

A displacement discontinuity, as originally defined, is the relative movement between the two surfaces of a crack [2]. This definition of a displacement discontinuity can be generalised to cover the relative movement between two points on a crack. Because the relative movement of opposing points on the surfaces of a crack is uniform along the length of the crack, it becomes possible to define the displacement discontinuity as the relative movement between surfaces. For the traditional displacement discontinuity element (Fig. 2a), the shear DD is calculated as $D_1 = u_1^+ - u_1^-$, while the DD in the normal direction is defined as $D_2 = u_2^+ - u_2^-$.

By examining the generalised definition of a DD, a third DD, which shall be named the lateral or confinement DD, D_c, can be defined for an element. It is the relative movement between the ends of a DD element as shown on Fig. 2b, and is defined by the relationship $D_c = u_c^+ - u_c^-$.

A strain nucleus d^* is the displacement discontinuity per unit volume in a continuum [18]. The cumulative or total displacement discontinuity, Ω, in a unit volume can be kept constant while the height of the volume is collapsed to zero. This can be written mathematically as $\Omega = \int d^* dV = \int d\, dA$, where d is a new quantity, which shall be

termed the displacement discontinuity per unit area, or surface displacement discontinuity density.

When a two-dimensional element of height h and length $2a$ in a homogeneous, linear elastic material is subjected to normal strain nuclei d_2^*, distributed throughout the element, stresses are induced in the medium. The stresses induced at a point q, sufficiently far from the element, by the distribution of strain nuclei can be (closely) replicated by replacing the element with a displacement discontinuity density, d, acting along the centreline of the element. (It is only when q is sufficiently far from the element that the stresses induced by strain nuclei distributed throughout the element will be well approximated by those induced by a displacement discontinuity density acting at the centreline of the element.)

Stresses induced by the strain nuclei distribution d_2^* can be determined using the following integral equation:

$$\sigma(q) = \int_{-h/2}^{+h/2} g(p,q) \cdot d^*(p)\, dx_2, \tag{1}$$

where g is a Green's function, and p is a point in the domain of the distribution of strain nuclei. Since the Green's function is continuous in the domain of integration $(-h/2, h/2)$, we can use the mean-value theorem to evaluate equation (1) as

$$\sigma(q) = g(p_o,q) \cdot d_2^*(p_o)\, h, \tag{2}$$

where p_o is the point between $-h/2$ and $h/2$ at which the integrand takes on its average value. p_o can be approximated to be located at the mid-height (centreline) of the element

in order to simplify computations. From this point forth, p_o shall be simply referred to as p.

Equivalent stresses at Q can be induced by a displacement discontinuity density d placed along the centre line of the element. These stresses can be evaluated from the formula:

$$\sigma(q) = g(p,q) \cdot d_2(p). \tag{3}$$

Equating (2) to (3), the strain nucleus distribution can be expressed in terms of the displacement discontinuity density as:

$$d_2^*(p) = d_2(p)/h \tag{4}$$

When the displacement discontinuity density d has a constant variation in the x_1-direction, it becomes equal to a displacement discontinuity D acting at the centre of the element (see further explanation in the next section).

Similar to the above development of the normal DD, a shear displacement discontinuity, D_1, can be formulated by replacing the normal strain nuclei with nuclei that produce shear displacements in the element.

We shall now consider another distribution of strain nuclei d_c^* that act on the element. We shall label these nuclei as confinement strain nuclei. This new distribution takes care of the effect of confinement in the element and produces lateral strain within the element. Analogous to the case of normal strain nuclei d_2^*, a lateral (or confinement) displacement discontinuity density d_c can be obtained from the confinement strain nuclei d_c^*. They are related through the equation

$$d_c^*(p) = d_c(p)/h \tag{5}$$

Assuming a constant distribution of lateral displacement discontinuity density in the x_1-direction, the total lateral displacement discontinuity in the element can be evaluated as

$$D_c(p) = \int_{-a}^{+a} d_c^*(p)\, dx_1 = d_c(p)\frac{2a}{h}. \tag{6}$$

Expression (6) defines the lateral (confinement) displacement discontinuity. This new DD will be employed in the development of the enhanced DD element, which will be presented in the next section.

3.2 Mathematical formulation

As mentioned earlier, distributions of shear and normal strain nuclei throughout an element of height h and length $2a$ located at a point p in a homogenous, linear elastic material, induce stresses in the continuum. The components of the stress tensor, σ_{ij}, and the displacements, u_i, that arise at a point q in the continuum due to the strain nuclei can be determined from the following equations:

$$\sigma_{ij}(q) = \int_{-a}^{+a}\int_{-h/2}^{+h/2} g_{ijk}^*(p,q) d_k^*(p) \varphi_m(x_2)\, dx_2 dx_1\,, \tag{7}$$

$$u_i(q) = \int_{-a}^{+a}\int_{-h/2}^{+h/2} h_{ik}^*(p,q) d_k^*(p) \varphi_m(x_2)\, dx_2 dx_1\,, \tag{8}$$

where the repeated indices represent the usual summation convention. For two-dimensional problems $i, j, k = 1, 2$. g^*_{ijk} and h^*_{ik} are normal and shear influence functions for stresses and displacements, respectively, due to the strain density at p. φ_m is an interpolation function. It can range from the simple square function, φ_0, to the Dirac delta function, φ_n (or δ) (Fig. 3).

We shall select the Dirac delta function for the problem at hand, *i.e.* $\varphi_m = \delta$, because of its unique properties, and shall also look to simplify the resulting expression $\int_{-h/2}^{+h/2} g^*_{ijk}(p,q) d^*_k(p)\, \delta(x_2)\, dx_2$ in equation (7). The Dirac delta function has an important property that for two functions $f(t)$ and $\varphi(t)$, both continuous at the origin, the following relationship holds [19]

$$\int_{-\infty}^{+\infty} [f(t)\ \varphi(t)]\ \delta(t)\ dt = f(0)\varphi(0) \tag{9}$$

Using the well-known property of the Dirac function: $\int_{-\infty}^{+\infty} f(t)\ \delta(t)\ dt = f(0)$, equation (9) can be written as:

$$\int_{-\infty}^{+\infty} [f(t)\ \varphi(t)]\ \delta(t)\ dt = \int_{-\infty}^{+\infty} f(t)\ \delta(t)\ dt\ \int_{-\infty}^{+\infty} \varphi(t)\ \delta(t)\ dt\,. \tag{10}$$

The above property, applied to the expression we are trying to simplify, leads to the following result:

$$\int_{-h/2}^{+h/2} g^*_{ijk}(p,q) d^*_k(p)\, \delta(x_2)\, dx_2 = \int_{-h/2}^{+h/2} g^*_{ijk}(p,q)\, \delta(x_2)\, dx_2 \int_{-h/2}^{+h/2} d^*_k(p)\, \delta(x_2)\, dx_2\,. \tag{11}$$

By letting

$$\int_{-h/2}^{+h/2} d_k^{\bullet}(p)\,\delta(x_2)\,dx_2 = d_k(p) \text{ , and } \int_{-h/2}^{+h/2} g_{ijk}^{\bullet}(p,q)\delta(x_2)\,dx_2 = g_{ijk}(p,q), \quad (12)$$

equation (11) can be reduced to the form:

$$\int_{-h/2}^{+h/2} g_{ijk}^{\bullet}(p,q) d_k^{\bullet}(p)\,\delta(x_2)\,dx_2 = g_{ijk}(p,q)\,d_k(p). \quad (13)$$

d_k is the displacement discontinuity density (where d_1 is the ride or shear DD density, and d_2 is the closure or normal DD density). Similar operations can be performed to simplify the corresponding expression in the equation for computing displacements.

These mathematical operations lead to the important result that for two-dimensional problems, the stresses and displacements in equations (7) and (8) can be calculated as:

$$\sigma_{ij}(q) = \int_{-a}^{+a} g_{ijk}(p,q) d_k(p)\,dx_1 \quad (14)$$

$$u_i(q) = \int_{-a}^{+a} h_{ik}(p,q) d_k(p) dx_1 \,. \quad (15)$$

g_{ijk} and h_{ik} are the normal and shear influence functions for stresses and displacements, respectively, due to the displacement discontinuity density d_k at the point p. These influence functions are given in [20]. The equations (14) and (15) constitute the formulation of the classical displacement discontinuity method.

We shall now consider the case of a crack divided into N discrete line segments or elements. Acting over each of these elements is a DD density. Each element is defined by nodes at which displacement discontinuities (DDs) can be evaluated. By multiplying values of the nodal DDs with coefficients of an interpolation function, the DD density

variation over the length of the crack can be approximated [1, 21]. The approximation of the DD density at a point p along the crack, coincident with the nodes of the elements, is represented by the expression:

$$d_k(p) = \sum_e \Phi_e(p)\, D_k^e, \quad k = 1, 2. \tag{16}$$

Φ is an interpolation function identical to the shape functions of elements [1], which is evaluated at the nodes e. Substituting eqn. (16) into eqns. (14) and (15) we obtain the following equations:

$$\sigma_{ij}(q) = \sum_e \int_a g_{ijk}(p,q)\Phi_e(p)D_k^e\, dx_1 \tag{17}$$

$$u_i(q) = \sum_e \int_a h_{ik}(p,q)\Phi_e(p)D_k^e\, dx_1 \tag{18}$$

If we assume a constant variation of the displacement discontinuity over each element, $\Phi_e(p)$ at node p is equal to unity and zero everywhere else, and eqns. (17) and (18) become:

$$\sigma_{ij}(q) = \sum_e D_k^e \int_a g_{ijk}(p,q)\, dx_1 \tag{19}$$

$$u_i(q) = \sum_e D_k^e \int_a h_{ik}(p,q)\, dx_1\,, \tag{20}$$

In this case the total number of nodes is equal to the number of elements N. Equations (19) and (20) form the classical formulation of the constant DDM.

The formulation of the enhanced displacement discontinuity (EDD) element shall begin with strain densities. Revisiting the problem of shear and normal strain nuclei acting at a point in a material, let an additional nucleus, d_c^*, orthogonal to the normal strain nucleus be included in the problem. Other than direction, this new strain nucleus

behaves similarly to the normal strain density. The solution of the new problem differs from the original only by the addition of an extra term to each of the equations (9) and (10), that accounts for the influence of the newly introduced strain density.

A new displacement discontinuity, D_c, which is perpendicular to the normal DD, can be formed from the new strain nucleus. Relying on the same approach used in the formulation of the classical DDM, the density d_c of this new lateral or confinement displacement discontinuity can be determined from the additional strain nucleus d_c^* using the relationship $d_c(p) = \int_{-h/2}^{+h/2} d_c^*(p)\,\delta(x_2)\,dx_2$. For discretized problems, the DD density at a point p along a crack can be approximated by nodal DD values through interpolation functions and the equation: $d_c(p) = \sum_e \Phi_e(p)\, D_c^e, \quad k = 1, 2$.

The stresses and displacements induced at an arbitrary point q in an infinite, homogeneous, linear elastic domain with the application of a shear, normal, and lateral constant DD can be written as (Fig. 3):

$$\sigma_{ij}(q) = \sum_e D_k^e \int_a g_{ijk}(p,q)\,dx_1 + \sum_e D_c^e \int_a v_{ij}(p,q)\,dx_1 \tag{21}$$

$$u_i(q) = \sum_e D_k^e \int_a h_{ik}(p,q)\,dx_1 + \sum_e D_c^e \int_a w_i(p,q)\,dx_1 \,. \tag{22}$$

v_{ij} and w_i are the confinement displacement discontinuity influence functions for stresses and displacements, respectively. Their mathematical definitions are as follow:

$$v_{11} = \frac{-G}{4\pi(1-\nu)}\left[2\frac{x_1^4}{r^6} + 2\frac{x_2^4}{r^6} - 12\frac{x_1^2 x_2^4}{r^6}\right] \tag{23}$$

$$v_{22} = \frac{-G}{4\pi(1-\nu)}\left[2\frac{x_1^4}{r^6} - 6\frac{x_2^4}{r^6} + 12\frac{x_1^2 x_2^2}{r^6}\right] \tag{24}$$

$$v_{12} = v_{21} = \frac{G}{4\pi(1-\nu)}\left[12\frac{x_1 x_2^3}{r^6} - 4\frac{x_1^3 x_2}{r^6}\right] \tag{25}$$

$$w_1 = \frac{G}{8\pi(1-\nu)}\frac{1}{r^2}\left[(1-2\nu)x_1 - 4\frac{x_2^2 x_1}{r^2}\right] \tag{26}$$

$$w_2 = \frac{-G}{8\pi(1-\nu)}\frac{1}{r^2}\left[(1-2\nu)x_2 + 4\frac{x_2^3}{r^2}\right] , \tag{27}$$

where $r^2 = x_1^2 + x_2^2$, and G and ν are the shear modulus and Poisson's ratio of the material, respectively. This newly formulated DD element is what shall be known as the enhanced DD element.

4. SYSTEM OF EQUATIONS FOR EDDM

The enhanced DD element can be applied to the problem of determining the total stresses and mining-induced displacements in the room-and-pillar or longwall mining of lenticular orebodies. As stated earlier, such mining involves slit-type excavations. It is necessary to identify the appropriate boundary conditions specific for problems of the type described above.

As a first step in solving the problem of mining lenticular orebodies employing room-and-pillar or longwall techniques, discrete EDD elements are placed along the centre lines of the excavations, pillars and panels. The next step is to determine values of normal, shear and confinement DDs that produce total stress and displacement components consistent with the boundary conditions of the problem. In general, if the problem involves boundaries that are represented by N elements, M of which are unmined

($M<N$), induced stresses σ_{ij}^{p} and displacements u_i^p at element p due to the distribution of normal, shear and confinement DDs at element q can be computed as

$$\sigma_{ij}^{p} = A_{ijk}^{pq} D_k^q + \delta_{ik} K_{jk}^{pq} D_c^q \tag{28}$$

$$u_i^p = B_{ik}^{pq} D_k^q + L_i^{pq} D_c^q \ , \tag{29}$$

where $i, j, k = 1, 2$ and δ_{ij} is Kronecker's delta. The influence coefficients A_{ijk}^{pq} are obtained from the expression

$$A_{ijk}^{pq} = t_{il} G_{lmk}^{pq} t_{mj} \ , \tag{30}$$

where G_{lmk}^{pq} is the integral in the element local coordinate system of $g_{lmk}(p,q)$ in equation (21), and

$$t_{il} = \begin{bmatrix} \cos\theta & -\sin\theta \\ \sin\theta & \cos\theta \end{bmatrix}. \tag{31}$$

θ is the angle between the local coordinate system of element q and the global coordinate system (Fig. 3). The other coefficients K_{jk}^{pq}, B_{ik}^{pq} and L_i^{pq} of equations (28) and (29) are determined in similar fashion through the integration and transformation of $v_{ij}(p,q)$, $h_{ik}(p,q)$, and $w_i(p,q)$ in equations (21) and (22), respectively.

Eqns. (28) and (29) represent a system of linear algebraic equations which, after substitution of the appropriate boundary conditions, can be solved for the unknown displacement discontinuities D_k^p and D_c^p.

In the solution of problems associated with underground excavations, it is convenient to separate total stresses σ_{ij} into two stress components - initial stresses

$(\sigma_{ij})_o$ and induced stresses due to excavation (or simply induced stresses) $(\sigma_{ij})'$. This is written mathematically as:

$$\sigma_{ij} = (\sigma_{ij})_o + (\sigma_{ij})' . \tag{32}$$

Crouch and Starfield [15] introduced mining-specific boundary conditions into the DDM. Naturally, these boundary conditions differ for mined and unmined rock or orebody zones. The boundary conditions for the EDDM are the same as those defined by Crouch and Starfield. However, because of the inclusion of a third DD, the confinement DD - D_c, an additional equation is needed to make the system of equations assembled for the EDDM fully determinate. This equation is supplied by the constitutive relationship for the seam material in unmined zones. Boundary conditions and the assembling of equations for the EDDM shall be discussed next.

Boundary conditions and system of equations for elements in mined zones

In the mined portions of a seam or orebody, generally, there is no contact between the roof and the floor of excavations. The boundary conditions[1] for the roof and floor are defined by Crouch and Starfield to be:

$$\sigma_{22} = -(\sigma_{22})_o \tag{33}$$

$$\sigma_{12} = -(\sigma_{12})_o , \tag{34}$$

where $(\sigma_{22})_o$ and $(\sigma_{12})_o$ are the initial normal stress and shear stress, respectively. These same boundary conditions are applied to EDD elements in mined zones. It is important to

[1] σ_{12} and σ_{22} in equations (33) and (34) are equivalent to the stresses denoted in [2] as σ_s and σ_n.

mention here that the lateral confinement of EDD elements in these zones is zero, because those elements have no material in them.

Writing the stresses in the normal and shear directions that arise out of eqn. (21) for EDD elements in mined zones, and using the above boundary conditions, the resulting system of equations is:

$$-(\sigma_{22}^{p})_{o} = A_{222}^{pq} D_2^q + A_{221}^{pq} D_1^q \tag{35}$$

$$-(\sigma_{12}^{p})_{o} = A_{122}^{pq} D_2^q + A_{121}^{pq} D_1^q . \tag{36}$$

$$D_c^p = 0 \tag{37}$$

Boundary conditions and system of equations for elements in unmined zones

To model material in the unmined zones of a seam, earlier works [2, 6, 7] use an elemental displacement discontinuity whose opposite surfaces are connected by springs (Fig. 4). The stiffness of each spring is chosen so that it has the same properties as the unmined material. In the original formulation of DDs, since simple one-dimensional stress-strain relations for compression and shear is assumed, only the normal stress, $(\sigma_{22})'$, and shear stress, $(\sigma_{12})'$, induced on an element are computed. These are determined, respectively, as:

$$(\sigma_{22})' = -\frac{E_s}{h_s} D_2 \tag{38}$$

$$(\sigma_{12})' = -\frac{G_s}{h_s} D_1 , \tag{39}$$

where h_S is the thickness of the seam, and E_S and G_S are the seam's Young and shear modulus, respectively. Material in unmined portions of a seam is thus modelled as an assemblage of springs, independently connecting the opposite surfaces of elements [2].

For elements in unmined zones, the EDDM accounts for the effect of confinement with the introduction of the confinement displacement discontinuity, D_c (Fig. 5). The equations for modelling the seam material change as a result of the new DD. If it is assumed that the seam material is homogeneous, isotropic, and linearly elastic, its constitutive relationship connecting stresses, σ_{ij}, and strains, ε_{ij}, can be written as:

$$\sigma_{ij} = \lambda_s \, \delta_{ij} \, \varepsilon_{kk} + 2G_s \, \varepsilon_{ij} \ , \tag{40}$$

where λ is Lame's constant defined by the relationship:

$$\lambda_s = \frac{2\nu}{(1-2\nu)} G_s \ .$$

Let strain nuclei acting on thin strips of material with height equal to element height h_S, be distributed along the length of a crack [17]. The strain nuclei, d_c^*, d_1^* and d_2^*, discussed earlier in the development of the EDD element (see section 3.1 of this paper), can be defined as

$$d_c^* = \varepsilon_{11} = \frac{\partial u_1}{\partial x_1} \tag{41}$$

$$d_2^* = \varepsilon_{22} = \frac{\partial u_2}{\partial x_2} \tag{42}$$

$$d_1^* = \varepsilon_{12} = \frac{1}{2}\left(\frac{\partial u_1}{\partial x_2} + \frac{\partial u_2}{\partial x_1}\right) \tag{43}$$

where ε_{11}, ε_{22}, and ε_{12} are the lateral, normal and shear strain, respectively. The strain nuclei distributions ε_{12} and ε_{22} corresponding to the displacement discontinuity densities d_1 and d_2 for an element of finite height h_s, as shown previously in eqns. (3) and (4), can be expressed as

$$\varepsilon_{12} = d_1^* = d_1 / h_s \tag{44a}$$

$$\varepsilon_{22} = d_2^* = d_2 / h_s \tag{44b}$$

The lateral strain in the element, ε_{11}, due to the lateral displacement discontinuity density can be defined as the total lateral deformation D_c over the length of the element $2a$ and thus can be represented as

$$\varepsilon_{11} = \frac{D_c}{2a} = \frac{1}{2a}\left(d_c \frac{2a}{h_s}\right) = \frac{d_c}{h_s}. \tag{45}$$

Subsequently, the following relationship holds true for ε_{11}:

$$\varepsilon_{11} = d_c^* = d_c / h_s. \tag{46}$$

When the variation of the displacement discontinuity density over the length of an element is considered to be constant, the values of d_k and d_c at a node equal D_k and D_c, respectively. Therefore, by replacing the strains in the constitutive relationship (34) with the quantities $\frac{D_k}{h_s}$ and $\frac{D_c}{h_s}$, the normal, lateral and shear stresses induced on an element in an unmined zone through the application of DDs are determined to be:

$$(\sigma_{22})' = \frac{(\lambda_s + 2G_s)}{h_s} D_2 + \frac{2G_s}{h_s} D_c \tag{47}$$

$$(\sigma_{11})' = \frac{(\lambda_s + 2G_s)}{h_s} D_c + \frac{2G_s}{h_s} D_2 \tag{48}$$

$$(\sigma_{12})^{\cdot} = \frac{G_s}{h_s} D_1 \tag{49}$$

The use of the constitutive relationship for the seam material has provided the additional equation needed to make the system of assembled equations fully determinate. Observation of equations (47) and (48) shows that only the confinement and the normal discontinuities are coupled. This is consistent with the expected behaviour of pillars under axial loads.

By assuming that initial deformations of unmined elements are zero, and that they deform only in response to induced stresses [2], the following system of equations:

$$0 = \frac{(\lambda_s + 2G_s)}{h_s} D_2^p + \frac{2G_s}{h_s} D_c^p + A_{222}^{pq} D_2^q + A_{221}^{pq} D_1^q + K_{22}^{pq} D_c^q \tag{50}$$

$$0 = \frac{(\lambda_s + 2G_s)}{h_s} D_c^p + \frac{2G_s}{h_s} D_2^p + A_{112}^{pq} D_2^q + K_{11}^{pq} D_c^q \tag{51}$$

$$0 = \frac{G_s}{h_s} D_1^p + A_{122}^{pq} D_2^q + A_{121}^{pq} D_1^q \tag{52}$$

can be combined with the system of equations (29) - (31) (*i.e.* for the mined material), and the combined system solved for the unknown DDs.

5. VERIFICATION OF THE ENHANCED DISPLACEMENT DISCONTINUITY METHOD

The newly formulated method - the EDDM for two-dimensional analysis - was verified through the solution of a number of sample problems. The sample problems involved excavations of simple geometry. Where closed-form solutions were available,

their computed stresses were compared with those produced by the EDDM. In cases where there were no closed-form or analytical solutions for the examples, stresses computed from the EDDM were compared with those calculated from other numerical procedures such as the FEM and the coupled FEM/BEM. These comparisons helped to establish the correctness of the results produced by the EDDM.

Example 1. Multiple Crack Problem

The first example solves for the stresses induced in an elastic material when an infinite row of equidistant collinear cracks of equal length in the material are subjected to internal unit pressures (Fig. 6). Each crack is discretised with 20 equal-sized EDD elements. The distance between the cracks (pillar width) is chosen to be equal to the length of the cracks, and is similarly discretised as the cracks. Although the material between the cracks ordinarily would not have been discretized for a homogeneous domain in either the EDDM or the DDM, doing so allows one to obtain an idea of the accuracy of the methods, when the material between cracks is different from that of the domain. In Fig. 6, the variation of the normalised normal displacement discontinuity over a crack width computed by the new formulation is compared with that obtained from the closed-form solution for the normal DD [22]. For this test case, the values of the normalised normal DD produced by the EDDM are in good agreement with the values from the closed-form solution. The results of the EDDM are better than the solution obtained with the DDM using the same mesh (Fig. 6). The error for the EDDM was 3.43%, while that for the DDM was 4.64%. The EDDM has increased accuracy because its representation of pillars is more realistic. The accuracy of the results of the EDDM

could be improved by increasing the number of elements used to model cracks and inter-crack spaces.

Example 2. Analysis of Pillar and Stope

The model of a pillar between two stopes presented by Brady and Wassyng [23] is analysed with the EDDM in the second example. The geometry of the problem is shown in Fig. 7. The pillar and each of the stopes were modelled with 12 discrete EDD elements. Since there are no analytical solutions for this problem, stresses computed in the pillar and around the stopes by the EDDM were verified by comparing them to those generated from the coupled FEM/BEM developed by Brady and Wassyng [23] (used in checking only stresses in the pillar), and to calculated stresses from *Phase*^{2}, an FE software program developed in the Rock Engineering Group of the University of Toronto [24]. In the finite element-boundary element coupling technique presented by Brady and Wassyng [23], the boundaries of the stopes (excavations) were modelled with boundary elements while a finite element mesh was used for the pillar. *Phase*^{2} wholly employs the finite element method.

Figure 8 contains plots of the major and minor stresses in the pillar computed by the three methods. From the results, it can be seen that all three methods give similar solutions to the problem. (The stress values at the ends of the pillar are different for the coupled FEM/BEM technique because a finer mesh is needed in that region for the technique.) Values of the normal stresses in the panels for the EDDM and FEM are illustrated in Fig. 9. The plot in Fig. 9 again shows that the EDDM gives results that are

consistent with those obtained from the FEM. In addition, it must be noted that a very fine finite element mesh was used to obtain the comparable *Phase*^{2} results.

These comparisons demonstrate that the EDDM, as well as its additional capability of including confining effects (which are very important when pillar yielding is modelled), can provide accurate results when used for elastic analysis.

6. FORMULATION OF THE THREE-DIMENSIONAL EDDM

In room-and-pillar mining, the modelling of pillar behaviour with two-dimensional analysis is inadequate, because plane strain conditions are violated. This violation occurs due to the three-dimensional nature of stress states in pillars [11]. In order to achieve a realistic analysis of the behaviour of pillars, therefore, a three-dimensional analysis is often required.

A three-dimensional formulation of the EDDM can be readily developed through straightforward extension of the two-dimensional model that was presented in section 3. The equations (3) to (16), used in the development of the lateral DD, can be applied to three-dimensional analysis by merely letting the indices i, j and k take integer values from 1 to 3 instead of from 1 to 2. In the conventional three-dimensional DDM, each element has three DDs - two shear (ride) components and one normal (closure) component (Fig. 10).

Similar to the development of the two-dimensional EDDM, two lateral strain densities are added to the formulation of the three-dimensional DD element. These lateral strain densities, as was the case in two dimensions, have properties similar to that of the

normal strain nucleus except for direction (see section 3). In direction, they are perpendicular to the normal strain density. They represent an averaged confinement value that acts along the axes perpendicular to the normal DD.

The three-dimensional EDDM is developed in a fashion analogous to the two-dimensional formulation. The influence functions of the confinement (lateral) DD in equations (15) and (16) change for the three-dimensional case. The influence functions of the lateral DD (which is formed from the two lateral singularities) for three-dimensional analysis are as follow:

$$v_{11} = -\frac{G}{4\pi(1-\nu)}\left[2(1-\nu)\frac{1}{r^3} - 3(1-2\nu)\frac{x_2^2}{r^5} - \frac{15x_1^2x_3^2}{r^7}\right] \tag{53}$$

$$v_{22} = \frac{-G}{4\pi(1-\nu)}\left[2(1-\nu)\frac{1}{r^3} - 3(1-2\nu)\frac{x_1^2}{r^5} - \frac{15x_2^2x_3^2}{r^7}\right] \tag{54}$$

$$v_{33} = -\frac{G}{4\pi(1-\nu)}\left[\frac{1}{r^3} + \frac{6x_3^2}{r^5} - \frac{15x_3^4}{r^7}\right] \tag{55}$$

$$v_{12} = v_{21} = -\frac{G}{4\pi(1-\nu)}\left[3(1-2\nu)\frac{x_1x_2}{r^5} - \frac{15x_1x_2x_3^2}{r^7}\right] \tag{56}$$

$$v_{23} = -\frac{G}{4\pi(1-\nu)}\left[\frac{3x_2x_3}{r^5} - \frac{15x_2x_3^3}{r^7}\right] \tag{57}$$

$$v_{13} = -\frac{G}{4\pi(1-\nu)}\left[\frac{3x_1x_3}{r^5} - \frac{15x_1x_3^3}{r^7}\right] \tag{58}$$

$$w_1 = \frac{-1}{8\pi(1-\nu)}\left[-(1-2\nu)\frac{x_1}{r^3} + \frac{3x_1x_3^2}{r^5}\right] \tag{59}$$

$$w_2 = \frac{-1}{8\pi(1-\nu)}\left[-(1-2\nu)\frac{x_2}{r^3} + \frac{3x_2x_3^2}{r^5}\right] \tag{60}$$

$$w_3 = \frac{-1}{8\pi(1-\nu)}\left[(1-2\nu)\frac{x_3}{r^3} + \frac{3x_3^3}{r^5}\right] \tag{61}$$

Boundary conditions for three-dimensional EDD elements in mined and unmined zones of orebodies do not differ from the boundary conditions of their two-dimensional counterparts. The assumptions underlying these boundary conditions remain the same for the three-dimensional case. However, the presence of two shear components (ride components) in three-dimensional analysis (Fig. 10) instead of one leads to an additional equation for each of the mining zones. The systems of equations for the three-dimensional EDDM assembled for elements in mined and unmined orebody zones are as follow:

System of Equations for EDD elements in Mined Zones

$$-(\sigma_{33}^{p})_{o} = A_{331}^{pq} D_1^q + A_{332}^{pq} D_2^q + A_{333}^{pq} D_3^q \tag{62}$$

$$-(\sigma_{32}^{p})_{o} = A_{321}^{pq} D_1^q + A_{322}^{pq} D_2^q + + A_{323}^{pq} D_3^q \tag{63}$$

$$-(\sigma_{31}^{p})_{o} = A_{311}^{pq} D_1^q + A_{312}^{pq} D_2^q + A_{313}^{pq} D_3^q \tag{64}$$

$$D_c^p = 0 \tag{65}$$

where D_1 and D_2 are shear displacement discontinuities, and the A_{ijk}^{pq}'s coefficients calculated from the influence functions. $(\sigma_{33}^{p})_{o}$ is the normal initial stress at the locale of an element, while $(\sigma_{33}^{p})_{o}$ and $(\sigma_{33}^{p})_{o}$ are the initial shear stresses at the same point.

System of Equations for EDD elements in Unmined Zones

$$0 = \frac{(\lambda_s + 2G_s)}{h_s} D_3^p + \frac{2G_s}{h_s} D_c^p + A_{331}^{pq} D_1^q + A_{332}^{pq} D_2 + A_{333}^{pq} D_3^q + K_{33}^{pq} D_c^q \tag{66}$$

$$0 = \frac{(\lambda_s + 2G_s)}{h_s} D_c^p + \frac{2G_s}{h_s} D_3^p + A_{113}^{pq} D_3^q + K_{11}^{pq} D_c^q \tag{67}$$

$$0 = \frac{G_s}{h_s} D_1^p + A_{311}^{pq} D_1^q + A_{312}^{pq} D_2^q + A_{313}^{pq} D_3^q \tag{68}$$

$$0 = \frac{G_s}{h_s} D_2^p + A_{321}^{pq} D_1^q + A_{322}^{pq} D_2^q + A_{323}^{pq} D_3^q \tag{69}$$

where D_c^p is the lateral DD of an element, and G_S and λ_S are material constants. h_S is the thickness of a seam (element). All the other quantities are the same as those define above.

With the systems of equations defined by (62) to (65) and (66) to (69), one can solve the problem of determining stresses and displacements in three dimensions induced by the mining of lenticular orebodies. It must be mentioned again that these equations are valid only for homogeneous, isotropic, linear, elastic seam material. However, the method allows analogous equations to be developed for other constitutive models, such as full plasticity models.

7. EXAMPLES OF THREE-DIMENSIONAL PILLAR ANALYSIS WITH THE EDDM

Two examples of the application of the three-dimensional EDDM are considered.

Example 1. Three-dimensional analysis of long pillar and stope

Underlying the solution of the two-dimensional example involving a pillar and two stopes given in [23], and solved earlier on in this paper, is the assumption of plane-strain conditions. These conditions can be simulated in the central cross-section of the

three-dimensional problem shown in Fig. 11, if the rooms and pillar are made sufficiently long. The tabular orebody problem illustrated in Fig. 11 was analysed with the three-dimensional EDDM. The configuration of discrete EDD elements used in modelling the problem is shown in Fig. 11b. For its results to be correct, quantities such as stresses, for example, calculated around the excavations and in the pillar in the central cross-sectional plane should match those obtained from the two-dimensional analysis. Because the two-dimensional EDDM was verified to correctly solve the planar problem, its results were used in validating those of the three-dimensional method. Another reason for the choice of the two-dimensional EDDM for validation purposes lay in the fact that since its results had been already shown to be accurate, DDs instead of stresses or displacements could be compared.

The normalised confinement displacement discontinuity, which is the ratio of the confinement DD to the maximum value of this DD, formed the basis for comparing the results of the two-dimensional and three-dimensional EDDMs. This ratio provides a good indication of the degree of confinement existing at a point in a material.

The variations of the normalised confinement DD across the width of the pillar for both the two- and three-dimensional EDDMs were plotted in Fig. 12. The plots indicate that the results of the two methods are in very good agreement.

Example 2. Three-dimensional analysis of a square pillar in a room

Confinement controls the overall behaviour of pillars. A detailed study of the failure process in pillars [9], showed that failure commenced on pillar boundaries and migrated towards the centres of the pillar, where the cores had not reached their full load-

bearing capacities. The observed increase in the strength of material from pillar boundaries towards the core is attributable to the effects of confinement.

It was mentioned earlier in this paper that previous approaches used in DD methods relied on manual approaches of accounting for the influence of confinement. In the technique employed in the commercial software package MULSIM, for example, users have to manually assign strengths to different elements according to the closeness of elements to pillar boundaries. Figure 13 shows a typical scheme for assigning stress-strain curves to the elements of a square pillar in a room-and-pillar mining scheme [25]. Elements used in discretizing the square pillar are designated with letters from A to D in Fig. 13 in accordance to the extents to which they experience confinement. Strength curves that model the different element types based on the degree of confinement are shown on the stress-strain diagram. The element at the core of the pillar, being in the most confined region, is assigned the highest strength curve (curve A). The normalised confinement DD adequately captures the degree of confinement in a pillar. Strength curves can be defined at a point in a pillar when the degree of confinement or confining stress at the point is known.

For the three-dimensional EDDM to be considered successful it must correctly capture the variation of the degree of confinement in pillars. An example of a single pillar in a room is depicted in Fig. 14. Fig. 15 shows the contours of equal normalised confinement DDs calculated for the square pillar. Due to the inclusion of the lateral singularity in the EDDM, it was able to effectively model confinement in the square pillar.

8. CONCLUSIONS

In a mine design environment in general, it is important to have a numerical tool that solves problems of calculating stresses and displacements around excavations and rock structures speedily and accurately, because of the need to quickly assess alternate mine layouts. The mining of lenticular orebodies using room-and-pillar methods creates conditions that require that the effect of confinement in pillars be modelled. Knowledge of confinement is necessary in pillar analysis for the reason that it significantly influences pillar behaviour and strength. Although numerical techniques such as the FEM and the FDM can address one or the other of the requirements, none of them is able to address the issues of speed and confinement modelling simultaneously.

Prior to the work reported in this paper, *ad hoc* approaches were used in the practical application of the DDM to include confinement effects in pillar analysis. The *ad hoc* methods including the approach employed in the commercial software program MULSIM, used manual means to assign different strength curves to DD elements based on the degree of confinement they were expected to experience. The research work in this paper was initiated in an effort to develop a numerical technique that exploited the computational speed of the DDM, and yet accurately modelled confinement. A new displacement discontinuity method referred to as the enhanced displacement discontinuity method (EDDM) was subsequently developed. The essential difference between the EDDM and the earlier DDM is the introduction of an extra centre of dilation singularity in the formulation of DD elements.

The new displacement discontinuity density was developed from a strain nucleus. From the effects of strain nuclei applied at a point in an elastic medium, it became possible to develop a new lateral (confinement) DD that effectively modelled confinement in pillar material. With the introduction of the lateral DD into the original DD element, the enhanced displacement discontinuity (EDD) element was created. Systems of equations for EDD elements in mined and unmined rock zones were developed with the consideration of appropriate boundary conditions. Both two-dimensional and three-dimensional models of the method were formulated in the paper.

The EDDM has a principal advantage over the classical DDM because of its ability to model different types of material behaviour. Whereas the DDM, due to its inability to use all components of the stress tensor, is limited in its application, the EDDM can accommodate general material constitutive equations including plasticity models. By explicitly accounting for confinement in its formulation, the new procedure generalises and automates the process of assigning strength curves to elements. As a result, it simplifies data preparation by eliminating the need for any artificial means for accounting for the effects of confining stresses.

Sample problems involving simple boundary and pillar geometries were solved in the paper to validate the performance of the EDDM. The results obtained from the EDDM compared well with analytical solutions for problems for which they were available, and showed good agreement with the results of other numerical techniques that have been established to perform well.

Although the examples used in validating the new formulation involved problems of simply geometry, the procedure is by no means limited to such cases. The EDDM

presented in the paper was formulated using constant DD elements. However, higher-order DD elements can be implemented with a few and relatively simple modifications. Also, owing to the fact that the newly formulated method uses all the components of stress and strain tensors for material, it can accommodate a variety of constitutive models including non-linear material models. This particular feature of the EDDM, combined with its ability to account for confinement, assumes greater attractiveness and importance in the analysis of failing or yielding pillars.

In order to simplify the development of the EDDM in this paper, only constant EDD elements were formulated. However, it is possible to develop higher-order EDD elements using the node-centric element approach outlined by Vijaykumar, Curran and Yacoub [26]. A node-centric formulation would allow the variation of the EDD along the lengths of adjacent elements to be continuous. A node-centric EDDM would have better accuracy compared to the constant EDD approach, and would allow continuous DD variation between adjacent elements.

Acknowledgement

The authors are grateful to S. Vijayakumar and R. Hammah for the valuable discussions related to this work. The financial support provided by NSERC through an operating grant (J. H. Curran) and postgraduate scholarship (T.E. Yacoub) and *Rocscience* Inc. are gratefully acknowledged.

REFERENCES

1. Beer G. and Watson J. O. *Introduction to finite and boundary element methods for engineers*, John Wiley & Sons, England (1992).
2. Crouch S. L. and Starfield A. M. *Boundary Element Methods in Solid Mechanics*, George Allen and Unwin, London, U.K. (1983).
3. Salamon M. D. G. Elastic Analysis of displacements and stresses induced by mining of seam or reef deposits, Part IV, *J. S. Afr. Inst. Min. Meallt.*, **65(5)**, 319-338 (1964).
4. Crawford A. M. and Curran J. H. Higher-order functional variation displacement discontinuity elements, *Int. J. Rock Mech. Min. Sci. & Geomech. Abst.*, **19**, 143-148 (1982).
5. Shou K. J. and Crouch S. L. A higher order displacement discontinuity method for analysis of crack problems, *Int. J. Rock Mech. Min. Sci. & Geomech. Abst.*, **32**, 49-55 (1995).
6. *NFOLD Program user manual*, Golder Associates, (1989).
7. Zipf R. K. *MULSIM/NL Theoretical and Programmer's Manual* BuMines IC 9322, (1992).
8. Andreev G. E. *Brittle Failure of Rock Materials, Test Results and Constitutive Models,* A. A. Balkema, Netherlands (1995).
9. Wagner H. Determination of the complete load-deformation characteristics of coal pillars, *3rd. Int. Congress on Rock Mechanics*, 1076-1081 (1974).
10. Bieniawski Z. T. Propagation of brittle fracture in rock, *Proceedings 10th Symposium on Rock Mechanics (AIME)*, 409-427 (1972).
11. Jeremic M. L. *Ground mechanics in hard rock mining,* A.A. Balkema, Netherlands (1987).
12. Kripakov N. P. Finite element analysis of yielded-pillar stability, *Comp. & Struct.*, **13**, 575-593 (1981).

13. Singh U.K. and Rao D.G. Evaluation of shaft pillar stability using numerical modelling methods - a case study, *J. Mines Metals & Fuels*, **XLII(8&9)**, 195-199 (1994).

14. Mack M. G. The displacement discontinuity method, *in Boundary Element Techniques in Geomechanics,* (Eds. G.D. Manolis and T.G. Davis) Computational Mechanics Publications, Elsevier Applied Science (1993).

15. Starfield A. M. and Crouch S. L. Elastic analysis of single seam extraction, *In New Horizons in Rock Mechanics* (Ed. H.R. Hardy Jr., R. Stefanko), Proceedings 14th. U.S. Rock Mechanics Symposium, 421-439 (1973).

16. Vandamme L. and Curran J. H. A three-dimensional hydraulic fracturing simulator, *Int. J. Numer. Meth. Engng.*, **28**, 909-927 (1989).

17. Hills D. A., Kelly P. A., Dai D. N. and Korsunsky A. M. *Solution of Crack Problems The Distributed Dislocation Technique* p. 297. Kluwer Academic Publishers, Netherlands (1994).

18. Westergaard, H. M. *Theory of Elasticity and Plasticity*, Dover Publications, (1964).

19. Wylie C. R. and Barrett L. C. *Advanced Engineering Mathematics*, McGraw-Hill, (1995).

20. Wiles T. D. and Curran J. H. General 3-D displacement discontinuity method, *Proceedings of the 4th Int. Conf. on Numerical Methods in Geomechanics*, (Z. Eisenstein, Ed.) Edmonton, Canada (1982).

21. Brady B. H. G. and Bray B. W. The boundary element method for elastic analysis of tabular orebody extraction, assuming complete plane strain, *Int. J. Rock Mech. Min. Sci. Geomech. Abstr.*, **15**, 29-37 (1978).

22. Sneddon I. N. and Lowengrab M. *Crack Problems in the Classical Theory of Elasticity* p. 221. John Wiley, New York (1969).

23. Brady B. H. G. and Wassyng A. A coupled finite element-boundary element method of stress analysis, *Int. J. Rock Mech. Min. Sci. Geomech. Abstr.*, **18**, 475-485 (1981).

24. *Phase*^{2}, *2D finite element analysis for excavations*, Rock Engineering Group, University of Toronto, Canada (1996).

25. Campoli A. A. Boundary element method applied to coal mine bump control, *Proceedings of the* 8^{th} *international conference on Computer Methods and Advances in Geomechanics*, (Siriwardane & Zaman, Eds.), **3**, 1817-1822, (1994).

26. Vijayakumar S., Yacoub T.E. and Curran J.H. A node-centric indirect boundary element method: Three-dimensional displacement discontinuities, *accepted for publication in Comput. and Structures.*

List of Figures

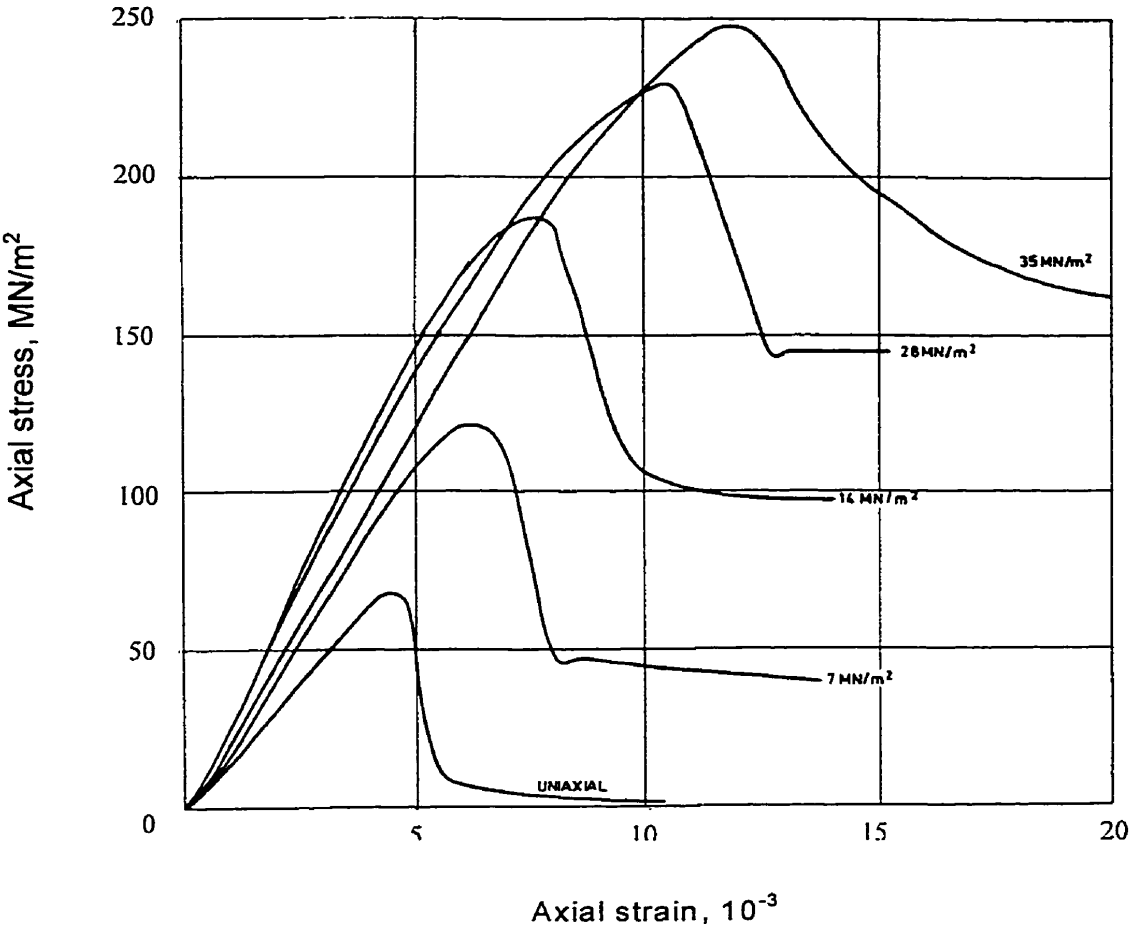

Fig. 1: Stress-strain behaviour of sandstone in triaxial compression for various confining pressures [10]

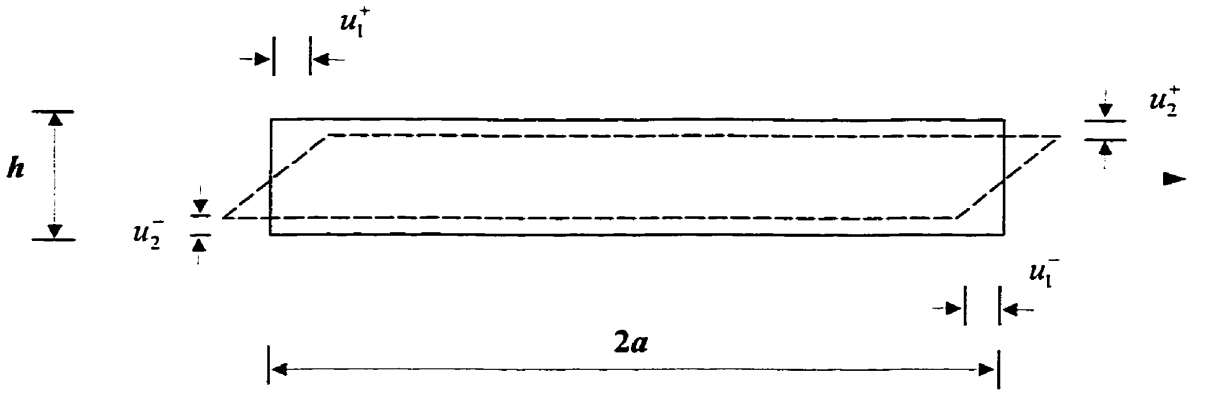

(a) Traditional DD element

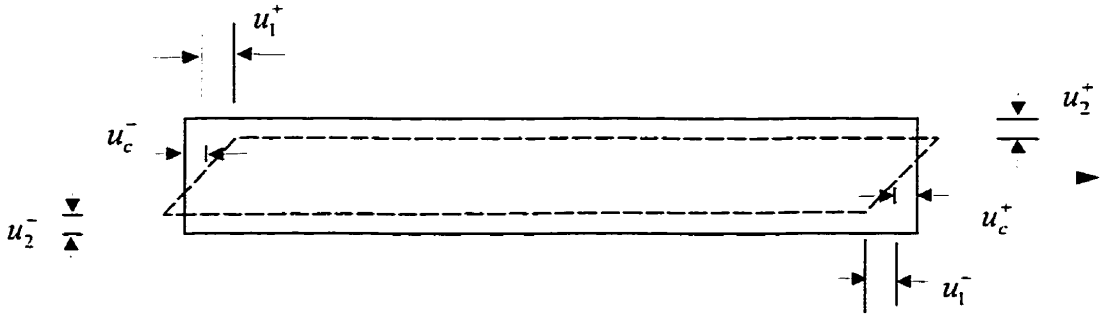

(b) New DD element

Fig. 2: Definition of displacement discontinuity

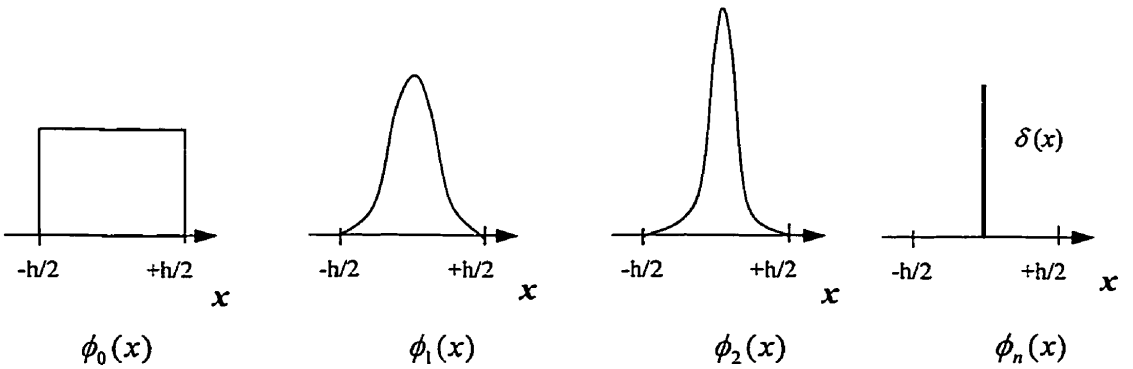

Fig. 3: Interpolation functions

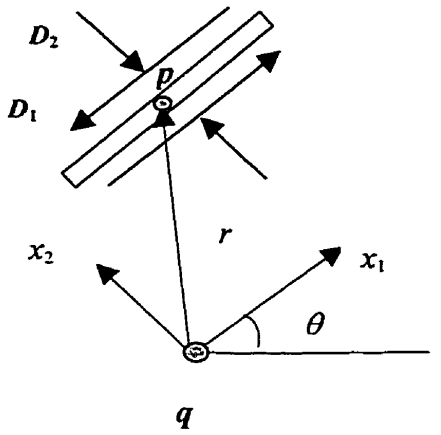

Fig. 4: Notations

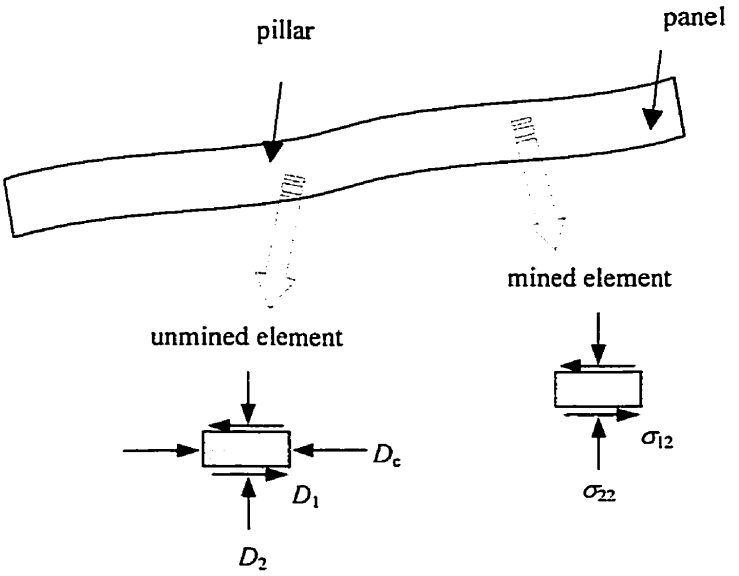

Fig. 5: Boundary conditions for mined and unmined elements in a seam

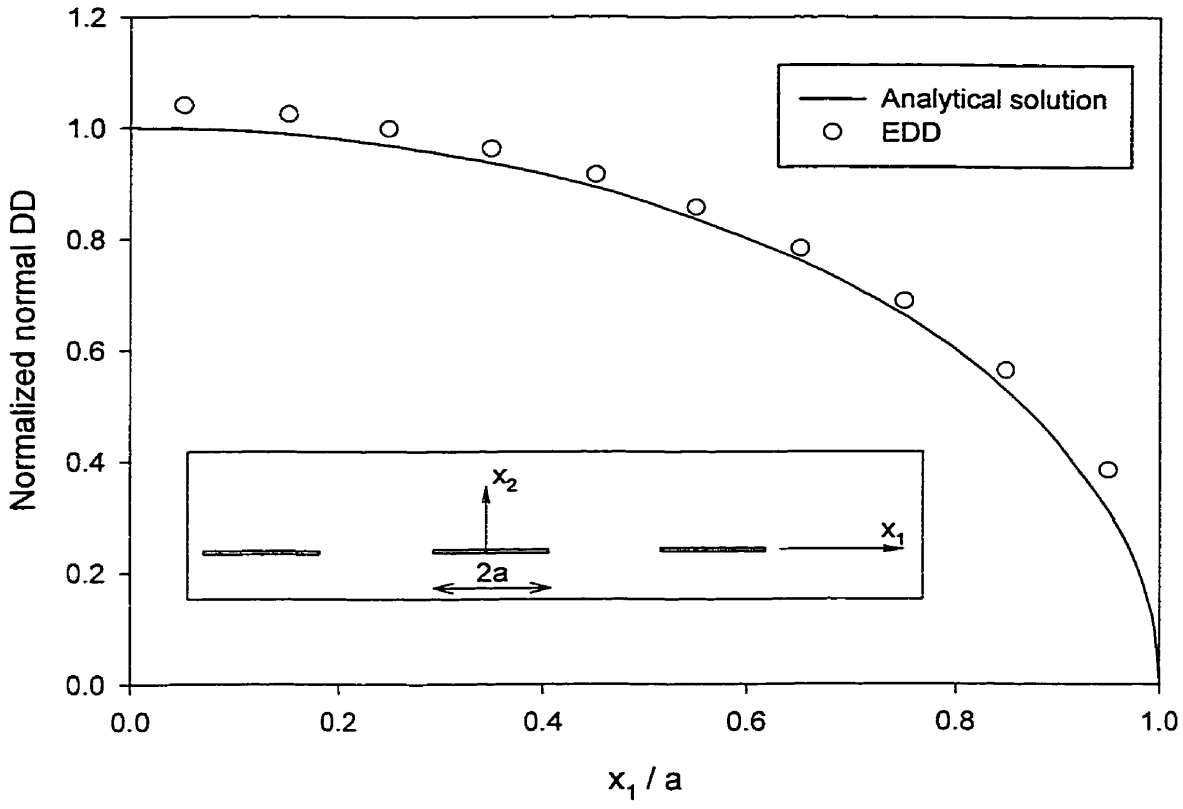

Fig. 6: Normal displacement discontinuity variation of central crack for a row of collinear cracks under unit internal pressure (G=100 MPa)

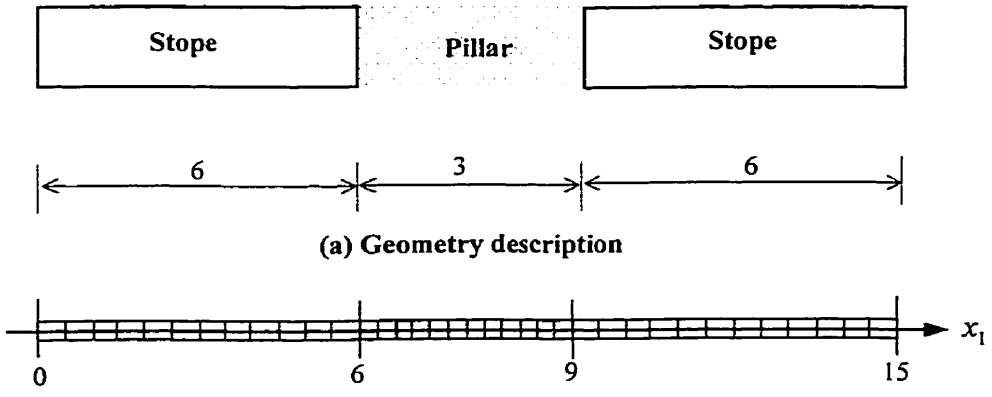

(a) Geometry description

(b) Discretized configuration

Fig. 7: Pillar and stopes geometry description

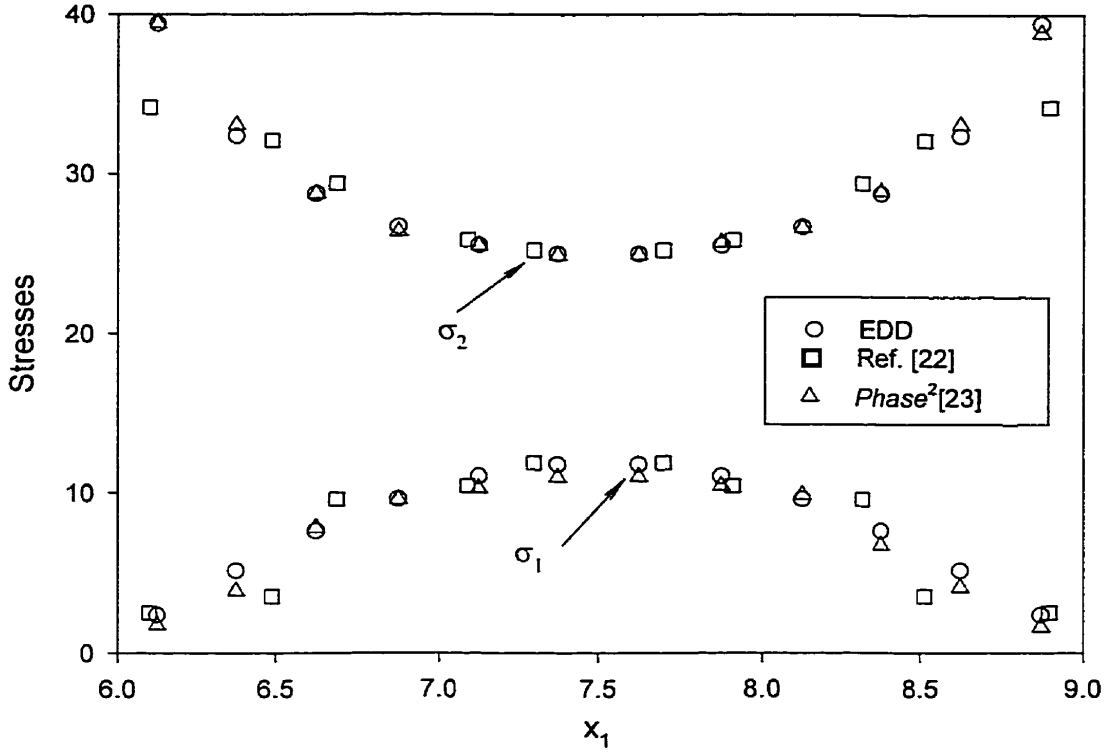

Fig. 8: Stress distribution for the pillar

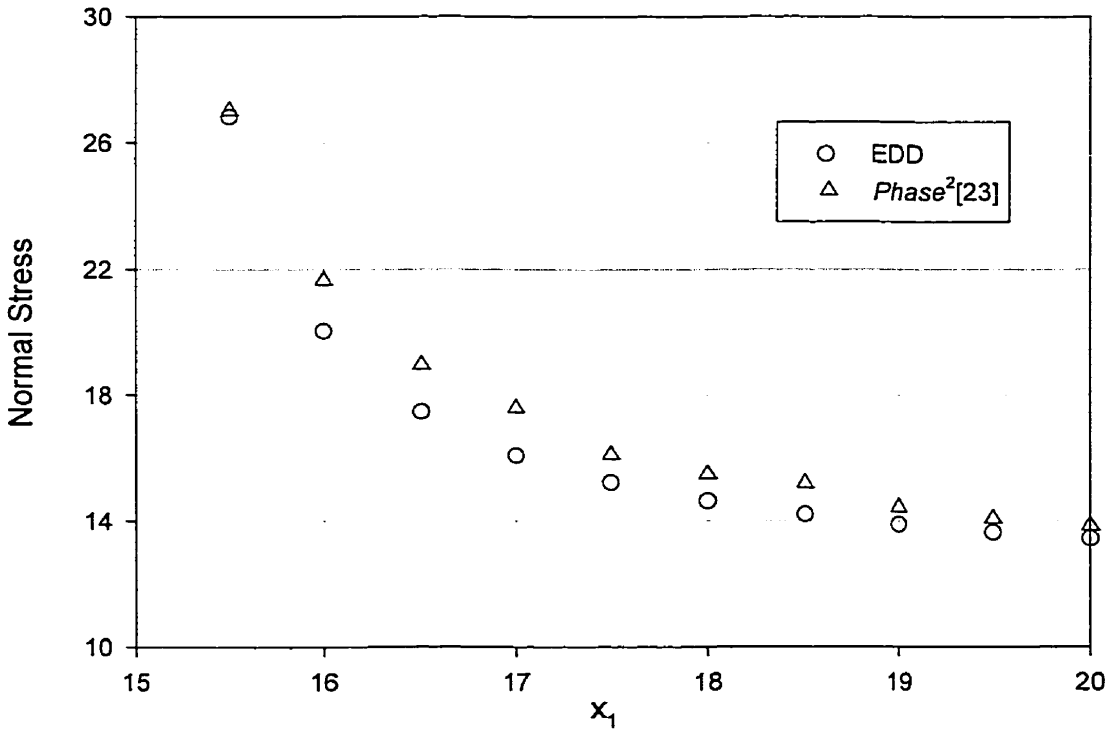

Fig. 9: Normal stress variation along the panel

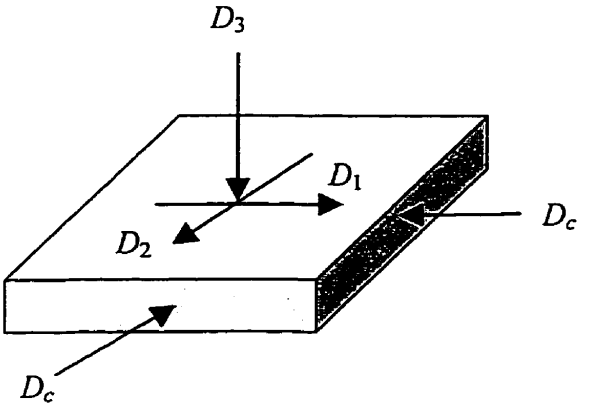

Fig. 10: Components of the three-dimensional displacement discontinuity

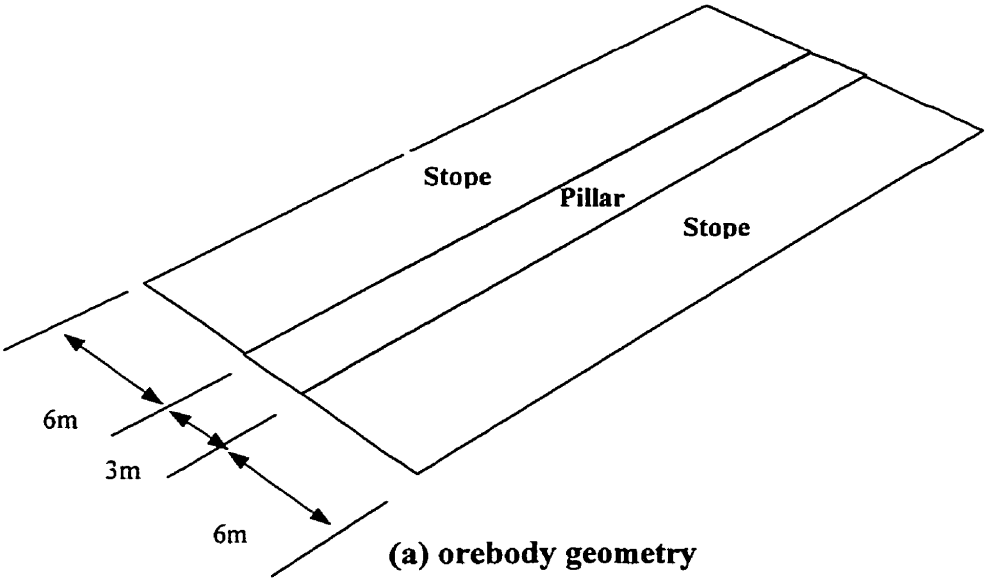

(a) orebody geometry

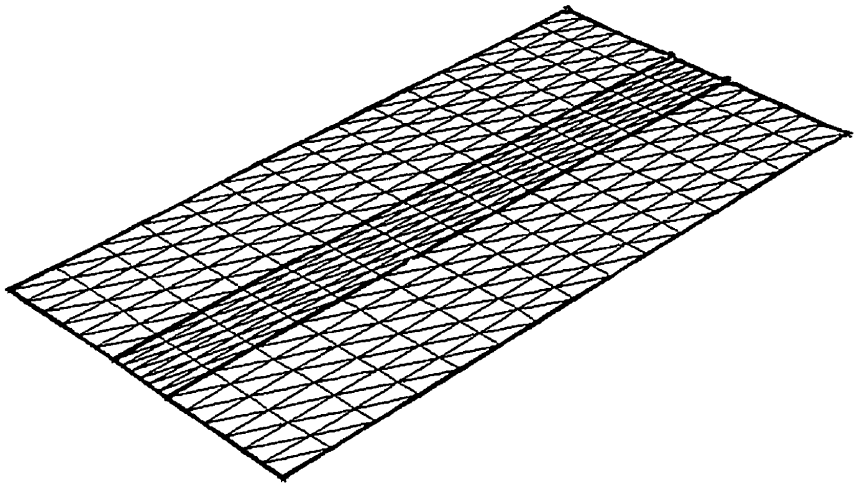

(b) discretization of the orebody

Fig. 11: Geometry and discretization of the orebody

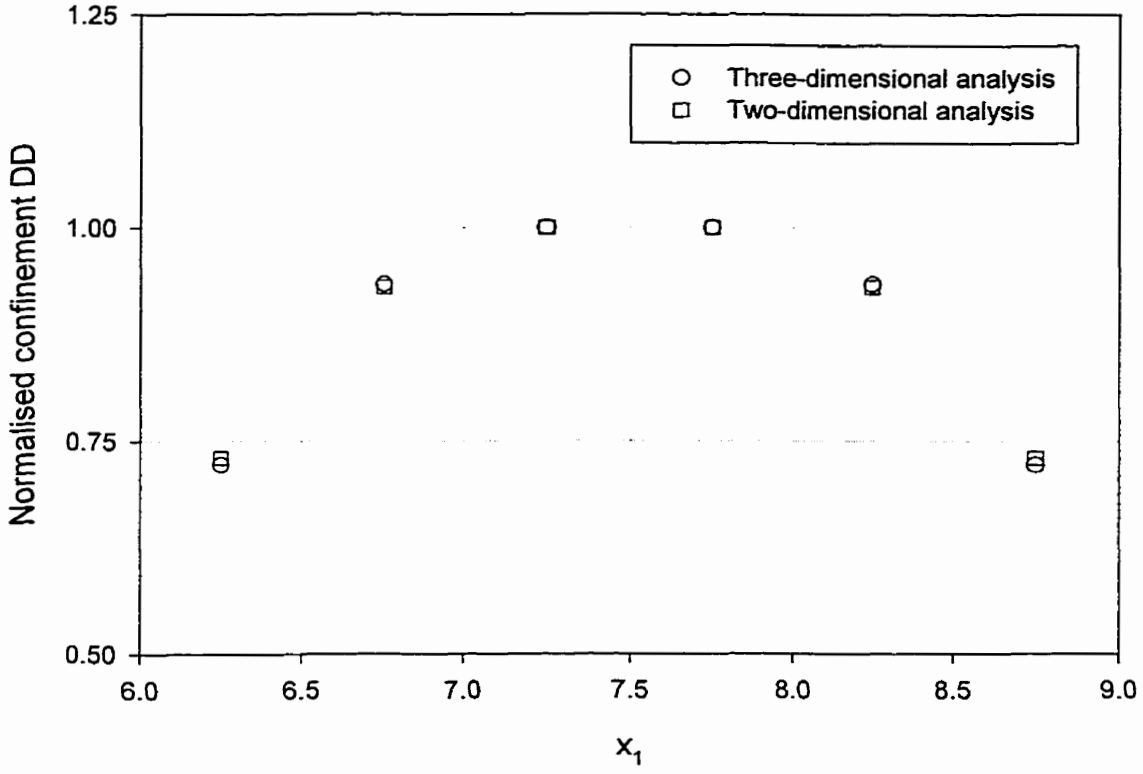

Fig. 12: Variation of the normalised confinement DD across the pillar width

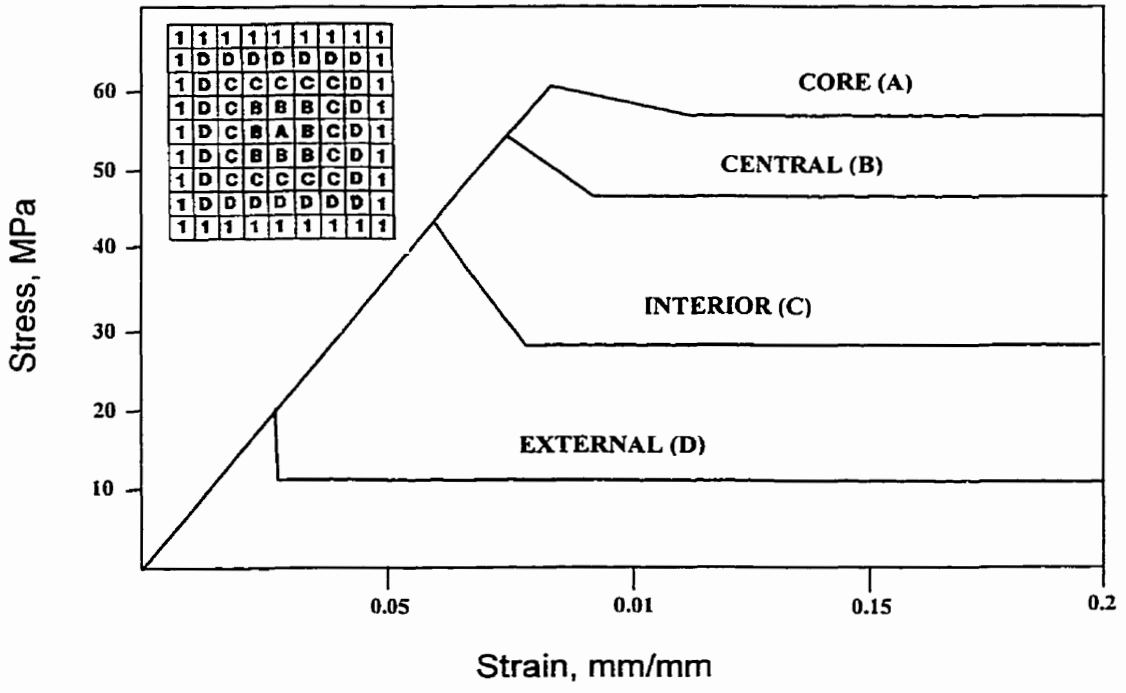

Fig. 13: Assignment of material properties to different elements [24]

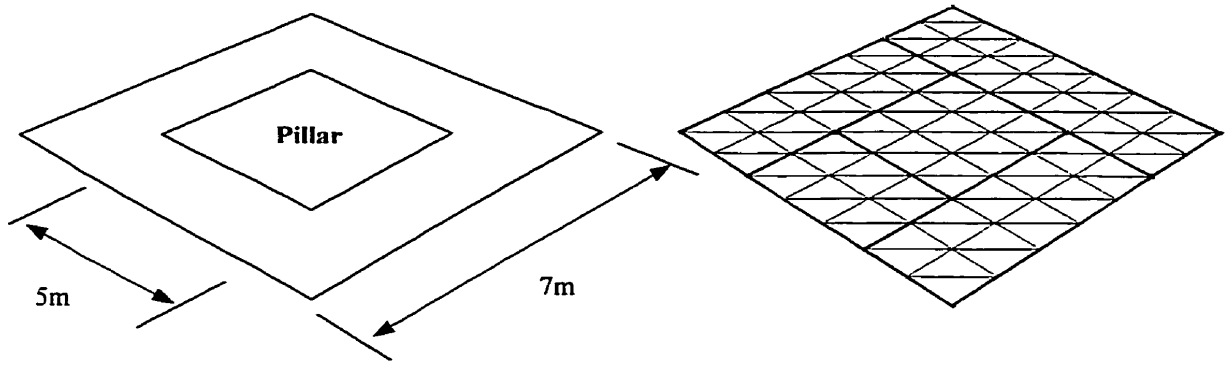

Fig. 14: Geometry and discretization of problem involving a square pillar and a room

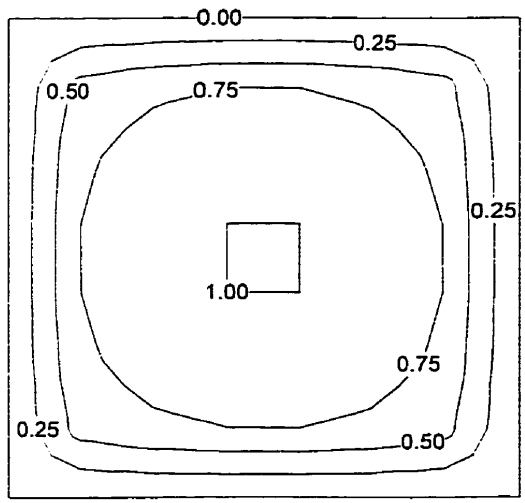

Fig. 15: Contours of normalised confinement DD for the pillar

Appendix D

Paper IV - "Modelling of the Post-Peak Behaviour of Pillars using the Enhanced Displacement Discontinuity Method"

To be presented in the 37th US Rock Mechanics Symposium

Modelling of the Post-Peak Behaviour of Pillars using the Enhanced Displacement Discontinuity Method

T. E. Yacoub[1] and J. H. Curran[2]

Rock Engineering Group, Dept. of Civil Engineering
University of Toronto
Toronto, Ontario
Canada, M5S 1A4

Abstract

The post-peak behaviour of pillars in underground mine structures is very important in the analysis of rock structures resulting from the mining of lenticular orebodies, because it can lead to catastrophic failure in mines. This behaviour can be modelled using the implementation of the progressive failure approach in the enhanced displacement discontinuity method (EDDM).

In the EDDM, a new DD element that explicitly considers the effect of confinement - the enhanced displacement discontinuity (EDD) element - is used. This newly formulated element has the capability of using any material constitutive relationships to model the post-failure behaviour of pillars. Failure of pillars is however simulated with the progressive failure procedure in this paper, because of the simplicity of the method. Progressive failure adopts a quasi-elastic approach to account for the residual strength of rock material after initial failure. The extent of pillar yielding is evaluated with failure criteria such as the Mohr-Coulomb and the Hoek-Brown criteria.

The potential benefits of using progressive failure and the EDDM for modelling the mining of lenticular type orebodies that utilise pillars as primary support are demonstrated through two- and three-dimensional examples in the paper. These examples provided were also intended to illustrate the flexibility and power of the proposed method in the simulation of pillar failure.

Keywords: Enhanced Displacement Discontinuity Method (EDDM); Progressive Failure; Pillar confinement effect; Post-failure analysis.

[1] Ph. D. Candidate and
[2] Professor

Introduction

The mining of lenticular or tabular orebodies results in the creation of thin slit-like excavations in rock masses. Support for such excavated rooms in orebodies is provided in the form of unmined columns of material. The material remnants left to support the excavated rooms are known as pillars. Since pillars provide support for slit excavations, the stability of the excavations in lenticular orebodies very much depends on the stability of pillars.

In the design of pillars, there are two competing demands that control pillar sizes. Mining economics demands that as much ore as possible be recovered from mining operations. This means that pillars must have minimal sizes. Safety demands however require that pillars be designed with thicker sections to ensure that they have adequate load carrying capacity in order to prevent catastrophic collapse of excavations. For an optimal solution between the competing factors to be reached, some failure of peripheral pillar material in practical mining is permitted [1]. Due to the effects of confinement, pillars do not experience failure uniformly across their cross-sections. Close to pillar surfaces, the degree of confinement is lesser than for points further away from exposed faces. Under such triaxial stress conditions, the strength of pillar material increases from the boundaries towards the core. In other words, pillar material strength increases with increasing confinement [2, 3].

Owing to the fact that due to confinement effects the strength of pillar material is not uniform across pillar cross-sections, practical pillar design and analysis without the use of confining stresses is inaccurate. Yielding of pillars or plastic pillar response must be considered [4]. In some contemporary design methods, parameters and relationships

used for computing pillar sizes are obtained through the back analysis of failed and stable pillars. Useful as this approach is, its range of application is limited to pillar design in the conditions from which the equations and parameters were obtained.

Other than through the empirical means described above, pillars can be analyzed and designed with numerical methods such as the finite element method (FEM) and the boundary element method (BEM). The FEM is a very powerful technique that can be used in solving a wide variety of engineering problems. It enjoys greater versatility than the BEM method, because it can accommodate a greater variety of material relationships, and more easily model problems involving non-homogeneous material. It can also provide more accurate details of stresses and displacements in pillars than the BEM. For the modelling of mining excavations, however, the BEM has significant advantages over the FEM. Because the problem domain in mining is practically of infinite size, discretization of a considerable region around excavations is needed in the FEM to sufficiently model mining problems. The BEM, however, involves the discretization of boundary surfaces only, and thus requires much lower numbers of elements than the FEM. The use of smaller numbers of elements in the BEM assumes greater significance in three-dimensional analysis. The smaller numbers of elements grant the BEM significant advantages in computational speed and mesh generation over the FEM in the solution of mining problems [5].

BEMs enjoy an additional advantage over FEMs in solving mining problems. It is often the case in mining that only a general idea of the stresses and behaviour of pillars, panels and excavations to be expected during mining operations is needed by the designer. The FEM can provide great detail of stress distributions in individual pillars and

panels of an orebody. A global view of the stresses and behaviour of the underground structures is however difficult to obtain amidst such detail. Also, it is unjustifiable to go to great extents to perform a very detailed analysis of the problem, when the information on the properties of rock masses and primitive stresses provided in a mine environment are often non-detailed and sketchy. With BEMs, however, the results obtained from analysis are consistent with the level of detail of the information provided on input parameters, and are usually sufficient for the mining rock mechanics specialist to make the necessary recommendations on excavation design.

A particular BEM technique, known as the displacement discontinuity method (DDM), is well suited for problems involving slit excavations with parallel surfaces, the very type encountered in the mining of lenticular orebodies [6, 7]. It models excavations as cracks with no material in them and pillars as linear or non-linear springs. The original formulation of the BEM omits the presence of confining stresses [8]. As a result, adjustments have to be made in its practical application to accommodate confinement effects [1]. Yacoub and Curran [2] developed a model of the DDM that incorporates confining stresses in its formulation. This method is called the enhanced displacement discontinuity method (EDDM). Because its formulation accommodates all components of the stress tensor at a point in a material, it can be used with all constitutive models.

Yielding behaviour in pillars can be modelled with constitutive relationships, such as elasto-plastic models. They can be used in various numerical techniques including the FEM and EDDM. The practical application of such models is however restricted due to the number of parameters involved, and the difficulties associated with the determination of the appropriate values of those parameters for the material being analyzed. A simpler

approach relies on the use of failure criteria such as the Mohr-Coulomb criterion or Hoek-Brown criterion to model yielding in pillars through iterative algorithms. One such approach is the progressive failure method developed for the FEM [10-14]. Although simple in formulation this method adequately captures the essence of the yield behavior of materials. The parameters needed for the failure criterion incorporated in the method are easy to determine thus making the practical application of the method very attractive.

Because the EDDM accounts for confining stresses, an approach is presented in this paper in which the progressive failure technique is implemented using the EDDM. Although the progressive failure procedure has been successfully implemented with the FEM to analyse pillars, the large number of elements required to adequately model the problem, and the lack of detailed input information do not make that approach especially convenient for practical mine design. The new approach proposed in this paper offers the all the advantages of the speed, and appropriate level of result detail of BEMs as well as the simplicity of progressive failure to the modelling of yielding pillars.

Stress-Strain Behavior of Rock

The stress-strain behavior of intact rock material depends to a great extent on the confining stresses acting on the material. The failure loads for intact rock samples in triaxial tests increases with increasing confining stresses. At low levels of confinement, the post-peak strength of rock is reduced to very small fractions of the load-bearing capacities of samples. The post-peak loss of strength is not so pronounced at high confining stresses. These results are shown on Fig. 1 and were obtained in studies by Bieniawski [2].

Experimental data by Bieniawski [2] also showed that the post-peak response of intact rock samples were characterised by a progressive decrease in both load-bearing capacity and elastic stiffness. Fractured rock has a reduced resistance to loads. This in turn leads to increased deformation under loads as a result of the increased external energy supplied to the rock.

In rock mass regions surrounding excavations, and for rock material in pillars, extensive redistribution of stresses occurs due to post-peak deformations. When local failure of material occurs at points in rock where stresses have exceeded strength, the loss of load-bearing capacity has to be sustained by surrounding material. Stresses are therefore redistributed with regions in the immediate vicinity of failed material acquiring increased stresses. Stress redistribution continues (progresses) until a stable state is attained in which no new local failures of material occur.

Simulation of Progressive Failure

Progressive failure of rock material was first included in analysis by Kidybinski and Babcock [15], when they represented failed rock zones around longwall faces with reduced elastic moduli. Pariseau and Eitani [16] automated the process of simulating progressive failure in analysis. They employed a simple model in which strata responded linearly elastically up to failure points. After failure the model assumed that the strata lost all strength due to fracture or flow.

Kripakov [10] developed a more sophisticated approach to simulating progressive failure. This approach, implemented in the FEM, more realistically modelled the process of progressive failure. The progressive failure approach of Kripakov used a pseudo-

elastic method of analysis to simulate the progressive yield zone in pillar material in an iterative manner. In the method, it was assumed that local failure of an element occurred at a point in a material, when the stress on the element exceeded the strength of the material at the point. The strength of the material at any point in the material was calculated from a failure criterion such as the Mohr-Coulomb criterion.

After stresses in all elements had been computed in an iteration, a new iteration was begun in which stresses were recalculated, with the difference between the calculated stress of a failed element and its admissible residual stress being distributed to surrounding elements. Redistribution of stresses was accomplished through the modification of the stiffnesses of elements. Each time the failure stress of an element was exceeded, its elastic modulus was reduced by the ratio of the failure stress predicted by a failure criterion to the stress computed at the element.

Since failure criteria generally do not provide any information on the post-failure behavior of material, the procedure developed by Kripakov necessarily had to rely on iterative means to model the post-peak constitutive behavior of material. The amounts by which both material strength and stiffness are reduced after failure are determined by an empirical local material factor of safety, F_S. This index is not a global safety factor that indicates the danger of collapse of excavations or mine pillars, but rather represents how close material at a point is to failure. The local factor of safety is computed from the formula:

$$F_S = \frac{maximum\ material\ strength}{applied\ stress} = \frac{\sigma_F}{\sigma_1}, \qquad (1)$$

where σ_1 is the maximum principal stress calculated at a point in the material. The maximum material strength, σ_F, is calculated from a failure criterion. A factor of safety greater than 1.0 implies that no failure has occurred, whereas factors of safety less than 1.0 indicate failure.

When the strength of an element is exceeded, it still retains a residual strength and stiffness. Thus in the implementation of progressive failure according to Kripakov, failure of elements is simulated with reductions in the modulus of elasticity of material and uniaxial strength (Fig. 2). The reduced modulus of elasticity and uniaxial strength are calculated as:

$$E_{(\text{modified})} = F_S \cdot E_{(\text{original})} \tag{2}$$

$$\sigma_{c(\text{modified})} = F_S \cdot \sigma_{c(\text{original})}, \tag{3}$$

respectively. If an element fails in tension, that element is assumed to have yielded completely and therefore does not retain any residual strength.

During the first iteration, the degrees of failure (factors of safety) of the elements of a discretized structure or domain are assessed for values less than 1.0 (indications of failed elements). If all elements have factors of safety greater than 1.0 the analysis is terminated. For elements that have factors of safety less than 1.0, reductions are applied to their stiffness and strength, and the analysis rerun. At the end of every iteration a termination condition is checked. The termination criterion compares element factors of safety from the previous iteration to that of the current. If the differences between previous and current values of the factors of safety for elements are smaller than a set tolerance, i.e. when the factors of safety practically stop changing, the algorithm is

adjudged to have converged. Results show that the criterion produces stable results that are not affected by the accuracy of the convergence ratio.

Failure criteria

When the stress at a point in a material, or on an element used in modelling the material, reaches the strength limit of the material, failure occurs. The stress limits at which failure of material occurs are determined or predicted from failure criteria [17]. For isotropic material, a failure criterion is an invariant function of the state of stress, and is commonly represented with principal stresses as:

$$f(\sigma_1, \sigma_2, \sigma_3) = 0, \tag{4}$$

where $\sigma_1, \sigma_2, \sigma_3$ are, respectively, the major, intermediate and minor principal stress components. Failure criteria for uniaxial stress conditions cannot always be used in progressive failure, because the stress-strain behaviour of rock material depends on the magnitude of confining stresses, as mentioned earlier.

The strength and deformation properties of rock masses are difficult to estimate, but are however critical to the design of underground excavations. The material properties (parameters) used in failure criteria for such design must therefore be estimated as realistically and reliably as possible [18]. Two failure criteria that are very widely used for predicting failure loads of rock under triaxial stress states that satisfy these conditions are the Mohr-Coulomb and the Generalised Hoek-Brown criteria. Another principal reason for employing these models in the practical application of progressive failure is their relative simplicity. Although more complicated models may, in theory, be able to more accurately predict failure stresses, the determination of the

appropriate values of the parameters in these models is very difficult. This renders complicated models impractical for routine use.

According to the Mohr-Coulomb failure criterion (Fig. 3a), the failure stress σ_{1_f} of rock masses can be predicted from the relationship:

$$\sigma_{1_f} = \sigma_{cm} + k\sigma_3 . \tag{5}$$

The uniaxial compressive strength of a rock mass, σ_{cm}, is defined by the equation

$$\sigma_{cm} = \frac{2c\cos\varphi}{1-\sin\varphi}, \tag{6}$$

while the slope of the failure envelope (Fig. 3a), k, can be expressed as

$$k = \frac{1+\sin\varphi}{1-\sin\varphi}. \tag{7}$$

c and φ in the above equations are the cohesive strength and the angle of internal friction of the rock mass, respectively.

The stress failure equation developed by Hoek-Brown (Fig. 3b) is a non-linear envelope. The functional form of this envelope (a parabolic curve close to the original Griffith theory) was determined based on experimental and theoretical considerations of rock fracture mechanics [18]. According to the Hoek-Brown criterion, failure of material will occur for all states of stress for which the major principal stress is expressed as

$$\sigma_{1_f} = \sigma_3 + \sigma_c\left[m_b\frac{\sigma_3}{\sigma_c} + s\right]^{\alpha}, \tag{8}$$

where m_b is the value of the constant m for the rock mass. σ_c is the uniaxial compressive strength of the intact rock pieces. s and α are constants that depend on the characteristics of the rock mass. These constants can be obtained after having classified a rock mass

using a simplified index called the Geological Strength Index (*GSI*) [18]. The constants in the Hoek-Brown criterion are determined in the following fashion:

$$m_b = m_i \exp(\frac{GSI - 100}{28}) \tag{9}$$

for $GSI > 25$

$$s = \exp\left(\frac{GSI - 100}{9}\right) \tag{10}$$

$$\alpha = 0.5$$

for $GSI < 25$

$$s = 0.0 \tag{11}$$

$$\alpha = 0.65 - \frac{GSI}{200}$$

m_i is a dimensionless constant which depends upon the shape and degree of interlocking of the individual piece of rock within the mass.

Overview of the Enhanced Displacement Discontinuity Method (EDDM)

The displacement discontinuity method (DDM) is a type of indirect boundary element technique that is well suited for the thin, slit-like openings commonly encountered in the mining of lenticular ore bodies (seam-type deposits). In the analysis of such features, both excavated and unexcavated regions can be represented as crack-line elements. Crouch and Starfield [7] present an excellent overview of the DDM. The conventional DD formulation for unmined regions of orebodies, however, has a major shortcoming - the important effect of lateral confinement is omitted from its formulation. The modelling of confinement in rock material is especially important in the simulation of progressive failure because, as discussed above, confining stresses are necessary for the prediction of failure stresses.

Yacoub and Curran [9] proposed an enhanced displacement discontinuity method (EDDM) that explicitly takes into account confining stresses in the element formulation. The enhancement is achieved through the addition of a new displacement discontinuity singularity, perpendicular to the normal displacement discontinuity (DD). With the addition of this new DD, three stresses - normal, shear and confining stresses, instead of two, are now accounted for in the modelling of unmined material. The x_1 - x_2 coordinate system can be rotated to a new system $x_n - x_s$ so that the stress state at a point p in the domain of a material due to a DD at an element q can be expressed as normal and shear components (Fig. 4).

The addition of confining stress to the formulation of enhanced DD (EDD) elements allows the enhanced method to accommodate in principle general constitutive relationships for rock. For ease of understanding, only the two-dimensional EDDM is described into detail in the current work.

In the EDDM for two-dimensional problems, the induced stresses σ_{ij}^p and displacements u_{ii}^p at an element p due to the distribution of normal, shear and confinement DDs at an element q can be computed from the formulae:

$$\sigma_{ij}^p = A_{ijk}^{pq} D_k^q + \delta_{ik} K_{kj}^{pq} D_c^q \tag{12}$$

$$u_i^p = B_{ij}^{pq} D_k^q + L_i^{pq} D_c^q \ , \tag{13}$$

where i, j, k = 1, 2, and A^{pq}, K^{pq}, B^{pq} and L^{pq} are influence coefficients. δ_{ij} is Kronecker's delta. D_1 and D_2 in equations (12) and (13) are respectively D_s and D_n in Fig. 4. These equations provide the formulation of the EDDM.

The EDD element can be applied to the problem of determining the total stresses and mining-induced displacements in the room-and-pillar or longwall mining of lenticular orebodies. In the first step in solving the problem, the boundary of the problem is divided into a total of N discrete EDD elements. In general, the stresses induced at element p due to the distribution of normal, shear and confinement displacement discontinuities at all elements ($q = 1 \ldots N$) can be computed as:

$$\sigma_n^p = \sum_{q=1}^{N} A_{nn}^{pq} D_n^q + \sum_{q=1}^{N} A_{ns}^{pq} D_s^q + \sum_{q=N-M}^{N} K_{nc}^{pq} D_c^q \tag{14}$$

$$\sigma_s^p = \sum_{q=1}^{N} A_{sn}^{pq} D_n^q + \sum_{q=1}^{N} A_{ss}^{pq} D_s^q \tag{15}$$

$$\sigma_c^p = \sum_{q=N-M}^{N} A_{cn}^{pq} D_n^q + \sum_{q=N-M}^{N} K_{cc}^{pq} D_c^q \tag{16}$$

where A^{pq} is the influence coefficient matrix and A_{nn}^{pq}, A_{ns}^{pq}, A_{nc}^{pq}, etc. are the members of this matrix defined in [19]. K^{pq} is the influence matrix defined in [9]. σ_n, σ_s and σ_c are the normal stress, lateral (confining) stress and shear stress, respectively, at the element p.

The values of the normal, shear and confinement DDs that produce total stress and displacement components consistent with the boundary conditions of the problem can be determined if the correct boundary conditions are inserted into eqns. (14-16). Of the N elements representing the boundary of the problem, M ($M < N$) of them are in unmined zones of the orebody. Fig. 5 shows the two different types of boundary conditions that represent the physical aspects of the problem of mining a lenticular orebody. For the elements in mined zones, boundary tractions should be equal to zero. This leads to the following system of equations for mined elements:

$$-(\sigma_n^p)_o = \sum_{q=1}^{N} A_{nn}^{pq} D_n^q + \sum_{q=1}^{N} A_{ns}^{pq} D_s^q \tag{17}$$

$$-(\sigma_s^p)_o = \sum_{q=1}^{N} A_{sn}^{pq} D_n^q + \sum_{q=1}^{N} A_{ss}^{pq} D_s^q \tag{18}$$

$$D_c^p = 0 \tag{19}$$

where $(\sigma)_o$ are the initial stresses present in the rock mass at the points at which these elements are inserted.

Material in the unmined zones of a seam is modelled through the constitutive equation establishing the relationship between stresses, σ_{ij}, and strains, ε_{ij}, in the material. Assuming a homogeneous, isotropic, linearly elastic material, with constitutive equation:

$$\sigma_{ij} = \lambda_s \delta_{ij} \varepsilon_{kk} + 2G_s \varepsilon_{ij} \ , \tag{20}$$

where λ_s is Lame's constant defined by the relationship:

$$\lambda_s = \frac{2\nu}{(1-2\nu)} G_s \ , \tag{21}$$

G_s and ν are the shear modulus and Poisson's ratio of a seam, respectively. The normal, lateral and shear stresses induced on an element in an unmined zone by the application of DDs can be computed from the formulae:

$$(\sigma_n)' = (\lambda_s + 2G_s)\frac{D_n}{h_s} + 2G_s \frac{D_c}{h_s} \tag{22}$$

$$(\sigma_c)' = (\lambda_s + 2G_s)\frac{D_c}{h_s} + 2G_s \frac{D_n}{h_s} \tag{23}$$

$$(\sigma_s)' = \frac{G_s}{h_s} D_s \tag{24}$$

By assuming that initial deformations of unmined elements are zero, and also assuming that they deform only in response to induced stresses [7], the following system of equations is obtained when these boundary conditions are inserted into the equations (14) to (16):

$$0 = (\lambda_s + 2G_s)\frac{D_n^p}{h} + 2G_s\frac{D_c^p}{h} + \sum_{q=1}^{N} A_{nn}^{pq} D_n^q + \sum_{q=1}^{N} A_{ns}^{pq} D_s^q + \sum_{q=N-M}^{N} A_{nc}^{pq} D_c^q \tag{25}$$

$$0 = (\lambda_s + 2G_s)\frac{D_c^p}{h} + 2G_s\frac{D_n^p}{h} + \sum_{q=1}^{N} A_{cn}^{pq} D_n^q \sum_{q=N-M}^{N} A_{cc}^{pq} D_c^q \tag{26}$$

$$0 = \frac{G_s}{h} D_s^p + \sum_{q=1}^{N} A_{sn}^{pq} D_n^q + \sum_{q=1}^{N} A_{ss}^{pq} D_s^q \tag{27}$$

The combined systems of linear algebraic equations (17) - (19) and (25) - (27) can be solved for the unknown DDs producing the boundary conditions stipulated above.

Three-Dimensional Formulation of EDDM

The three-dimensional EDDM is similarly developed to the two-dimensional enhanced DD model. The three-dimensional element is obtained by adding two lateral singularities to the formulation of the conventional three-dimensional DD element. The two lateral singularities are equal in magnitude and are an averaged value of the confinement stresses at a point in a material domain. The three-dimensional EDD element thus has a normal and a confinement component, and two shear components. As a result, when compared to the equations in the two-dimensional EDDM, the systems of equations for both mined and unmined zones for three-dimensional analysis have an extra equation to account for the additional shear component. Detailed information on the formulation of the three-dimensional EDDM can be found in [9].

The Progressive Failure Technique for the EDDM

It must be reiterated that it is possible to implement progressive failure in the EDDM, because the EDDM supplies all the components of the stress tensor needed by the various failure criteria to compute strengths. The classical DDM, on the other hand, does not account for confining stresses and cannot therefore produce all the stress components needed by failure criteria for the computation of failure envelopes.

The iterative process for implementing the progressive failure technique using the EDDM is given in the form of the flow chart in Fig. 6.

Sample Applications

Three examples of the application of progressive failure with the EDDM are provided in the paper. These examples help to demonstrate the applicability of the method proposed in this paper to mine pillar analysis. The examples presented in the paper were selected such that the results obtained from analysing them with progressive failure in the EDDM could be readily verified. Subsequently, the examples involve excavations and pillars of very simple geometry. The method however is not limited to problems involving simple shapes only. It is general enough to handle more complicated problem geometry. In all the examples it is assumed that the host rock is much stronger than the seam or orebody. Under such conditions, the host rock behaves in a linear elastic manner. Only material in the seam undergoes yielding.

Example 1

The first of the examples demonstrates the application of progressive failure with

the EDDM to the two-dimensional analysis of a pillar. Figs. 7a and 7b provide a description of the problem and the discrete representation of the stopes and pillar with EDD elements. Representative elastic properties and parameters for determining the strength of both the host rock and orebody in the problem are provided in Table 1 [20]. This problem was first solved in [12] with progressive failure in the FEM. It is assumed in the problem that only vertical stresses due to the weight of rock overburden are applied to the excavations. The underground excavations shown in Fig. 7a are at a depth of 457m.

Table 1: Rock properties for Example 1

Rock type	*E (MPa)*	*ν*	*ϕ (degree)*	*C (MPa)*	*m*
Host	11324	0.3	40	4	9
Orebody	3248	0.3	30	2	7

In the analysis, stresses in the pillars were calculated using the EDDM. The ratios of the normal stresses to the vertical stress, p, (normalized normal stresses) at various points across the width of the pillar were plotted in Fig. 8. From the plots it is evident that the results of the approach advocated in this paper compare very well with those obtained from the FEM with progressive failure modelling. In addition to verifying the stresses in the pillar, the stresses computed for the panels were also checked. Normalised normal stresses for the panels are plotted in Fig. 9. Again, there is good agreement between the results of the EDDM with progressive failure, and those computed from progressive failure in the FEM. Plots of the normalised normal stresses in the pillar and panels

produced by an elastic analysis are supplied in Figs. 8 and 9, respectively, for comparison with stresses obtained from the yield models.

Plots of the normalised normal stresses for different ratios of pillar width to excavation width (Fig. 10) were also generated in order to establish the correct behaviour of the proposed method. The changes in the yield zones with increasing values of the pillar width to stope width ratios predicted by progressive failure in the EDDM, reflect the expected physical behaviour of yield zones in mine pillars.

Example 2

Example 2 considered the analysis of a pillar in a longwall mining scheme in which ore from a panel was removed in two stages. This example was analyzed by Kripakov *et al* [12] using progressive failure in the FEM. The material properties of the host rock and orebody analyzed in the example are provided in Table 2. The mining depth is assumed to be at 457m with the primitive stress field assumed to be uniform and equal to overburden pressure. Fig. 11a shows the geometry and dimensions of the excavations, panels and pillar at each of the mining stages. If the length of the panels, orebody, and pillar were to be infinitely long, this three-dimensional problem would be equivalent to a two-dimensional analysis of the central cross-section of the problem. For practical purposes, however, an infinite length is not possible for the simulation of the two-dimensional problem. Therefore, a length to width ratio of 4:1 was selected for the problem.

Table 2: Rock properties for Example 2 and 3

Rock type	*E (MPa)*	*ν*	*ϕ (degree)*	*C (MPa)*	*m*
Host	17241	0.3	30	4	9
Orebody	1724	0.3	30	2	7

The mesh used in discretizing the problem domain is shown in Fig. 11b. This mesh remained unchanged for both stages of the problem. Boundary conditions, however, were chosen to correctly represent the physical conditions prevailing at the different stages.

Stresses around the excavations and in panels and pillars were computed for the different stages of the analysis. During stage I, no failure occurred in either pillar or panel material. Progressive failure of rock occurred only during stage II of mining. The normalized normal stresses computed in the plane of the central cross-section of the pillar are plotted in Fig. 12. These results are compared with the results of a two-dimensional analysis of the central cross-section of the problem. There was good agreement between the results of the three-dimensional and two-dimensional analyses, even though the mesh used for the latter was much finer.

Example 3

The three-dimensional analysis of a single square pillar in an excavated room was performed in Example 3. The dimensions of the room and pillar are provided in Fig. 13. The material properties of the orebody and surrounding rock mass, mining depth, and stresses remained the same as those found in the second example.

Normal stresses at different points in the pillar were calculated and normalized with the primitive vertical stresses acting at the mining depth. Contours of equal normalized stresses in the pillar are depicted in Fig. 14. These contours agreed with the experimental results in [3], which demonstrated that under low confining stress, high stress zones in yielded pillars migrated towards the core.

Summary and Conclusions

The yield behaviour of rock pillars and the analysis of yielding pillars are generally very difficult to model numerically because of the non-linearity of the yielding process. The prediction however of pillar behaviour is of great importance to the design of room-and-pillar mining schemes. Due to difficulties in estimating the *in-situ* strength properties of pillar material and the complexities of pillar loading conditions, any tool for the practical analysis of yielding pillars must be simple and yet capable of producing acceptable results. The progressive failure technique, implemented in the EDDM, meets the necessary requirements. It was initiated in an effort to develop a quick and efficient numerical technique for pillar post-failure analysis in the mining of lenticular orebodies.

One of the principal advantages of the EDDM in solving mining problems is that it provides optimal information on the global behaviour of pillars in a mining zone. Progressive failure in the EDDM produces analysis results sufficient enough for correct recommendations on pillar design to be made. The EDDM is used over the classical DDM in simulating the progressive failure of rock, because whereas the former provides all components of the stress tensor needed to compute failure envelopes, the DDM does not.

In the progressive failure technique, the yielding of pillars is modelled iteratively in a pseudo-elastic fashion. During each iterative step, elements representing the material being modelled are assigned elastic and strength properties based on the extents to which they have failed. Elements that have not undergone any failure retain their initial elastic properties while those that have failed experience reductions in their modulus of elasticity and strength. The reduced stiffness and strength values of failed elements are computed as functions of a key numerical value in the progressive failure method - the local factor of safety of a material. This quantity is defined as the ratio of the strength of the material computed at a point in the material to the major principal stress at the point. For a failed element, the progressive failure technique assumes that the degree of material weakening (or softening) of the element in an iteration is inversely proportional to the factor of safety calculated for the element in the previous iteration. The reductions in the elastic modulus of failed elements allow stresses to be redistributed from the failed elements to the more competent ones in each iteration. The iterations continue until there are practically no further changes in the computed factors of safety for all elements. In this paper, the elements used in conjunction with the progressive failure method are enhanced displacement discontinuity (EDD) elements.

Simple as the progressive failure technique is, it overcomes many of the numerical programming difficulties associated with the simulation of strain-softening behaviour. It also is an efficient way of way of generating results that conform to real rock behaviour in pillars and panels. The results of the analysis of sample problems in both two and three dimensions with the progressive failure procedure in the EDDM

proposed in this paper, compared very favourably with those obtained from progressive failure modelled with the FEM, and with experimentally obtained results.

For the sake of simplicity, only the EDD model with constant elements was considered in this work. It is possible to formulate higher-order EDD elements using the node-centric element approach outlined by Vijaykumar, Curran and Yacoub [22]. Using a node-centric formulation that allows continuous variation of the DD along the lengths of adjacent elements would definitely have some advantages in accuracy compared with the constant EDD approach. The node-centric elements enjoy the additional advantage that they allow more realistic boundary conditions to be used in analysis. This is possible because in the node-centric method the nodes of elements are actually located on the physical boundaries of excavations.

Although the progressive failure method was used only with the EDDM in this paper, additional models for analysing pillar yielding in the EDDM could be readily developed. The EDDM in its formulation uses or supplies all the components of the stress tensor and assumes a homogeneous stress distribution along the height of pillars or panels. It can therefore accommodate any material constitutive relationships.

Acknowledgment

The authors are grateful to R. Hammah for the valuable discussions related to this work. The financial support of the Natural sciences and Engineering Research Council (NSERC) and *Rocscience* Inc. are gratefully acknowledged.

References

1. Jeremic M.L. *Ground mechanics in hard rock mining,* A.A. Balkema, Netherlands (1987).
2. Bieniawski Z.T. Deformational behavior of fractured rock under multiaxial compression. *Proc. Int. Conf. Structures Solid Mech. Engng Materials,* Southampton, England, Paper 50, 589-598 (1969).
3. Wagner H. Determination of the complete load-deformation characteristics of coal pillars, *3rd. Int. Congress on Rock Mechanics*, 1076-1081 (1974).
4. Duncan Fama M.E. Numerical modeling of yield zones in weak rock, *Comprehensive Rock Engineering* (Eds. J.A. Hudson, E.T. Brown, C. Fairhurst and E. Hoek), Chp. 3, Vol.2, 49-75 (1993).
5. Beer G. and Watson J. O. *Introduction to finite and boundary element methods for engineers*, John Wiley & Sons, England (1992).
6. Mack M.G. The displacement discontinuity method, *in Boundary Element Techniques in Geomechanics,* (Eds. G.D. Manolis and T.G. Davis) Computational Mechanics Publications, Elsevier Applied Science (1993).
7. Crouch S.L. and Starfield A.M. *Boundary Element Methods in Solid Mechanics* p.322. George Allen and Unwin, London, (1983).
8. Zipf R.K. *MULSIM/NL Theoretical and Programmer's Manual* BuMines IC 9322, (1992).
9. Yacoub T.E and Curran J.H. An enhanced displacement discontinuity method for the analysis of lenticular orebodies. *Submitted for publication* (1998).

10. Kripakov N.P. Finite element analysis of yielded-pillar stability, *Comp. & Struct.*, **13**, 575-593 (1981).

11. Kripakov N.P. and Melvin M.T. A computer procedure to simulate progressive rock failure around coal mine entries. *Proceedings of the 1st conference on the use of computers in the coal industry,* (Eds. Y. J. Wang, R.L. Sanford), Chp. 56, 487-502 (1983).

12. Kipakov N.P., Sun M.C. and Donato D.A. ADINA applied toward simulation of progressive failure in underground mine structures, *Comp. & Struct.*, **56**, 329-344 (1995).

13. Ash N.A. and Park D. 3-D finite element modeling of longwall mining using progressive failure concept. *Proc. 28th US Symp. Rock Mech.*, (Eds. I.W. Farmer, J.J. K. Daemen, C.S. Desai, C.E. Glass, S.P. Neuman), Tucson, 725-734 (1987).

14. Park D. and Gall V. Supercomputer assisted three-dimensional finite element analysis of a longwall panel. *Proc. 30th US Symp. Rock Mech.*, (Ed. A. Wahab Khair), 133-140 (1989).

15. Kidybinski A. and Babcock C. O. Stress distribution and rock fracture zones in the roof of longwall face in a coal mine. *Rock Mech. J.* **5(1)** (1973).

16. Pariseau W.G. and Eitani I. M. Comparisons between finite element calculations and field measurements of room closure and pillar stress during retreat mining. *Int. J. Rock Mech. Min. Sci. & Geomech. Abstr.* **18**, 305-319 (1981).

17. Chen W.F. *Plasticity in reinforced concrete*, McGraw-Hill, New York (1982).

18. Hoek, E., Kaiser P.K. and Bawden W.F. *Support of underground excavations in hard rock*, A. A. Balkema, Netherlands (1995).

19. Wiles T.D. and Curran J.H. General 3-D displacement discontinuity method, *Proceedings of the 4th Int. Conf. on Numerical Methods in Geomechanics*, (Z. Eisenstein, Ed.) Edmonton, Canada (1982).

20. Bieniawski, Z.T. *Rock mechanics design in mining and tunneling,* A.A. Balkema, Netherlands (1984).

21. Duncan Fama M.E. and Wardle L.J. Numerical analysis of coal mine chain pillar stability, *Int. Congress on Rock Mechanics* (Eds. G. Herget and S. Vongpaisal), Vol. 2, 859-863 (1987).

22. Vijayakumar S., Yacoub T.E. and Curran J.H. A node-centric indirect boundary element method: Three-dimensional displacement discontinuities, *to appear in Int. J. of Computers & Structures.*

LIST OF FIGURES

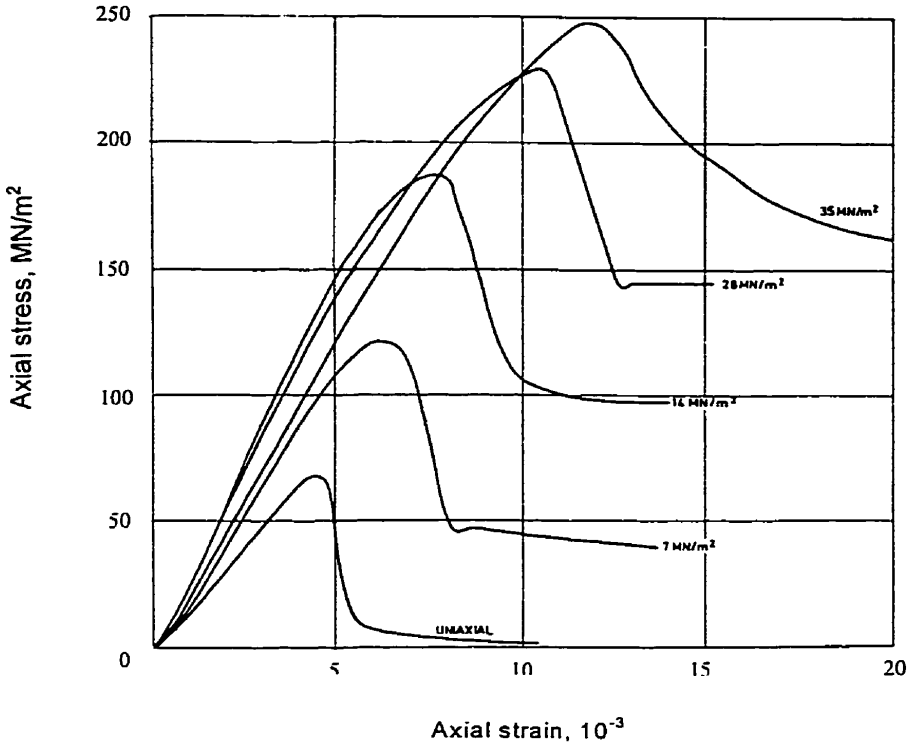

Fig. 1: Stress-strain behaviour of sandstone in triaxial compression for various confining pressures[2]

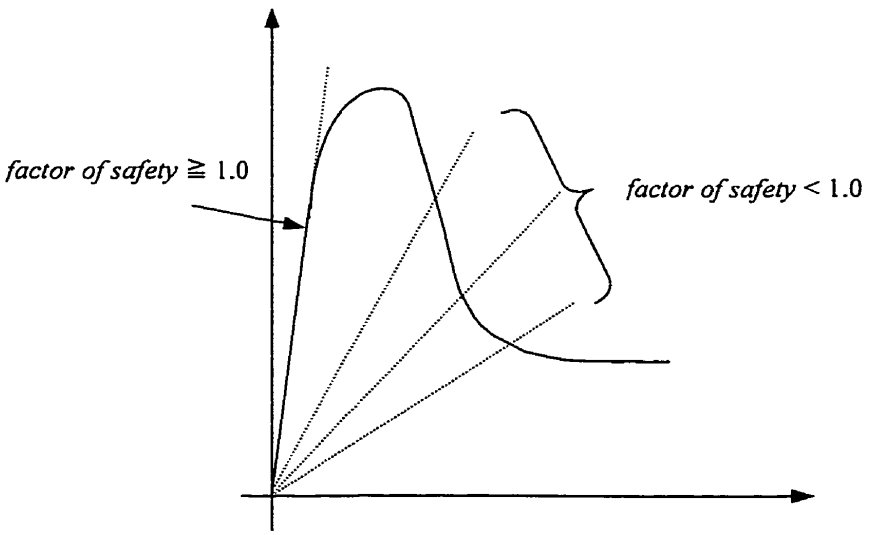

Fig. 2: Reduced post-peak elastic moduli of material

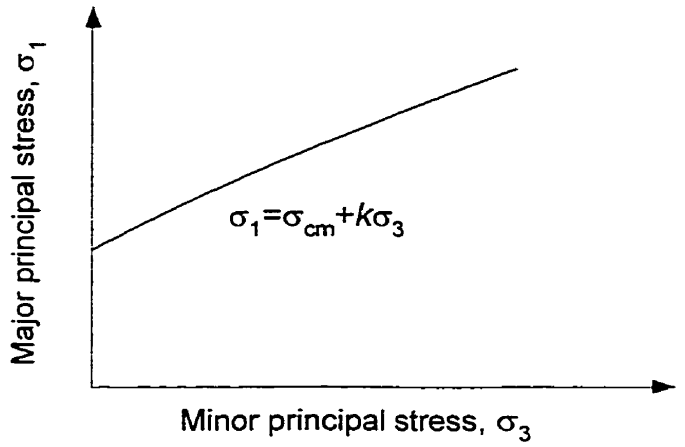

(a) Mohr-Coulomb criterion

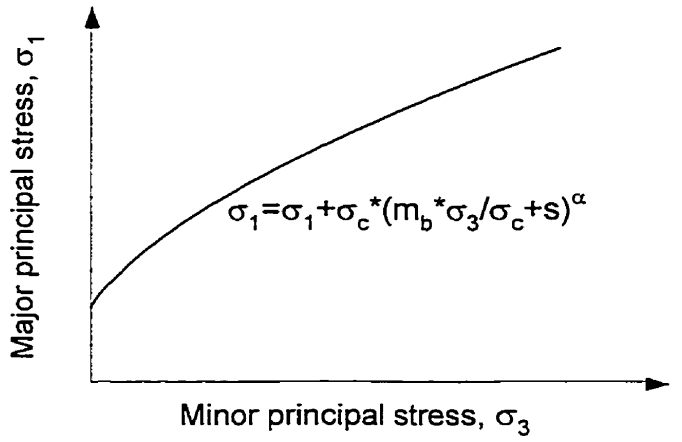

(b) Hoek-Brown criterion

Fig. 3: Relationships between principal stresses

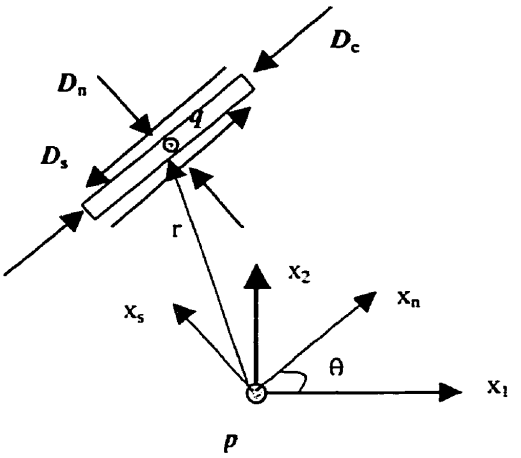

Fig. 4: Notations

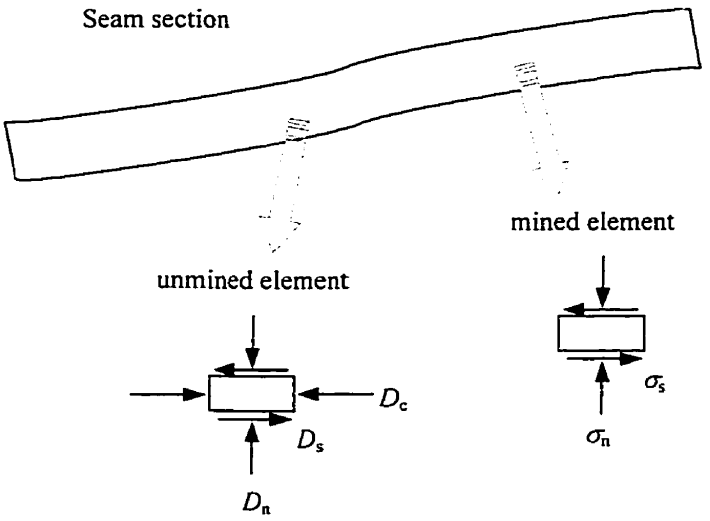

Fig. 5: Boundary conditions for mined and unmined EDD elements

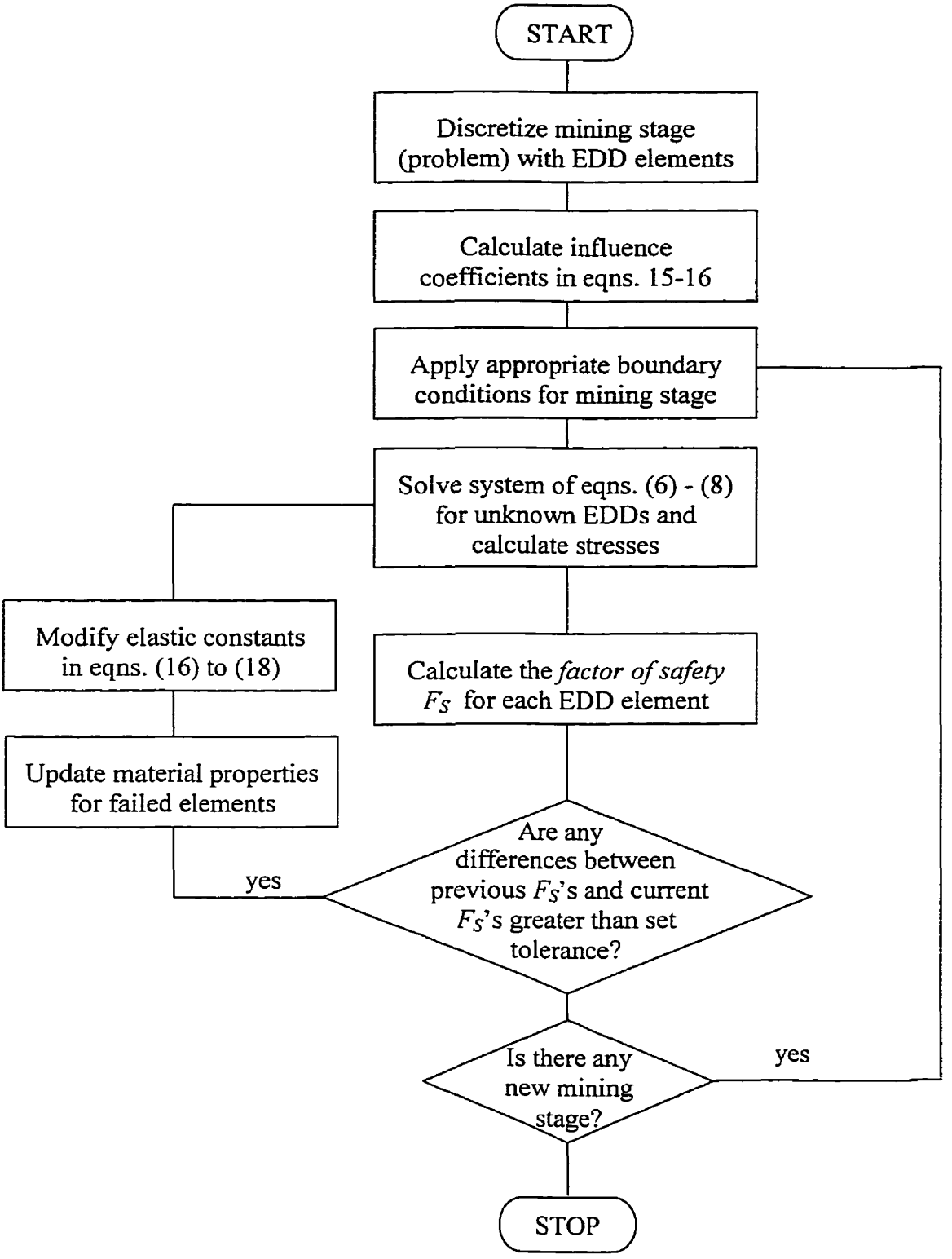

Fig. 6: Flowchart for the progressive failure algorithm using EDDM

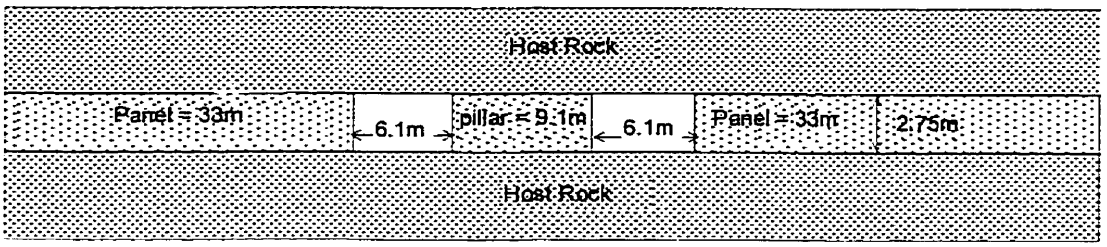

(a) Geometrical description

(b) Discretized mesh

Fig. 7: Two-dimensional model for mining problem

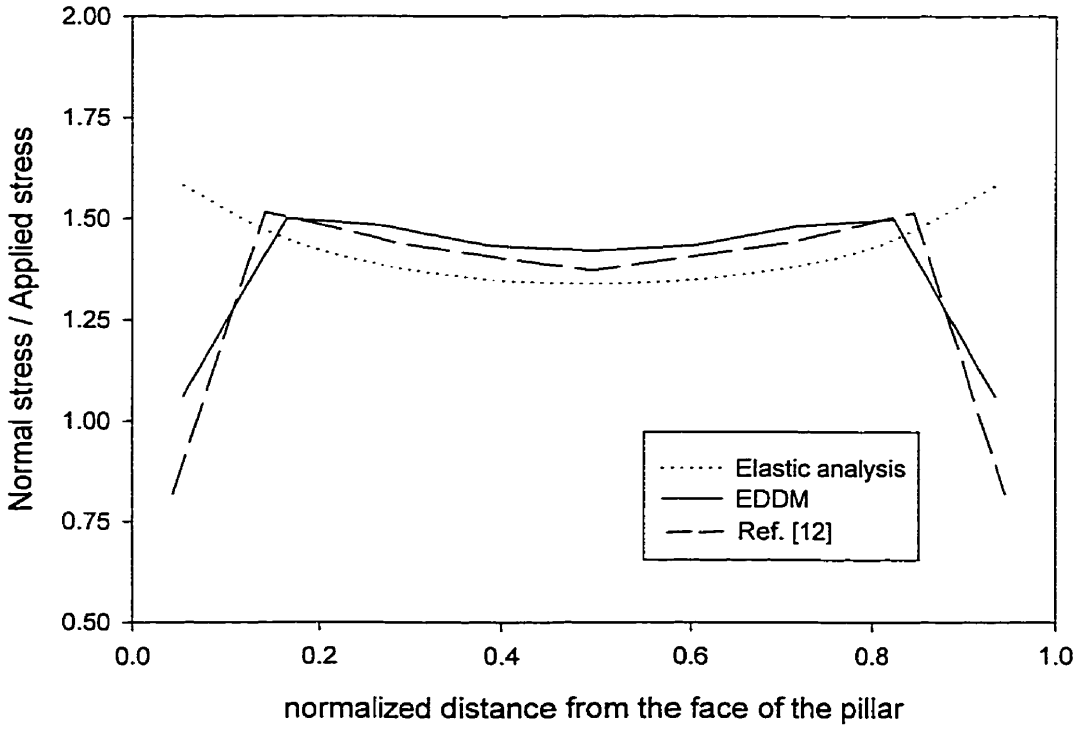

Fig. 8: Normal stress variation across the pillar

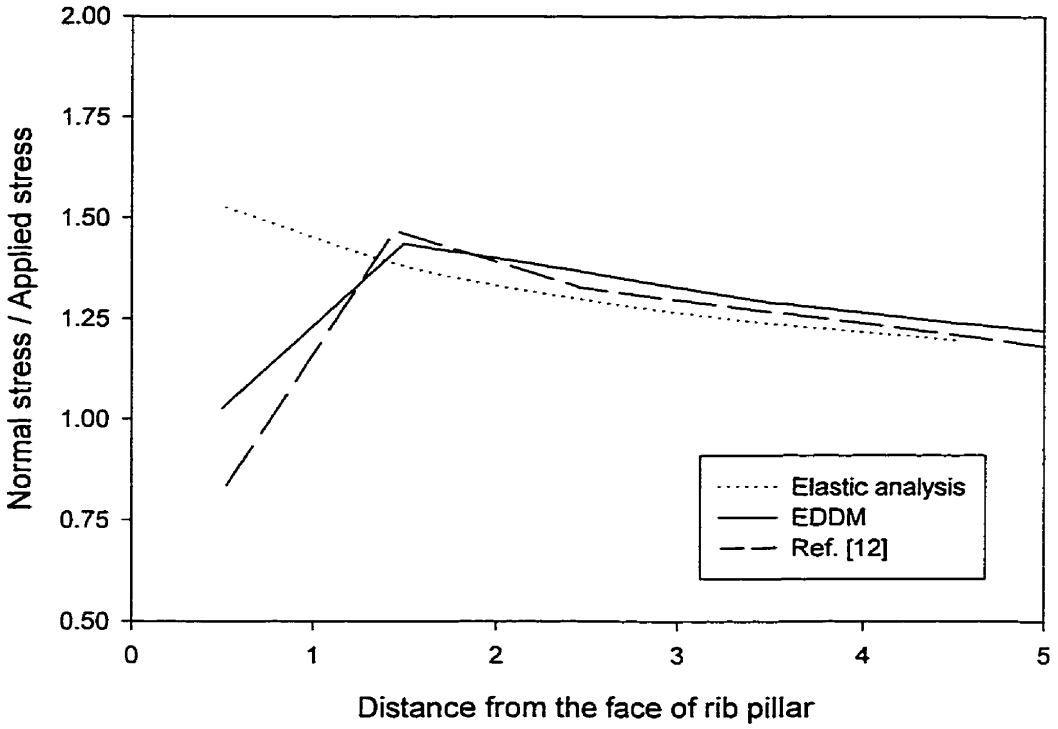

Fig. 9: Normal stress variation along the panel

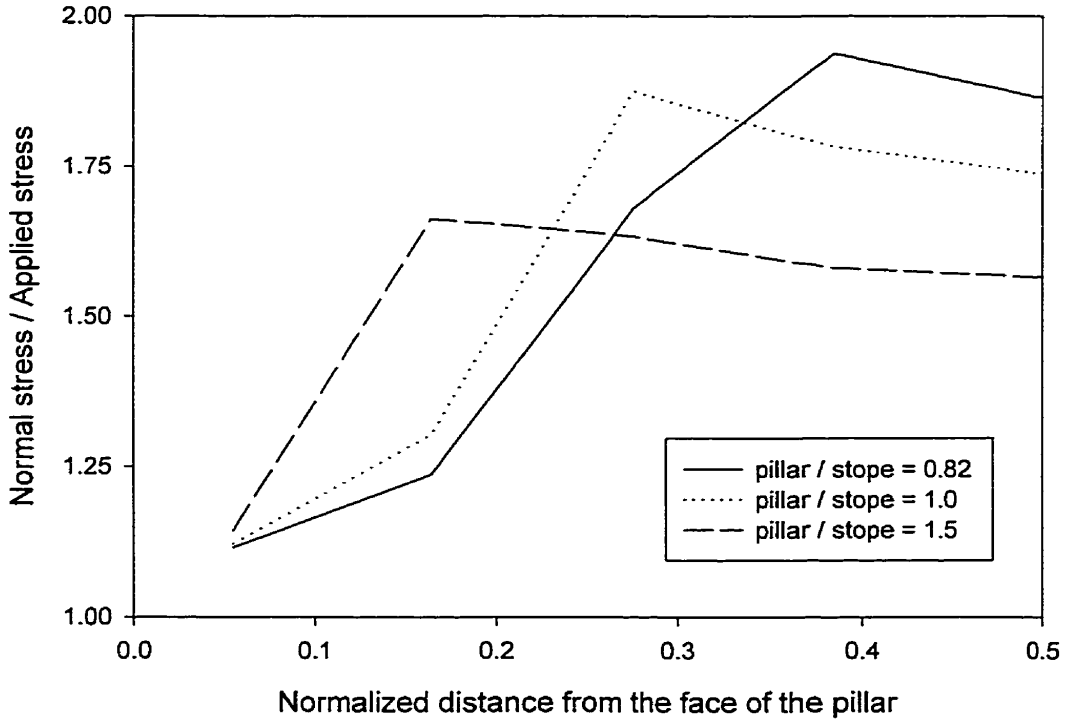

Fig. 10: Influence of pillar to stope ratio on the normal stress

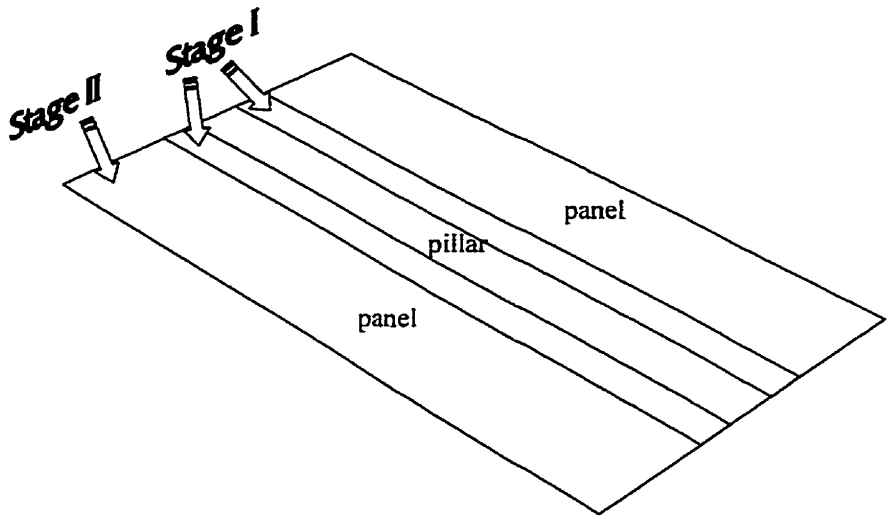

(a) Geometry description

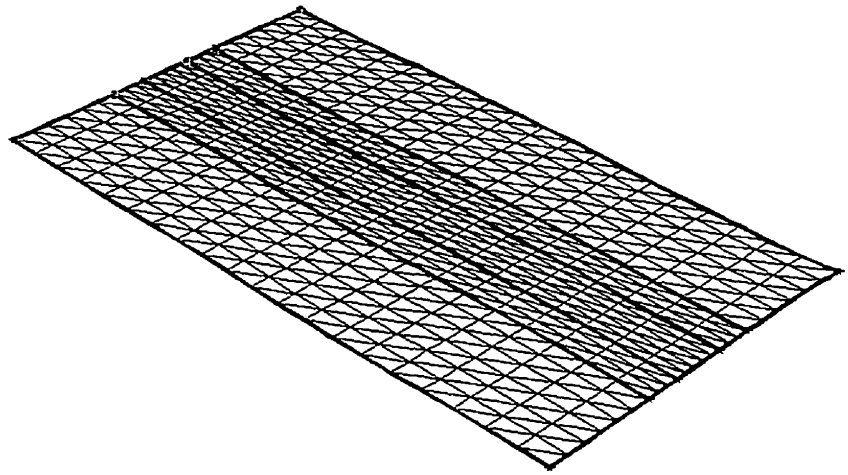

(b) Used mesh

Fig. 11: Geometry and discretization of the orebody

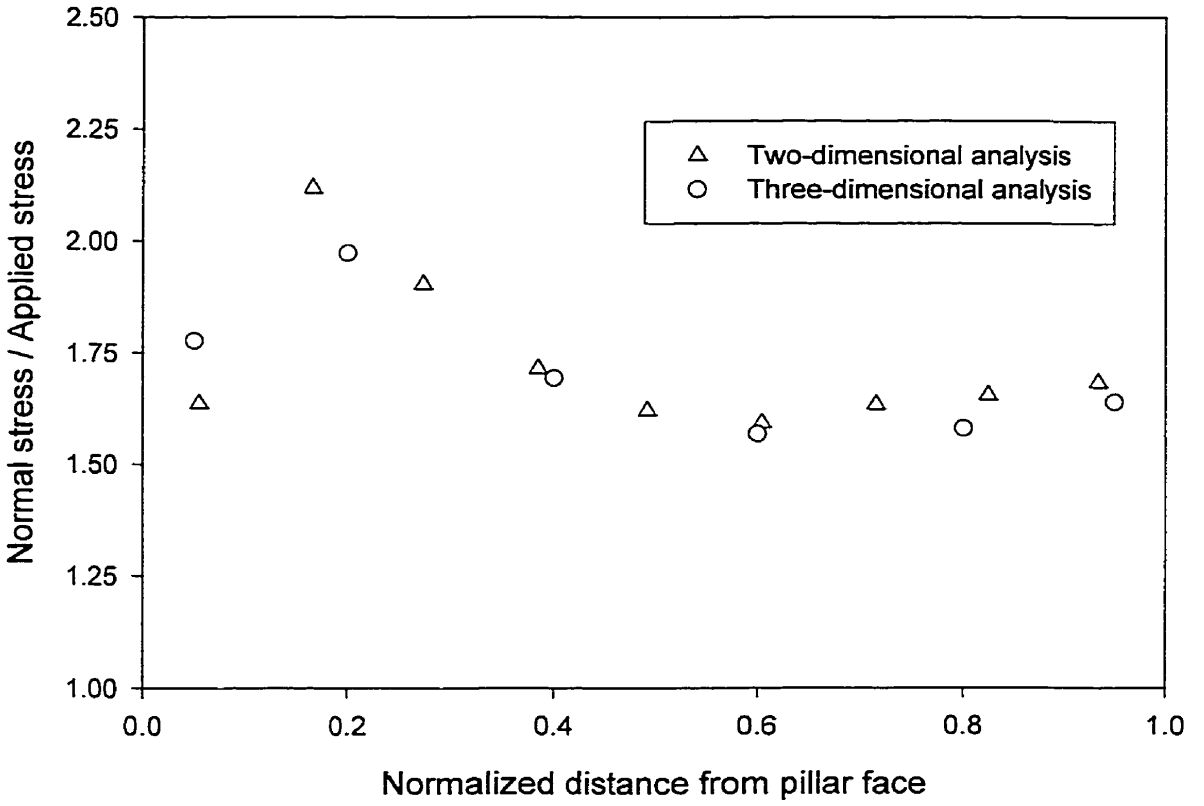

Fig. 12: Variation of normal stress across the pillar for stage II

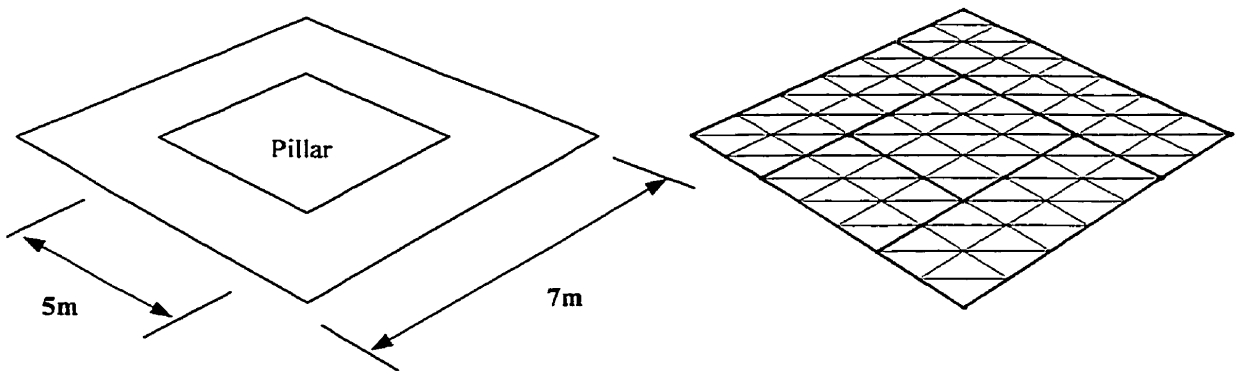

Fig. 13: Geometry and discretization of a pillar and a room excavation

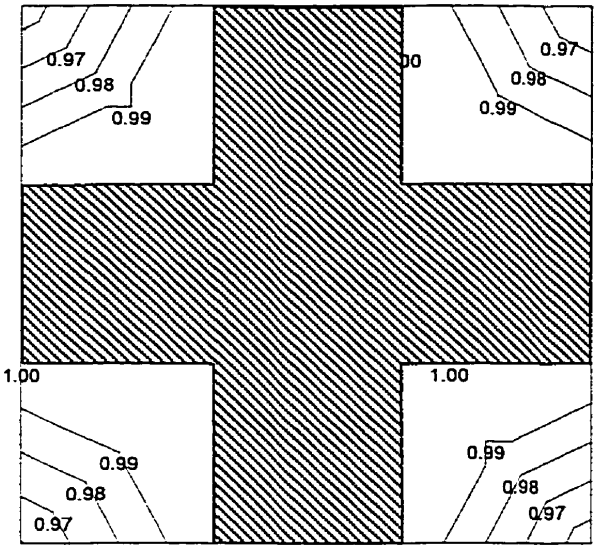

(a) Elastic pillar analysis

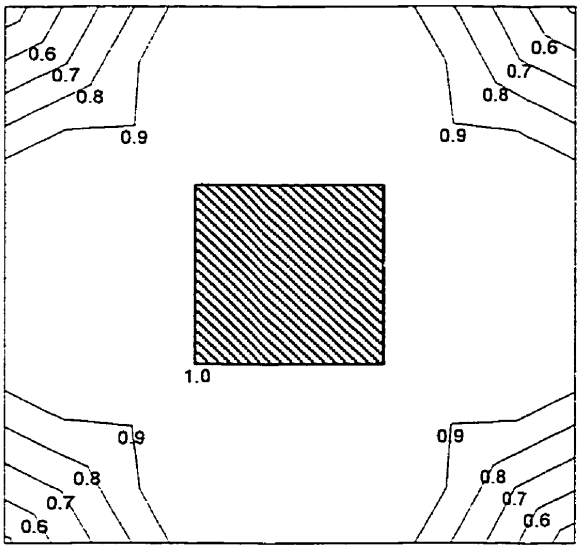

(b) Yielded-pillar

Fig. 14: Contours of the factor of safety for pillar